AD NUMBER
AD506976
CLASSIFICATION CHANGES
TO: unclassified
FROM: confidential
LIMITATION CHANGES
TO: Approved for public release, distribution unlimited
FROM: Distribution: Further dissemination only as directed by Office of Naval Research, Attn: Coded 102-05, Washington, DC 20390, OCT 1969, or higher DoD authority. NOFORN.
AUTHORITY
ONR ltr, 31 Jan 2006; ONR ltr, 31 Jan 2006

AD NUMBER

AD506976

CLASSIFICATION CHANGES

TO

confidential

FROM

secret

AUTHORITY

31 Oct 1972, DoDD 5200.10

SECURITY MARKING

The classified or limited status of this report applies to each page, unless otherwise marked.
Separate page printouts MUST be marked accordingly.

SECRET
NOFORN

MC REPORT 002
Copy ___ of ___ Copies

MEDITERRANEAN SEA ENVIRONMENTAL ATLAS FOR ITASS (U)

October 1969

Special Handling Required
Not Releasable to Foreign Nationals

OCEAN SCIENCE PROGRAM
MAURY CENTER FOR OCEAN SCIENCE
Department of the Navy
Washington, D.C.

[redacted]

SECRET

SECURITY

This document contains information affecting the national defense of the United States within the meaning of the Espionage Laws, Title 18, U.S.C., Sections 793 and 794. The transmission or revelation of its contents in any manner to an unauthorized person is prohibited by law.

MEDITERRANEAN SEA

ENVIRONMENTAL ATLAS

FOR JTAGS (U)

October 1968

OCEANOGRAPHER

OF THE

NAVY

CONTENT IS CLASSIFIED

In addition to [illegible] and must be [illegible] with specific [illegible] by the holder only to this document

Naval Res Lab

OCEAN SCIENCE PROGRAM

MAURY CENTER FOR OCEAN SCIENCE

Department of the Navy

Washington, D.C. 20390

SECRET

FOREWORD (S)

This Atlas is a departure from the usual approach to presenting environmental and acoustic data in that it was tailored from its conception solely to support the deployment of the Interim Towed Array Sonar System (ITASS) in the Mediterranean Sea. It is the intent of this Atlas to provide sufficient environmental and acoustic information for the optimum deployment of the ITASS, and to provide a source of general information on environmental effects to those charged with its operations.

This Atlas was requested by Manager, ASW Systems Project Office; compiled by the Undersea Surveillance Oceanographic Center of the Naval Oceanographic Office with technical direction by the Maury Center for Ocean Science, and financed by the Long Range Acoustic Propagation (LRAP) Project.

It is considered that this document is an interim Atlas designed to fill an urgent need. It is intended to upgrade and reissue the Atlas based on experience in its use.

Users of this Atlas are invited to forward their comments to Deputy Assistant Oceanographer for Ocean Science, Office of Naval Research (Code 102-OS), Navy Department, Washington, D. C. 20360.

J. B. HERSEY
Director
Maury Center for Ocean Science

SECRET

CONTENTS

LIST OF FIGURES

CONTENTS

INTRODUCTION

(S) This atlas provides environmental information pertinent to the operation of an Interim Towed Array Sonar System (ITASS) in the Mediterranean Sea, and describes how the environment may affect its operation. The atlas provides graphic information on bathymetry, surface winds, sea, swell, surface and subsurface currents, sound velocity, convergence zones, acoustic propagation, transmission loss, ambient noise and the application of this information. Transient environmental parameters are described monthly or seasonally.

(S) Environmental effects on sound detection over ranges greater than 100 miles are discussed as well as how the experimental ITASS equipment can be used most effectively.

THE MEDITERRANEAN ENVIRONMENT

BATHYMETRY AND PHYSIOGRAPHY

(U) The bathymetry of the Mediterranean Sea is shown in Figure 1 by means of 100 fathom contours which are based upon an assumed velocity of sound in sea water of 4800 ft./sec. However, a nomogram (Figure 2) provides separate depth corrections in four regions of the Mediterranean Sea for variations of vertical sound velocity from the assumed values. The following is a brief summary of the bathymetric features.

(U) The floor of the Strait of Gibraltar is a sill, which divides the Mediterranean Sea from the Atlantic Ocean, and has a limiting depth of approximately 175 fathoms. The bottom relief is extremely rugged. In the Alboran Sea there is no break to distinguish between the continental shelf and the slope. The basin floor lies at about 700 fathoms, and a maximum depth of about 840 fathoms occurs at the eastern end of the basin where it narrows to a submarine valley which descends into the deeper Balearic Basin.

(U) The floor of the Tyrrhenian Basin is flat to mildly sloping and lies at depths of 1400 to 1800 fathoms. The continental shelf is narrow to non-existent over most of the basin. The greatest depth of the basin exceeds 1800 fathoms.

(U) The floor of the Tyrrhenian Basin is irregular, but in some places at depths of 1800 fathoms or more it is relatively flat. Numerous peaks and knolls rise from the basin floor and slopes. The Tyrrhenian Basin is separated from the Ionian Basin by a sill with a depth of slightly less than 200 fathoms in the Strait of Sicily and less depths of less than 50 fathoms in the Strait of Messina.

(U) The continental shelf reaches a maximum width of about 300 n.m. east of Tunisia. There are northwest-southeast trending troughs on the continental shelf between Sicily and Tunisia where depths are about 700 to 800 fathoms.

(U) The Adriatic Sea lies mostly on the continental shelf. The floor of the Adriatic Basin is 600 to 700 fathoms deep and has little local relief. The maximum depth of 765 fathoms is in the Strait of Otranto adjacent to the sill which separates the Adriatic from the Ionian Basin. Limiting depths on the sill are approximately 450 fathoms.

(U) The floor of the Ionian Basin has considerable local relief consisting of seamounts, and many large and small elevations, depressions, and valleys.

(U) Most of the Levantine Basin floor is mildly undulating with several relatively flat regions. Several deep depressions lie off Turkey and Rhodes, three of which exceed 2000 fathoms.

(U) The physiography of the Mediterranean may be divided logically into western and eastern regions. The western region, west of Sicily, consists of continental margins descending to abyssal plains formed by turbidity flows (Figure 3). The eastern region is much more complex structurally and physiographically, in many respects being atypical of the usual oceanic divisions. An example of this is a series of basins paralleling and abutting the Mediterranean Ridge. Tectonic activity in this region has reportedly destroyed abyssal plains of the past similar to those which occur in the western Mediterranean. There are, however, many small abyssal plains in the deepest parts. Most are a few miles across.

SECRET

[illegible]

(U) Surface wind roses compiled from U. S. Weather Bureau records are shown for each month in 5° quadrangles. In Figures 4 through 38 winds, sea and swell are described by month and season. The winter months are January, February, March; the spring months are April, May, June; summer consists of July, August, September; and autumn of October, November and December.

(U) The winds are distributed among 8 direction and 5 speed groups and plotted to the nearest whole percent. To determine the percentage of winds from a particular direction the total length of the rose facing that direction is measured and compared with the rose scale in the legend. The total frequency of wind falling within a certain speed group may be estimated by measuring the length of each speed group on the bar graph located at the base of each rose.

(U) An eastward extension of the Azores High is the predominant climatic feature in the western Mediterranean during most of the year. In winter the Siberian High occasionally extends westward to cover most of Europe leading to the formation of deep low pressure centers in the Mediterranean off southern France and northern Italy. These lows are partly responsible for the greater number of strong winds and gales reported during the cold season. When a cold high is located over the interior of France, persistent strong winds blow out to sea through the river valleys of southern France. In the Gulf of Lion wind speeds in excess of 40 knots occur 15 percent or more of the time in winter.

(U) In the eastern Mediterranean, the western extension of the climatic [illegible] around the deep thermal low in Iran and Pakistan is the predominant climatic feature of summer. Its greatest development occurs during July and August causing the northwesterly winds to be stronger and more persistent than in any other months.

(U) In winter migratory low pressure centers enter the western Mediterranean through the Strait of Gibraltar and usually cross the Balearic Sea, the northern Tyrrhenian Sea, Italy, and the Adriatic Sea. A secondary storm path extends from the upper Tyrrhenian Sea through the Straits of Messina and into the Ionian Sea.

[illegible]

(U) In winter the eastern Mediterranean is affected by high pressure that prevails over the European continent. The contrast between cold European air and warm African air causes many cyclones to form. Other cyclones enter the area from the western Mediterranean. These lows cause increased precipitation and variability of wind direction and more frequent gales during the cold season although winds seldom exceed 40 knots. The spring transition season in the western Mediterranean is characterized by greater persistence of northwest winds and increased thunderstorm and shower activity followed by a rapid decrease in cloudiness and in the amount and intensity of precipitation. The frequency of 40-knot winds decreases to about 8 percent in the Gulf of Lion and is extremely low elsewhere in the western Mediterranean.

(U) In the eastern Mediterranean in the spring transition season an increase of northwesterly winds and cyclonic activity is followed by a decrease in the amount and intensity of precipitation.

(U) Cloudiness of any type is rare in the western Mediterranean in summer and there is almost no precipitation except for thunderstorm activity in the north. Cyclone activity is extremely rare. In the Gulf of Lion about 1 percent of the winds are greater than 40 knots. Winds of this strength seldom occur elsewhere in the western Mediterranean.

(U) In summer there is almost no precipitation in the eastern Mediterranean except for thunderstorm activity in the northern Aegean Sea and other near shore regions in the northern part of the area.

(U) In fall shower and thunderstorm activity increases as the first cool air masses arrive in the western Mediterranean. Cyclones enter the area by way of Gibraltar and the Rhone Valley and cyclogenesis occurs in the Ligurian and northern Tyrrhenian Seas. Winds greater than 40 knots increase in frequency.

(U) During fall, shower and thunderstorm activity increase in the eastern Mediterranean beginning in the Ionian Sea in October and reaching the southeastern Mediterranean in December. Cyclones enter the area from the western Mediterranean and the Adriatic Sea.

SEA AND SWELL

(i) The surface of the ocean is described by the terms sea and swell. Sea refers to waves caused by the local wind, whereas swell refers to waves that have progressed beyond the influence of the generating wind. The direction of swell is largely independent of the local wind but may coincide with it. Both sea and swell frequently are present at the same time although the presence of one may mask the other. Although the surface of the ocean is not a series of rythmic waves, it is possible to observe the direction, height, length and period of the more conspicuous waves making up sea and swell.

(ii) Sea and swell roses show the direction and frequency of occurrence of various wave height ranges, and histographs show the frequency of various sea height ranges for all directions. These figures represent accumulated observations for each month in 5° quadrangles. Summary scales show predominant sea direction (from which the sea is moving) and constancy. The quality and quantity of sea and swell data are sufficient to make these charts reliable.

SURFACE CURRENTS

(ii) Surface currents in the western Mediterranean are determined principally by the prevailing winds and surface evaporation. Throughout the year surface water from the Atlantic Ocean moves through the Strait of Gibraltar into the western Mediterranean and is driven generally in a counter-clockwise direction by the prevailing northwesterly winds. Southerly winds that occur for varying periods in winter interrupt this counter-clockwise flow. When the wind from any one quarter has been strong and continuous, drift currents are set up. During gales, current speeds of 4 to 5 knots may occur. Water from the west can extend the influx of

Adriatic surface water, depending on the [illegible] forces. Wind drift currents [illegible] to 100 feet but are negligible below this depth, however wind drift usually is weak because wind speeds in this area range from Beaufort force 0 to 3. Strong winds from the west in summer and the east in winter can develop appreciable crosscurrents.

(U) Rapid evaporation of surface water in the western Mediterranean, particularly in the northern part of the Balearic and Ligurian Seas, produces surface water of high salinity which sinks and is replaced by less saline Atlantic surface water that flows east through the Strait of Gibraltar. The salt balance between the Mediterranean and the Atlantic is maintained by a bottom countercurrent of high salinity that flows out of the Mediterranean through the Strait of Gibraltar. Mixing occurs between the surface and bottom currents forming a transition zone which has strong vertical movements and weak, variable currents.

(U) Strong tidal currents superimposed on the surface and subsurface currents reduce the inflow when they set from the Mediterranean into the Atlantic Ocean, and increase the inflow when they set from the Atlantic into the Mediterranean.

(U) The most persistent part of the prevailing surface current in the western basin flows east between Gibraltar and Tunisia where about 50 to 65 percent of all current observations show a set between northeast and southeast, and of these most show a set due east. Transient westerly sets are caused by easterly gales. The most variable currents (in direction) occur in the central parts of the basins. There is a westerly return current along the north slope.

(U) The surface current sets southeastward into the eastern Mediterranean through the Strait of Sicily at speeds ranging from 0.2 to 1.0 knot. In the Malta channel the current is influenced by the wind but generally sets east-southeast at 1.2 knots. Along the south coast of Sicily the southeast setting current is weak except when accelerated by west to northwest winds. During strong southerly winds a northeast setting current may occur along the south coast of Sicily and during gales it may attain a speed of 2.0 knots. The

counter-clockwise circulation of the eastern Mediterranean deficit the 0.1 to 1.0 knot southeast setting currents off Tunisia and Libya toward the coast. Except for a counter current in the Gulf of Sirte, the surface currents set eastward along the coast of eastern Libya and into the Levantine basin at speeds of 0.4 to 0.8 knot.

(U) In the Levantine basin the surface currents set east at 0.4 to 1.0 knot paralleling the coast of Egypt. However, off the coast of Libya and Egypt this current may set westward for brief periods under the influence of strong southerly winds that occur most frequently in winter. The surface current parallels the coast around the Levantine basin at speeds of 0.4 to 1.0 knot off Israel and Lebanon, 1.0 to 1.5 knots between Syria and Cyprus and 0.4 to 1.0 knot off Turkey and between Crete and Turkey into the Aegean Sea. Part of this current veers south to southwesterly around the west tip of Cyprus at speeds of 0.2 to 0.6 knot and completes the counter-clockwise movement of the Levantine basin. North of Crete a portion of the southward flowing Aegean current divides. One branch sets eastward at speeds of 0.2 to 0.7 knot, part rejoining the northward currents in the Dodecanese and part passing around the eastern tip of Crete and setting westward south of the island. The other branch veers westward at speeds of 0.2 to 0.7 knot between the coast of Greece and Crete and continues northwestward along the west coast of Greece toward the Ionian Sea.

(U) The surface current which enters the Ionian Sea from the Aegean Sea also divides. One branch flows northward along the western coast of Greece at speeds of 0.2 to 0.6 knot and joins the counter-clockwise circulation of the Adriatic Sea. The other branch veers southwestward and joins the southeast flowing currents in the Ionian Sea.

(U) This branch completes the counter-clockwise circulation of the eastern Mediterranean Sea. The prevailing circulation pattern of the eastern Mediterranean

Sea does not exist as a single face. [illegible] and the degree of variability cannot be predicted.

SUBSURFACE CURRENTS

(U) The direction and speed of subsurface currents in the Mediterranean Sea were computed from the difference in the specific volume of the water at different locations and at different levels within the water column. The differing specific volume values were contoured for several levels and for several seasons. The contours indicate the speed and direction of the current at the upper level, or depth, referred to on the figure. The lower level is the assumed level of no current motion (Figure 41 et seq.).

(U) The subsurface current profiles are the only ones available and represent measured current velocities and directions to about 300 meters below the surface. The profiles indicate current velocity in knots. Mean current directions at 5, 10, 25, 50, 100, 200, and 300 meters are given by abbreviated compass directions: ESE = East South East. The profiles are grouped into four seasons and identified by month. Geographical location of each current profile is indicated by a number keyed to the chart (Figure 46 et seq.).

SOUND VELOCITY STRUCTURE

(U) Sound velocity variations in the Mediterranean Sea are shown seasonally by mean sound velocity profiles in selected one-degree quadrangles. Typical monthly sound velocity profiles are shown for each of four major basins (Figures 53-57).

(U) Variation of surface sound velocity from year to year in the eastern Mediterranean is not significantly greater than the possible variation within a single month. Maximum surface sound velocity variations in the eastern Mediterranean occur in the summer months and are commonly as much as 15 to 20 feet per second (fps). During summer the isothermal layer depth varies from 0 to 100 feet. Variation in sound velocity during the winter months is not likely to exceed 5 fps near the surface. Variation decreases with depth, and seasonal

effects are small in areas 500 to 600 feet where changes occur slowly over 6 months to a year. At this depth, variation with location within one of the boxes mentioned should not exceed about 5 fps. The total annual sound velocity variation decreases to about 3 fps at 1000 feet, 2 at 2000, 1 at 3000, 0.5 at 5000 and should be less than 0.5 fps below 8000 feet. Surface sound velocities vary about 5 fps in August. The depth of the isothermal layer is highly variable during the period from April to August and has variations of about 50 feet through December. The depth of the sound channel axis (point of minimum velocity) is most uncertain during the spring. Local surface warming can give an axis depth of 20 feet in January through March, although this is quite rare.

(U) Variability of sound velocity in the western Mediterranean is about ±5 fps in fall and winter and ±10 fps in spring and summer for the upper 100 feet. These limits decrease gradually to the 600 foot limits of the deep profiles. A mixed layer at the surface is most common during the fall and winter, but an occasional warming period can produce a temporary shallow negative gradient layer characteristic of early spring. Warming during spring and early summer makes negative-gradient surface layers most common, with occasional surface mixing due to high winds or short cooling periods. After mid-August the shallow mixed layer, characteristic of early fall, is more likely to exist.

(U) In the summer, isovelocity layers are generally only 50 to 60 feet deep coinciding approximately with the summer maximum isothermal layer depth. Little cyclonic activity occurs in this region during the summer. The shallow isothermal layers result principally from convection with a minimum of wind mixing. Mixing is aided by high insolation and evaporation rates which create very stable negative temperature and sound velocity gradients below the layer depth. Summer conditions prevail approximately between April and October.

(U) The climatology of the Mediterranean Sea shows that maximum storm conditions occur in the winter. With the onset of cyclonic activity in October, the clear cover, wind increase and the rate of insolation

deep sea resulting in a decrease of ice melt to practically zero. Increased wind mixing combined with convective mixing results in a deep ming of the isothermal layer to 500 feet or more by January. Winter conditions prevail roughly between November and March. Changes in the thermal situation of the Mediterranean Sea last from 24 to 48 hours after a storm.

SONAR PROPAGATION

INTRODUCTION

(5) This section describes how the ocean environment affects the acoustic operation of ITASS and discusses a rationale for the best effective deployment of this sonar in relation to depth and geographic location for various parts of the Mediterranean Sea. It contains an elementary account of sound detection to ranges of well over 100 nautical miles. It provides the background for understanding the sound propagation curves used as the basis for choice of best depth for the ITASS. Measurements of ambient noise in the Mediterranean are reviewed.

THE SONAR EQUATION

(6) The passive detection equation can be written in a simplified form as follows (in decibels):

$$SE = SL - TL - NL - RD + AG$$

where, SE = Signal Excess

SL = Average Source Level

TL = Transmission Loss

NL = Noise Level at the sensor

RD = Recognition Differential (this is nearly equivalent to Detection Threshold)

AG = Array Gain

The source level (SL) stated dB relative to 1 microbar (dbμ/cm^2), is extrapolated to a range of one yard from measurements at greater distances.

(S) Source levels of foreign submarines are commonly established by taking measurements of targets of opportunity. These measurements are not taken under ideal or controlled conditions which means that they contain a degree of uncertainty. These uncertainties include target factors such as changes in speed, aspect, depth and machinery modes of operation. Such factors must be taken into account in the establishment of a source level value for a given class of target and conditions of operation. Another uncertainty is the spectrum of the sound on which the source level is based. It is usual to assume that the source is a line in the spectrum of the target having a width less than the narrowest filter in the signal processor. In applications of towed arrays, at least a part of the test program will include detection employing a 10Hz processor capable of 1/4 Hz. The target line can be considerably broader than 1 Hz, and this fact must be allowed for in making detection range estimates. For example, a target line 2 Hz wide should be compared with a noise term, NL, which is 3 dB larger than the spectrum level usually employed.

(U) Transmission loss is a complicated function of range and, in addition, fluctuates in a manner that can best be described statistically. It will be covered in considerable detail in a later section.

(U) The noise at the sensor (NL) consists of natural sounds of the sea, ship traffic, flow-noise and the self noise of the towing ship. Below 200 Hz shipping dominates the ambient noise spectrum while above 200 Hz sea state and occasionally marine animals dominate the spectrum. This frequency limit is not exact, and exceptions to the above generalizations abound. Nevertheless, shipping is a dominant cause of low-frequency ambient noise with sea state being the principal cause of high frequency noise.

(U) The development of noise statistics in the sonar detection equation depends on the nature of the target signal and on the signal processing and display. The spectrum level of noise (i.e. noise in a band 1 Hz wide) is the

usually into the detection equation for NL including those cases where detection of a single line of the target spectrum is sought. This is the level in a band 1 Hz wide at the anticipated frequency of the target. A variability of ± 5dB should be expected in the noise spectrum level.

(S) The recognition differential (RD), is a characteristic of the operator as well as the signal processing and detection components. It can be defined as the amount by which the signal level exceeds the noise when there is a 50% probability of detection. RD is dependent on the properties of the signal and the noise. It generally becomes smaller as other terms become less favorable for detection. Values assigned to recognition differential are best determined from actual field experience, i.e. measurements at sea. The assigned value is the result of averaging a large number of sample cases. A variability of ± 3dB can be expected.

(S) The array gain (AG) can be defined as the ratio, in decibels, of the signal-to-noise ratio of the array to the signal-to-noise ratio of a single element. The array gain of ITASS is a function of several variables such as directionality of the noise, the beam within which the target appears, and the bearing of the target within the beam. Array gain figures are normally based on isotropic noise; i.e. total noise at a point is composed of noise arriving from all directions with equal intensity. This is a reasonable assumption, in the horizontal plane, for noise generated by breaking waves caused by local winds; i.e. in the spectrum above 200 to 500 Hz. It may be a rather poor assumption where noise is generated by a half a dozen or more ships which may be clustered or scattered in bearing from the array. Array gain assumes that a coherent signal is received along the length of the array, which is also an idealization. For these reasons, AG is not a dependable factor. It does provide an approximate upper limit on performance estimates. A variability of some ±3dB can be expected from the average value of AG.

(S) All the terms in the sonar equation are variable. Therefore, the longer the time available for seeking the target signal, the better the chances are for the fluctuations which occur to combine in a favorable manner to give a detection. This means that averaging the received signals to smooth out fluctuations is not necessarily advantageous. Estimates of these fluctuations or inaccuracies are as follows:

SL ± 5 dB

TL ± 5 dB to 60 miles, ± 3 dB beyond 60 miles

RL ± 5 dB

RD ± 3 dB

AG ± 3 dB

(S) These numbers are an estimate of the degree to which the observed data will tend to spread about an average value. Statistically, when one adds together a series of terms each of which has its own degree of uncertainty, the result has a degree of uncertainty which is approximated by the square root of the sum of the squares of the individual uncertainties. For the sonar equation:

SE = SL - TL - RL - RD + AG

the combined uncertainty (σ) in signal excess (at ranges greater than 60 n.m.) is given by:

$$\sigma^2 = 5^2 + 3^2 + 5^2 + 3^2 + 3^2$$

$$\sigma^2 = 25 + 9 + 25 + 9 + 9$$

$$\sigma = \sqrt{77}$$

$$\sigma = 8.8 \text{ dB}$$

The statistical interpretation of this variability figure is that the observed signal excess will be within ± 8.8 dB of the computed value approximately three fourths of the time.

(U) There are no measures of environmental effects on SL, AG and RD even though we know them to be environmentally affected. The uncertainties stated above are empirically based and will have to be altered as our experience grows.

(U) At a distance fr[illegible] large compared with the dimensions of the source, sound spreads out as though it had been generated at a point. Thus, a few miles from a ship or submarine, its sound behaves in this way. Because sound speed varies in the ocean, the sound is bent by the water as it spreads out just as air, glass, (or water) bends light. This phenomenon is called refraction, and can be studied by rays of sound which trace out the path followed by the sound. The separation of neighboring sound rays is inversely proportional to the intensity of the sound. The bending and spreading of rays can be computed precisely and rapidly through regions where sound speed varies both vertically and horizontally through the ocean. Since sound spreads in all directions from its source, some of the sound strikes both the surface and the bottom. These rays reflect partially and continue to travel by successive reflections at the surface and bottom. Some of the energy striking these surfaces is transmitted into the air or down into the earth. Much of this transmitted energy is lost to the ocean, though some may be reflected back by rock layers below the bottom. These paths are illustrated in the following series of sketches:

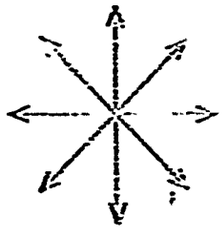

Figure A-1. Divergence of Sound Rays - sound goes outward from a source in all directions. (U)

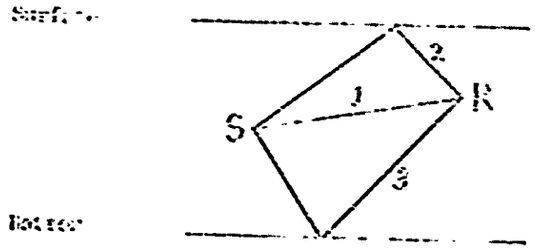

Figure A-2. Reflection of Sound Rays. (U)

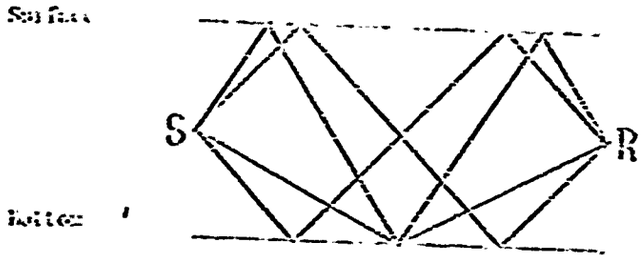

Figure A-3. Reflection of Sound Rays with One Bottom Bounce. (U)

These are four paths by which sound from a source (S) reaches a receiver (R) with one bottom bounce.

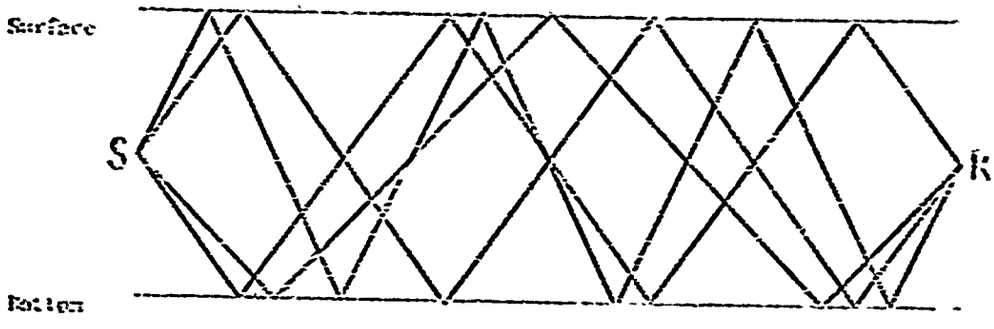

Figure A-4. Reflection of Sound Rays with Two Bottom Bounces (U)

There are also four paths by which sound from a source (S) reaches a receiver (R) after two bottom bounces.

(U) This type of sketch could be extended indefinitely to show that there are four paths from source to receiver for any number of bottom bounces. The

sound propagation. All three paths must be regarded as related randomly in phase. Thus the average transmission loss in dB for a given bottom bounce is 6 dB less than that due to a single direct path. Neglect of this term is a common mistake.

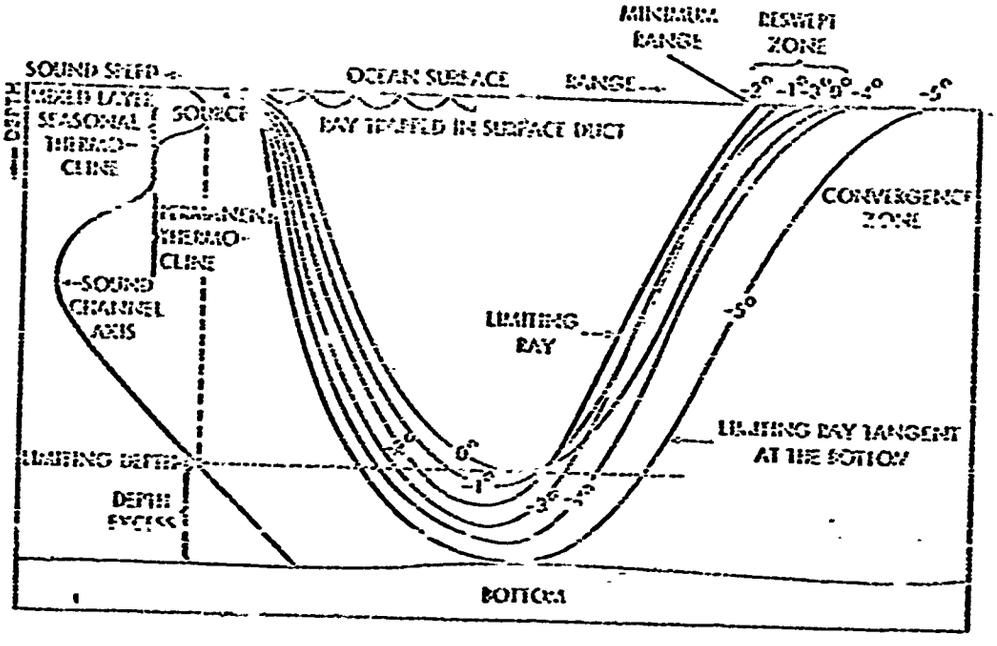

Figure A-5. Refraction of Sound Rays (U)

(U) The above figure illustrates how sound rays are refracted according to constraints imposed on them by the sound velocity in the water.

(U) The sound travelling along each path in the previous sketches is spreading according to the constraints imposed upon it by the sound velocity in the water, being partially absorbed by the water itself and partially scattered by material distributed through the water, and losing energy to the surface and to the bottom upon reflection. The intensity associated with each ray can be computed, and the total intensity at a point can be computed by adding the contributions from all of the rays.

(U) The vertical bending of sound paths by the variations in sound speed in the ocean limits where sound energy goes. In order to understand these effects, a few simple facts about the ocean are needed. The ocean waters are layered and consist of very extensive horizontal sheets within which the physical and chemical properties such as temperature, sound speed, salinity, oxygen content, etc., are nearly the same. Sound speed increases with increasing temperature, salinity and pressure so that, other things being equal, high temperature, high salinity and high pressure implies high sound speed. In Mediterranean winter, most of the sea, except for the southeastern part, is nearly the same temperature, top to bottom, close to 13 degrees centigrade (55.4°F). Thus, sound speed increases nearly uniformly from surface to bottom. Sound paths from a source at any depth are bent toward the region of lowest sound speed, the surface. There they are reflected and continue following paths that are approximately segments of circles interrupted by successive surface reflections, as shown in Figure A-6.

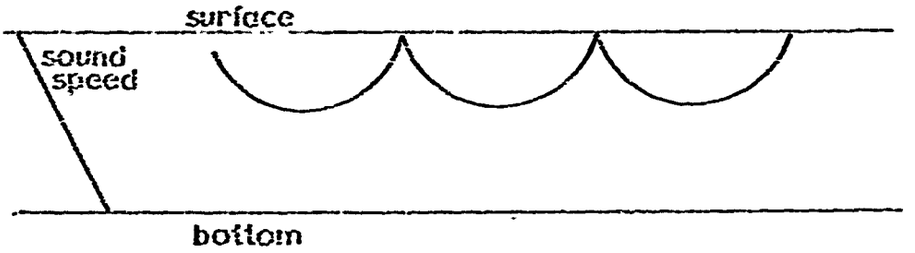

Figure A-6. Successive Surface Reflections - a typical Mediterranean sound path in the winter. (U)

(U) As sound travels through the water, some energy is absorbed by the water itself, and some is randomly scattered by material distributed throughout the water. These two effects, which seldom can be separated, vary with frequency. The combined effect, displayed as an attenuation coefficient, is shown in figure A-7.

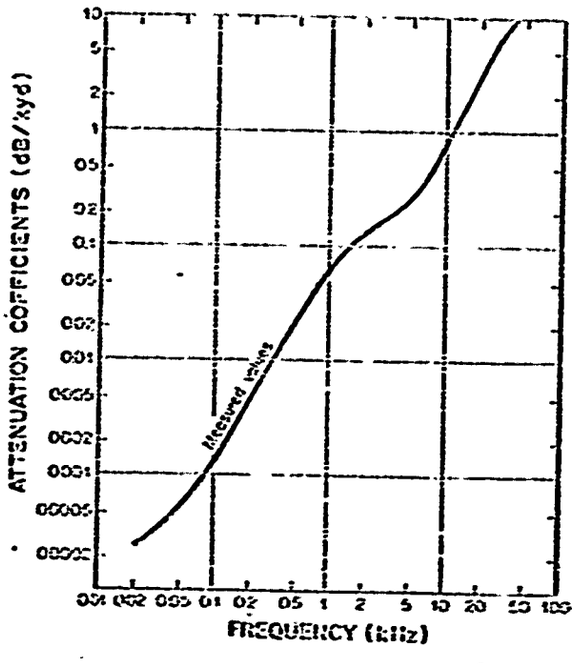

Figure A-7. Sound Attenuation. (U)

(U) The loss of acoustic energy at low frequencies on reflection from the surface is very small, while that from the bottom can be from 0 to well over 99%. The contribution to the received intensity by bottom reflected sound varies widely. The bottom reflection loss is greatest when the bottom is rough or is composed of soft mud. Loss is also high over a rock surface, smooth or rough. The least loss appears to result from reflection from a smooth sandy sea floor. In any case surface losses are less than bottom losses except under unusually stormy conditions. The angle at which the sound strikes the bottom affects the loss as well. The angle between the bottom and the sound path is called the grazing angle. When this angle is large, the loss tends to be largest; when the angle is small (less than 15 to 25 degrees) the loss is smallest. Bottom loss measurements made over a very large ocean area including

the Mediterranean has been divided into 5 classes according to bottom loss. These correspond roughly to different magnitudes of bottom roughness. Bottom loss is frequency dependent as well. The average bottom loss curves and their variance vs. grazing angle, frequency, and loss class used in the present prediction model are given in Figure 65.

(S) In the detection of submerged submarines the radiation of sound from a source within a few hundred feet of the surface is of prime concern. Figures 74 and 76 present a sampling of sound rays emitted from the source at equal angular intervals. They illustrate propagation in Mediterranean winter from a source 300 feet deep. Bearing in mind that the separation of neighboring sound rays is approximately inversely proportional to the intensity, many regions of great intensification can be seen. The most intense sound occurs in regions where the crossing rays form long smooth curves called caustics. It is useful to imagine a sensor such as an array towed at, say 1000 feet. The transmission loss along this line, computed from ray theory, is given in Figure 72. The sharpness of the peak of intensity at the caustic is striking. It can be observed in the ocean under the right conditions. However, as will be discussed below, there are several other influences that also produce intensity peaks and still others that tend to blunt the sharp caustics illustrated here. Nevertheless, if a choice is presented, it is always best to place the array where the maximum number of caustics will be encountered. Transmission loss will be least in such regions.

(U) As the seasons progress from winter to summer, the surface waters of the Mediterranean are heated producing a layer of warm water (high sound speed) near the surface below which both temperature and sound speed decrease to a depth of about 300 feet. Below 300 feet the temperature is relatively constant so that sound velocity increases with depth in response to increasing pressure.

Such a sound velocity structure is called a sound channel and its depth of minimum velocity is called the sound channel axis. A typical vertical profiles is shown in Figure A-8.

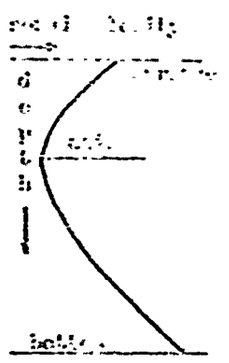

Figure A-8. Velocity Profile Showing Sound Channel. (U)

(U) The differences between these winter and summer profiles are illustrated in Figure 67-72.

CONVERGENCE ZONES

(U) In sound channels the sound is refracted toward the region of minimum sound speed. Figure A-9 shows regions of high intensity. These are called convergence zones and occur approximately every 12-20 miles in the Mediterranean Sea

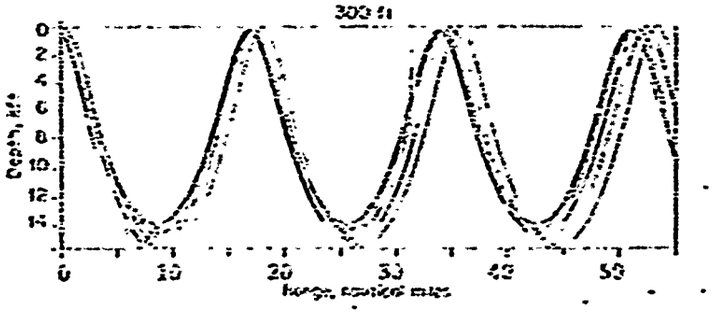

Figure A-9. Convergence Zones

if sufficient depth of water exists. The occurrence of convergence zones in different seasons is shown in Figures 67 through 70. The sound intensity may be increased by a factor as much as ten to a hundred in such zones. In any case, they are zones of marked intensification and are well worth using in any detection system.

(U) One more important feature of sound refraction in the ocean is the limitation on the horizontal range that can be covered by a single bottom reflection. Paths having a large grazing angle strike the bottom and return to the surface at comparatively short range. As the path becomes less steep, a point is reached where rays recurve before they strike bottom. A single bottom reflected ray from this source can extend no farther than the ray which is tangent to, but just misses striking the bottom at the point of reflection. Similarly, if two bottom bounces are considered, then the effective range will be approximately doubled and so on.

(S) Deepwater sound velocity data used in computation of convergence zones were obtained from unpublished data on file at the Oceanographic Office and National Oceanographic Data Center. The sound velocity profiles selected were considered to be the most representative deep profiles available for each one-degree quadrangle in each season. Where the sonic structure was not uniform in a quadrangle, two or more profiles were selected. Velocity gradients below the sound channel axis were calculated for the profiles by ten-degree quadrangles for each season. However, near Gibraltar the gradients were so variable that they were calculated for each profile. The average depth was calculated for one-degree quadrangles. Ranges were computed by using pertinent sound velocity and depth data. Basic assumptions were that a flat bottom extended between the source and the receiver and that there was no appreciable horizontal variation of sound velocity. Convergence zone calculations could not be made for fall because of insufficient data. Convergence zone transmission generally does not occur in winter.

(S) Ranges to the inner margin of the zone of convergence in spring (Figure 59) vary from less than 10 kiloyards southwest of Greece to more than 35 kiloyards east of the Balearic Islands. In summer (Figure 62), these ranges vary between 30 and 45 kiloyards throughout most of the Mediterranean. These differences are accounted for by the pronounced negative, near-surface gradients which produce extreme refraction of the ray paths in the upper layers.

(U) The degree of certainty of occurrence of convergence zone transmission is very much dependent on depth excess. The depth excess is the difference between the bottom depth and the depth where the near-surface maximum velocity reappears below the sound channel axis. The greater the depth excess, the greater is the probability of convergence zone formation.

(S) One method of estimating the probability of convergence zone formation indicates that if a depth excess variability of 300 fathoms is assumed, then an average depth excess of greater than 600 fathoms results in a probability of convergence zone occurrence of greater than 95 percent and assures reliable transmission. Where the average depth excess is between 480 and 600 fathoms, the probability of occurrence is between 75 and 95 percent and this transmission mode is likely. Convergence zone transmission is marginal where the average depth excess is less than 480 fathoms, and the probability of occurrence is less than 75 percent.

(S) The surface insonification intervals represent the difference between the range to the convergence zone and the range of the ray which just grazed the bottom and returns to the surface. The surface insonification interval is substantially wider in spring than in summer. A result of the increased surface heating in summer produces the longer range to the convergence zone and thereby reduces the insonified interval. In spring the interval varies from less than 5 kiloyards to greater than 40 kiloyards, and in summer the interval varies from less than 5 kiloyards to more than 15 kiloyards.

(S) In the Mediterranean as elsewhere in the oceans, the top few tens of a hundred feet may be mixed to a uniform temperature. Sound from a source within such a layer is transmitted by recurving at depth and reflecting from the surface. This layer is called either the surface mixed layer or the isothermal layer. It is a sound channel and can be an efficient sound duct for frequencies whose wave length is a small fraction of the thickness of the layer. In the Mediterranean, this layer is 10 to 60 feet thick in summer. Most frequencies employed in long range detection leak rapidly out of this surface duct and it is of little use for towed arrays in the Mediterranean.

(U) In summary, the sound will either reflect from the surface or bottom, or it may be refracted prior to striking either interface.

(S) The total sound intensity received by an omnidirectional sensor is the sum of all the paths that reach the sensor. A prediction model must account for them all. The various paths are:

1. Direct (very short distances only).

2. Bottom reflected by one or more bottom bounces, but including all combinations of surface and bottom reflection. It turns out that reliable predictions are not achieved with less than 7 or 8 bottom reflections per 100 miles, and more may be required.

3. Surface duct. Contributes little to long range detection (over 100 miles).

4. Convergence zones. Important contributor, especially in the Mediterranean.

5. Deep sound channel paths, reflecting neither from surface nor bottom. The receiver and source must both be within the sound channel for use of these paths.

6. In winter, paths 3, 4 and 5 are replaced by the half channel whose axis is at the surface over much of the Mediterranean (Figure A-6). Convergence zones are rarely individually identifiable, but caustics of the winter half channel provide zones of intensification.

(S) The prediction model now in operation at the Fleet Numerical Weather Central, Monterey, California traces the necessary rays for each type of path and computes the corresponding intensities from the spacing of the rays. Bottom reflection takes place from a model bottom that approximates the known bathymetric profile. The model responds to horizontal changes in the vertical sound speed structure of the water. When all the individual path intensities have been computed, the computer identifies all the paths that are superimposed along the transmission track at the depth assumed for the array. The corresponding intensities are added together for points every half mile along the track to the limit of the computation, thus providing a complete prediction of transmission loss along the chosen track and depth. Bottom reflections and convergence zones from a shallow source at short range can be recognized by their shape as is shown in Figure A-10.

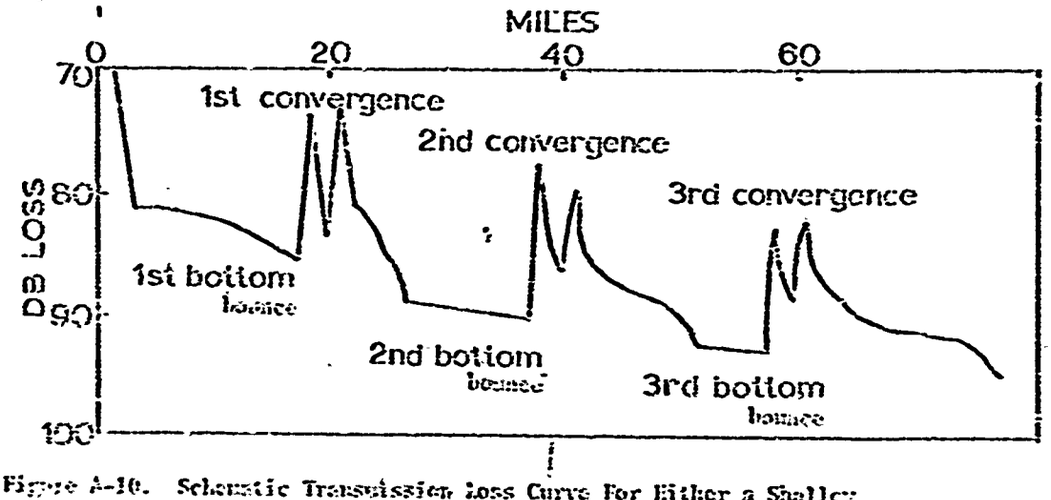

Figure A-10. Schematic Transmission Loss Curve For Either a Shallow Source or a Shallow Receiver. (U)

(S) When the first convergence zone is entered, a sharp increase in intensity occurs followed by a gradual decrease and then a sudden drop at the edge of the first zone is left. Then for an interval, the second bottom reflection dominates until the second convergence zone is entered, and so on as suggested in Figure A-10. The successive convergence zones broaden in proportion to their ordinal number until they overlap. At greater ranges, the leading edge of the convergence zone (which generally consists of two or more peaks) rises above the general level. When the source lies well within the sound channel and the receiver is not at very shallow depth, these features just described are not obvious and the prediction curve, though it may be jagged, cannot readily be analyzed into individual types of path.

TRANSMISSION LOSS

(S) Figures 67 to 72 are a set of predictions representing loss at 60 and 300 Hz to be anticipated for various source/receiver combinations in summer and in winter in the Balearic Basin, in the Ionian Sea and in the Levantine Basin. The path structure for many of the curves can be identified by comparison with Figure A-10. A class 3 bottom was assumed as the best single designator of bottom reflectivity for all three areas. This assumption is pessimistic for the Balearic Sea where the basin floor is smooth and an excellent reflector. The Ionian and Levantine regions have a generally rough floor, but with some smooth areas.

(S) The quality of these predictions has been tested by comparing them with two series of transmission measurements derived from explosive sound sources in the Balearic and Ionian Seas (Figure 75). The comparisons are not exact because the measurements were made in 1/3 octave bands at 55, 100 and 200 Hz whereas the predictions were made for 60 and 300 Hz. Nevertheless, the differences

associated with such frequencies are generally small except where the duct transmission is reflected by the bottom. The method of measurement has been thoroughly tested. The observed points are compared (Figure 73) with the nearest available combination of frequency and source and receiver depths. The measured levels lie within 2 or 3 dB (and commonly less) of the prediction curve except at short ranges. There, the measured levels are higher than the predicted ones by different amounts up to 5 or 6 dB. This discrepancy may be due in part to the choice of bottom class 5 instead of class 1. The observed values also show less variation between peaks and dips than do the predictions. These discrepancies are probably due to known deficiencies of the ray model such as failure to account for sound scattering or diffraction. While not an exhaustive test of the model, the measurements suggest it is valid to within a few dB in average level and that it successfully predicts the level of the peaks.

(S) For reasons to be explained later, it is recommended that for best detection, towed arrays be maintained near the central and deepest parts of the basins. The predictions of Figure 67 to 72 were made for such locations and are not designed for use elsewhere, for example, over shallow slopes or in the several gradually shoaling trenches leading into the basins.

(S) Figure 77 presents the peak levels (minimum transmission loss) for 69 ft at a range of 200 miles for all the predictions of Figure 67 to 72. Similarly, Figure 77 presents the arithmetic mean of the greatest and least transmission loss near 200 miles. In the absence of extensive transmission data for the Mediterranean, the assumption is made that average levels will approximate those of Figure 77 but that peaks as high as those of Figure 67-72 will be observed. The latter assumption is the weaker. From the average transmission loss of Figure 77, the source at 69 ft. depth is seen to have generally higher losses by about 4 to 7 dB than the 500 foot source except for a shallow (90 foot) sensor in summer (or for any sensor depth in the winter). The results for any

source deeper than about 200 feet should be similar to the loss at 500 feet. This prediction agrees with comparisons between 60 feet and 500 feet shots made by [illegible] (1968). The transmission loss vs. depth data for all areas suggest that there is no significant advantage in towing deeper than 700 feet for detecting any target 500 feet deep or shallower. There is some possibility, as yet untested, that an array towed at 4000 to 4500 feet might do well against a shallow target. For periscope depth targets, there appears to be a distinct advantage to towing at 90 feet or less, but the penalty against deep target detection in so doing amounts to 6 to 8 dB.

(S) The prediction model has not been tested enough to permit reliance on some of the finer distinctions apparent on these graphs. It is suggested that experiments with different depths be referred to repeated tests at 500 feet.

GEOGRAPHIC CONSIDERATIONS

(S) The entire transmission loss discussion thus far has assumed a bottom having the same average depth along the transmission track. The Mediterranean Sea consists of several basins with sides of varying steepness. They are separated by ridges or extensive and complicated shallow water areas such as the Strait of Sicily. Very few transmission loss measurements have been made across these boundaries and very few have been made across the sloping sides. Prediction models for such areas are available but they have not been tested. Nevertheless, it is known that sound levels are not heavily attenuated on transmission over a slope until the water depth is within 200 to 400 feet of the bottom of the sound channel. This is a serious problem in the Mediterranean only when the axis of the channel is below the surface, or largely during the warm half of the year. This condition is depicted in Figures 54-57. Within the area designated as not bottom limited, the predictions of Figures 67 to 68 apply. During the winter, the predictions apply in water deeper than about 300 to 500 fathoms and may be a reliable guide in 200 fathoms of water.

(S) Several long narrow embayments such as the gulf between Barcelona and the Balearic Islands should probably stay from the deep basin. Sound from a shallow target is transmitted better downslope than upslope. Therefore, the proper position for the array for best surveillance is near the center of the embayment, preferably also near the deeper end. Some experimentation with this possibility is indicated.

(U) Predictions of transmission loss in the deep basins of the Mediterranean Sea (except the Tyrhenian Sea) have been furnished. Charts showing where the predictions apply in summer and winter are given in Figure 77.

(S) The average transmission loss increases 3 dB for each doubling of the range beyond about 50 miles. For periscope depth targets, transmission loss is higher by 4 to 7 dB than for deeper targets. These losses are highest in summer and in the eastern Mediterranean. They amount to 92 to 96 dB at 200 miles for 60 Hz. In winter, the transmission loss for the target at 60 foot depths does not exceed 92 dB and may be considerably less at 200 miles.

(S) Transmission losses for targets at depths between 200 and 500 feet probably will not exceed 90 dB at 200 miles in any seasons with proper array depth. Usually losses at this range for such targets will not exceed 88 dB at 60 Hz.

(S) The basis for interpretation is provided by comparison of some of the predictions with measurements made under somewhat similar conditions. Agreement is within 3 to 5 dB or better with the predictions having higher loss except where the agreement is within 0 to 2 dB.

(S) A practice of towing the array at 300 feet is recommended, with an aggressive campaign to compare these results with both shallower and deeper tow depths. Their choice should depend on sonar conditions and knowledge of target depth. It is always an acoustic advantage to tow at the depth of the target even though this practice may not be desirable for reasons of safety. It appears that there is little advantage in towing at great depth, with the

exception that depths of about 4600 to 4800 feet may be advantageous against a periscope depth target.

AMBIENT NOISE

(U) Ambient noise in the ocean is the sum of sounds from shipping, weather-induced wave noises, mostly the noise of breaking waves, rain or hail on the water, seismic disturbances, animal sounds, industrial noise and others. The sources are listed here in rough order of dominance in general. At any particular place and time, any of the later items on the list may dominate altogether. Wenz (1962) has summarized the effects due to shipping and weather in Figure A-11.

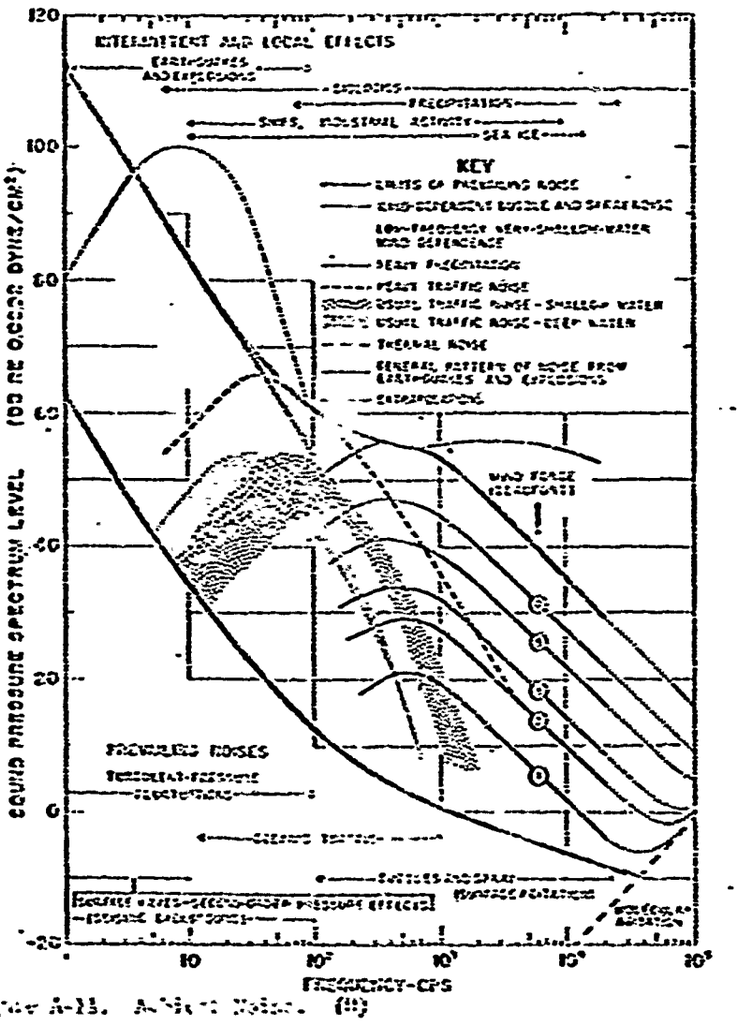

Figure A-11. Ambient Noise. (U)

(S) These are based on measurements in the ocean. Probably, the weather induced noise at the higher frequencies of Figure A-11 are applicable to the Mediterranean. At frequencies below about 500 Hz reliance should be placed on measurements in the Mediterranean itself. Unfortunately, there is little data concerning the Mediterranean. An analysis has been made of traffic noise through Gibraltar. In 1968, scientists from Hudson Laboratories and the Woods Hole Oceanographic Institution made three independent sets of measurements in the Balearic, Tyrhennian, Ionian and Levantine Seas. The most extensive set, made by Arase and Arase, has been reported and its results are summarized in Figure 78. The Woods Hole Oceanographic Institution measurements corroborate the Arases' work. Despite the considerable flurry of recent work, we remain rather ignorant about noise conditions in the Mediterranean Sea. It is important that every reasonable opportunity be taken to measure ambient noise by means of the towed array. For example, nothing is known either of azimuthal distribution of noise nor whether there are depth dependent effects. Both can be measured by means of towed arrays.

(S) Experience with other low frequency detection systems in the Atlantic and Pacific Oceans shows that the spectrum level of noise at 100 Hz is -15 to -20 dB in a rather noisy location; -25 dB is representative of locations within 100 miles or so of shipping lanes; -27 to -29 dB is observed at locations well removed from shipping but capable of detecting distant shipping and -31 to -35 dB has been observed in truly remote ocean areas. Thus, it is plain that the Mediterranean is an especially noisy place since levels of -15 dB are common and 0 dB are observed. However, it is also true that levels as low as -20 dB or lower often prevail. At this writing, too little is known of ambient noise in the Mediterranean to do more than speculate.

(S) In experimental operations, the level of noise at the array should be measured virtually constantly, and steps should be taken to determine whether

(S) In [illegible], the level of noise at the array should be measured directly or [illegible] should be taken to determine whether the noise is caused by [illegible] ships, flow noise, or is the ambient noise of the sea. Attempts should be made to correlate ambient noise with local shipping. In addition to constant monitoring, procedures should be adopted for running quietly at frequent intervals so as to measure ambient noise. It may be possible to identify relatively quiet areas which still permit broad surveillance coverage. It seems unlikely that there will be large differences in noise at different depths of array, but this possibility should be tested. If differences are found, then the noise advantages should be weighed against any penalties that may be incurred in transmission loss.

(S) It is suggested that the peak of the noise distribution in the appropriate basin be assumed to prevail unless a measurement is available. For example, in the Ionian Sea, the -10 dB level is the most frequently measured spectrum level at 100 Hz. Suppose that at 200 miles a detection is made 50% of the time. The loss is 92 dB (for a 60 foot target). Assume BB is 7 dB and AG is 18 dB. Then

$$SE = SL - 92 + 18 + 7 + 18$$

$$0 = SL - 64$$

$$SL = 64$$

If as suggested earlier, the various uncertainties are considered, it is plain that the target could be a noisy 75 or a very quiet 47 dB according to the estimates on page 15. If the noise has been measured, then the uncertainty is reduced by 10 dB between 65 dB and 52 dB -- i.e., to an uncertainty factor of forty. Possibly AG has been measured and is known to be 25 dB -- the source level now stands at 65 dB to 52 dB. Possibly we might know enough about transmission to reduce the uncertainty in the average transmission loss to ±1 dB making the source level 65 dB to 54 dB, or a factor of eight. How well is BB known? How variable is that target likely to be? How did we know the target was at 200 miles? Or at periscope depth? Good luck.

REFERENCES

The information and most of the charts contained in this atlas were taken, in some cases with little or no modification, from the following sources:

Arase, E. M. and T.: Ambient Noise in the Mediterranean Sea, Hudson Laboratories, Columbia University, 1968. (CONFIDENTIAL)
Figure 78.

Brockhurst, R. R.: Acoustic Structure of the Western Mediterranean Sea, U. S. Navy, J. Underwater Acoustics, 16:1 (1966). (CONFIDENTIAL)

Kaufman, O. and S. [illegible]: Convergence Zone Transmission in the Mediterranean and Black Seas, U. S. Naval Oceanographic Office Tech. Rept. [illegible], [illegible]. (CONFIDENTIAL)
Figures 58 through 64.

Matthews, D. J.: Tables of the Velocity of Sound in Pure Water and Sea Water for Use in Echo-Sounding and Sound-Ranging. Hydrographic Department, Admiralty, London, 1939.
Figure 2

Officer, C. B.: Introduction to the Theory of Sound Transmission with Application to the Ocean, International Series in the Earth Sciences, McGraw-Hill, New York, 1958.
Figures A-1, A-5

Swenson, R. E.: Oceanography for Long Range SONAR Systems, Part II Computer Transmission and Operational Planning, U. S. Naval Oceanographic Office Spec. Publ. SP-79, August 1966. (CONFIDENTIAL)
Figure A-5

Urick, R. J.: Principles of Underwater Sound for Engineers, McGraw-Hill, New York, 1967.
Figure A-9

Wenz, G. M.: Acoustic Ambient Noise in the Ocean: Spectra and Sources, J. Acoust. Soc. Am., 34:1936 (1962).
Figure A-11

Basic Features of the Geological Structure of the Hydrologic Regime and Biology of the Mediterranean Sea, L. M. Fomin ed., Oceanographic Commission, Academy of Sciences, USSR, Science Publishing House, Moscow, 1965.
Figures 40, 41, 42, 43, 44

Current Data Compiled by the U. S. Naval Oceanographic Office, 1969. Unpublished:
Figures 46, 48, 50, 52

Marine Geophysical Survey Program 1965-1967 North Atlantic Ocean, Norwegian Sea and Mediterranean Sea Area 6- Volume 5 Geology and Geophysics, Texas Instruments Inc., U. S. Naval Oceanographic Office Contract N62306-1687, October 1967.
Figure 3

REFERENCES (continued)

Mediterranean and Black Seas, Marine Climate and Oceanography, Section 2-Oceanography, Naval Intelligence Posty Atlantic Fleet, Part IV, 1965. (SECRET)
Figure 1 (revised by Underse Surveillance Oceanographic Center)

Mediterranean Sea Project, Propagation Loss, Fleet Numerical Weather Central, Monterey, Cal., 1969. Unpub. (CONFIDENTIAL)
Figures 65 through 72, 75 (also Hays, F. E. Woods Hole Oceanographic Institution, 1966), 74, 75, 76 and A-10

Operational Oceanography of the Western Mediterranean Sea for Submarines, U. S. Navy Hydrographic Office, Spec. Publ. SP-49, 1962. (CONFIDENTIAL)

Operational Oceanography of the Eastern Mediterranean Sea for Submarines, U. S. Naval Oceanographic Office Spec. Publ. SP-50, June 1962. (CONFIDENTIAL)

Charts from the preceding two references were combined to form Figures 4 through 38, 45, 47, 49, 51 and 53 through 56.

Sound Velocity Data Compiled by the U. S. Naval Oceanographic Office, 1969 Unpublished.
Figure 57

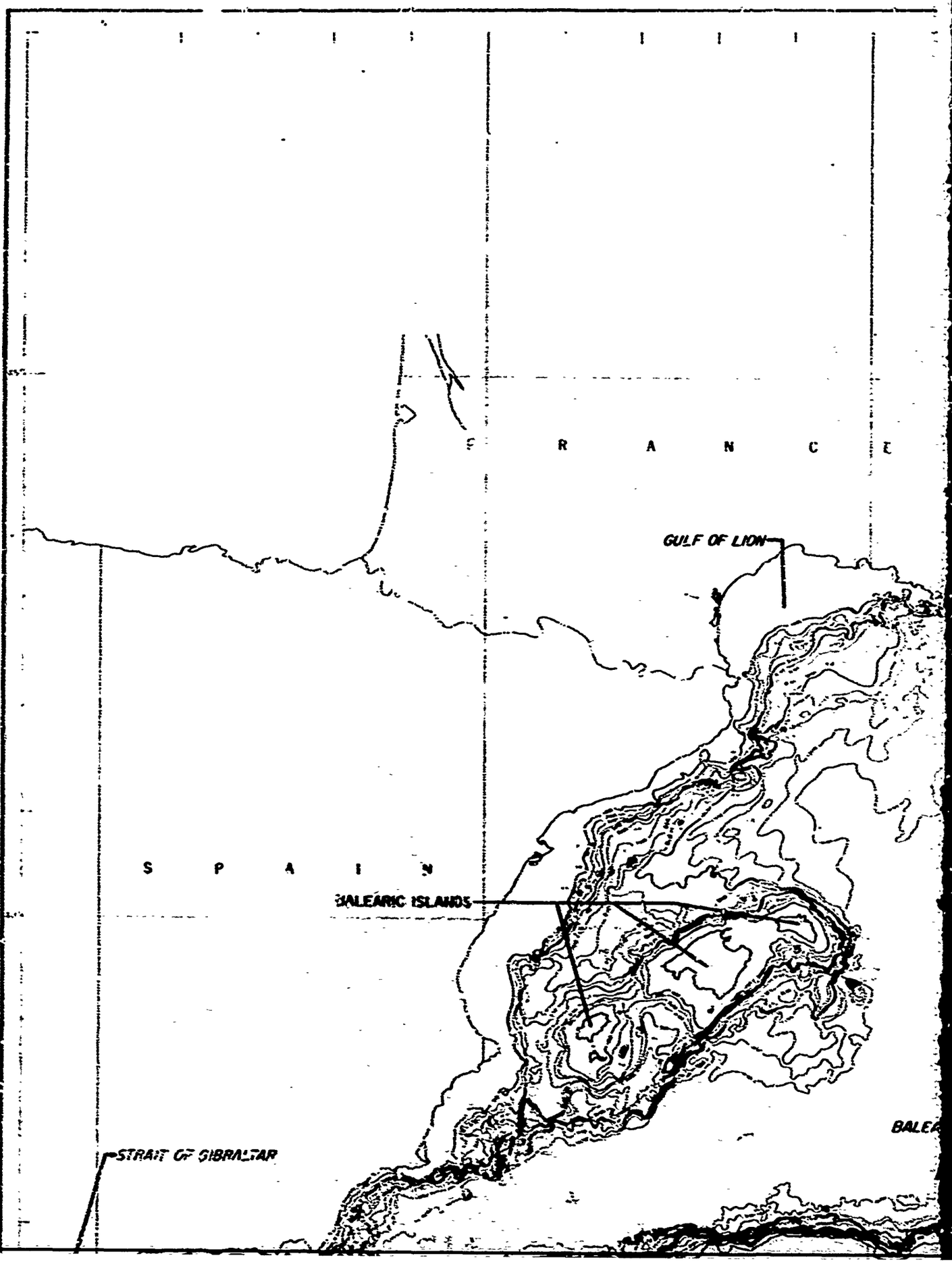
F R A N C E
GULF OF LION
S P A I N
BALEARIC ISLANDS
STRAIT OF GIBRALTAR

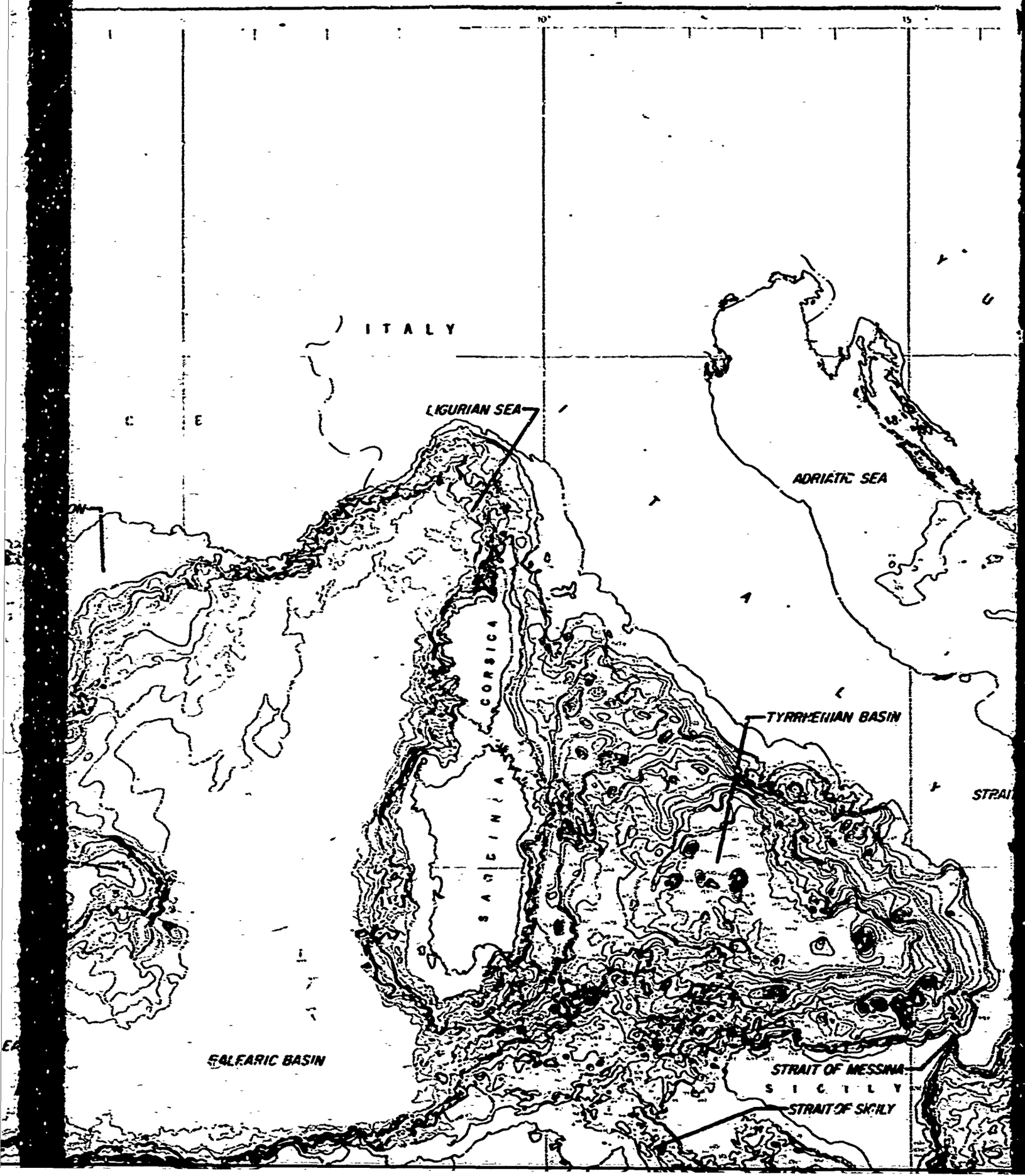
ITALY
LIGURIAN SEA
ADRIATIC SEA
CORSICA
SARDINIA
TYRRHENIAN BASIN
BALEARIC BASIN
STRAIT OF MESSINA
SICILY
STRAIT OF SICILY

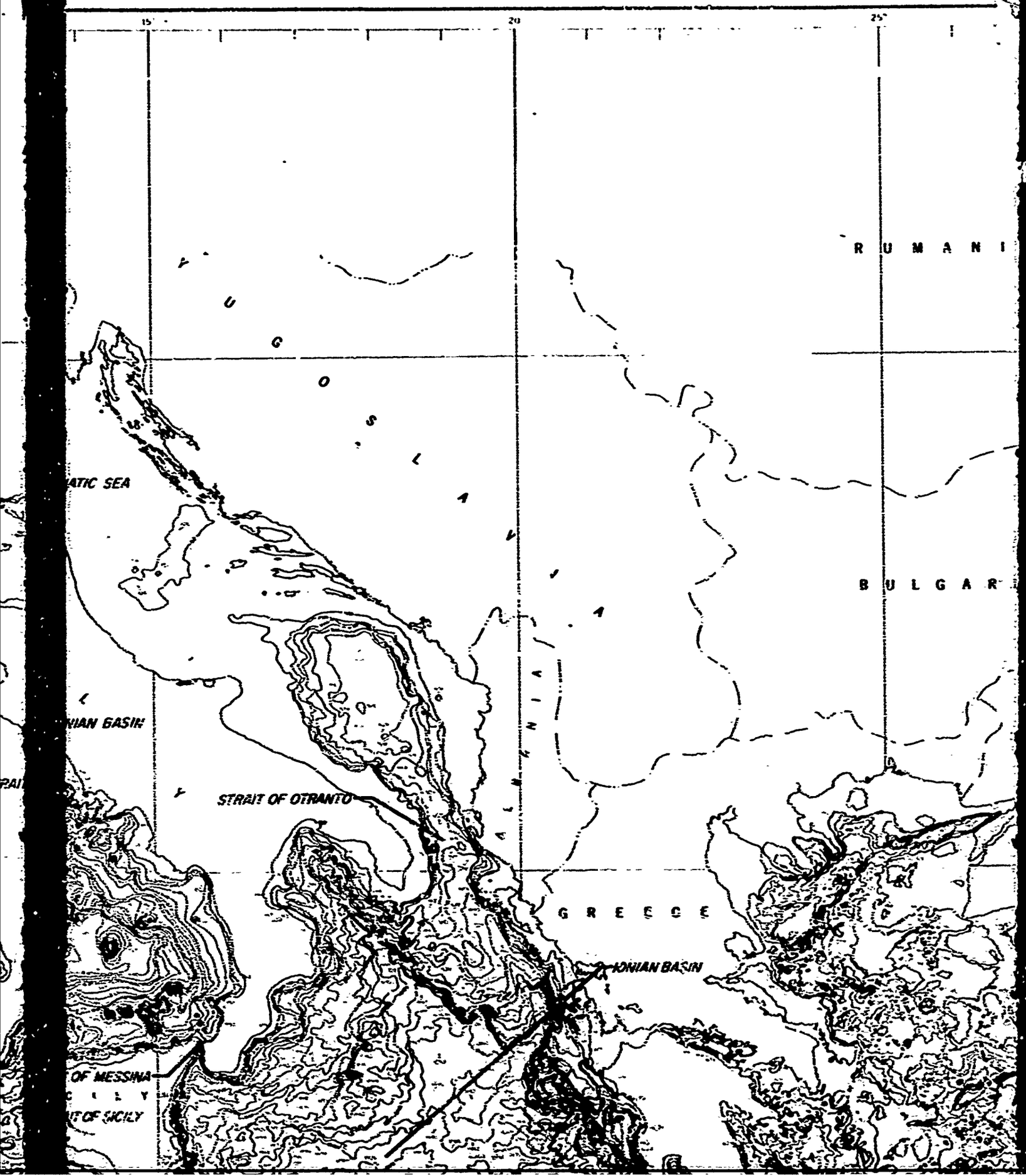
15°
20°
25°
R U M A N I
ATIC SEA
B U L G A R
IAN BASIN
STRAIT OF OTRANTO
G R E E C E
IONIAN BASIN
OF MESSINA
OF SICILY

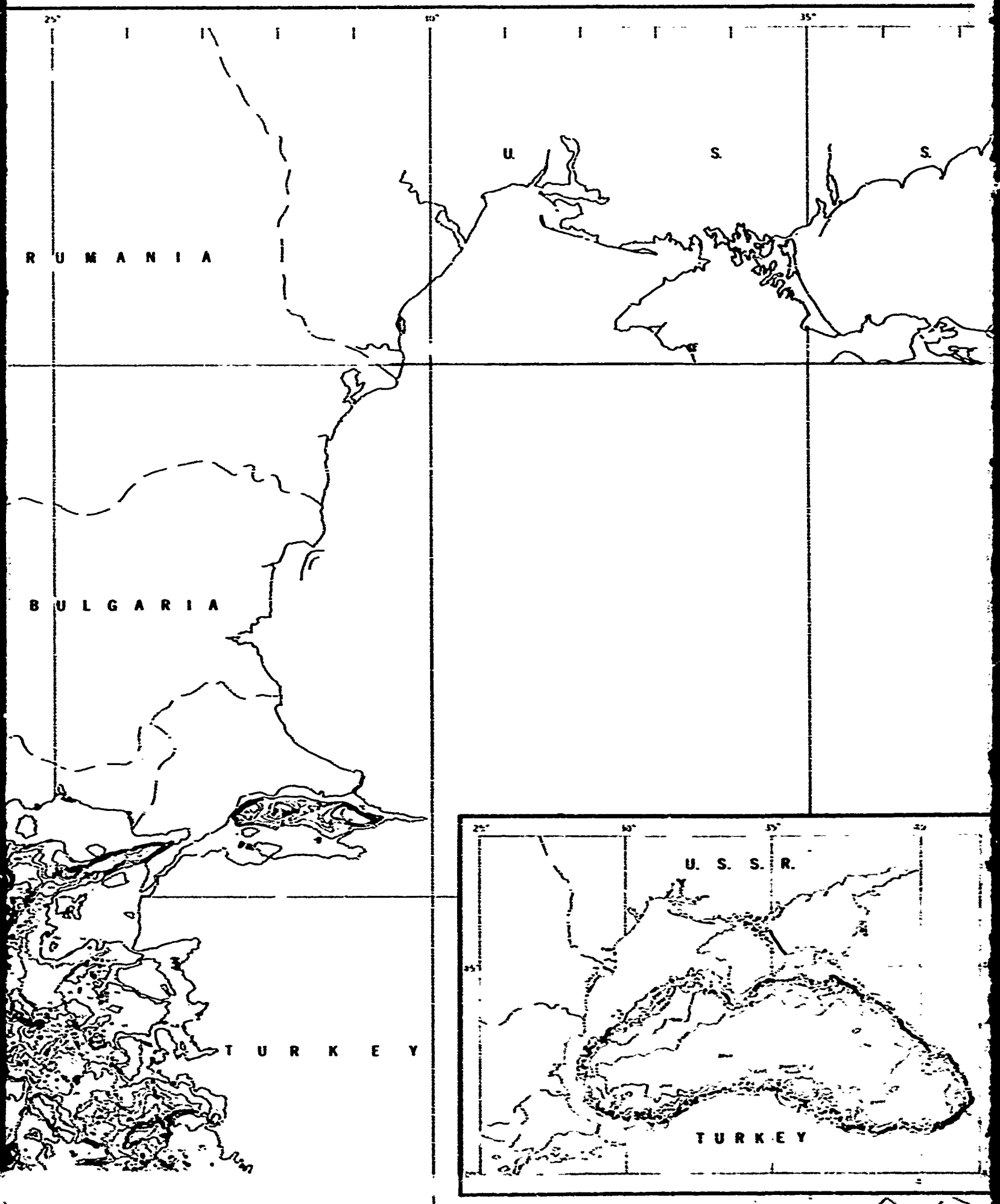

BLACK SEA BASIN

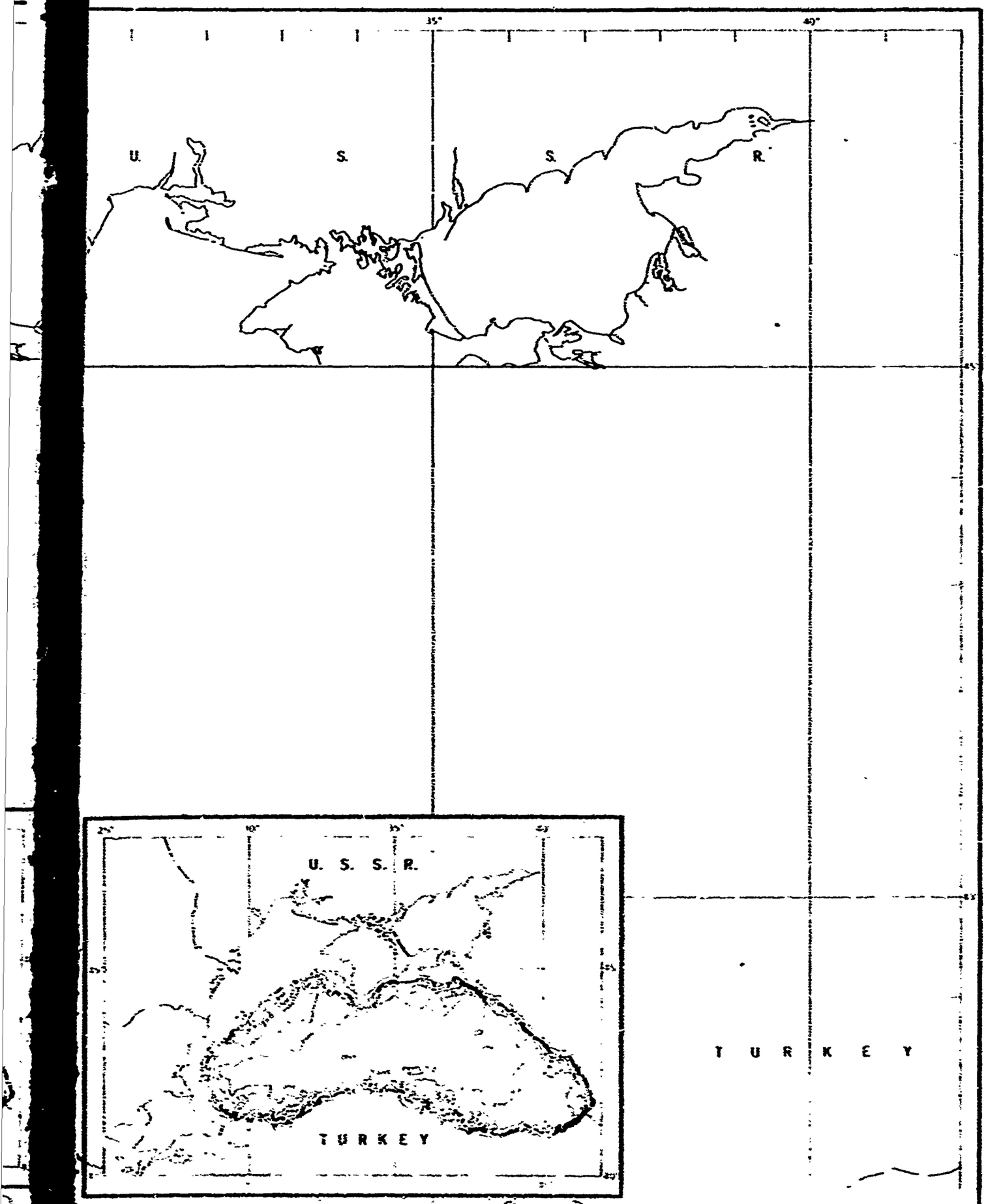
35°
40°
U.
S.
S.
R.
U. S. S. R.
TURKEY
T U R K E Y
LEVANTINE BASIN

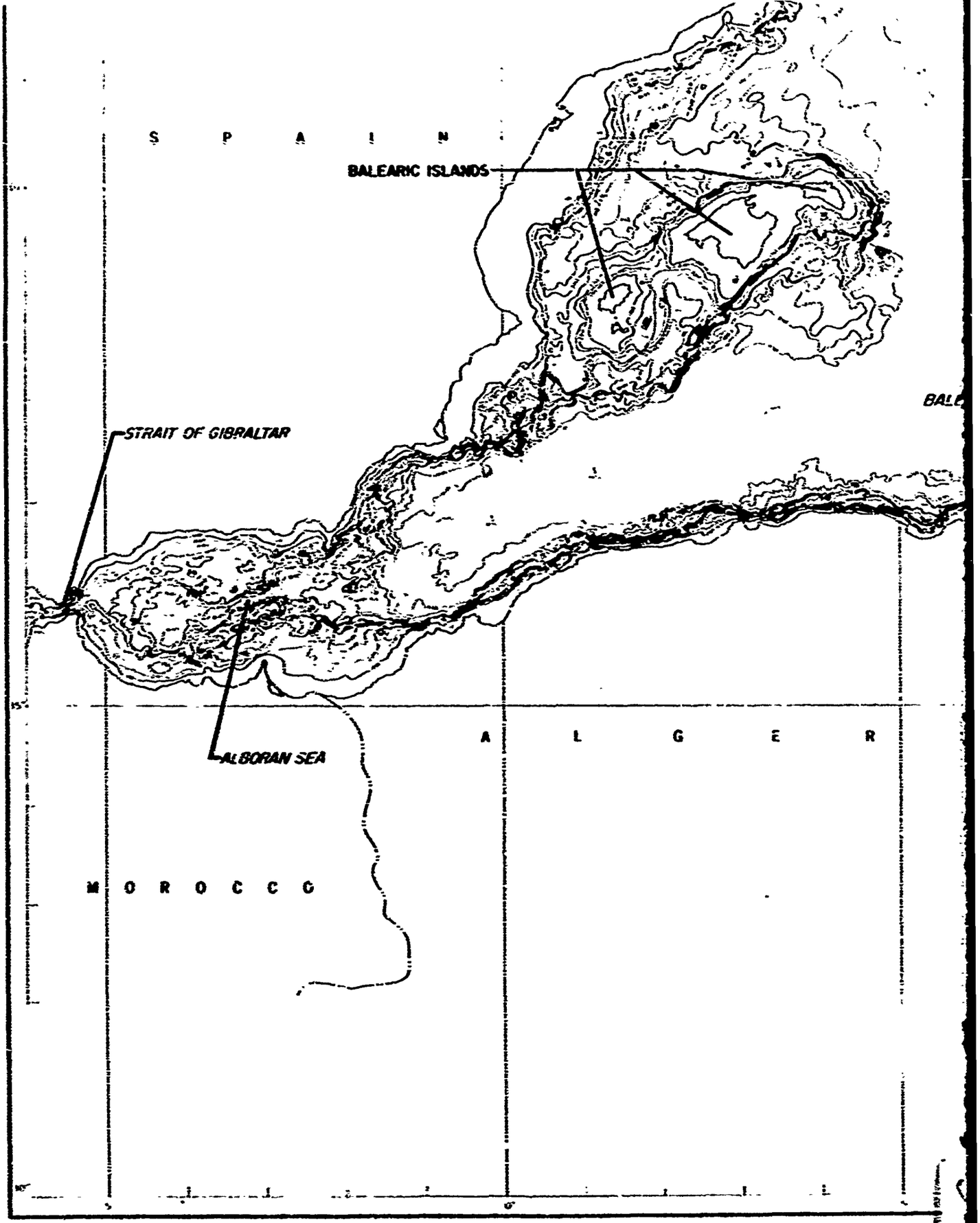
S P A I N
BALEARIC ISLANDS
STRAIT OF GIBRALTAR
ALBORAN SEA
A L G E R
M O R O C C O

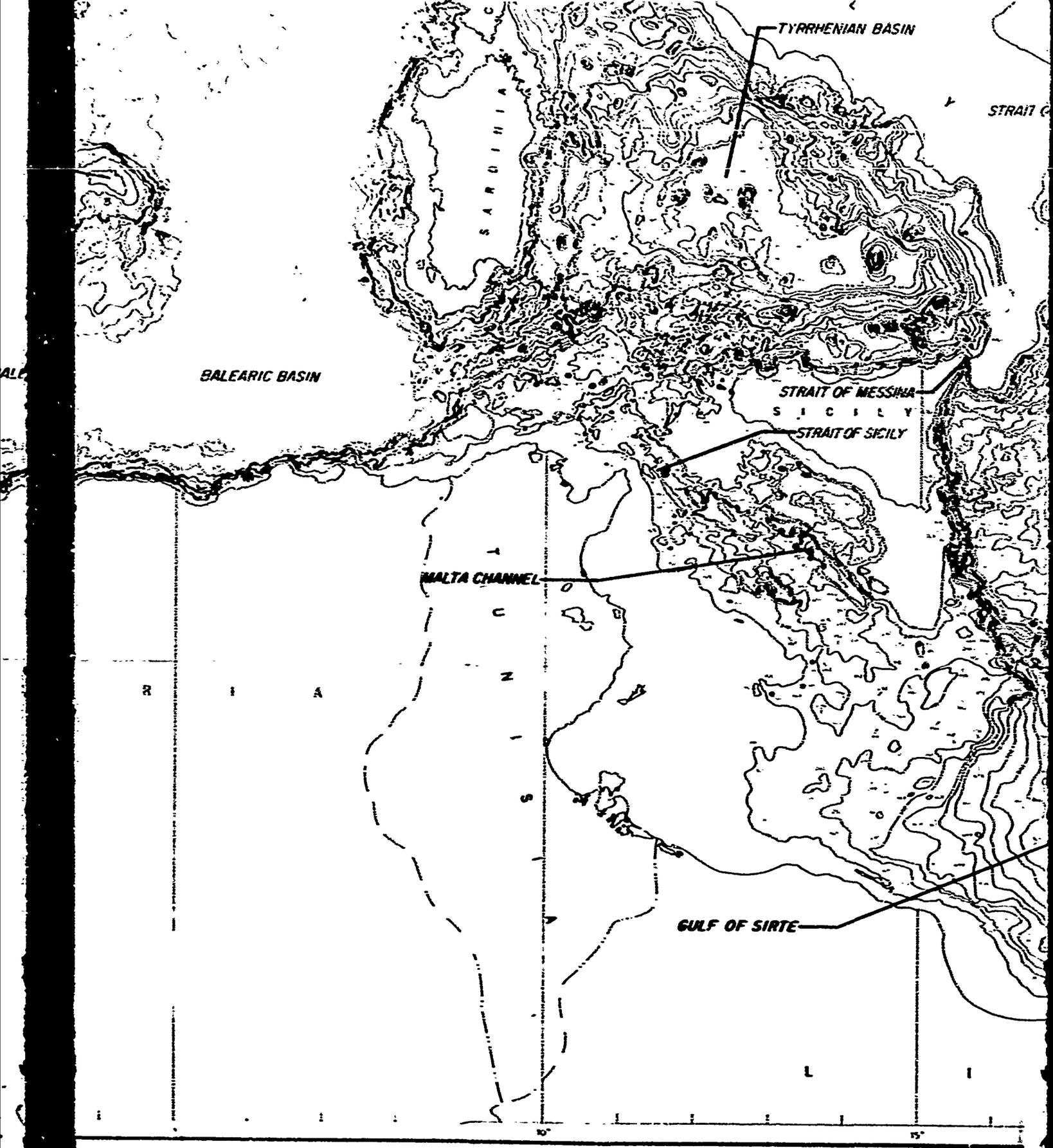

FIGURE 1 BATHYMETRY OF THE

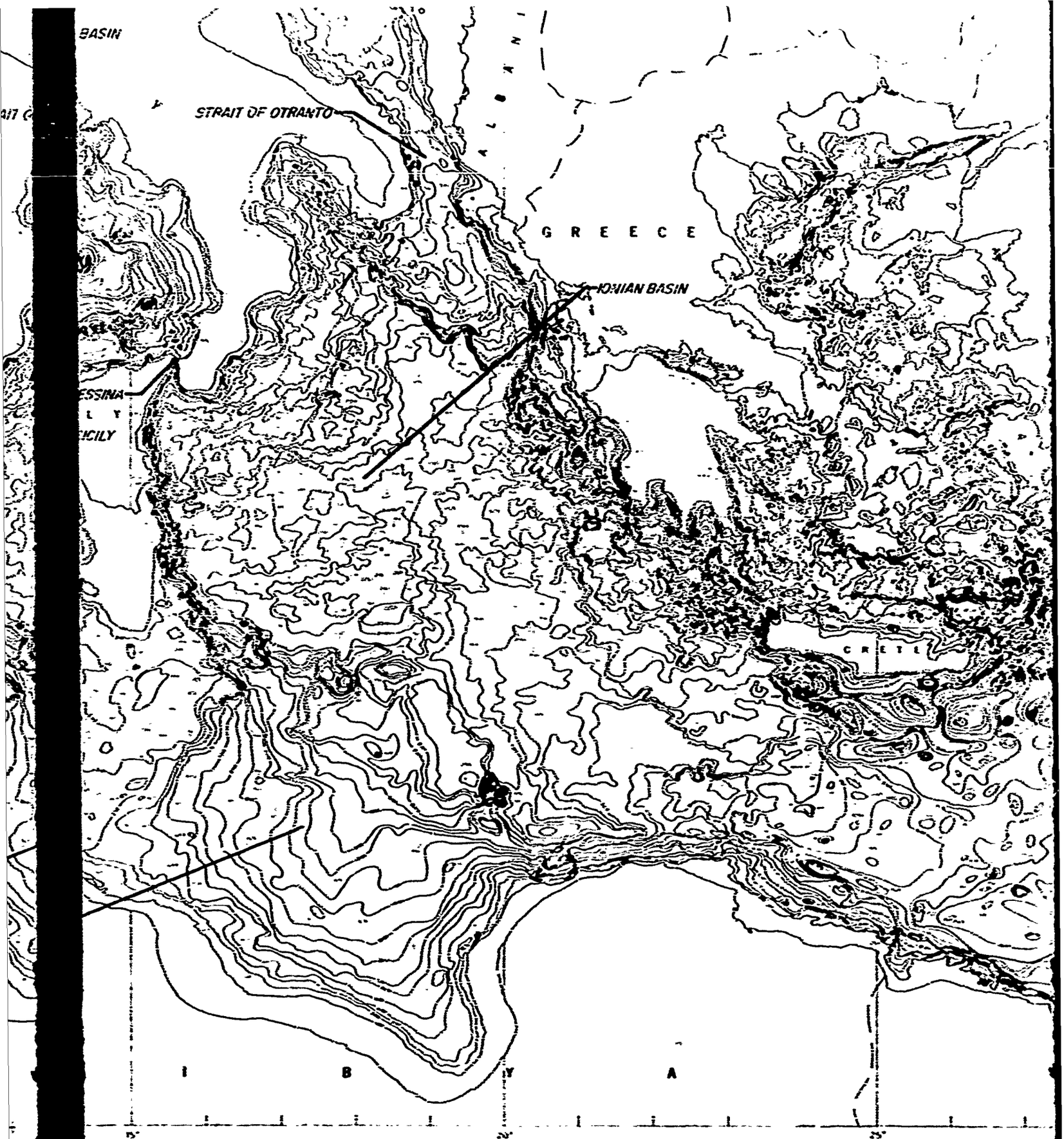

BATHYMETRY OF THE MEDITERRANEAN SEA (DEPTHS IN FATHOMS UNCORRECTED FOR VARIATION IN SOUND VELOCITY IN SEA WATER FROM 4800 FT SEC)

8

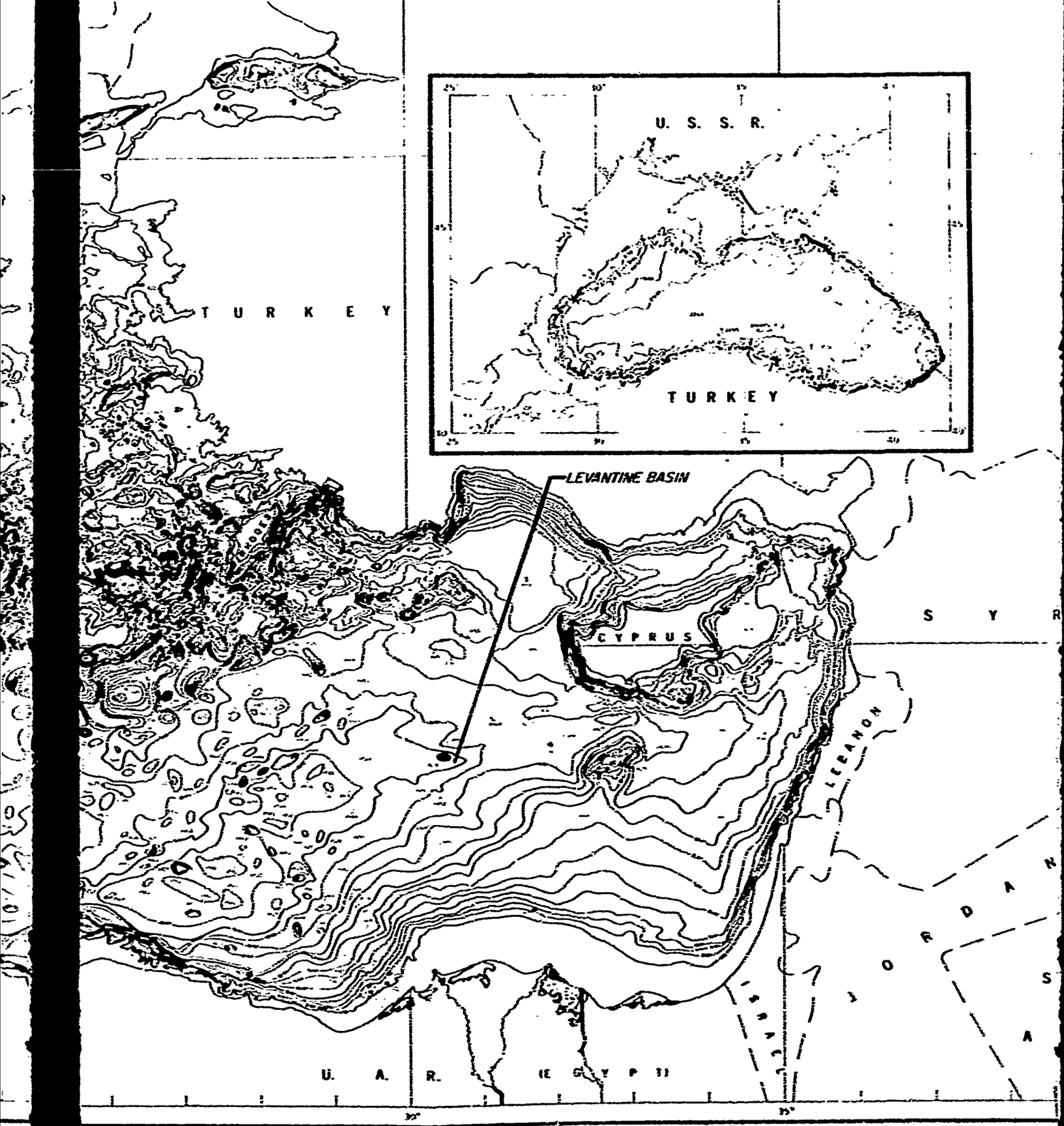
U. S. S. R.
TURKEY
TURKEY
LEVANTINE BASIN
CYPRUS
S Y R
LEBANON
J O R D A N
U. A. R.
(E G Y P T)

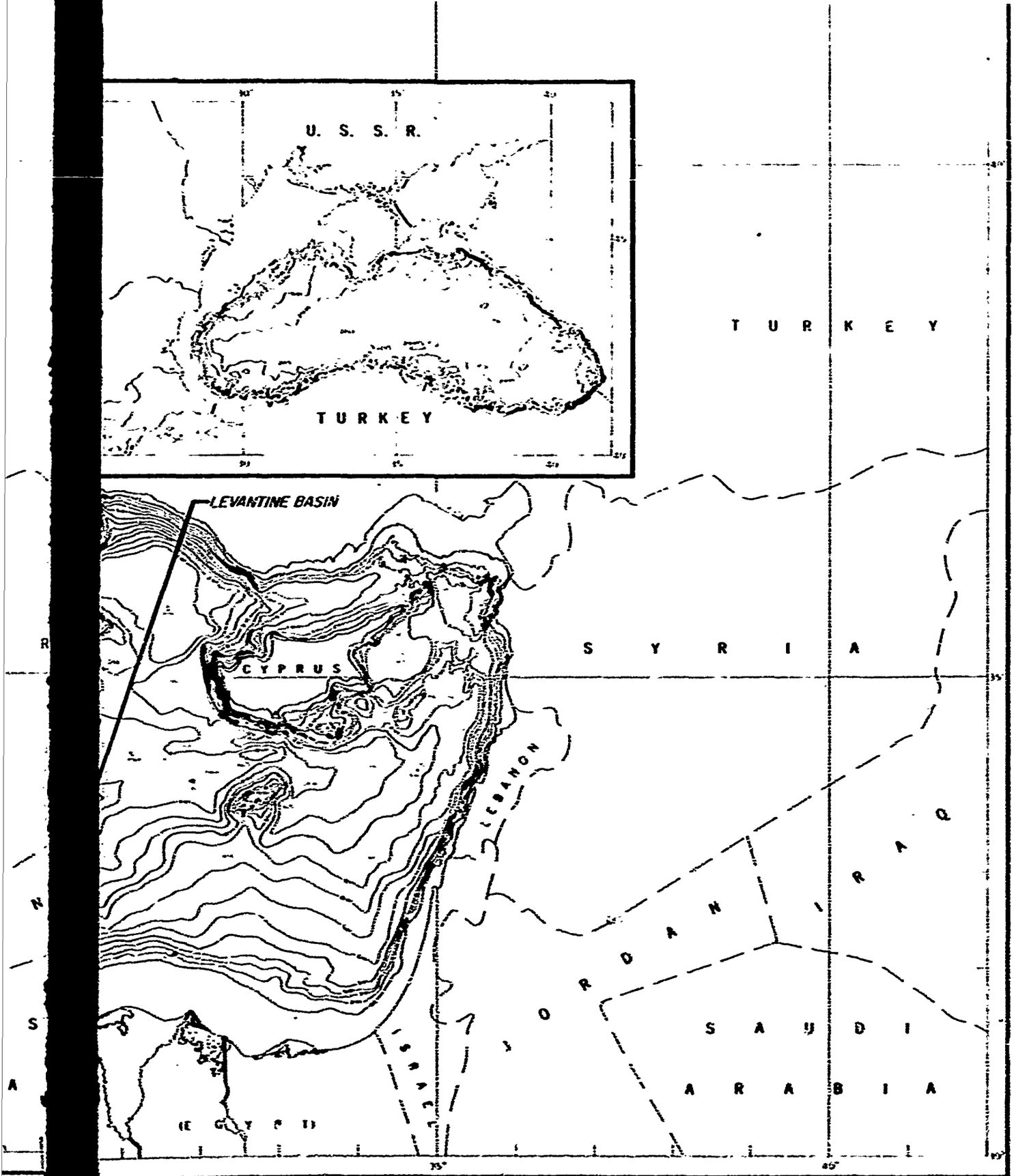
U. S. S. R.
TURKEY
LEVANTINE BASIN
CYPRUS
T U R K E Y
S Y R I A
LEBANON
I R A Q
J O R D A N
S A U D I
A R A B I A
(E G Y P T)

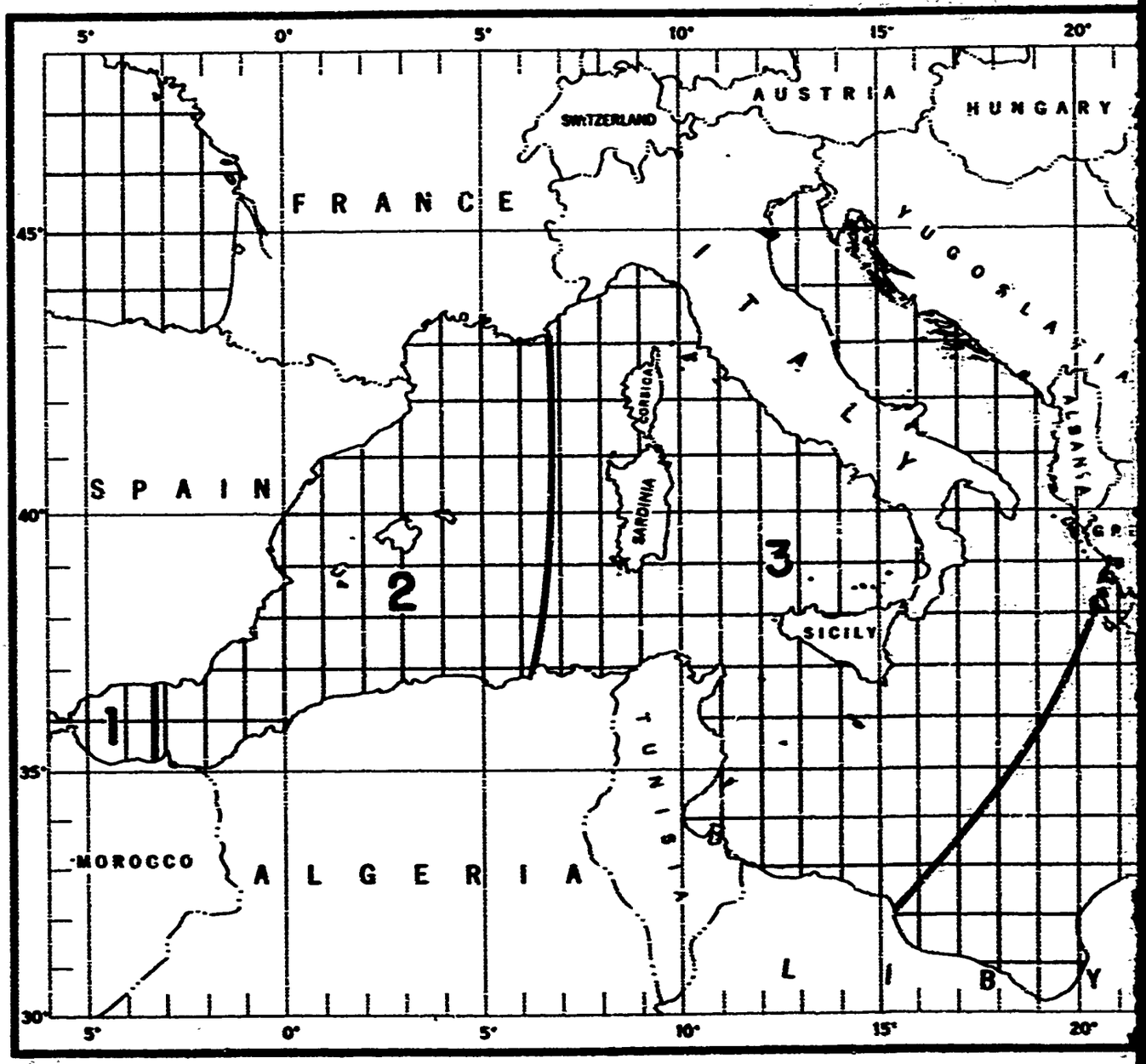

FIGURE 2. SOUND VELOCITY CORRECTIONS FOR DEPTHS

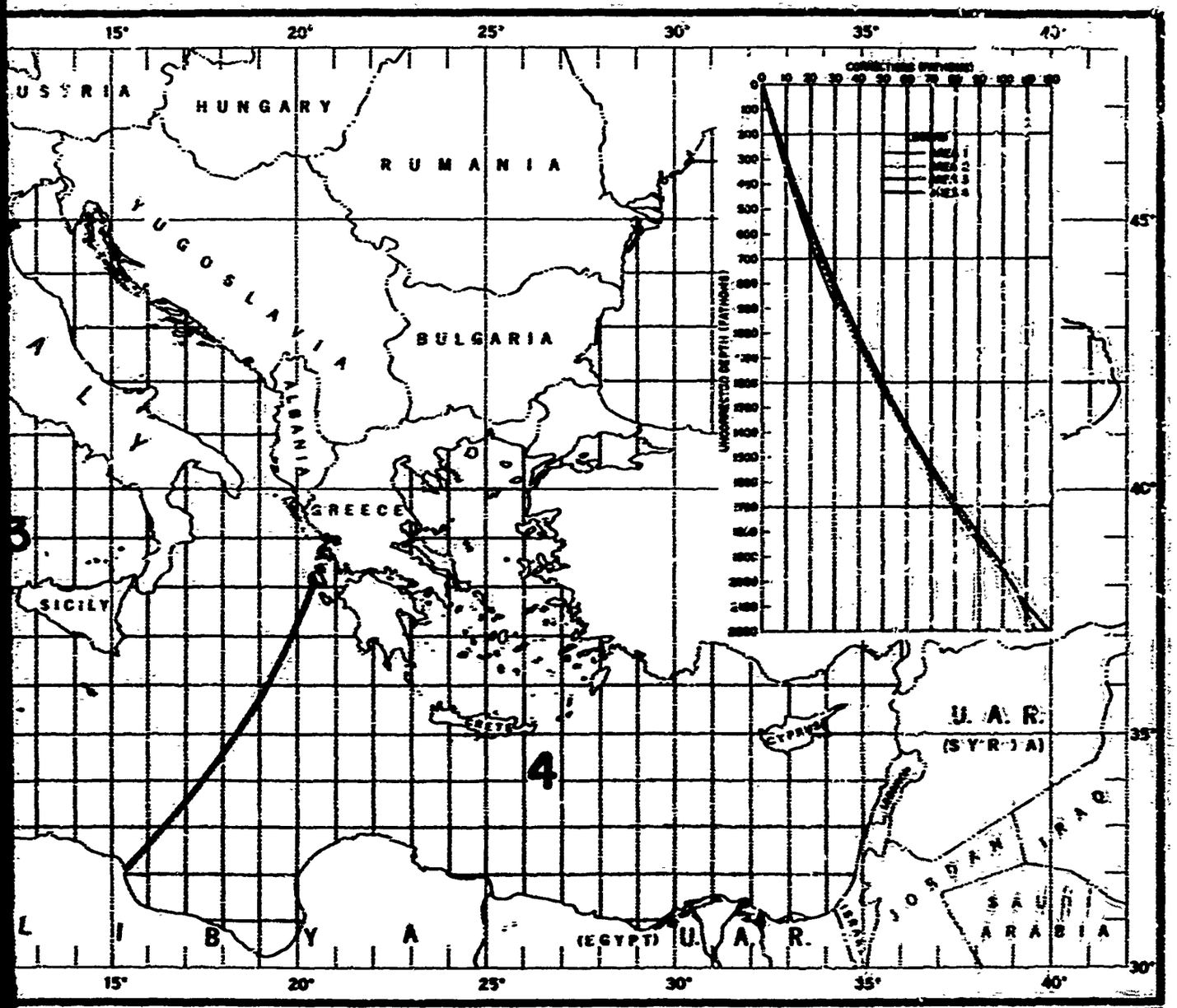

FIGURE 2. DEPTH CORRECTIONS FOR SOUND VELOCITY

. SOUND VELOCITY CORRECTIONS FOR DEPTHS SHOWN IN FIGURE 1.

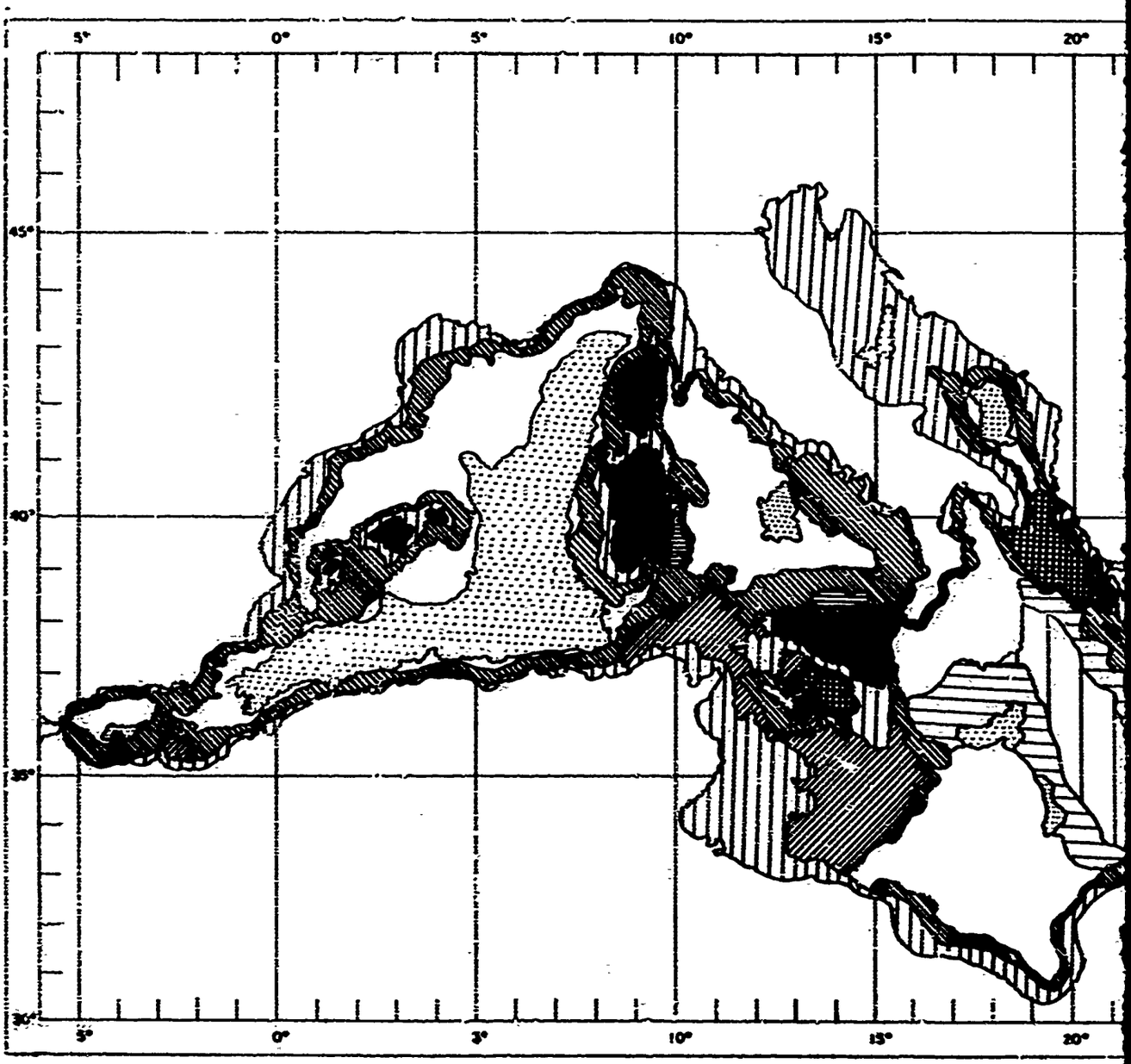

FIGURE 3. PHYSIOGRAPHIC PROVINCES OF

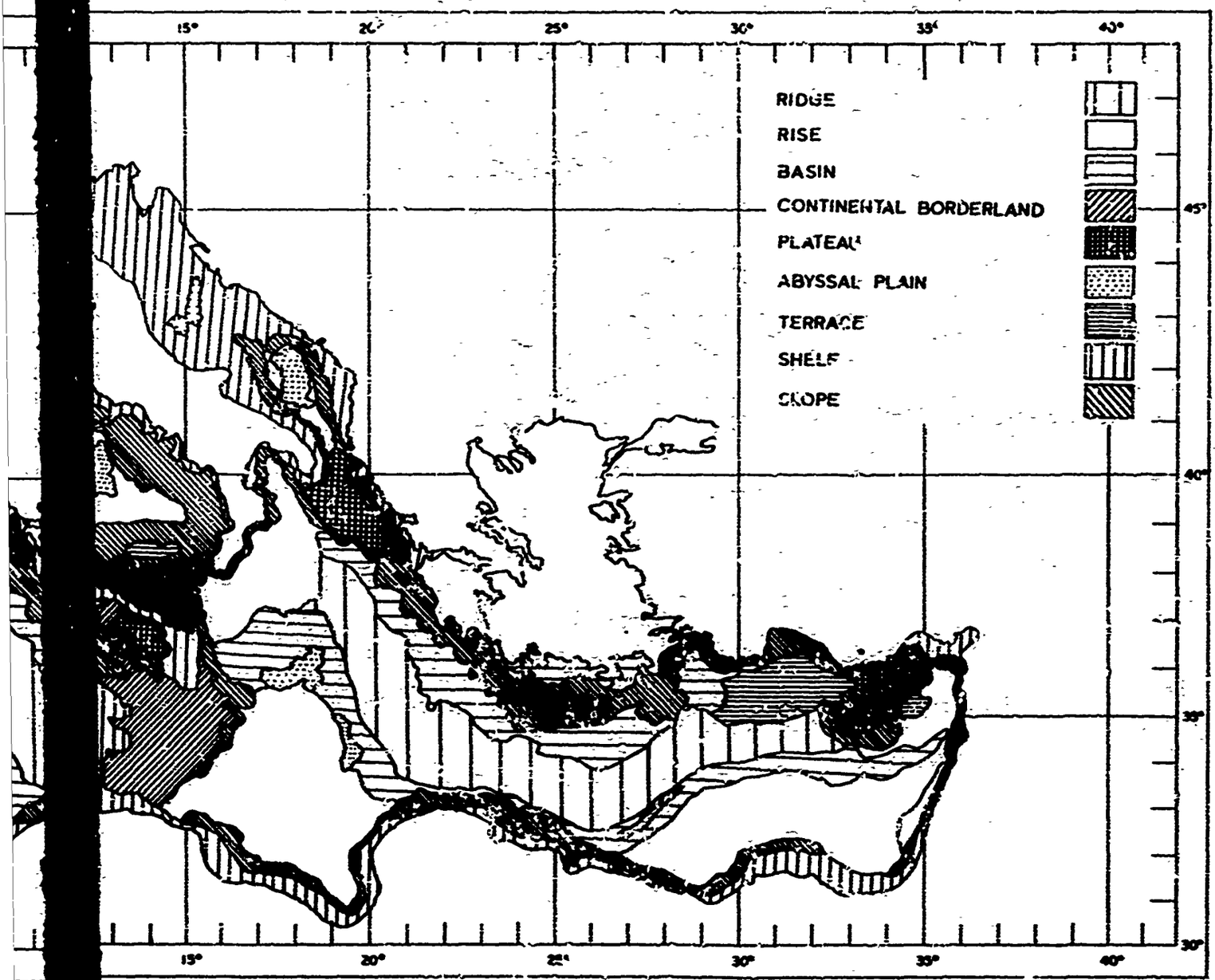

FIGURE 3. PHYSICGRAPHIC PROVINCES OF THE MEDITERRANEAN SEA

FIGURE 3. PHYSIOGRAPHIC PROVINCES

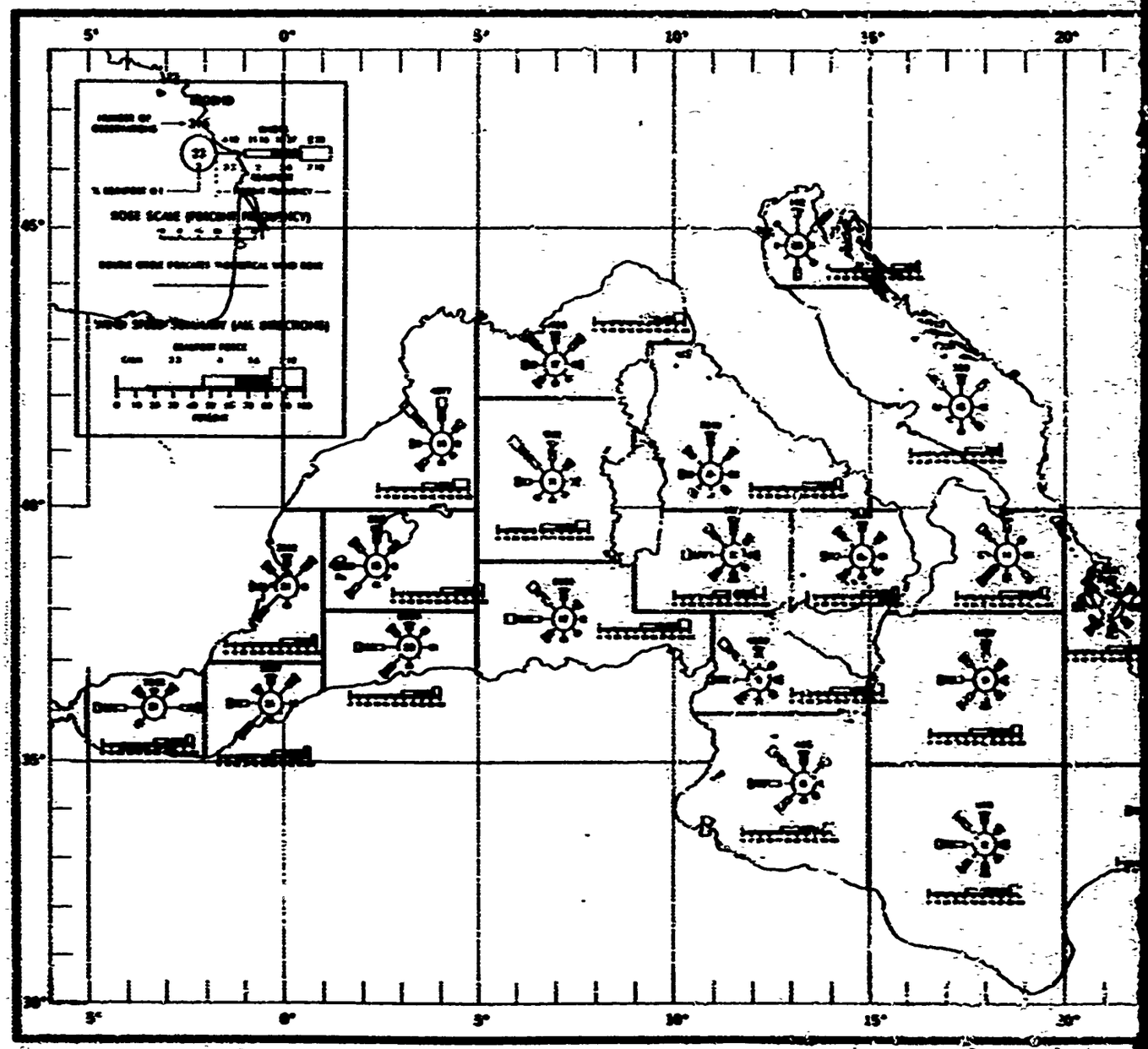

FIGURE 4. SURFACE WIND ROSES, THE MEDITERRANEAN SEA

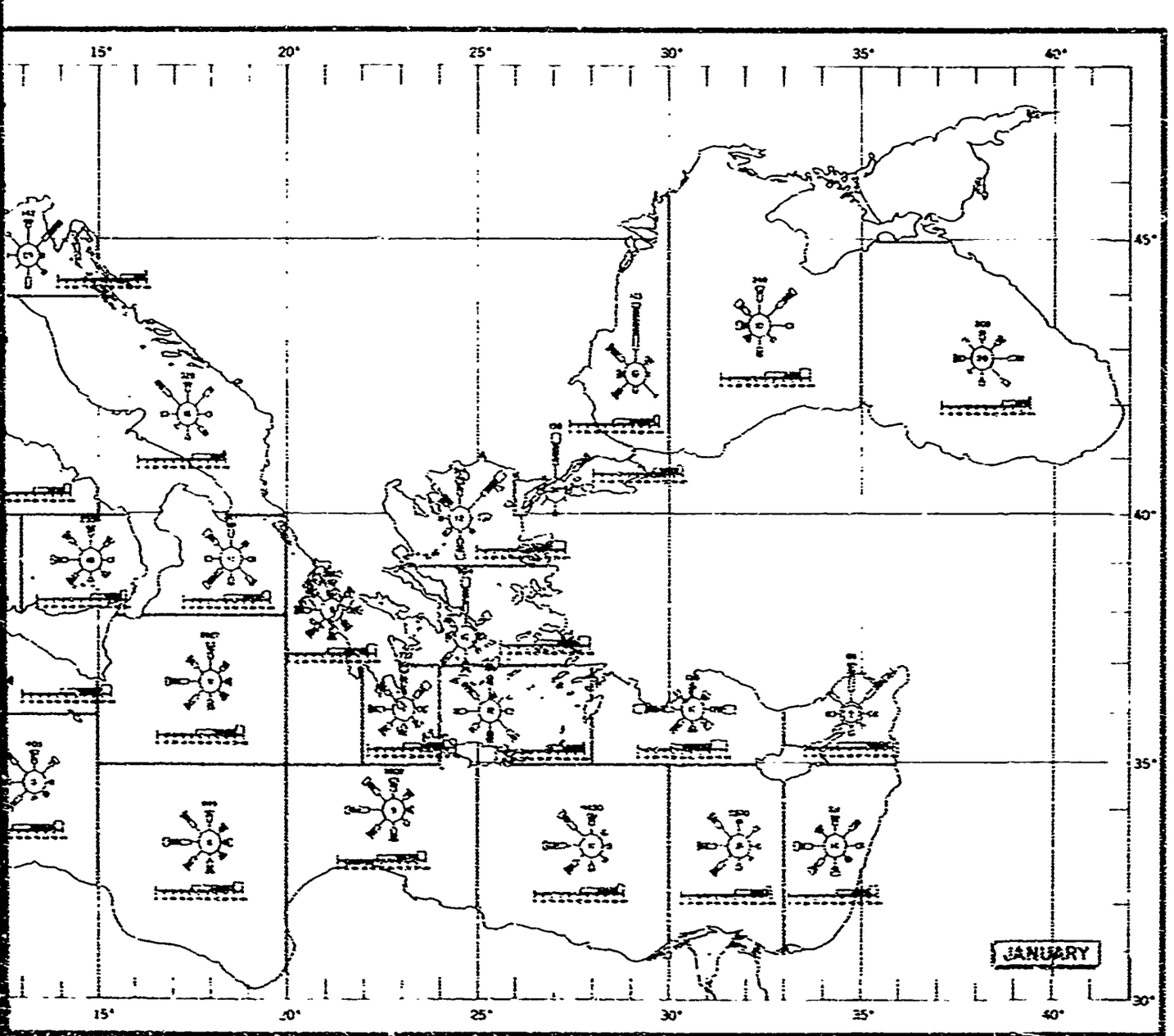

SURFACE WIND ROSES, THE MEDITERRANEAN SEA, JANUARY

FIGURE 4. SURFACE WINDS, JANUARY

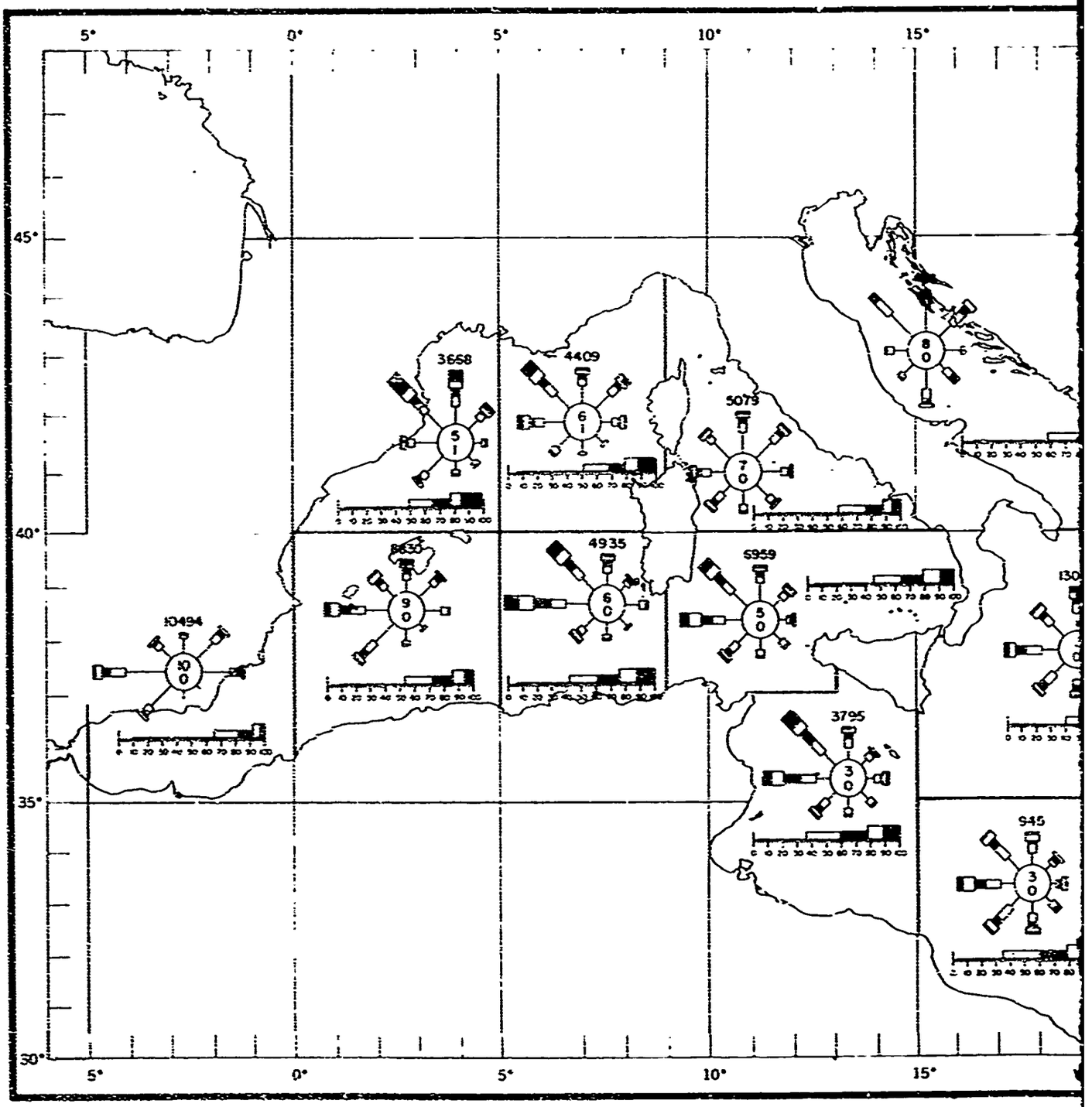

FIGURE 5. STATE OF SEA IN THE MED

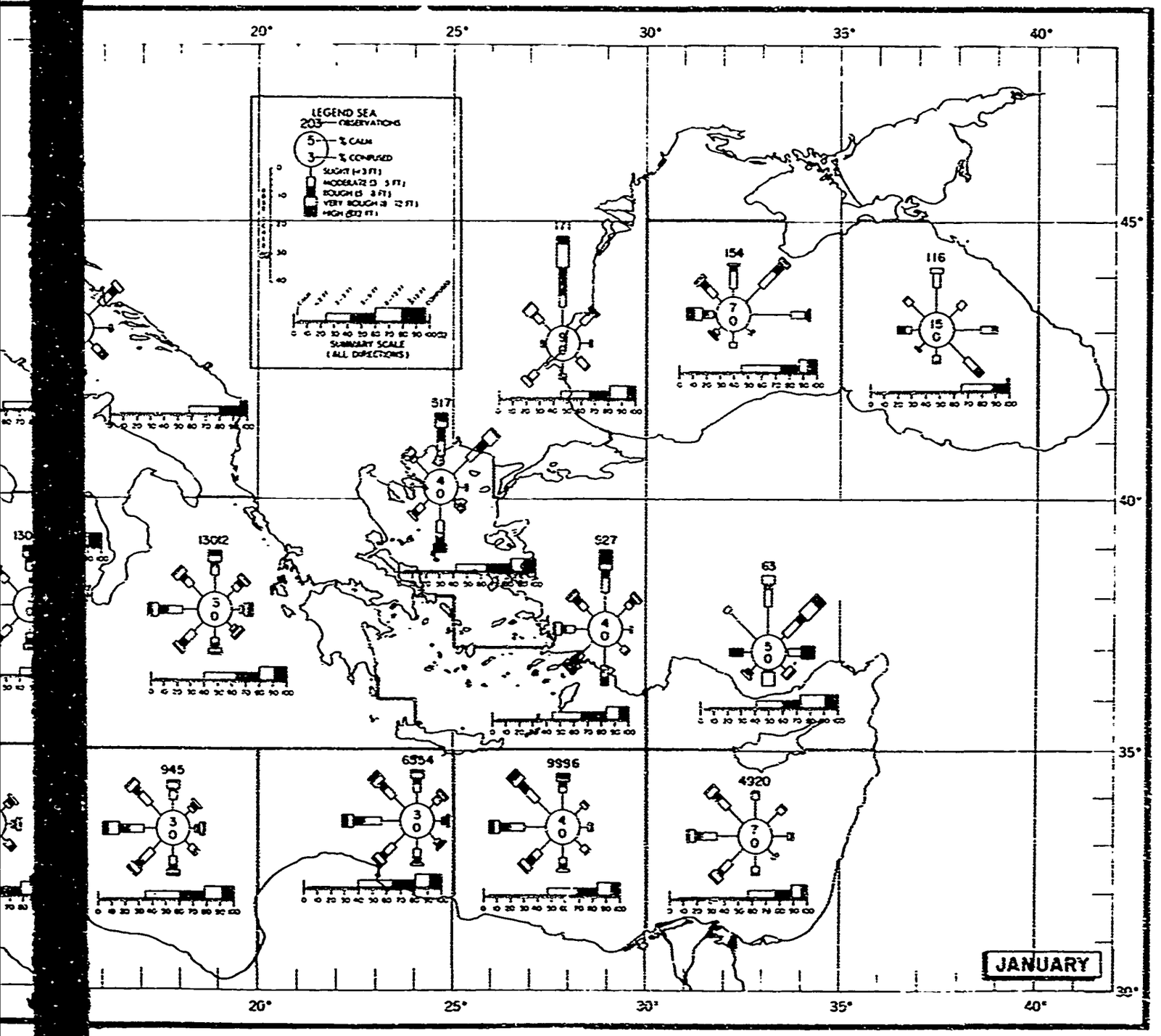

F SEA IN THE MEDITERRANEAN SEA, JANUARY

FIGURE 5. SEA, JANUARY

2

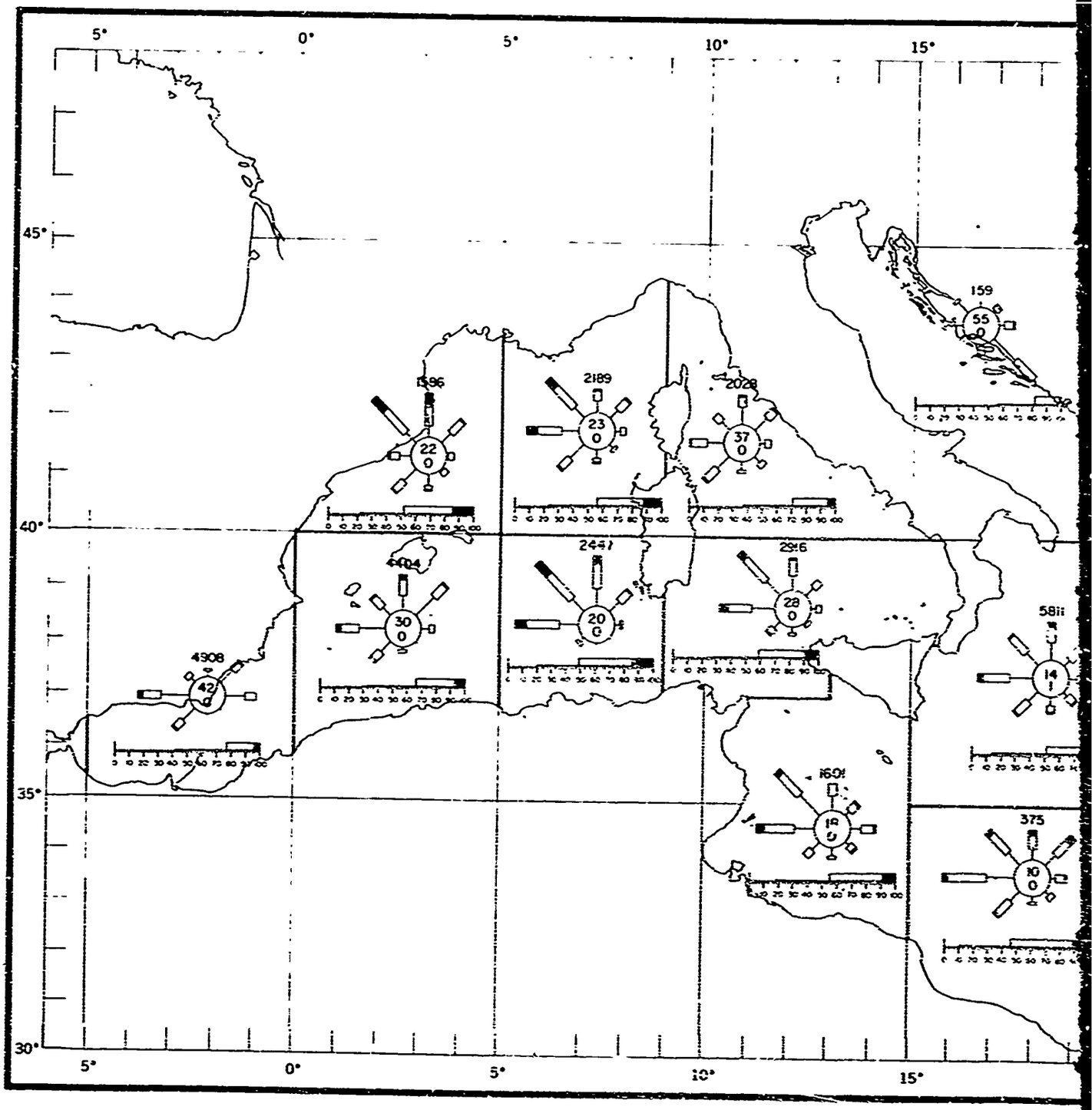

FIGURE 6. SWELL IN THE ME

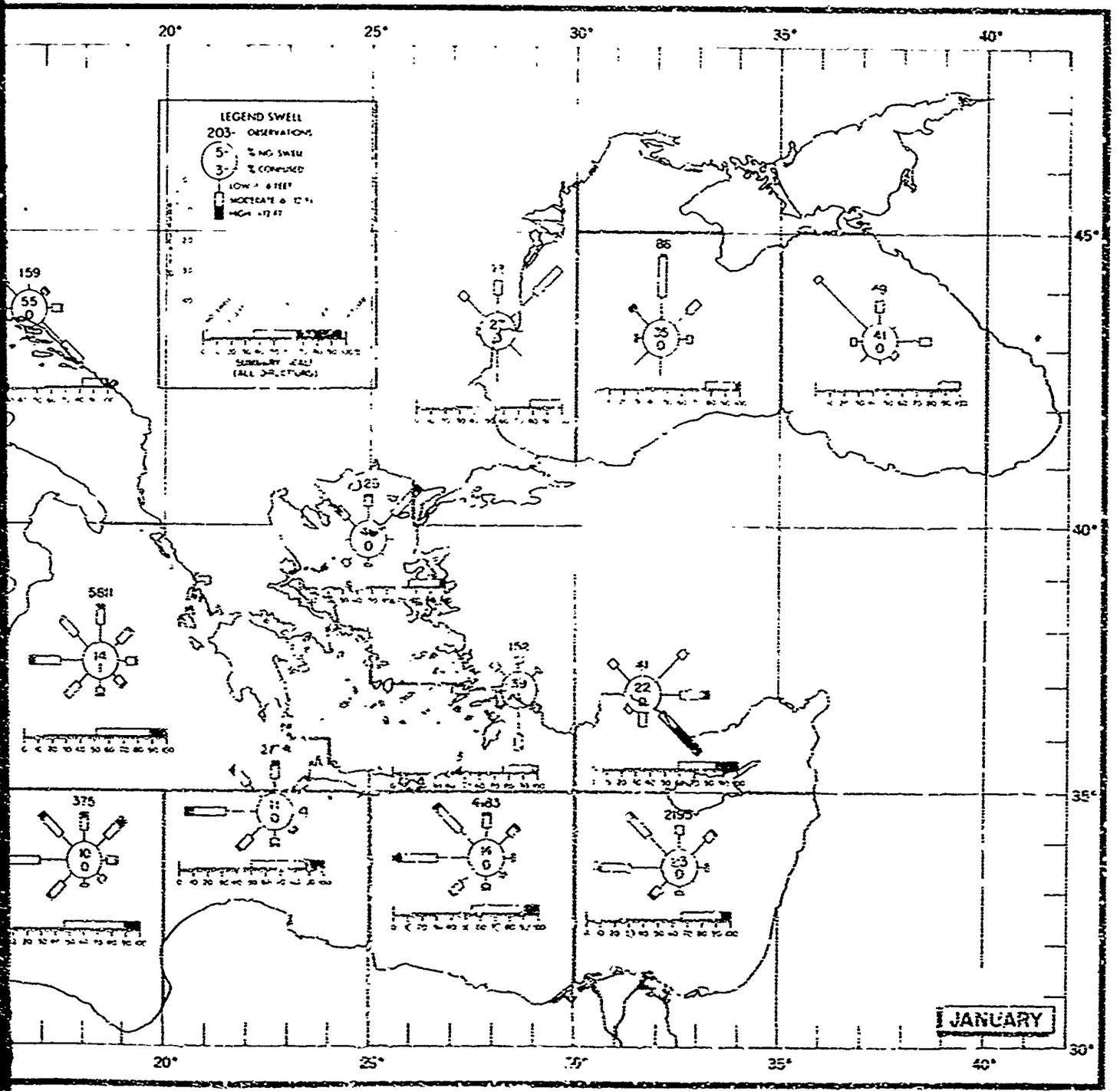

SWELL IN THE MEDITERRANEAN SEA, JANUARY

FIGURE 6. SWELL, JANUARY

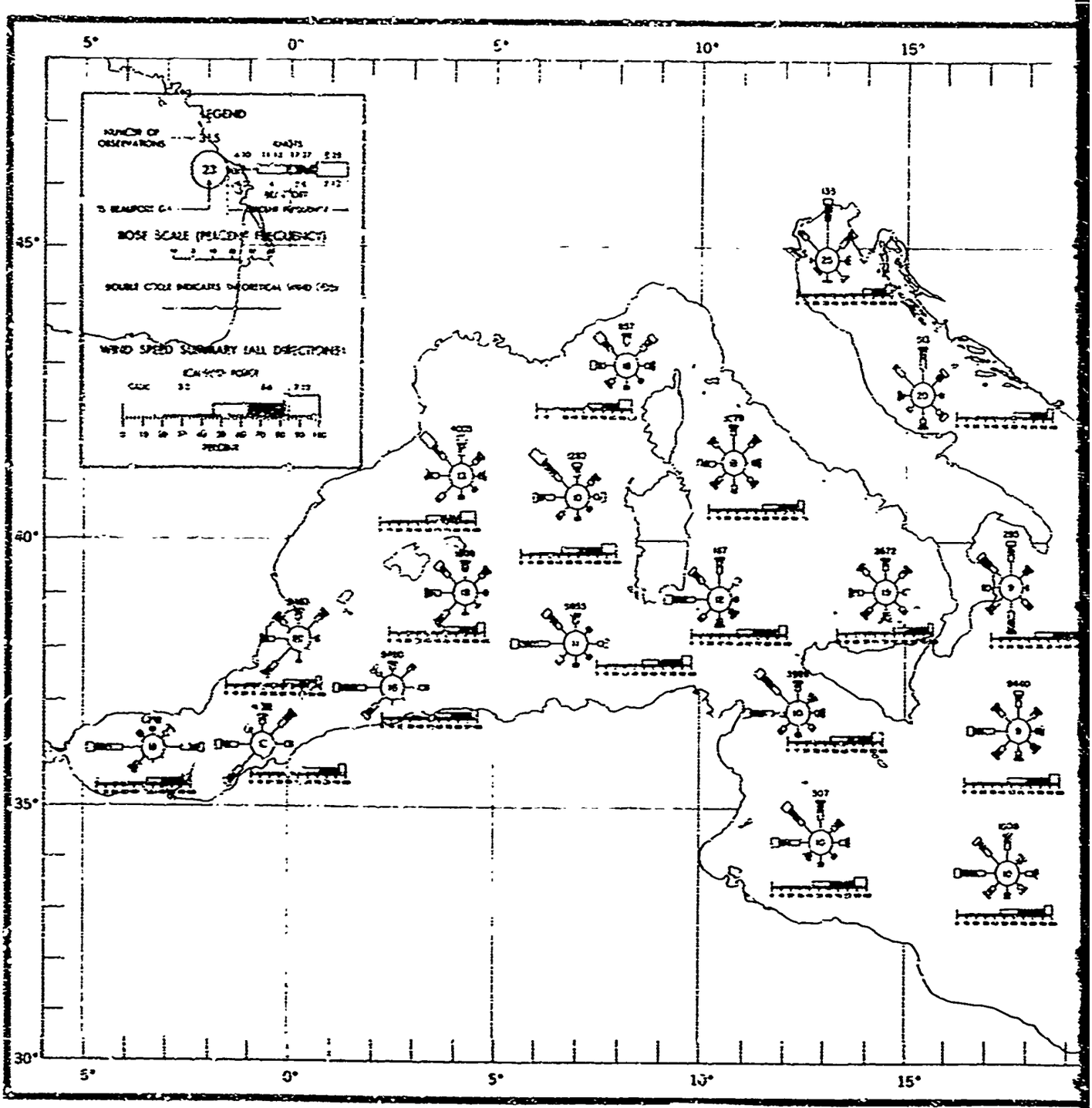

FIGURE 7. SURFACE WIND ROSES, THE MEDITERR

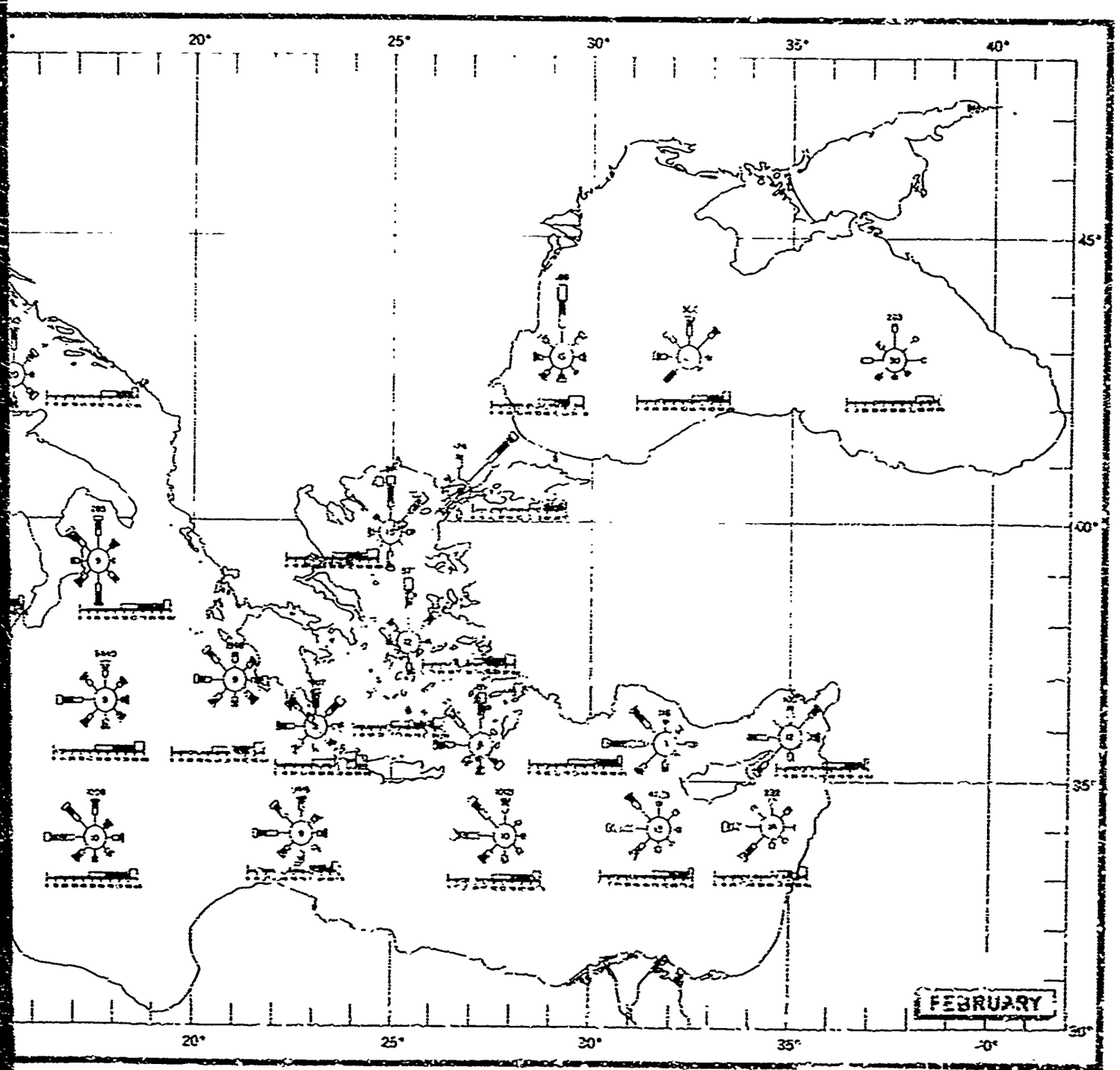

OSES, THE MEDITERRANEAN SEA, FEBRUARY

FIGURE 7. SURFACE WINDS, FEBRUARY

2

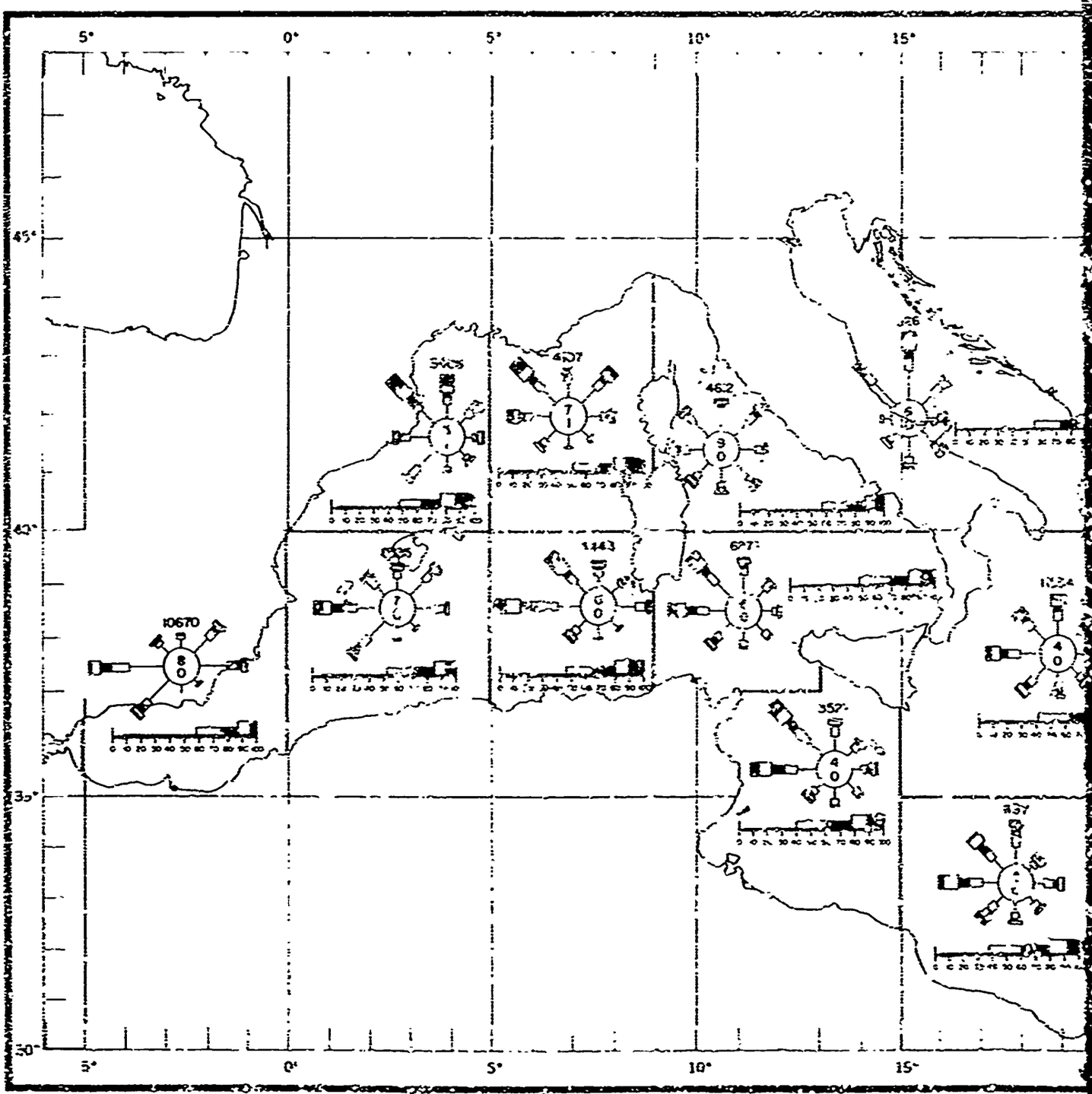

FIGURE 9. STATE OF SEA IN THE MEDITERRANEAN

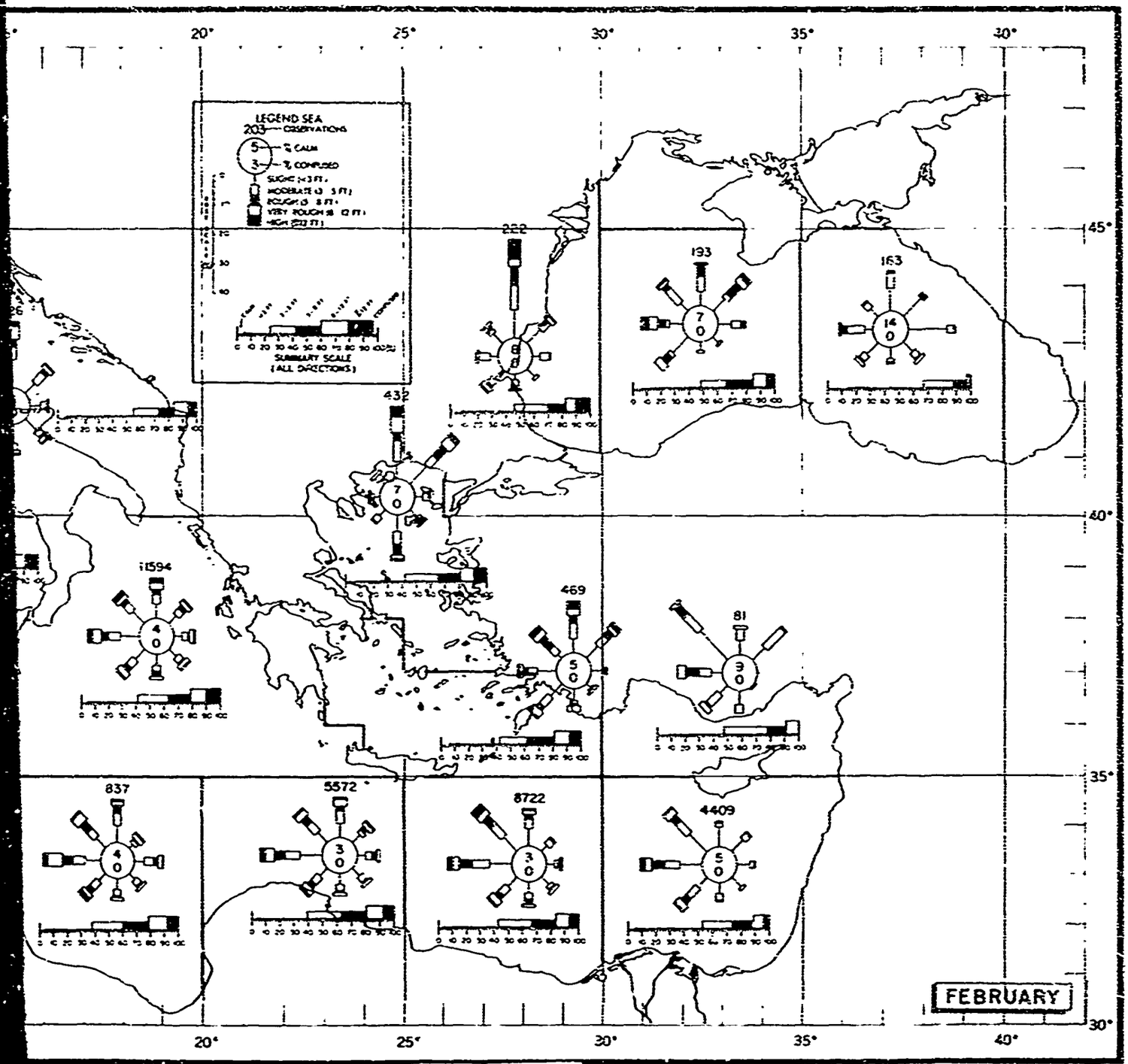

IN THE MEDITERRANEAN SEA, FEBRUARY

FIGURE 8. SEA, FEBRUARY

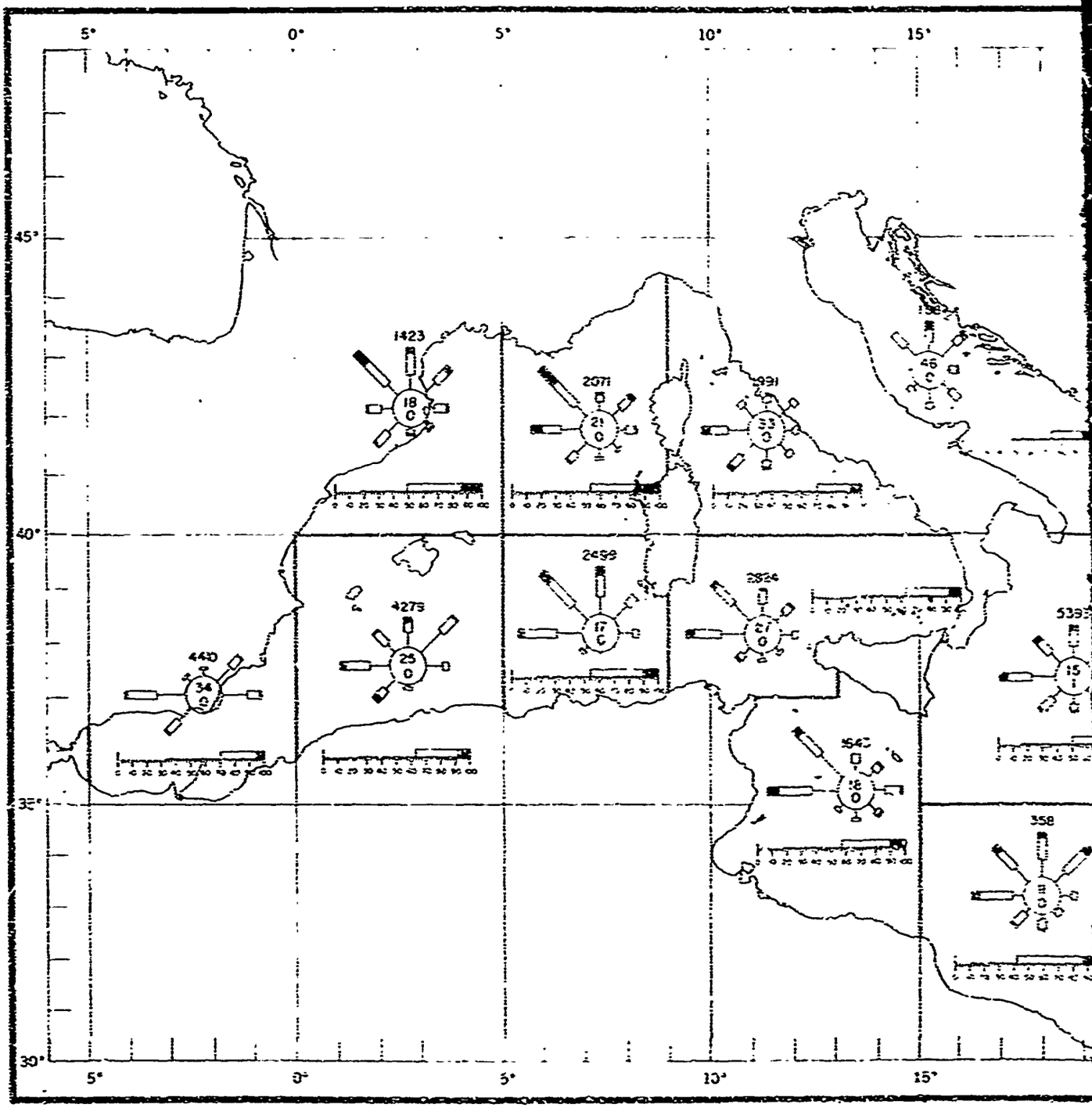

FIGURE 9. SWELL IN

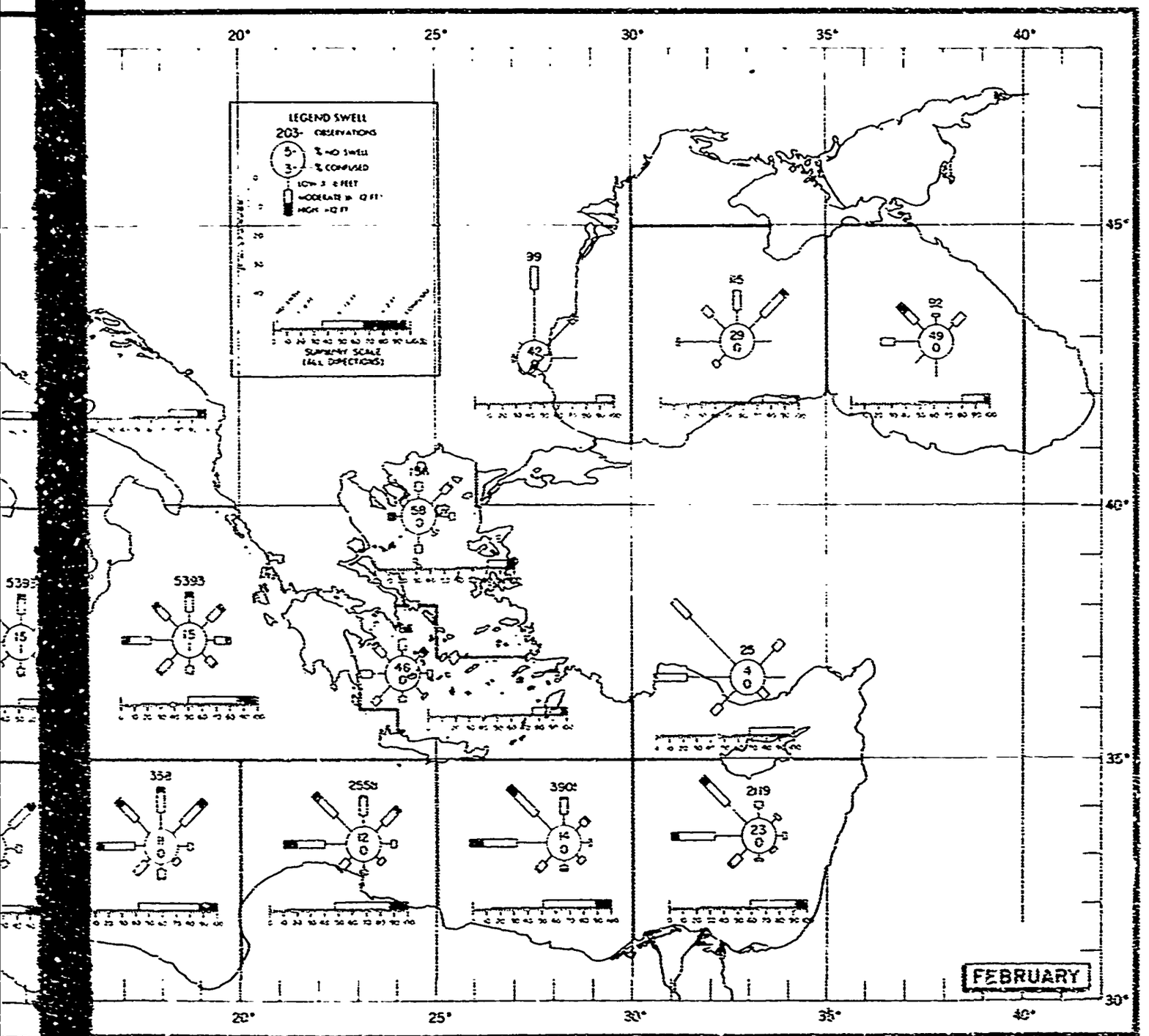

9. SWELL IN THE MEDITERRANEAN SEA, FEBRUARY

FIGURE 9 SWELL, FEBRUARY

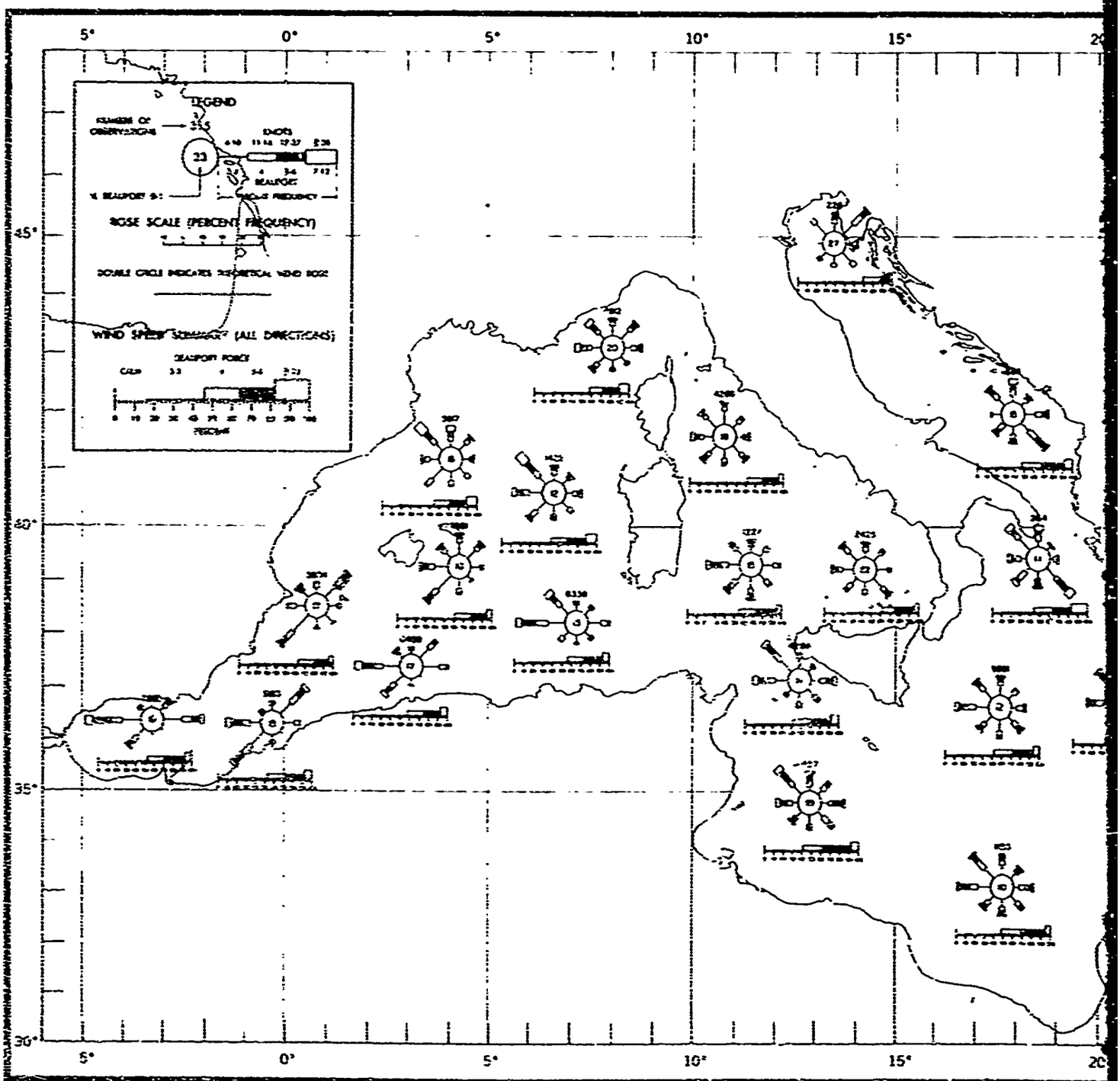

FIGURE 10. SURFACE WIND ROSES, THE MEDITERRANEA

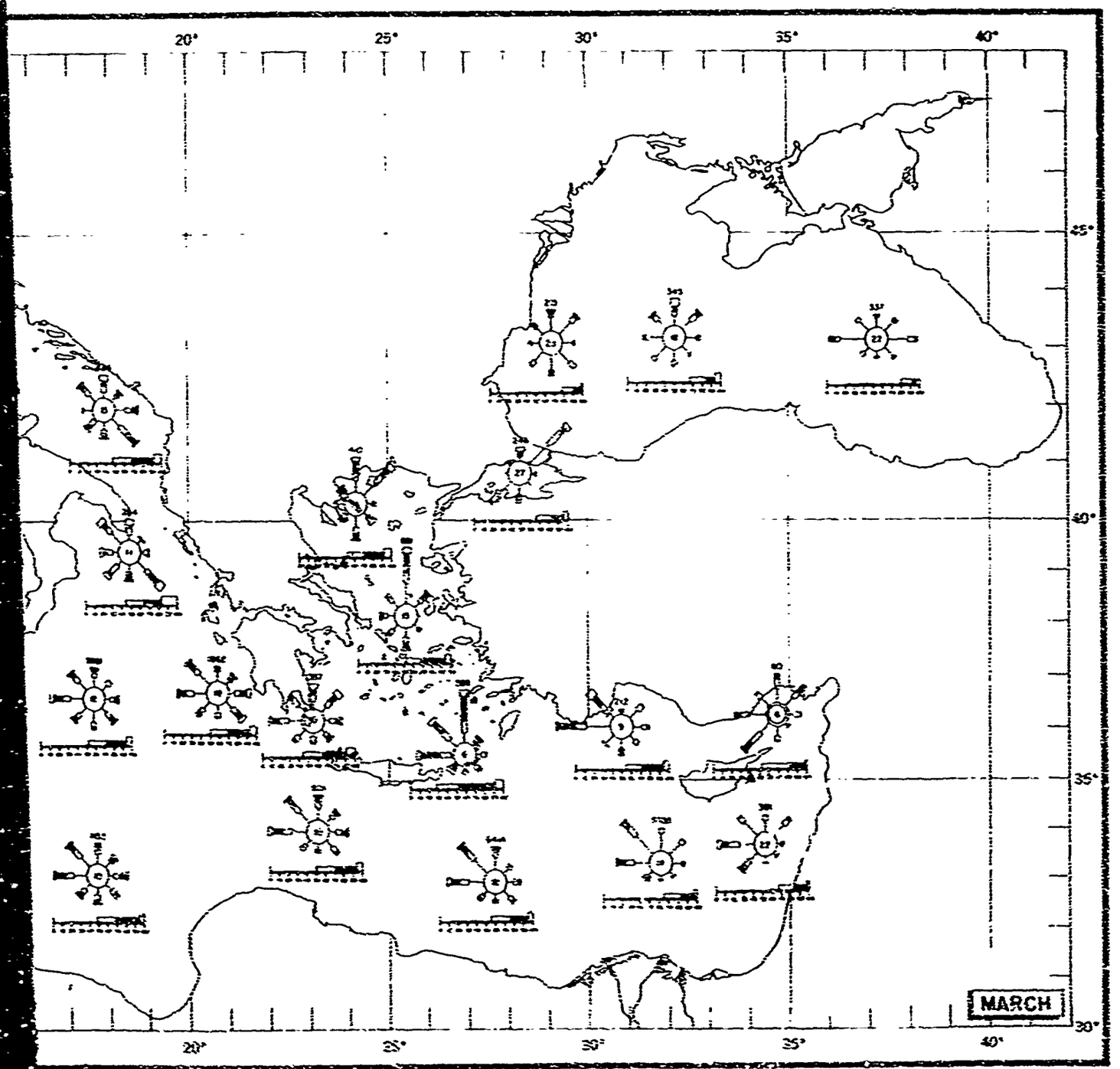

ES, THE MEDITERRANEAN SEA, MARCH

FIGURE 10. SURFACE WINDS, MARCH

2

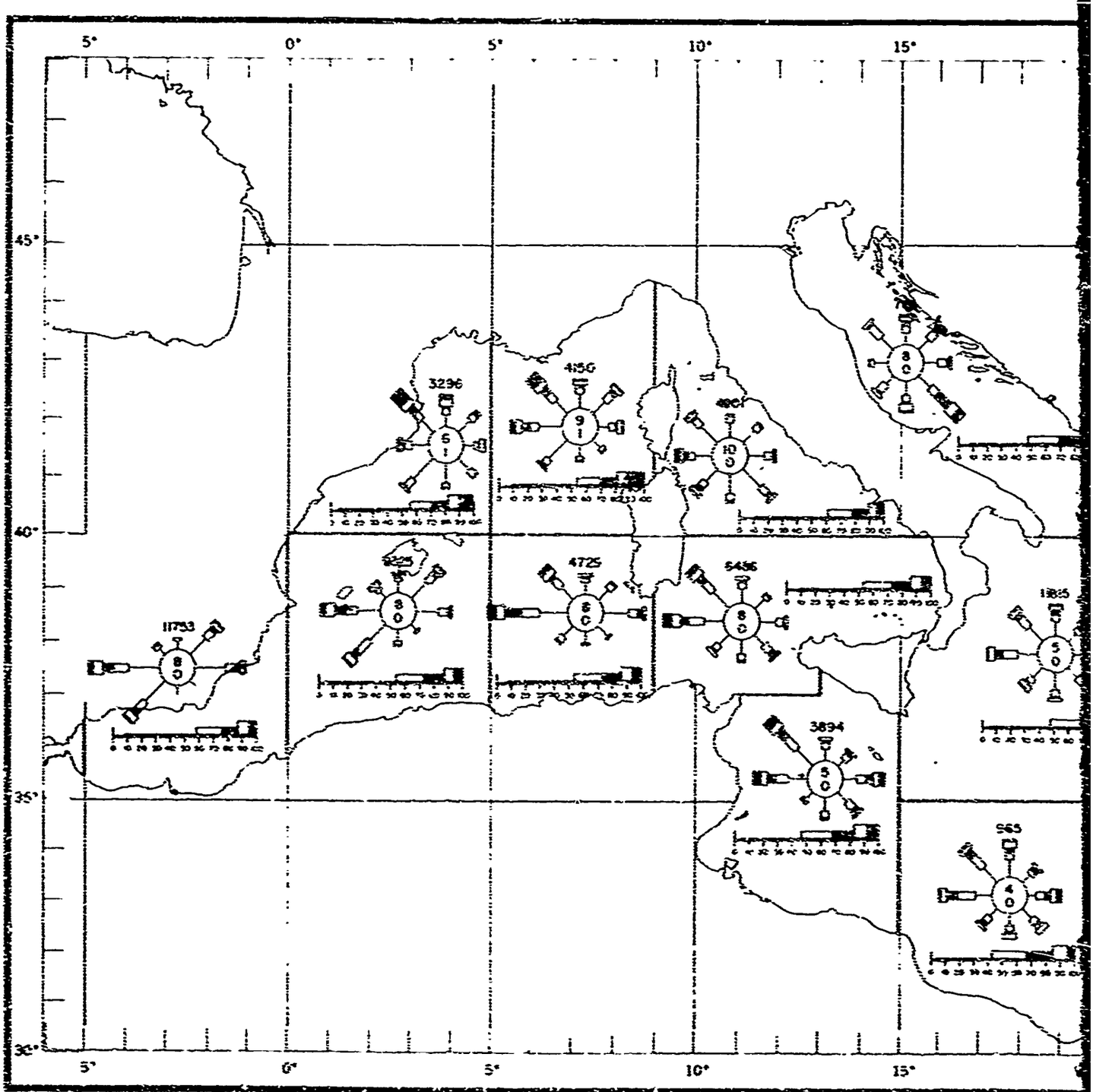

FIGURE 11. STATE OF SEA IN TH

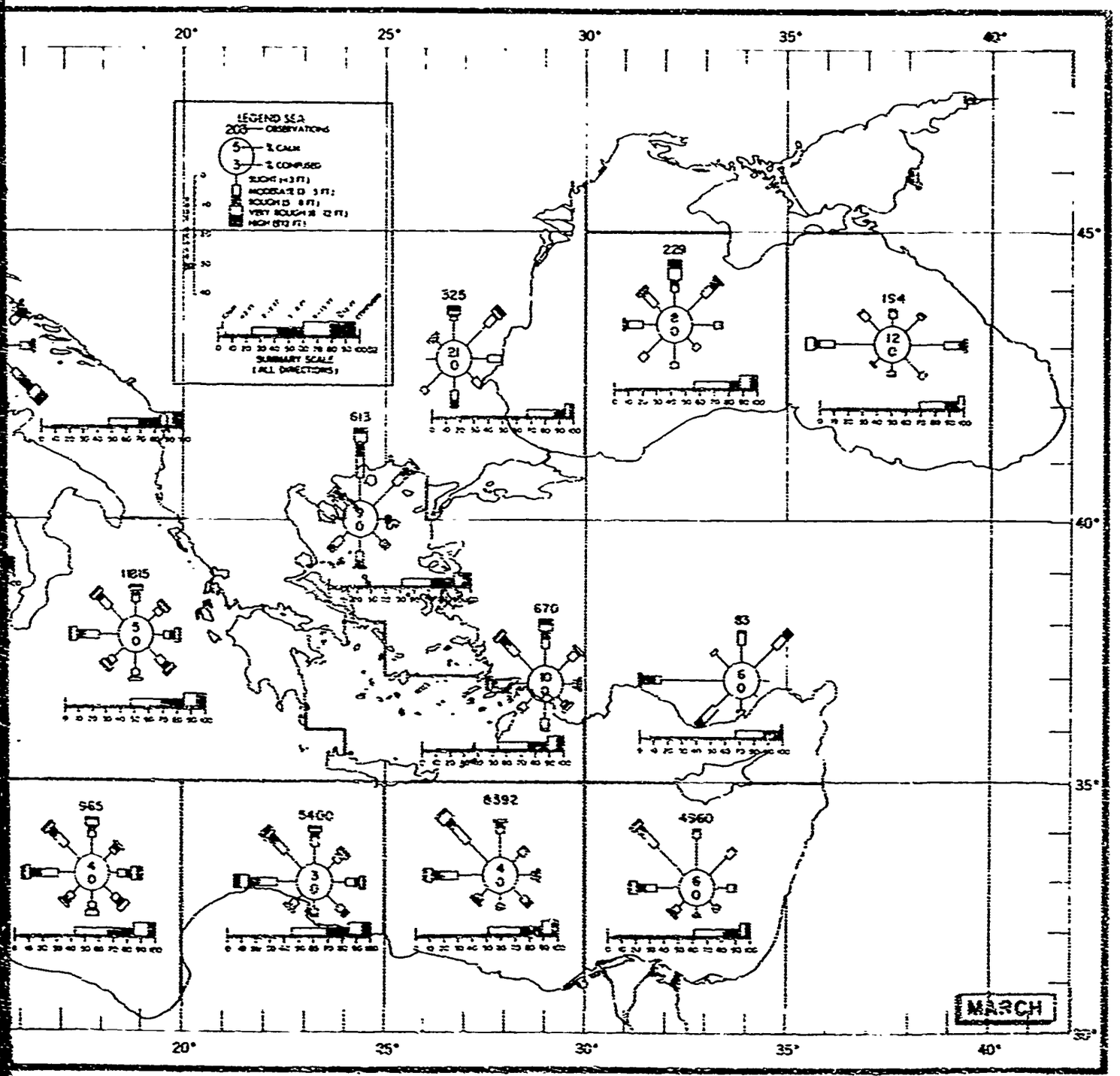

STATE OF SEA IN THE MEDITERRANEAN SEA, MARCH

FIGURE 11. SEA, MARCH

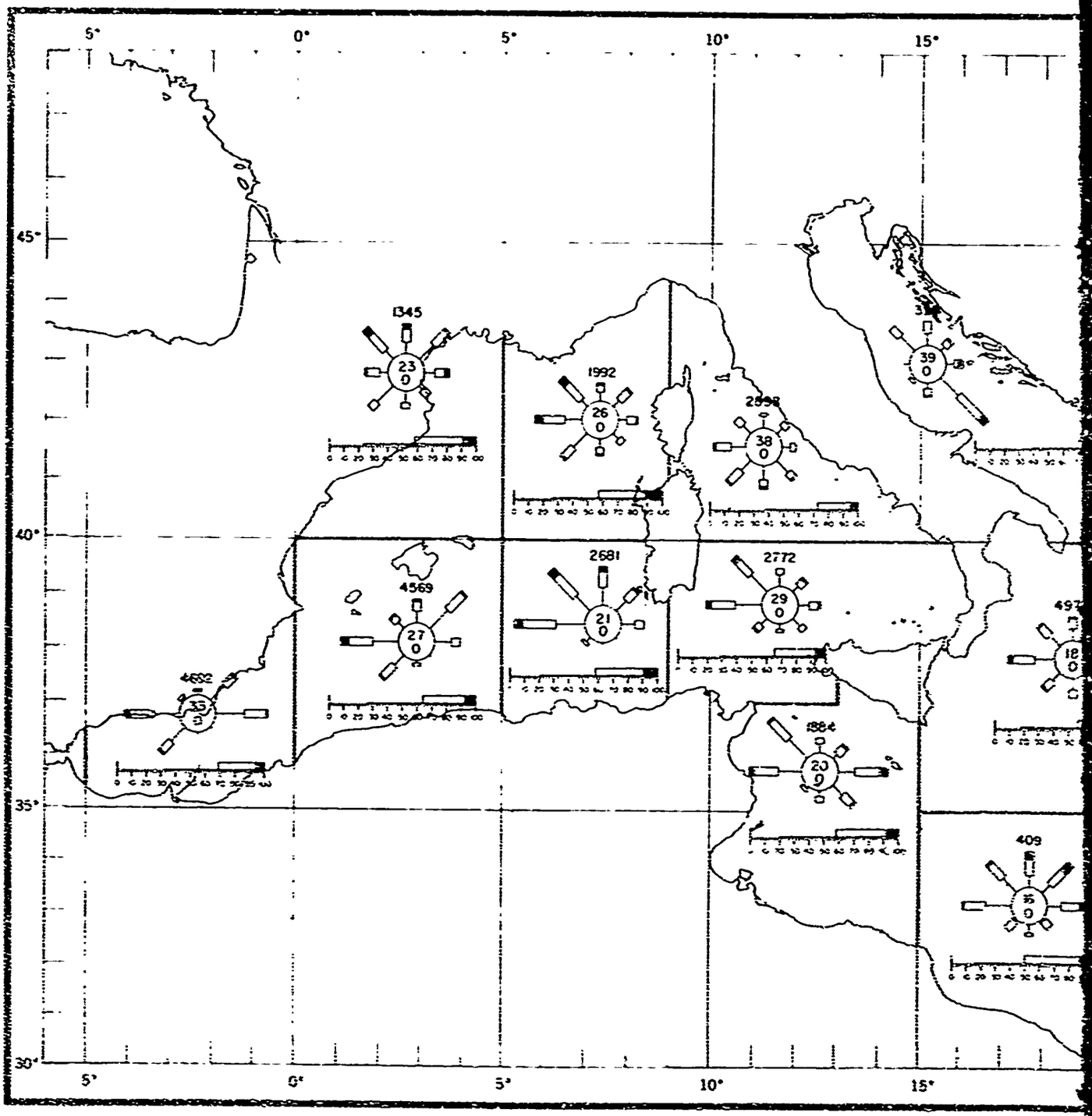

FIGURE 12. SWELL IN THE MEDITERRAN

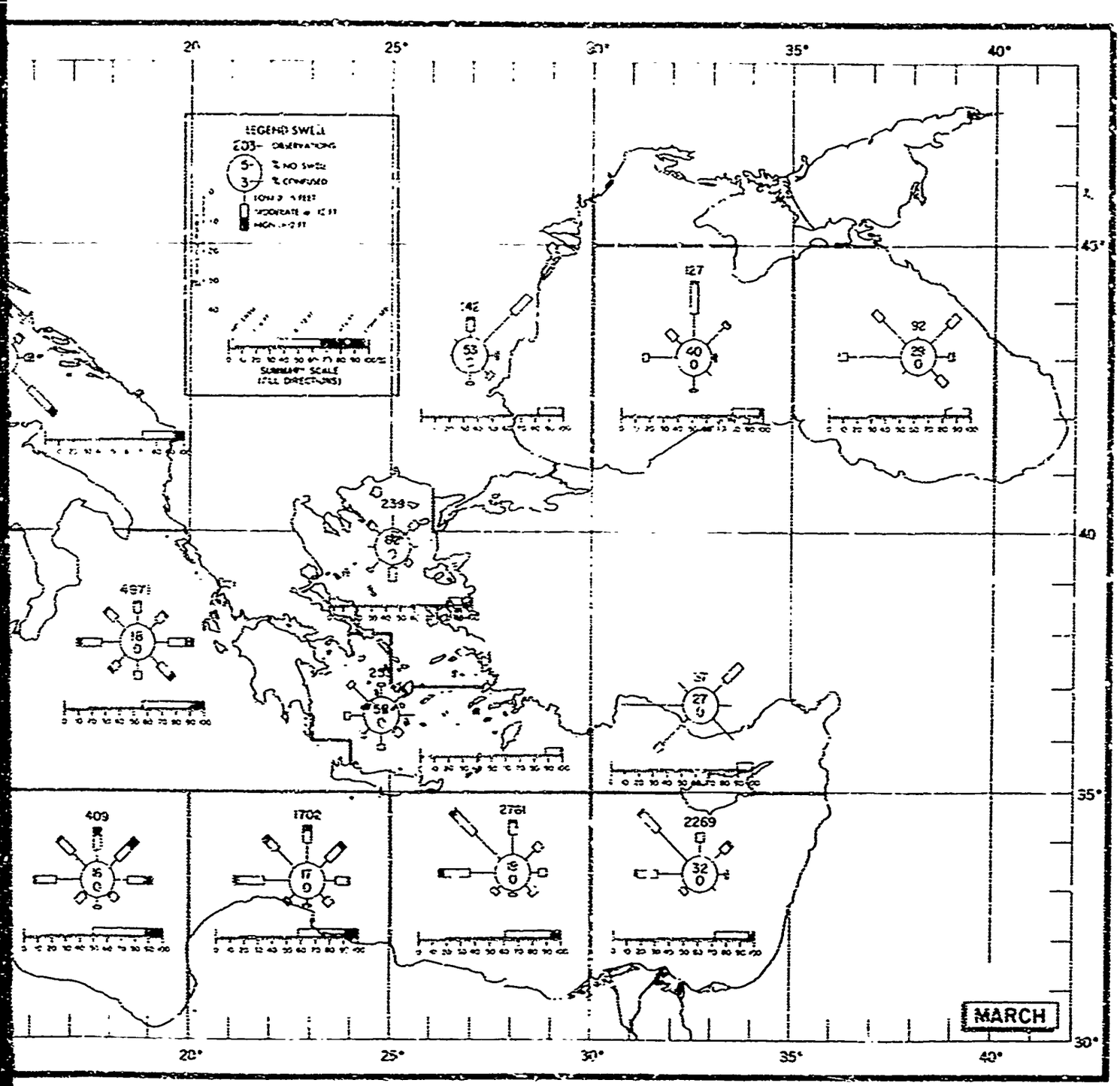

N THE MEDITERRANEAN SEA, MARCH

FIGURE 12. SWELL, MARCH

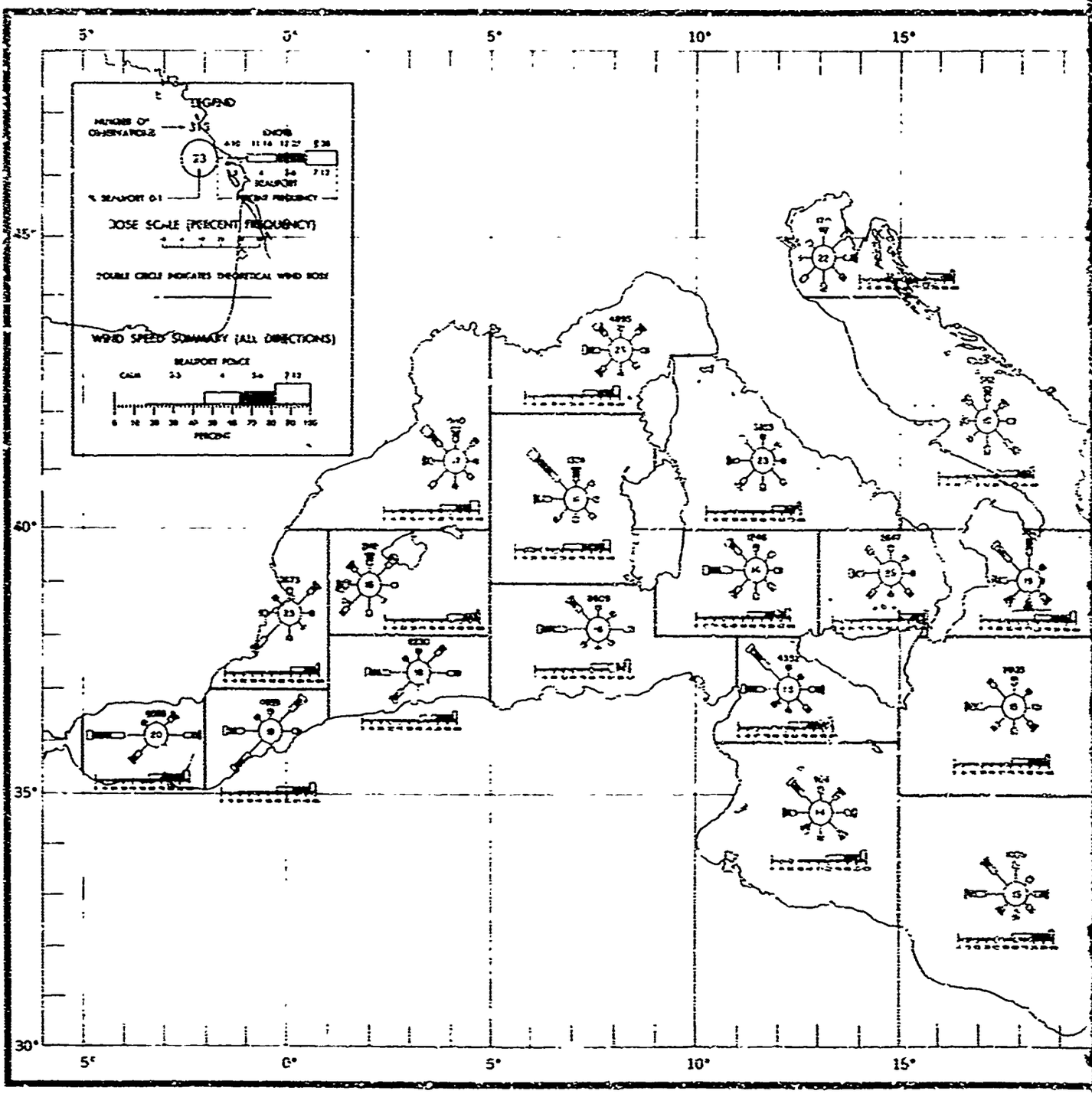

FIGURE 15. SURFACE WIND ROSES, THE MEDITERR

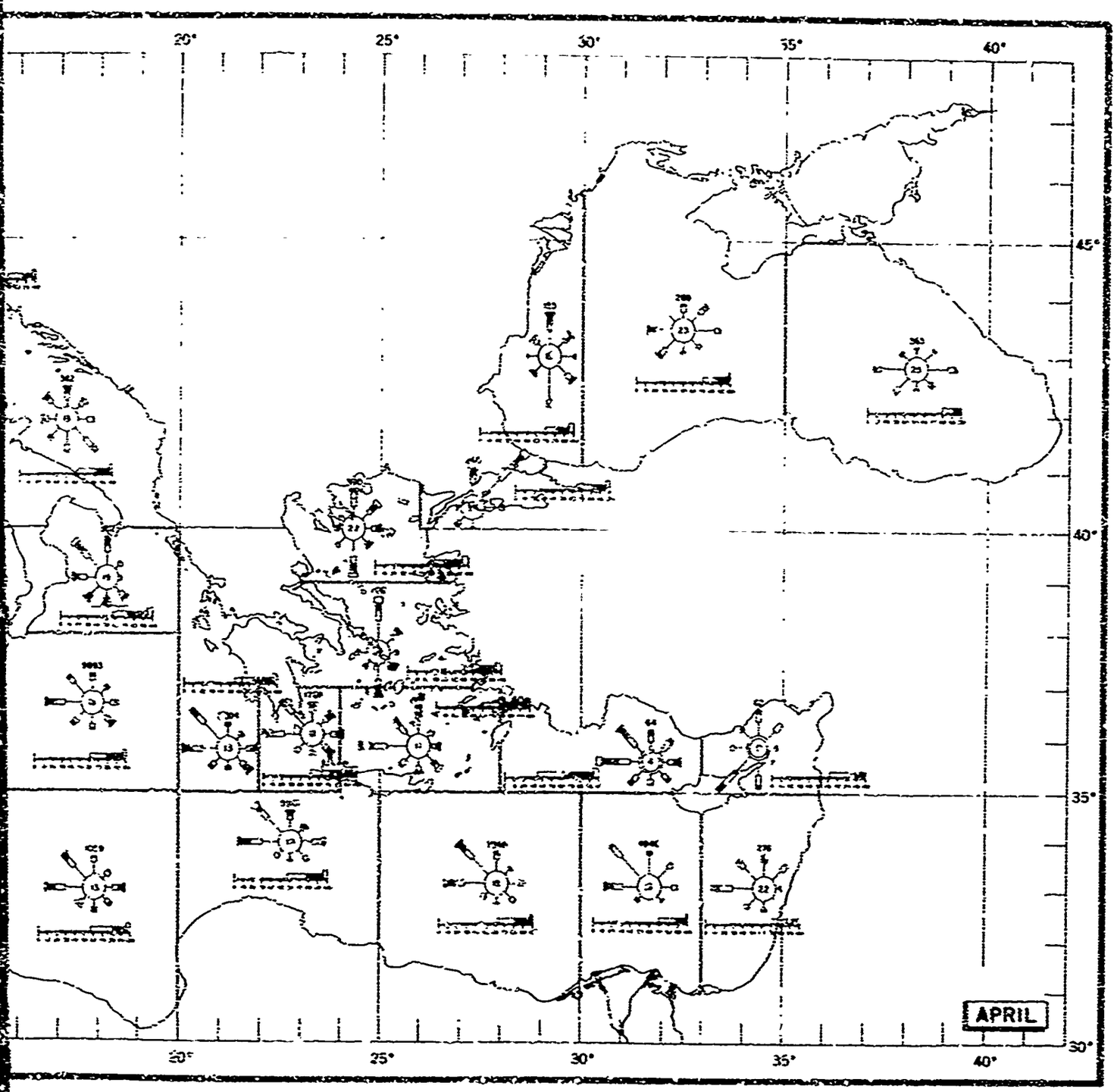

POSES, THE MEDITERRANEAN SEA, APRIL

FIGURE 13. SURFACE WINDS, APRIL

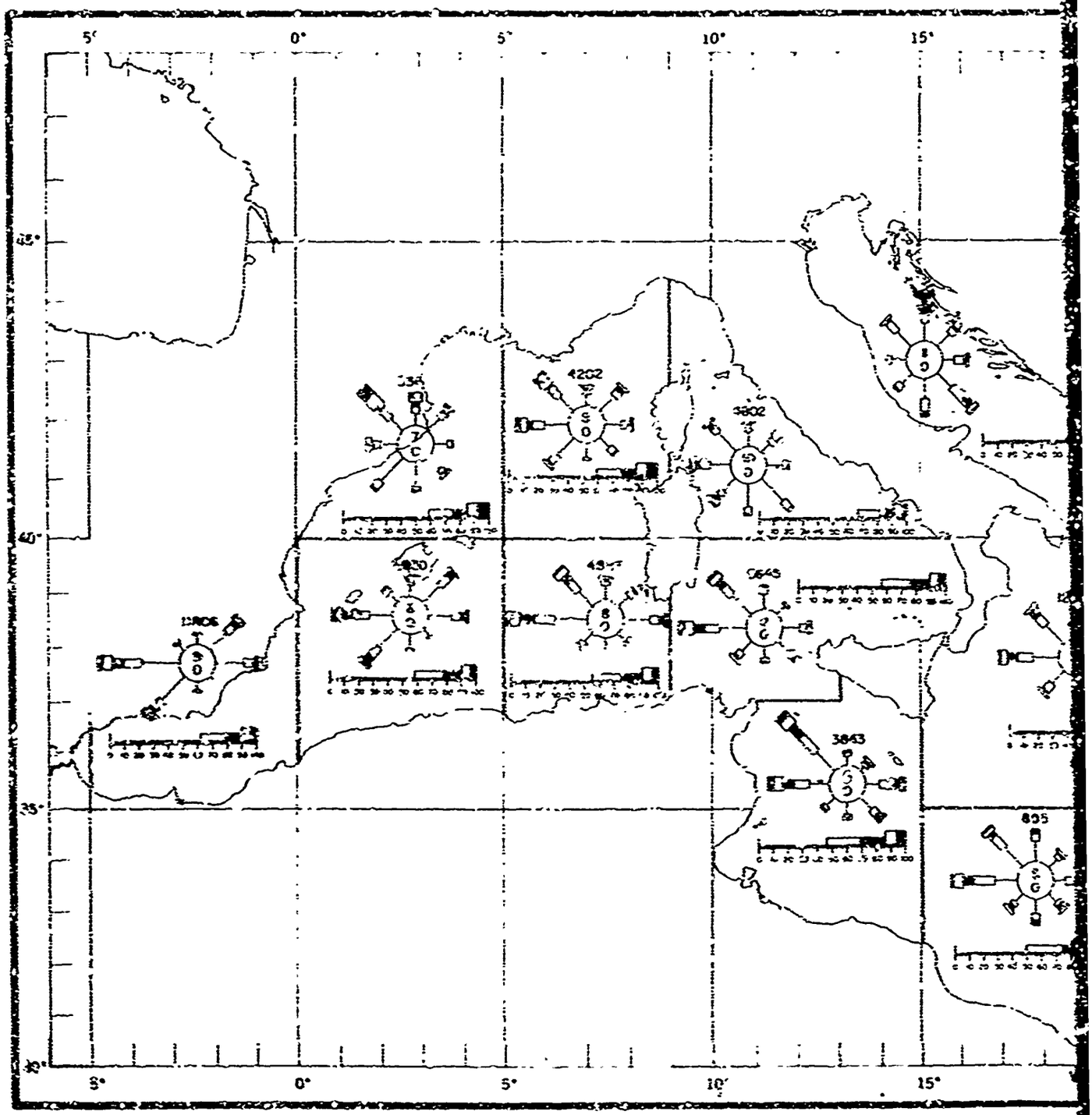

FIGURE 11. STATE OF SEA IN THE MED

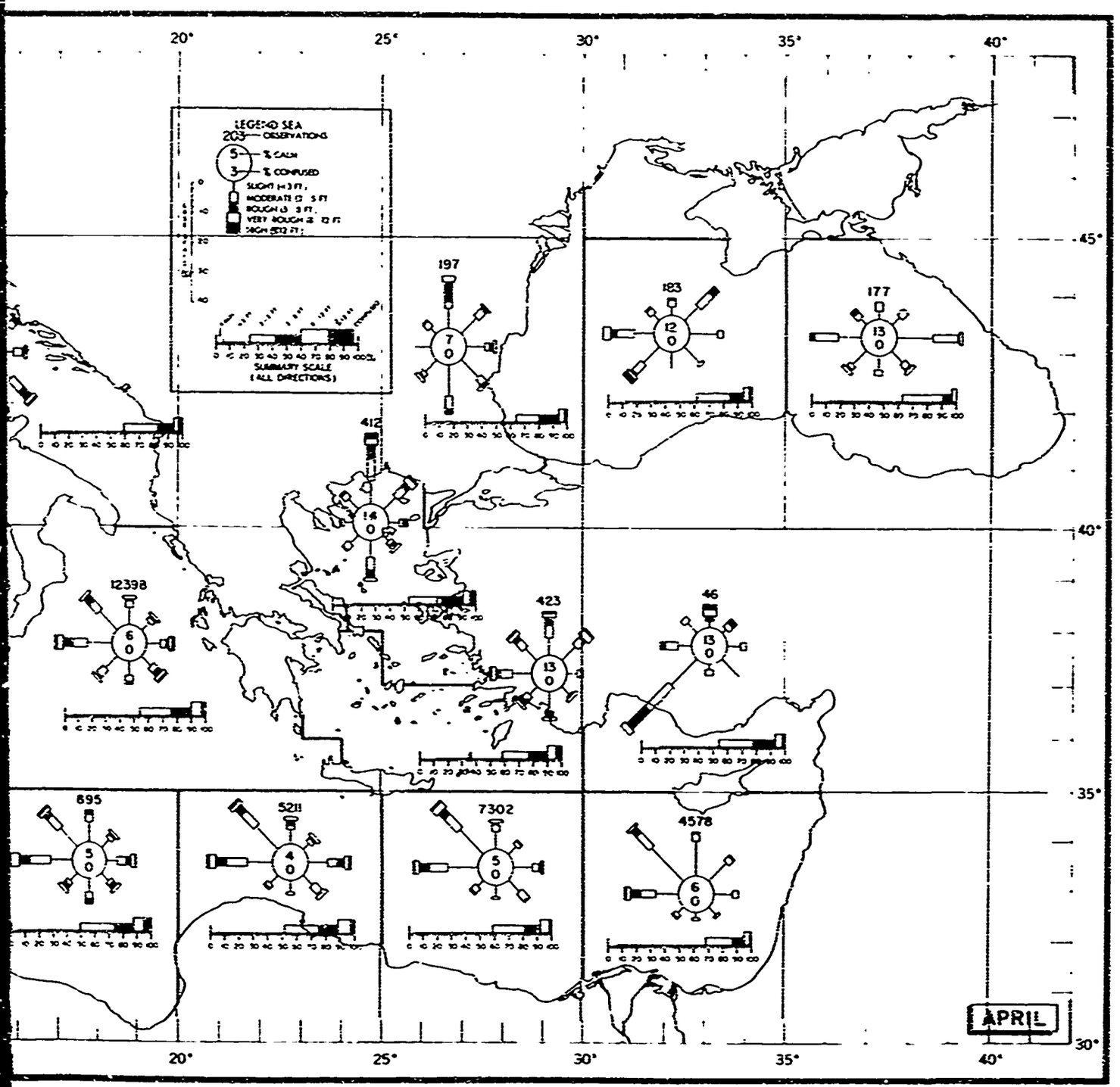

SEA IN THE MEDITERRANEAN SEA, APRIL

FIGURE 14. SEA, APRIL

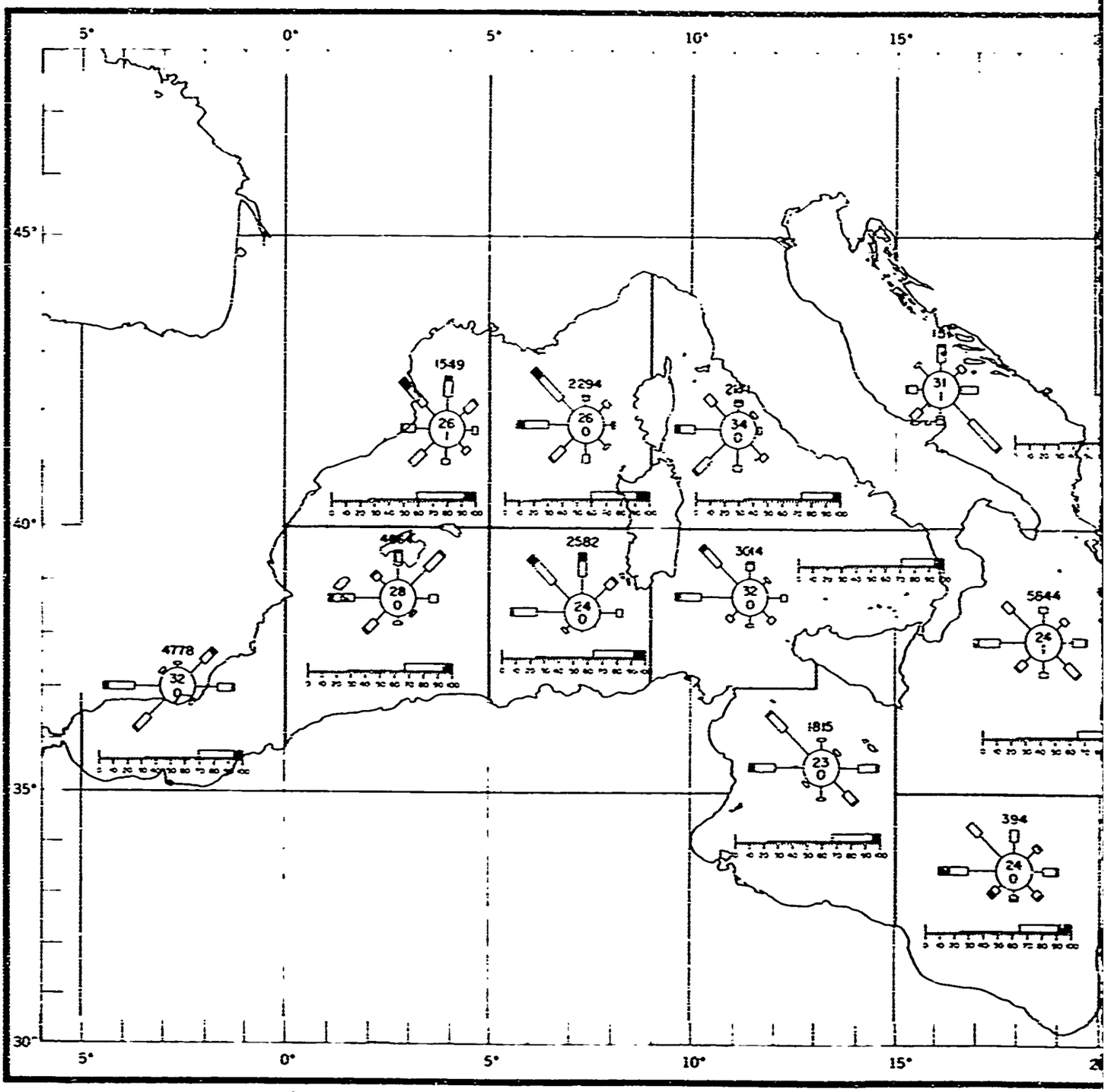

FIGURE 15. SWELL IN THE MEDITERRANEAN SE

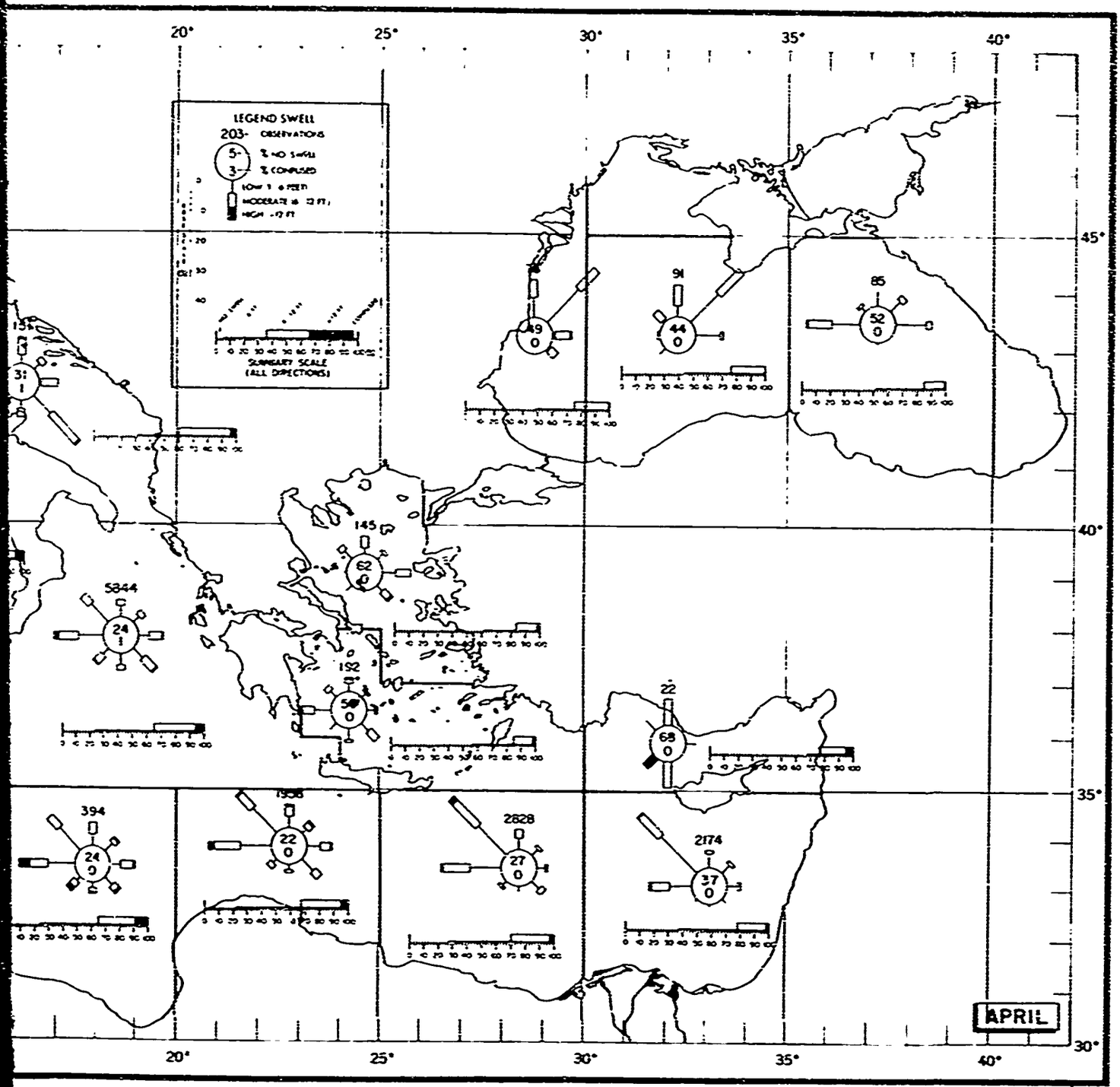

E MEDITERRANEAN SEA, APRIL

FIGURE 15. SWELL, APRIL

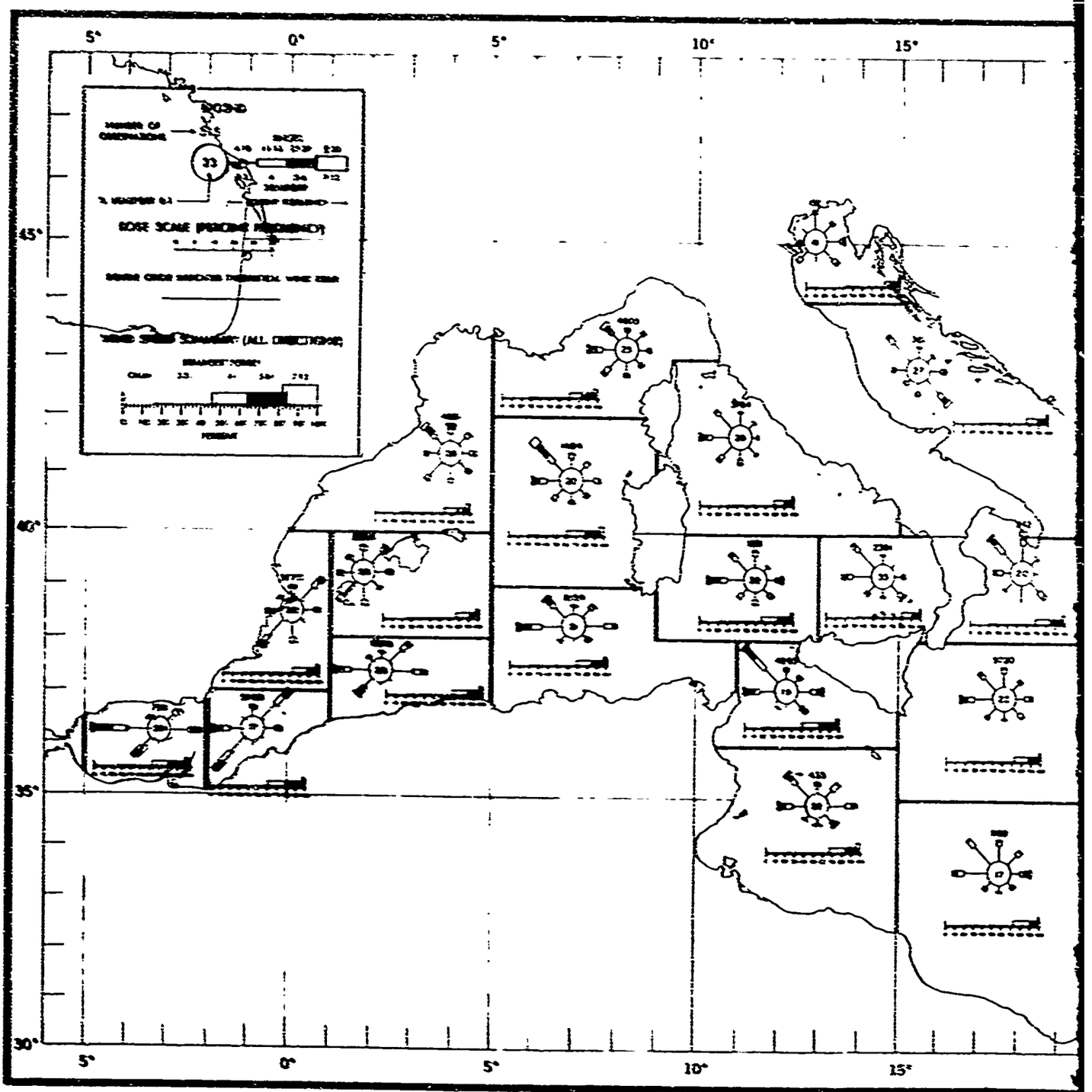

FIGURE 16. SURFACE WIND ROSES, THE MEDITERRA

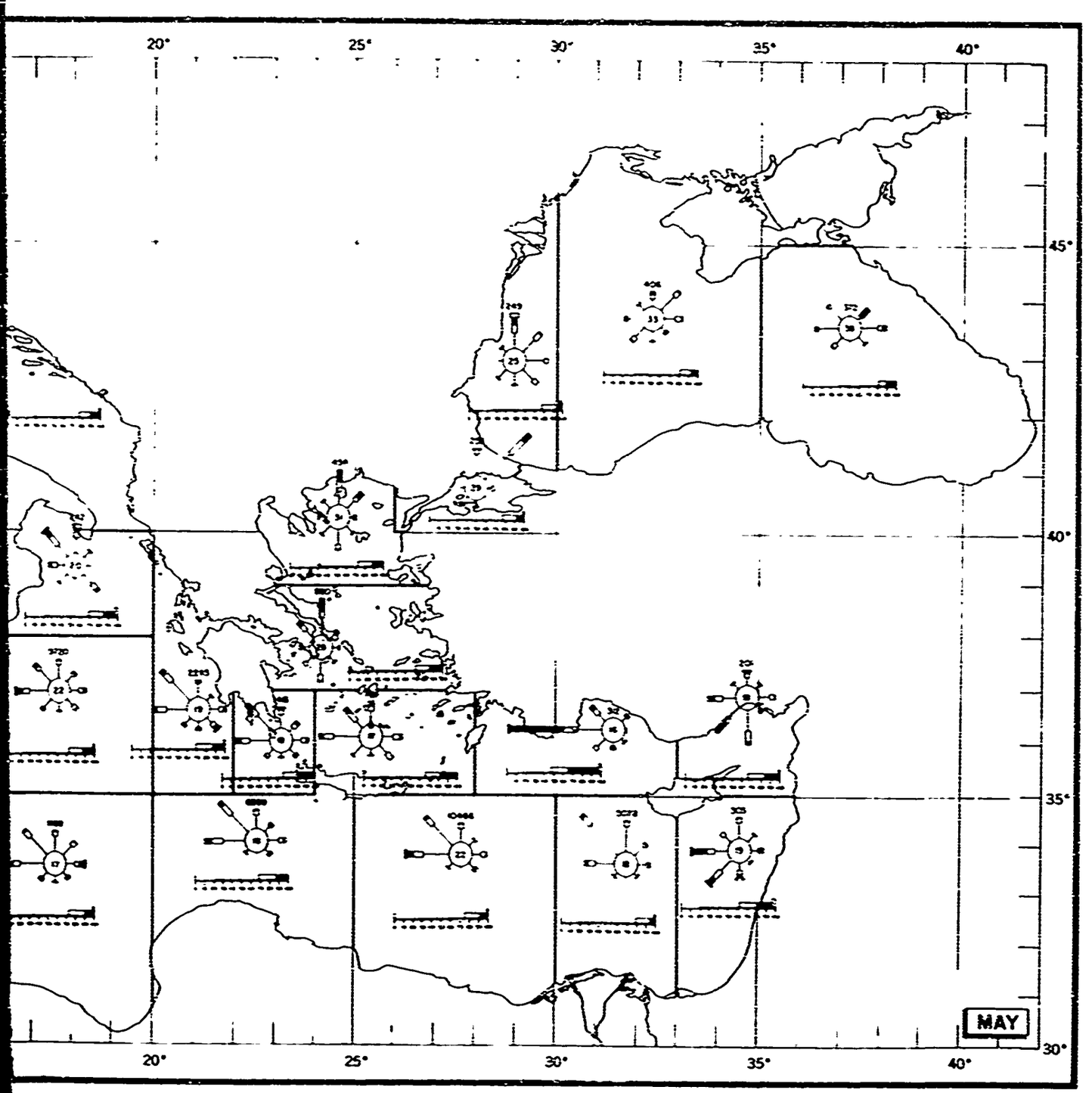

THE MEDITERRANEAN SEA, MAY

FIGURE 16. SURFACE WINDS, MAY

2

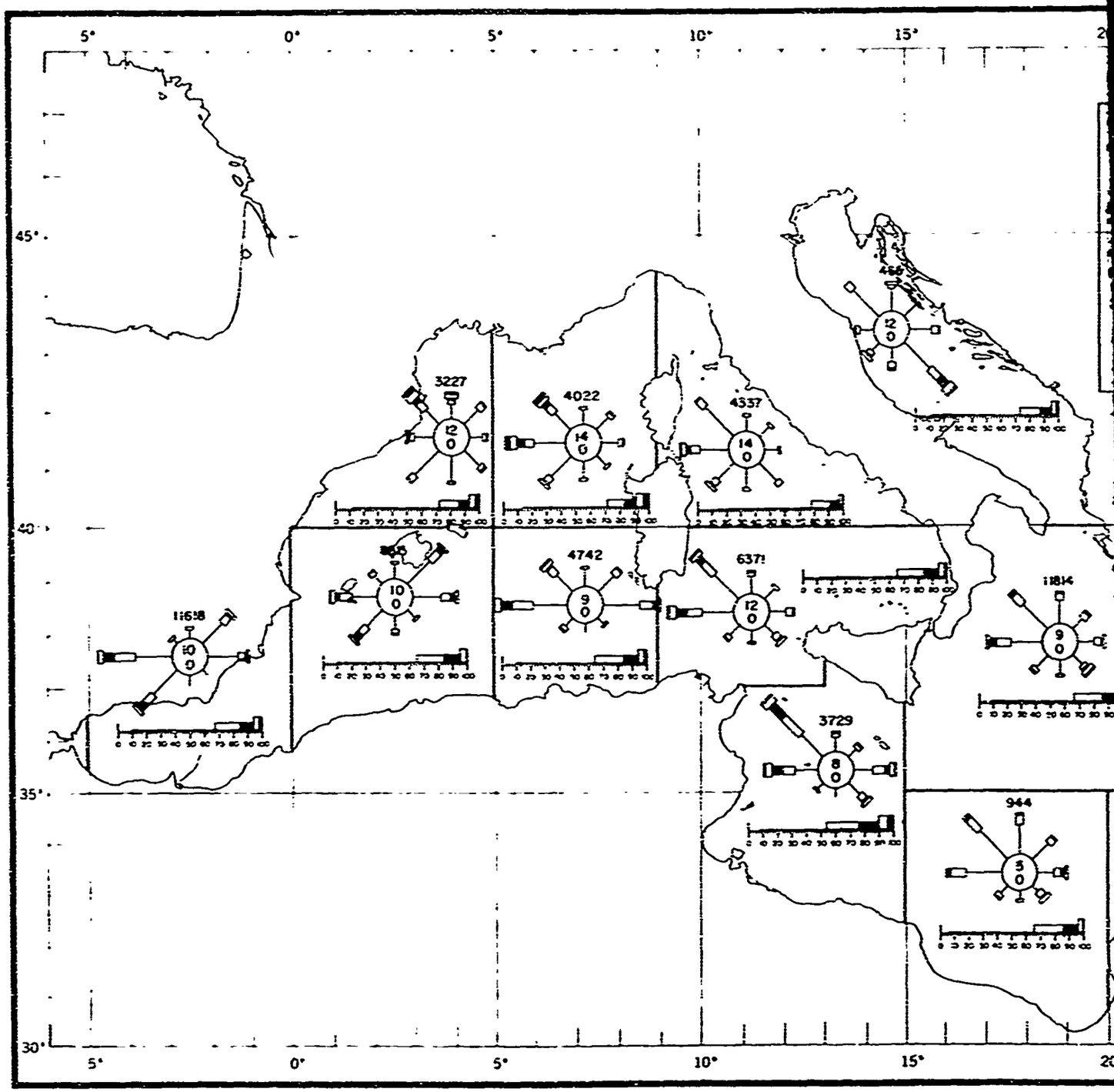

FIGURE 17. STATE OF SEA IN THE MEDITERRANE

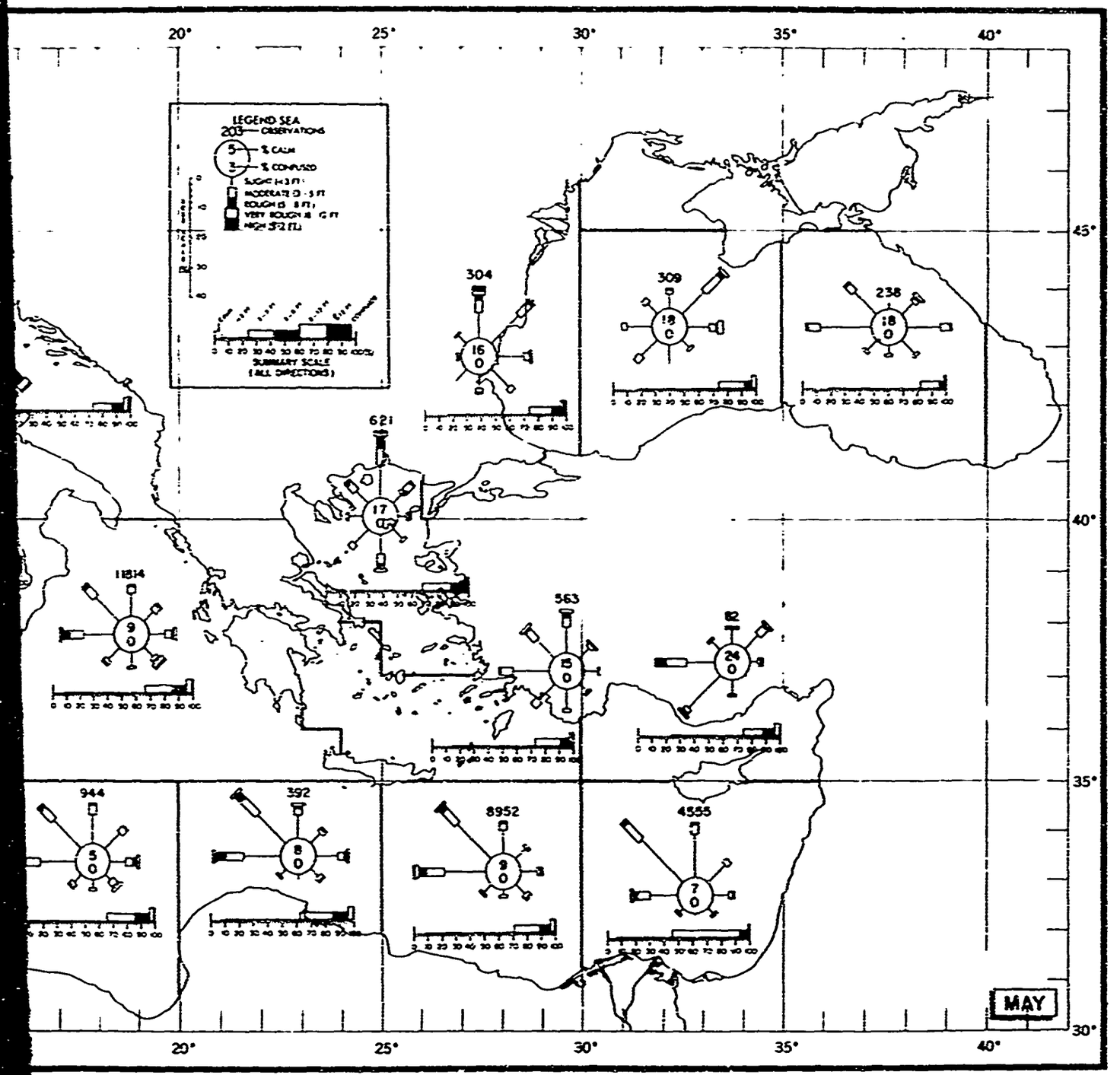

IN THE MEDITERRANEAN SEA, MAY

FIGURE 17. SEA, MAY

2

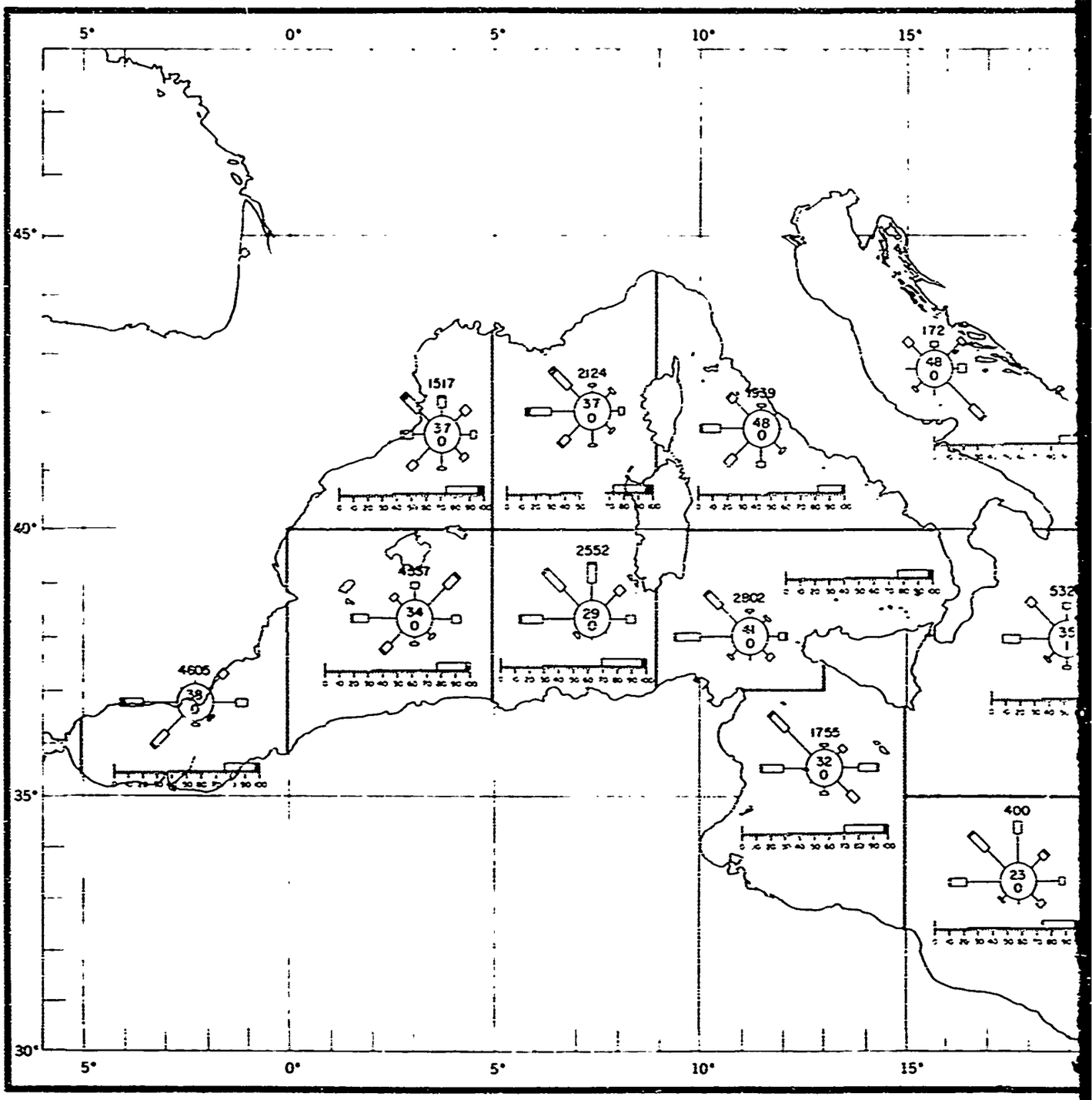

FIGURE 18. SWELL IN THE MEDITER

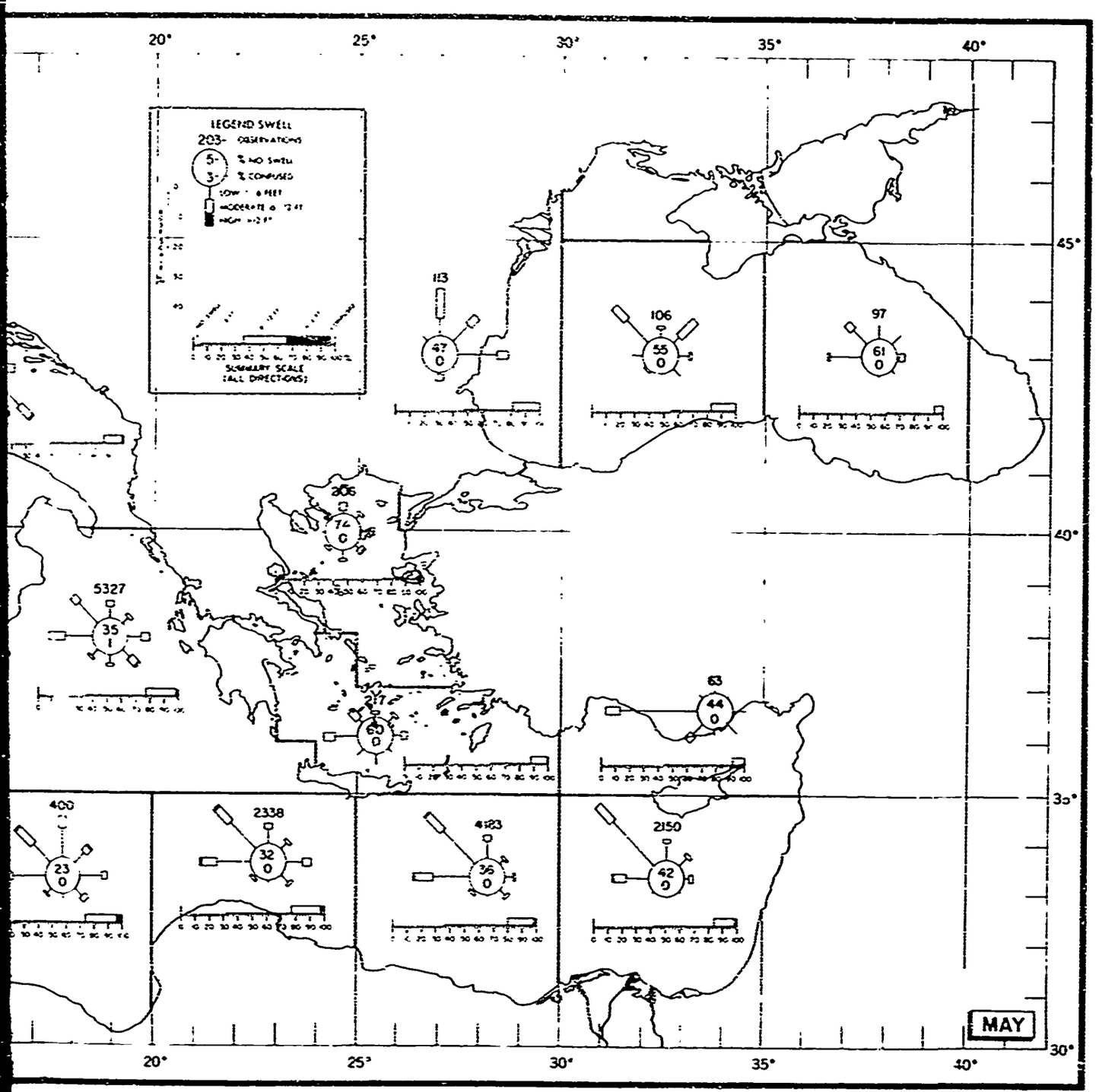

N THE MEDITERRANEAN SEA, MAY

FIGURE 18. SWELL, MAY

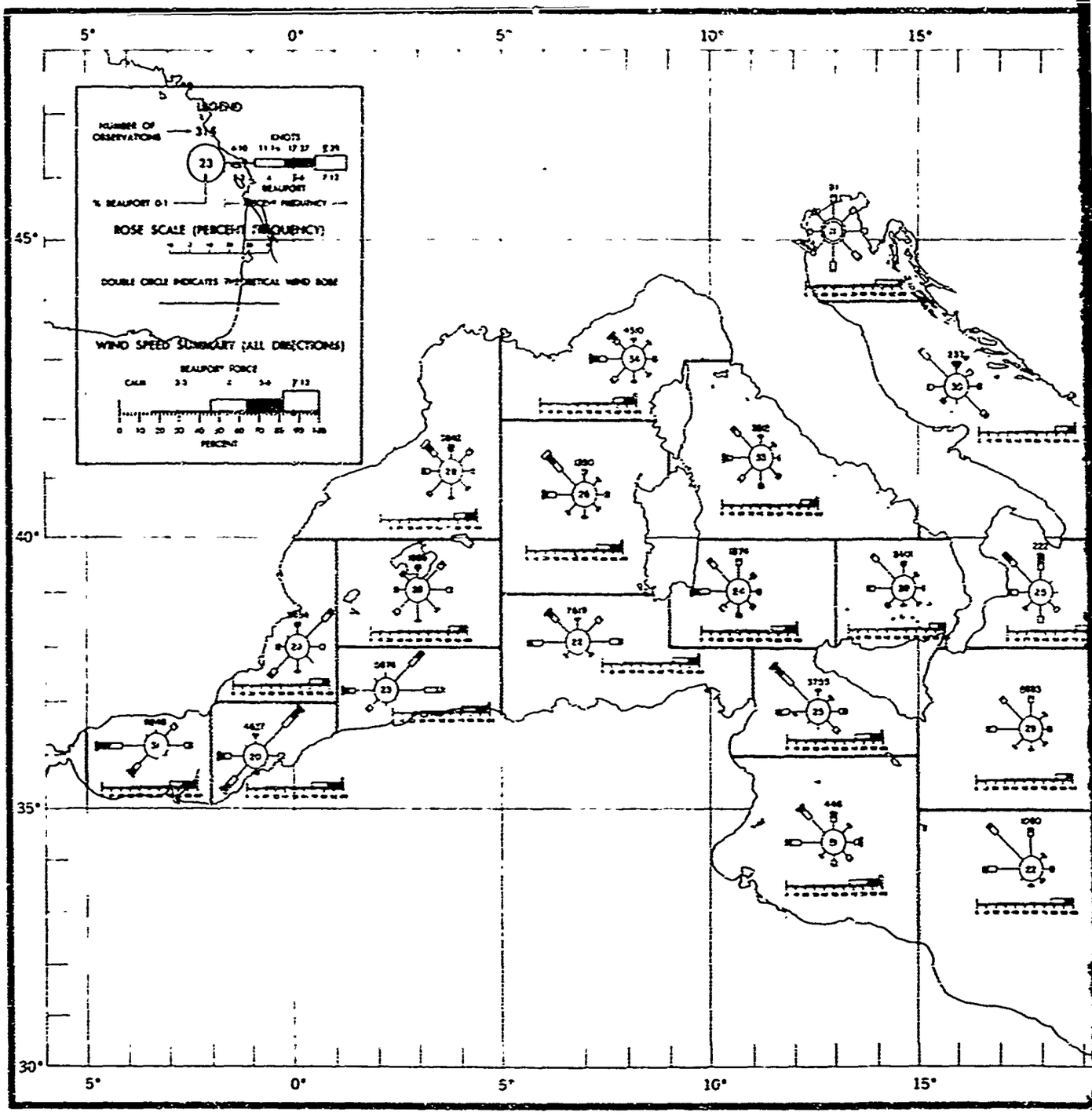

FIGURE 19. SURFACE WIND ROSES, THE MEDITE

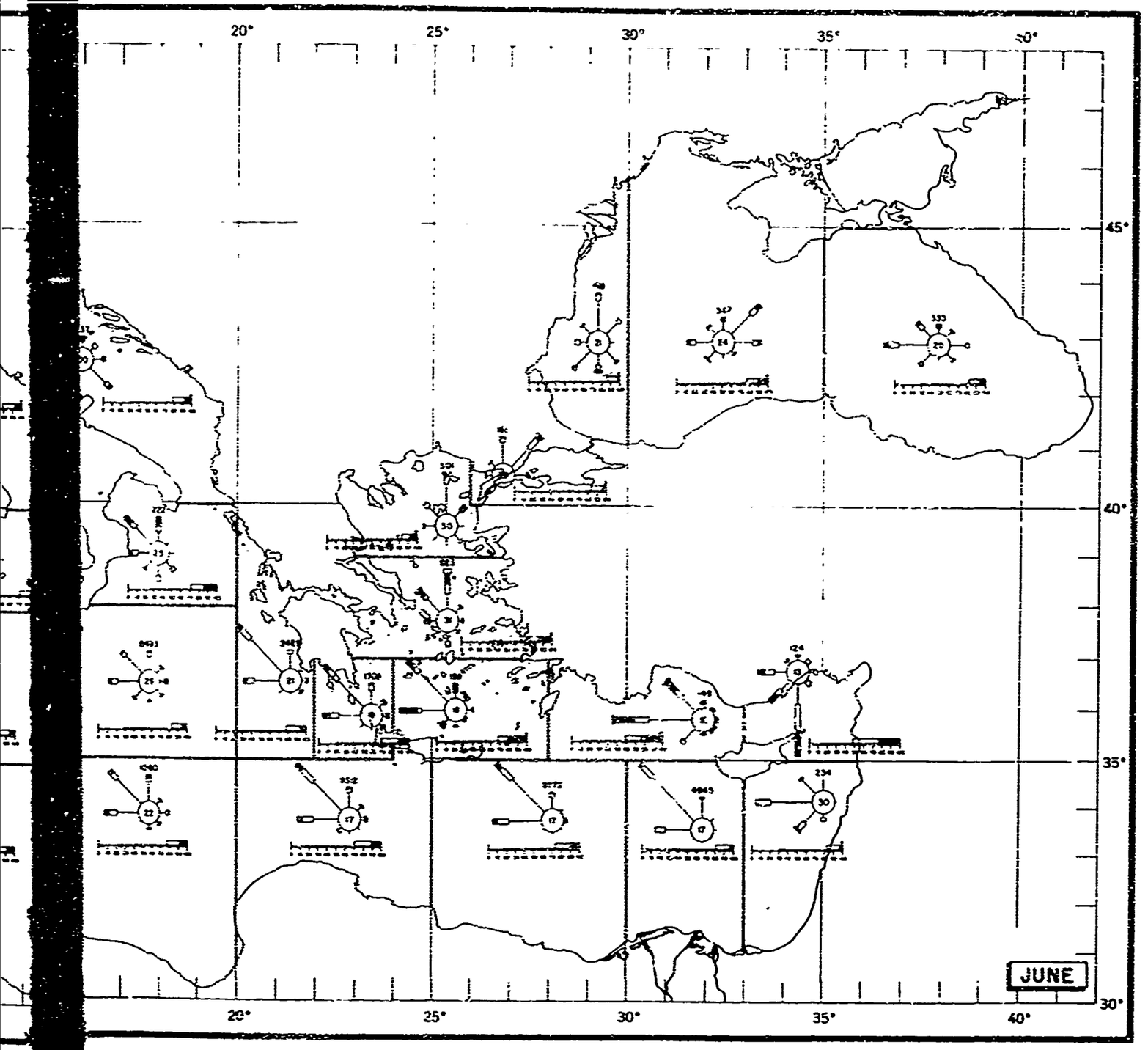

SES, THE MEDITERRANEAN SEA, JUNE

FIGURE 19. SURFACE WINDS, JUNE

2

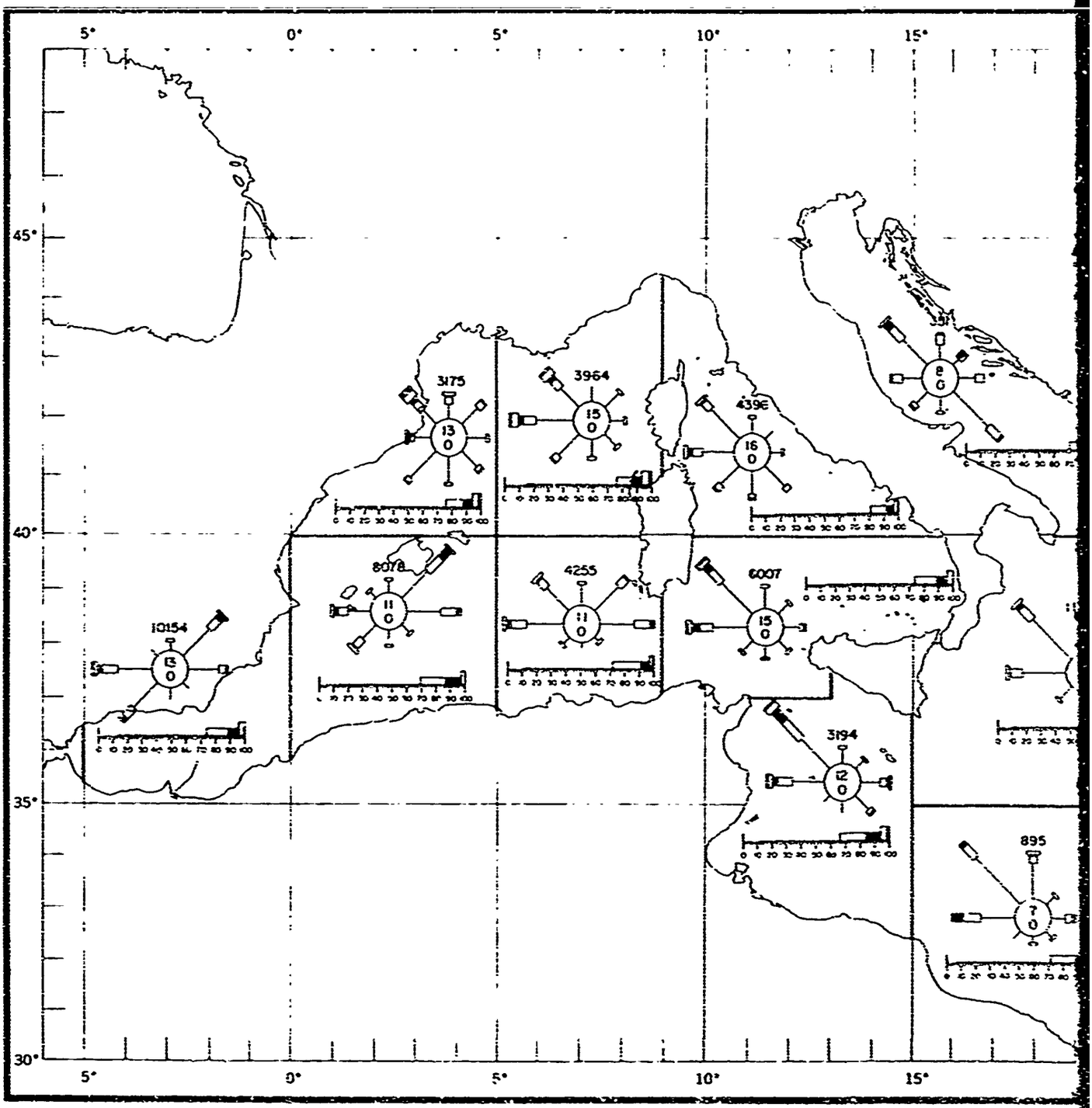

FIGURE 20. STATE OF SEA IN THE M

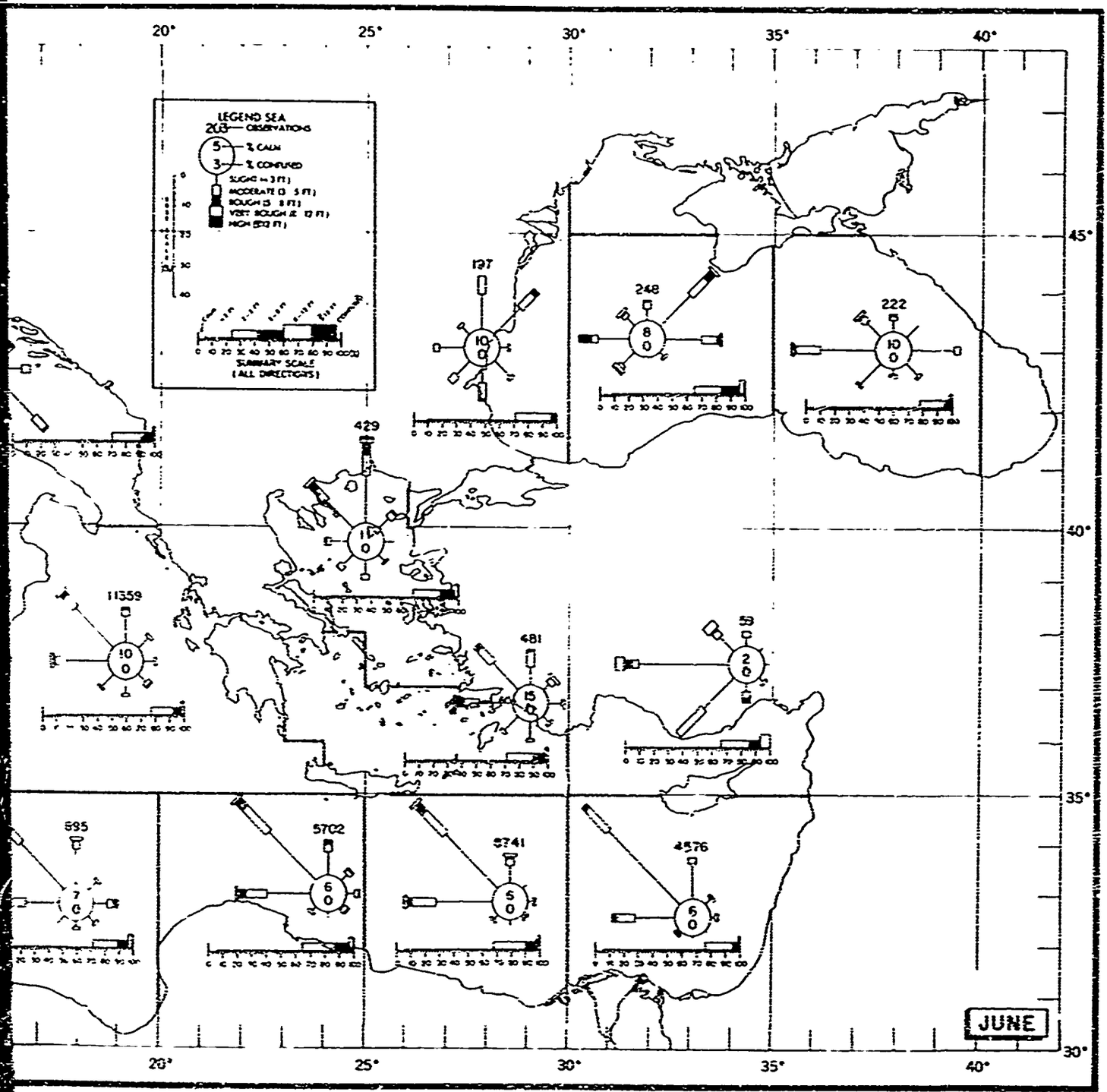

SEA IN THE MEDITERRANEAN SEA, JUNE

FIGURE 20. SEA, JUNE

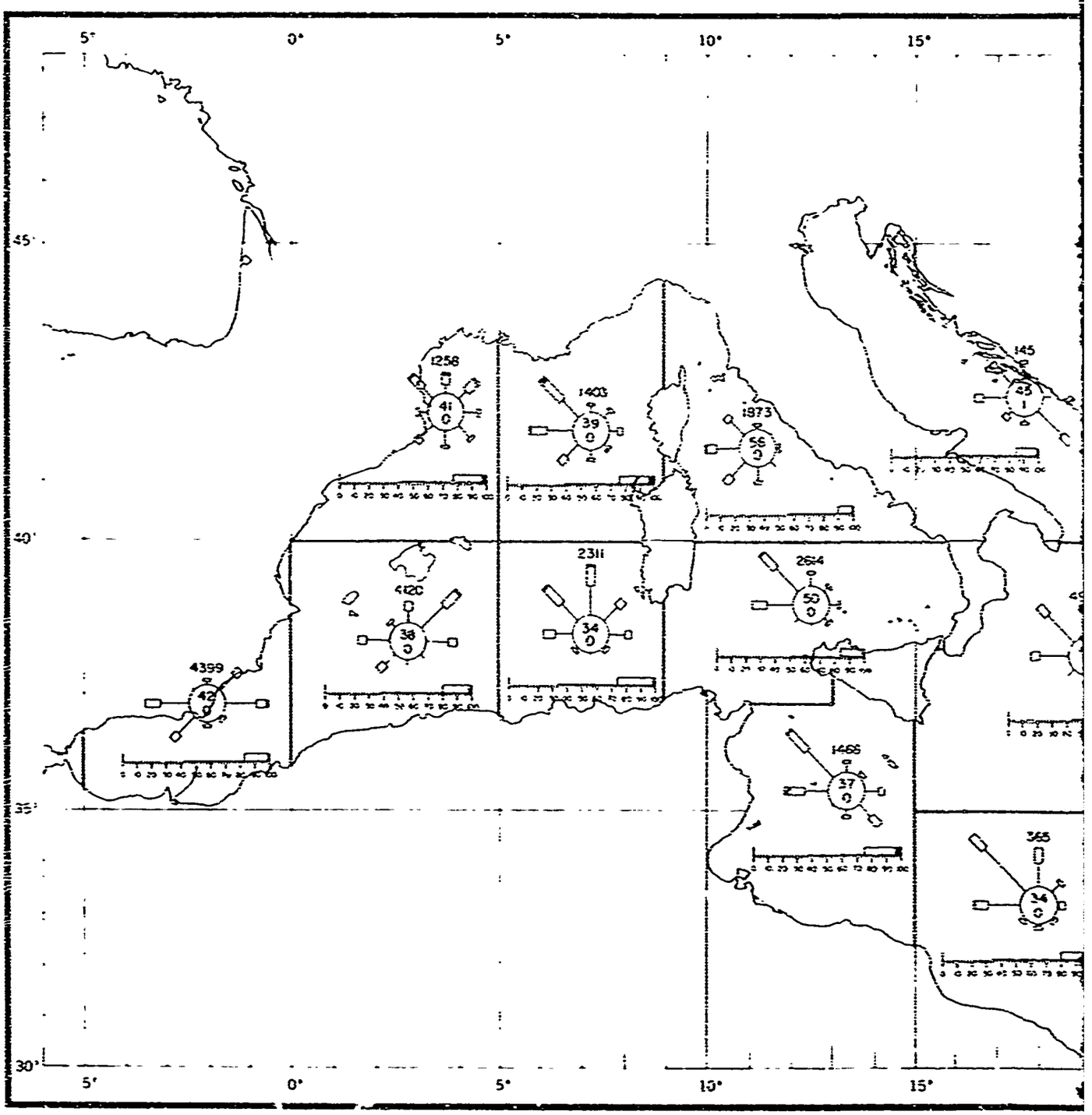

FIGURE 21. SWELL IN TH

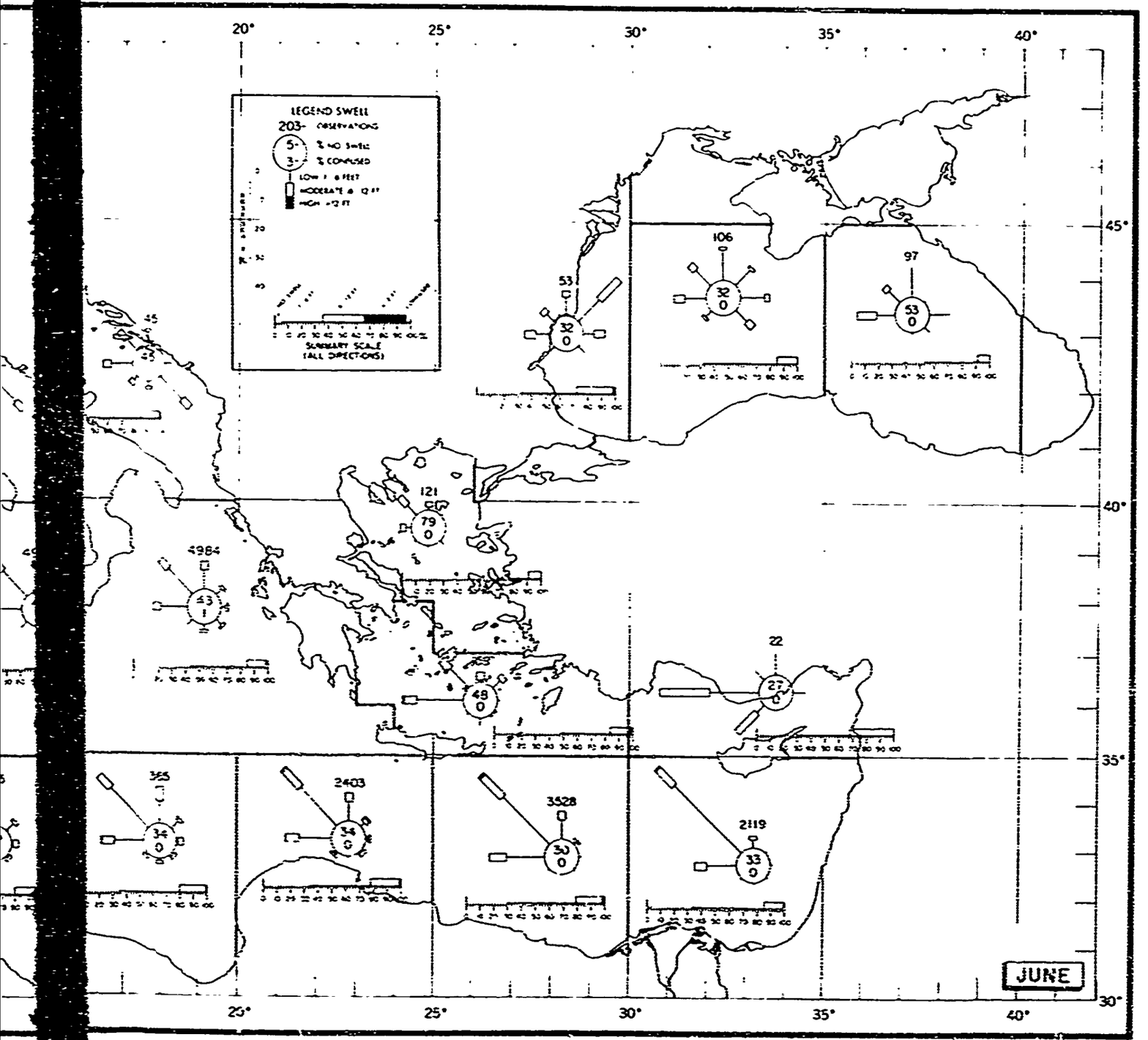

SWELL IN THE MEDITERRANEAN SEA, JUNE

FIGURE 21. SWELL, JUNE

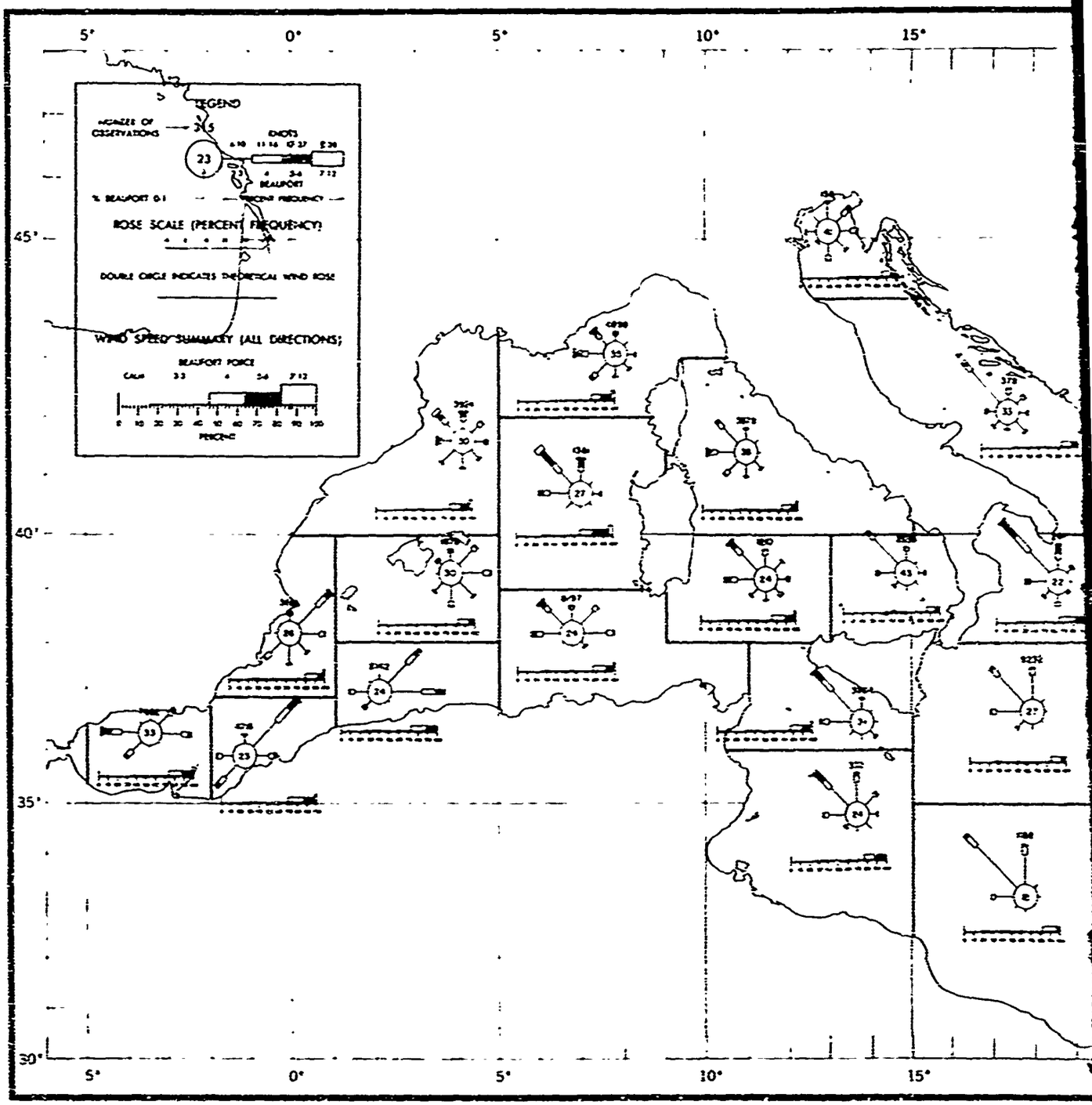

FIGURE 22. SURFACE WIND ROSES,

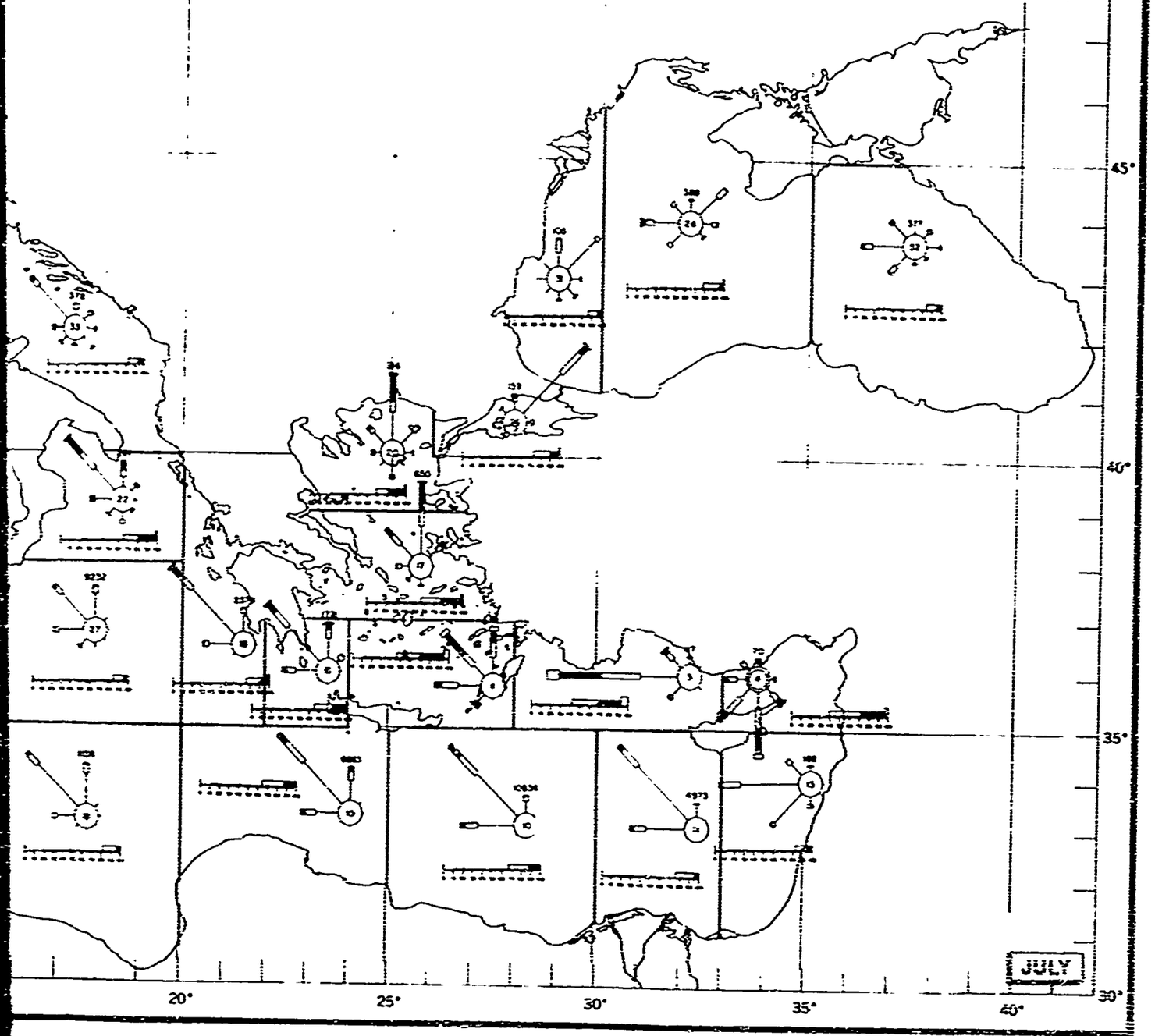

ACE WIND ROSES, THE MEDITERRANEAN SEA, JULY

FIGURE 27. SURFACE WINDS, JULY

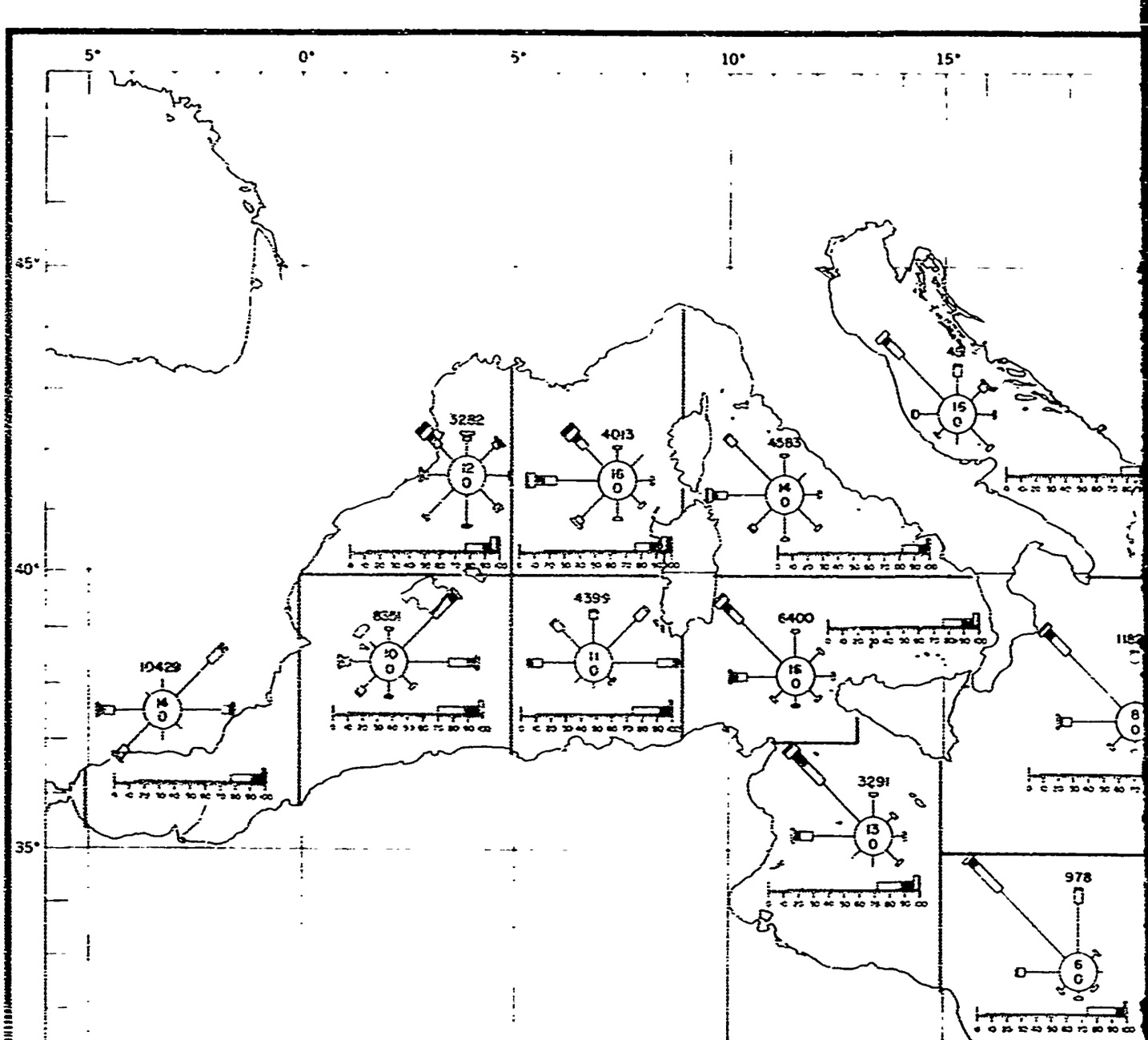

FIGURE 23. STATE OF SEA IN THE MEDITERRANEAN

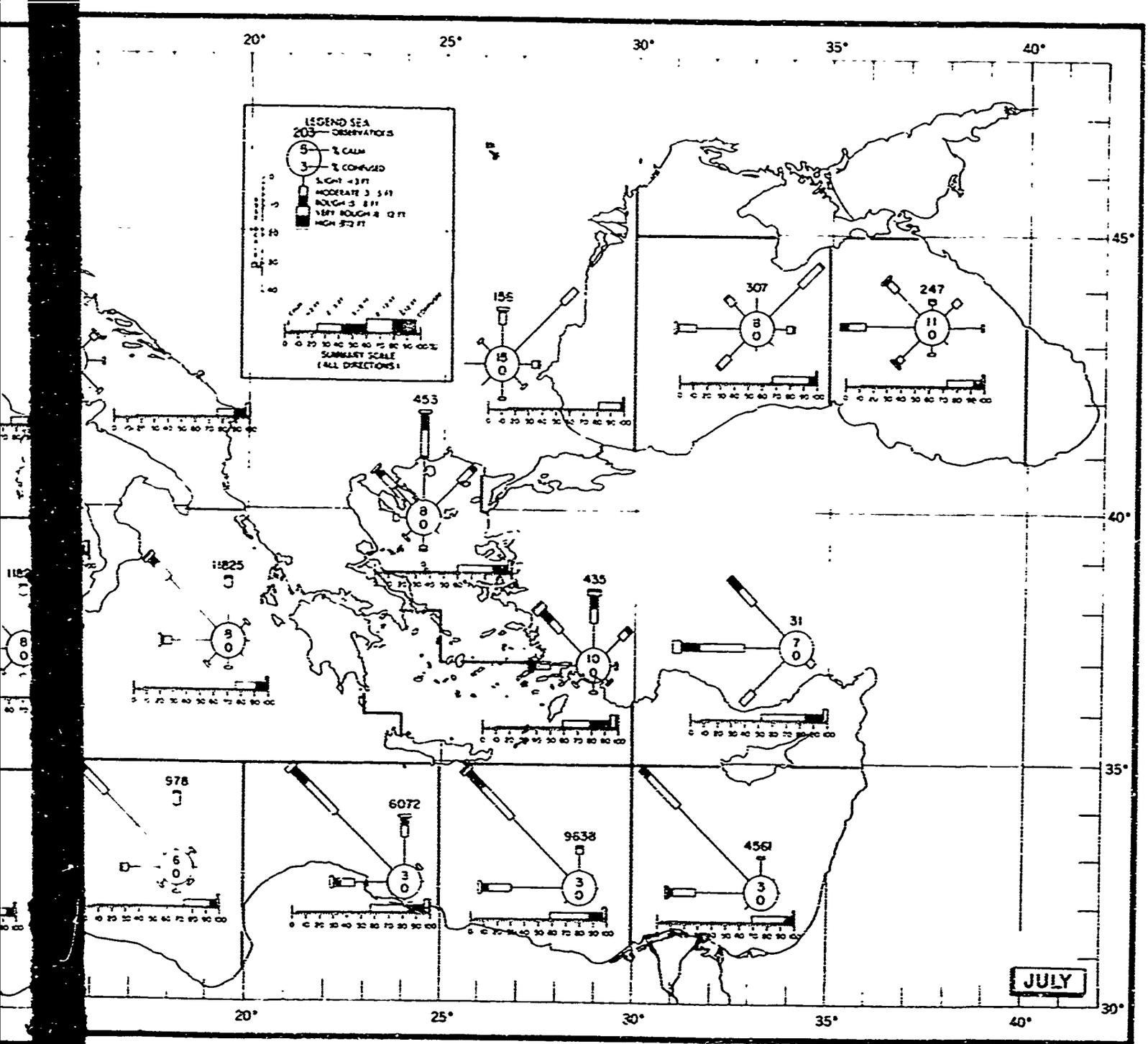

HE MEDITERRANEAN SEA, JULY

FIGURE 23. SEA, JULY

2

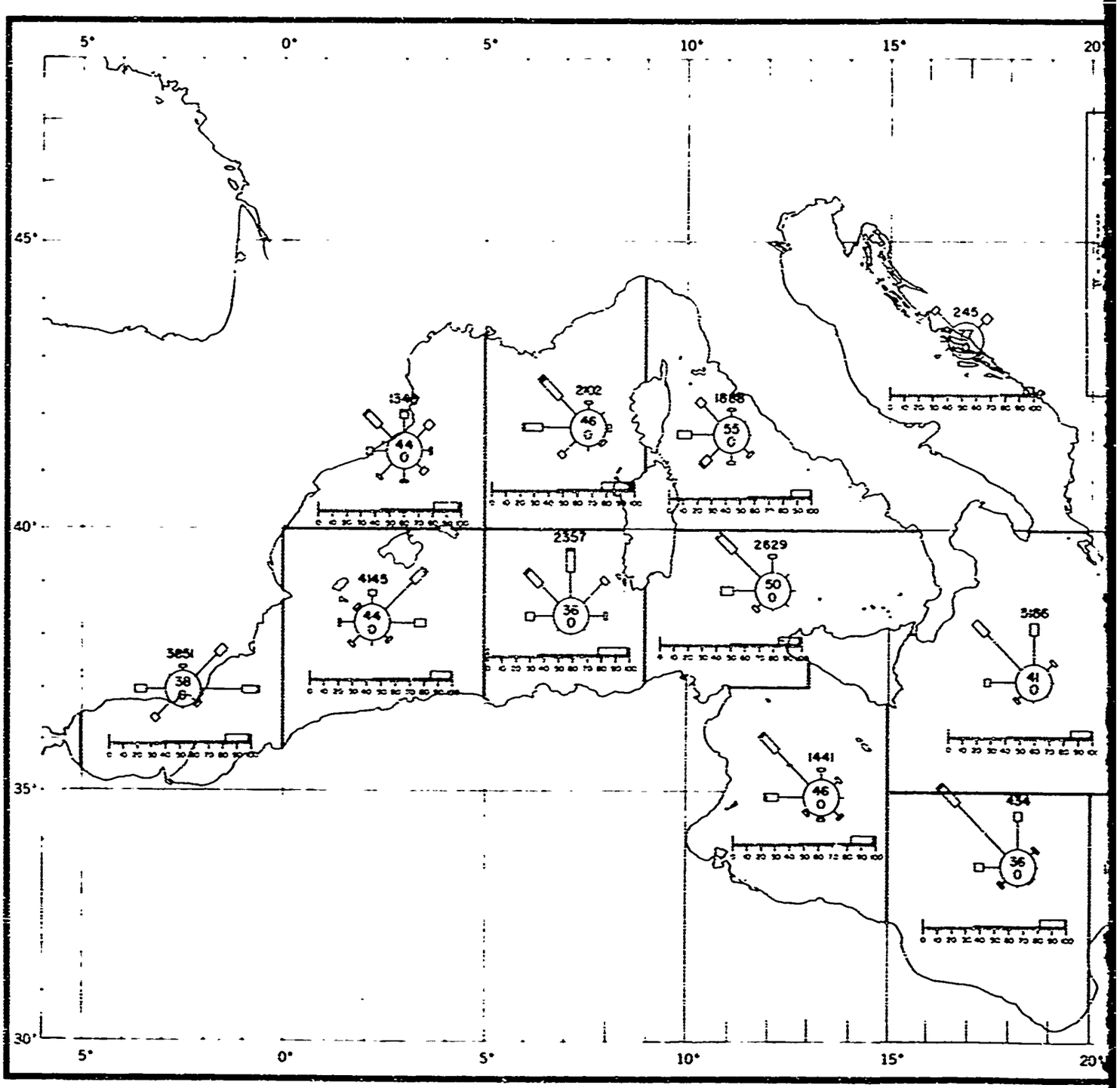

FIGURE 24. SWELL IN THE MEDITERRANEAN

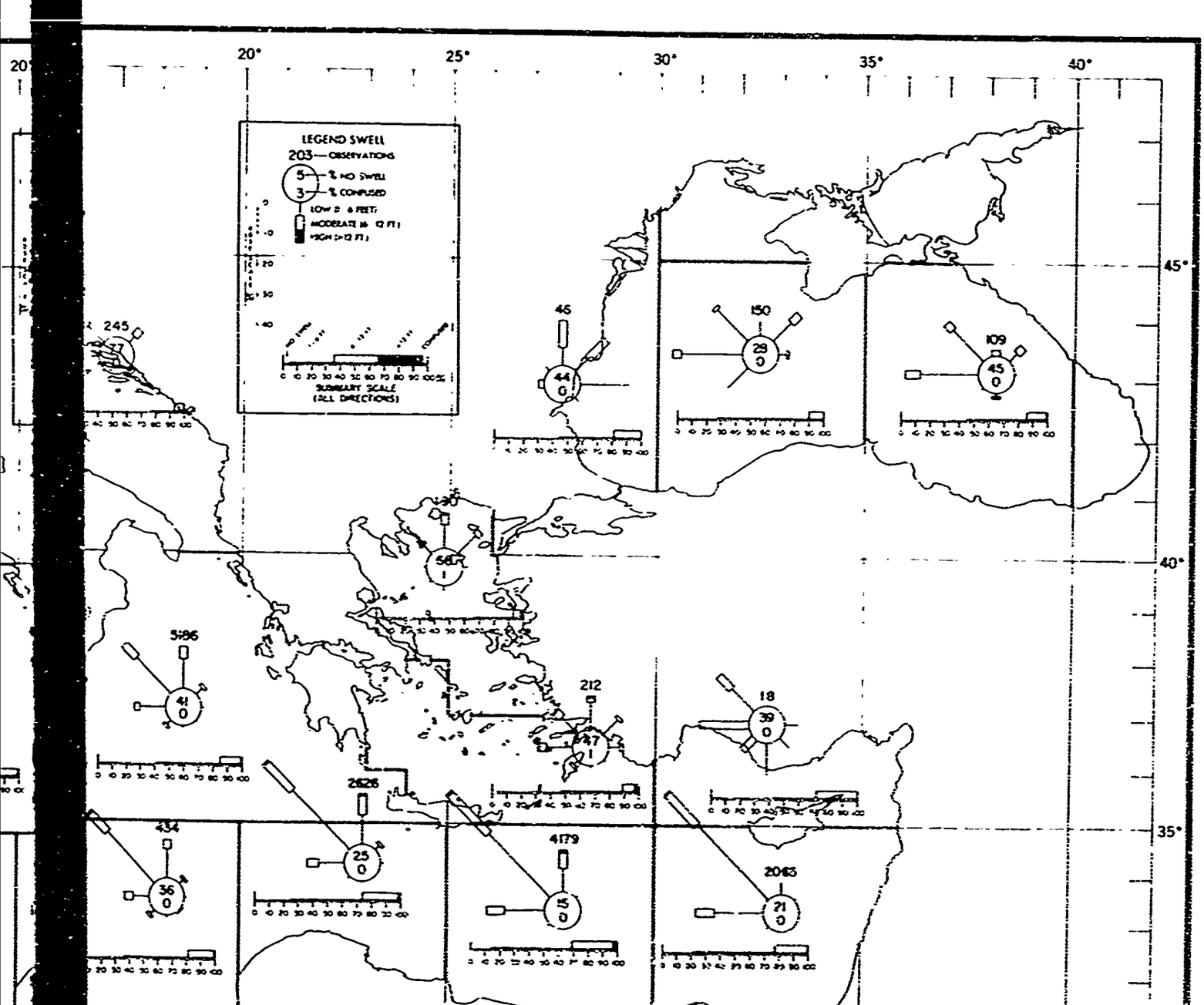

N THE MEDITERRANEAN SEA, JULY

FIGURE 24. SWELL, JULY

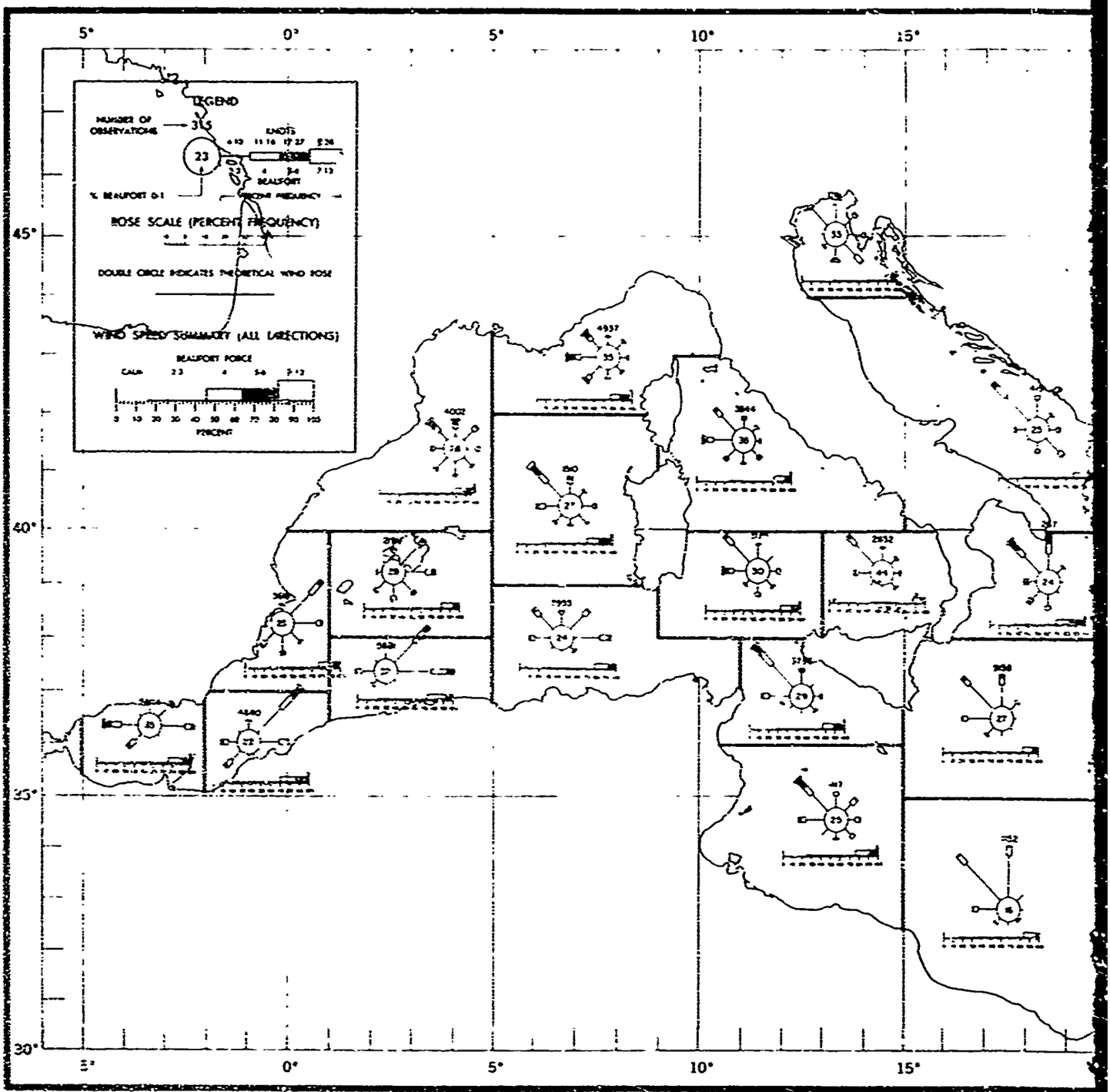

FIGURE 25. SURFACE WIND ROSES, THE MEDI

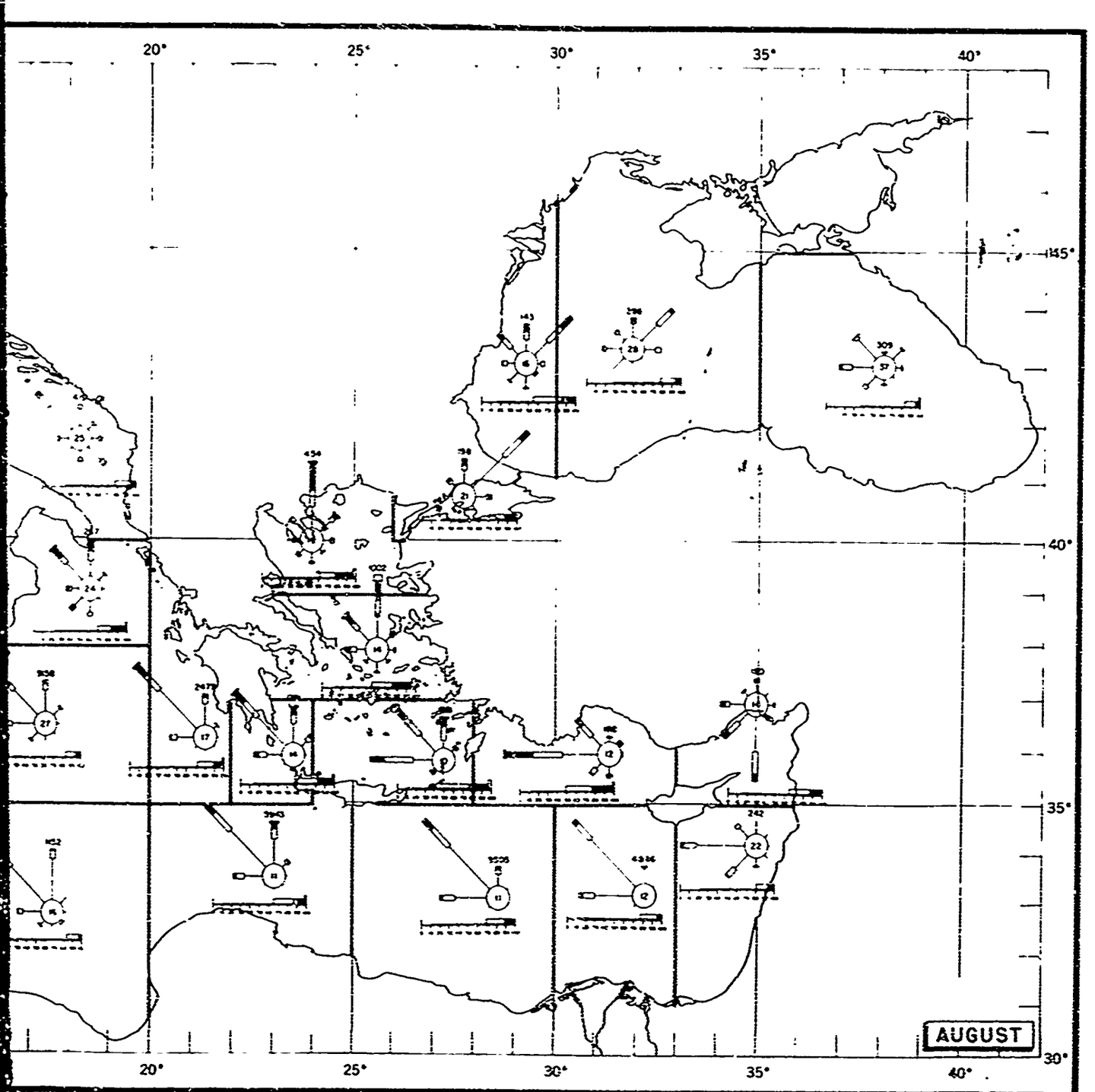

OSES, THE MEDITERRANEAN SEA, AUGUST

FIGURE 25. SURFACE WINDS, AUGUST

2

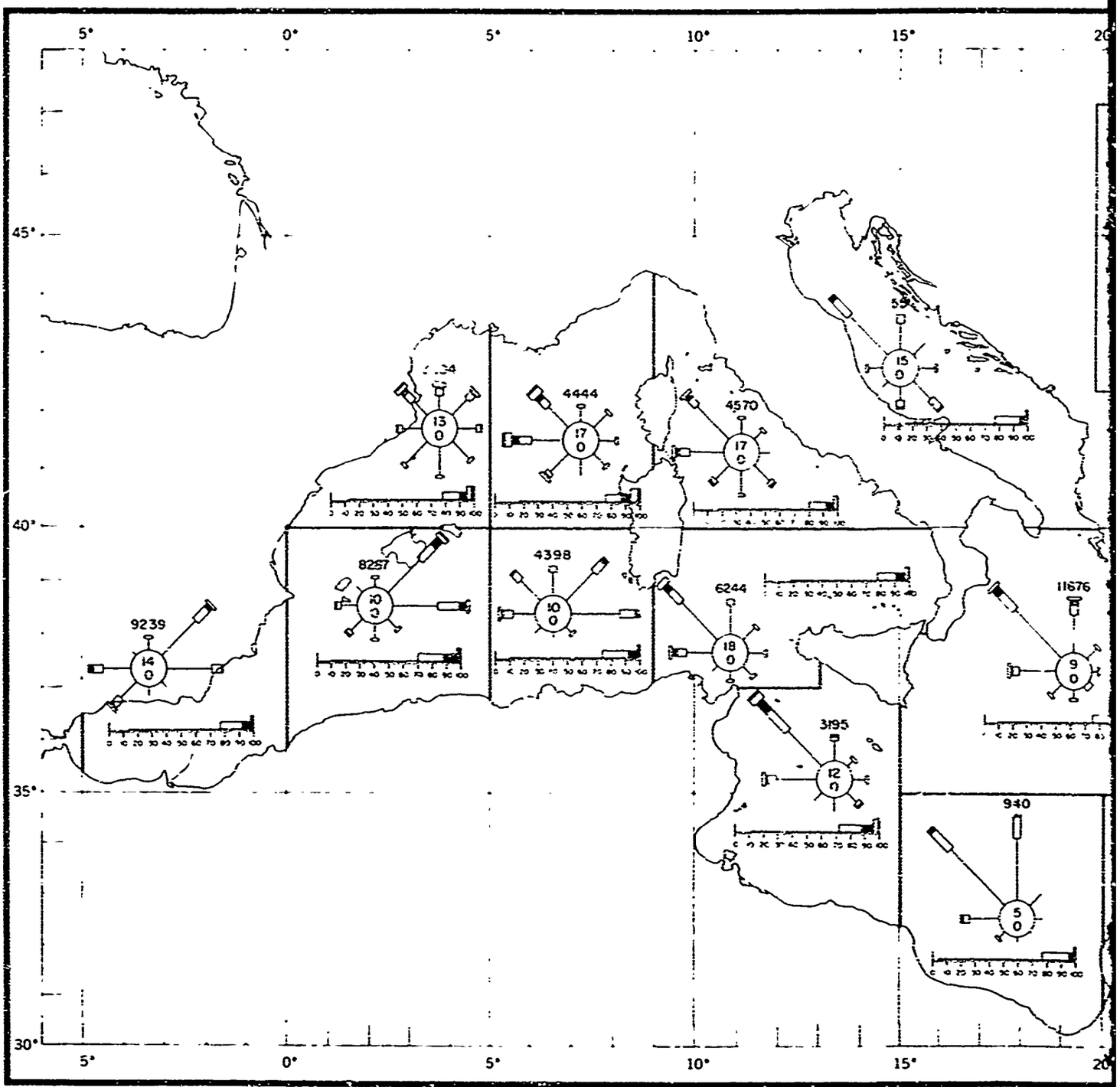

FIGURE 26. STATE OF SEA IN THE MEDITERRA

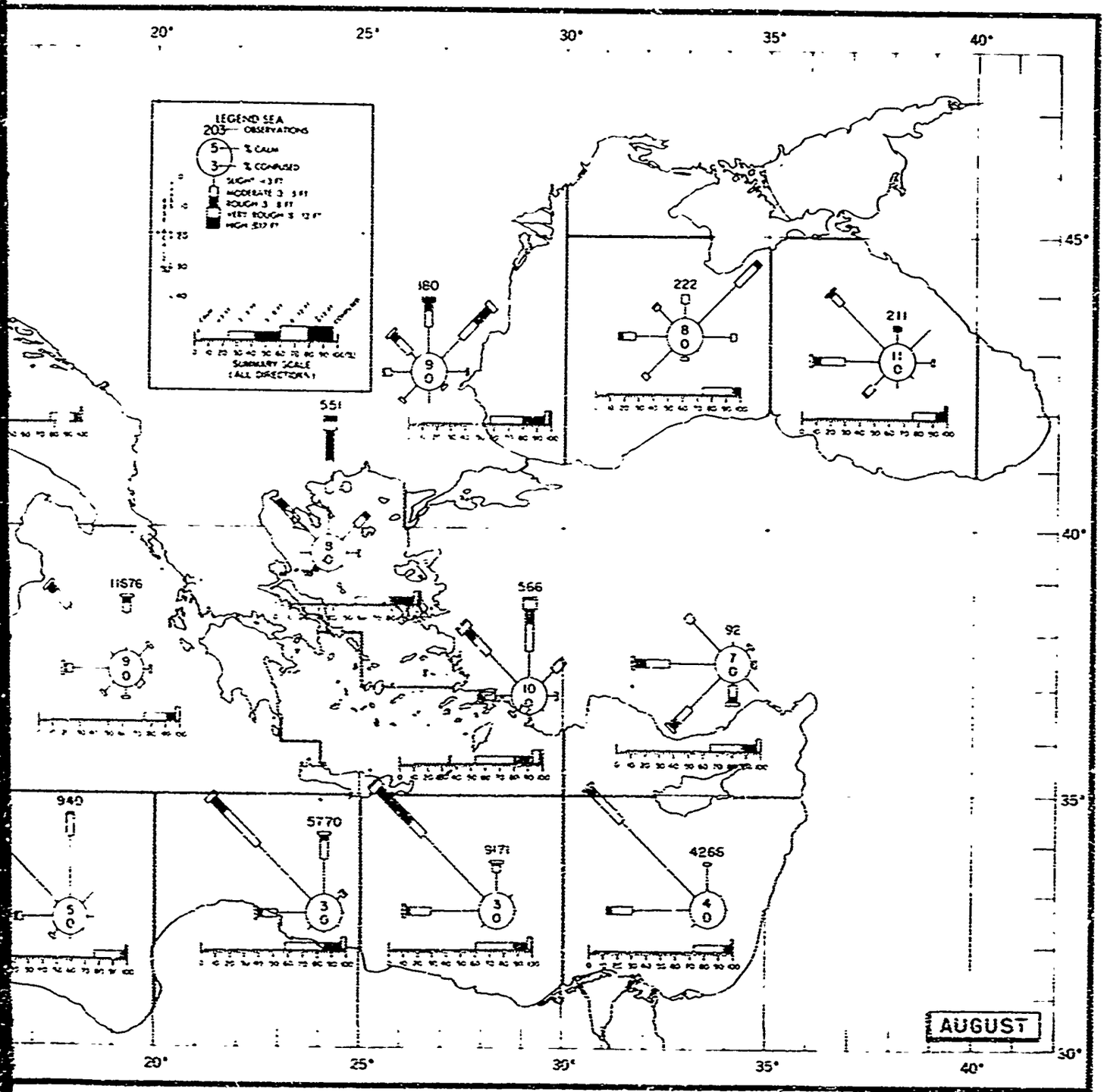

A IN THE MEDITERRANEAN SEA, AUGUST

FIGURE 26. SEA, AUGUST

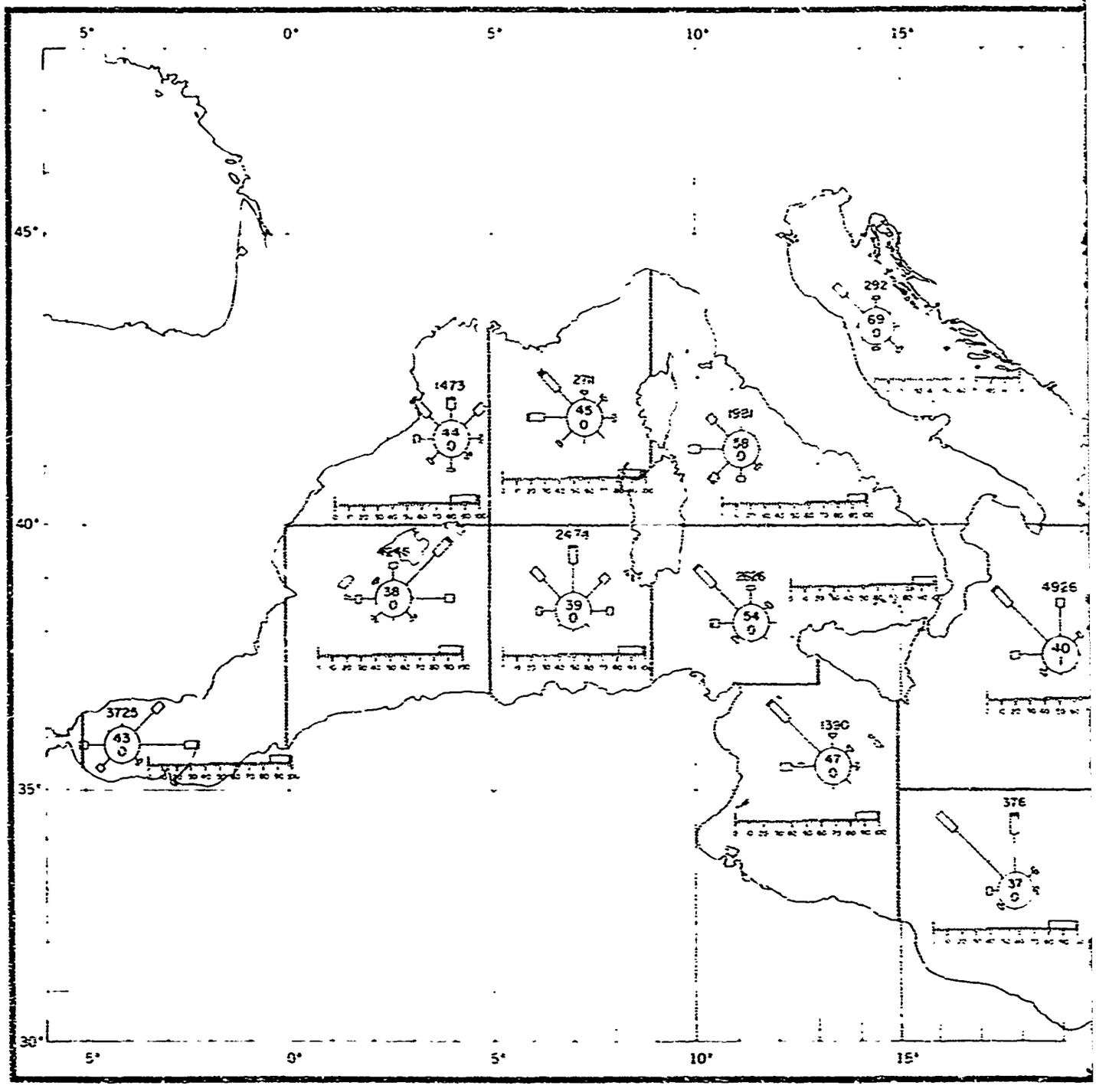

FIGURE 27. SWELL IN THE MEDITER

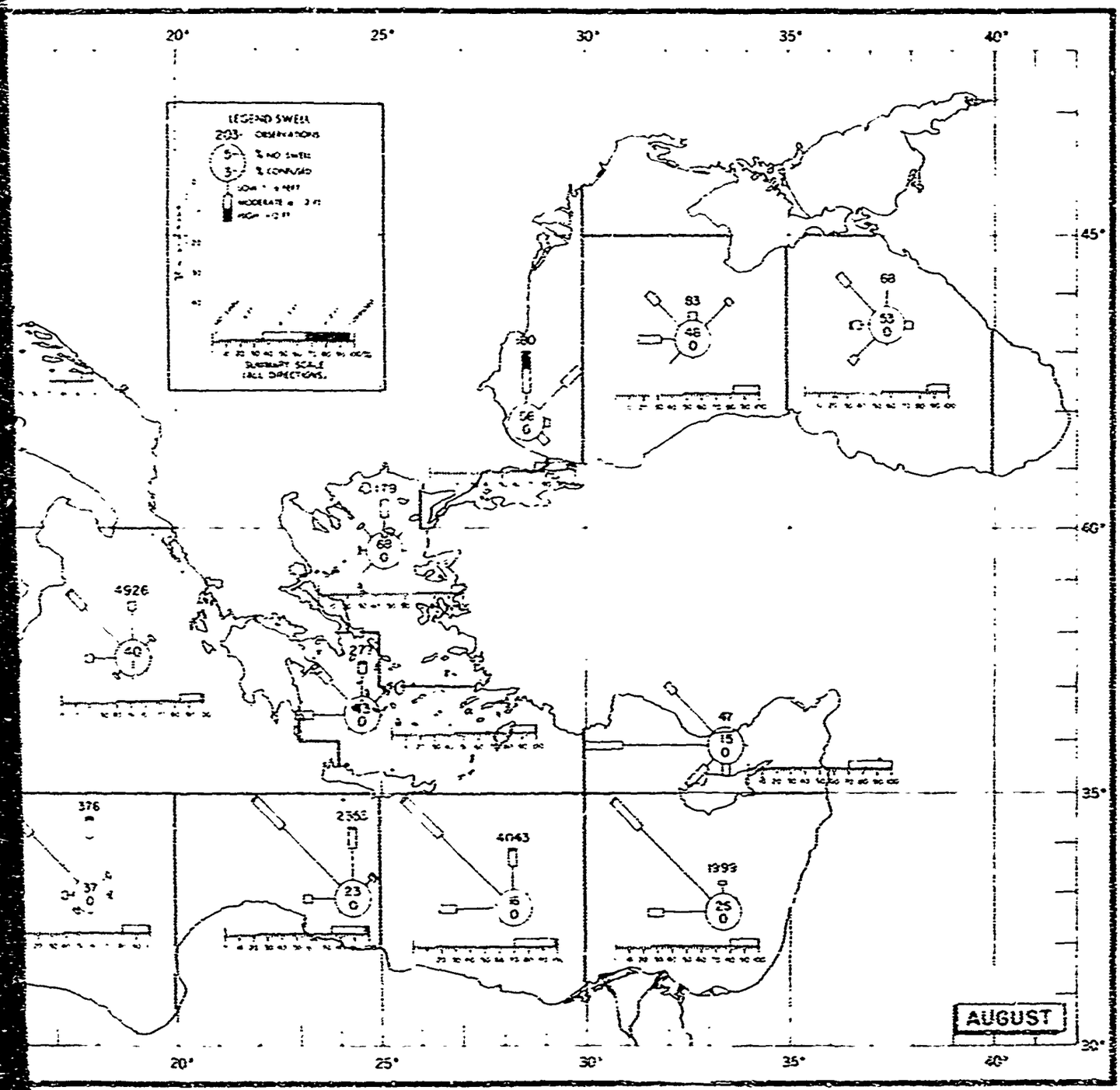

L IN THE MEDITERRANEAN SEA, AUGUST

FIGURE 27. SWELL, AUGUST

2

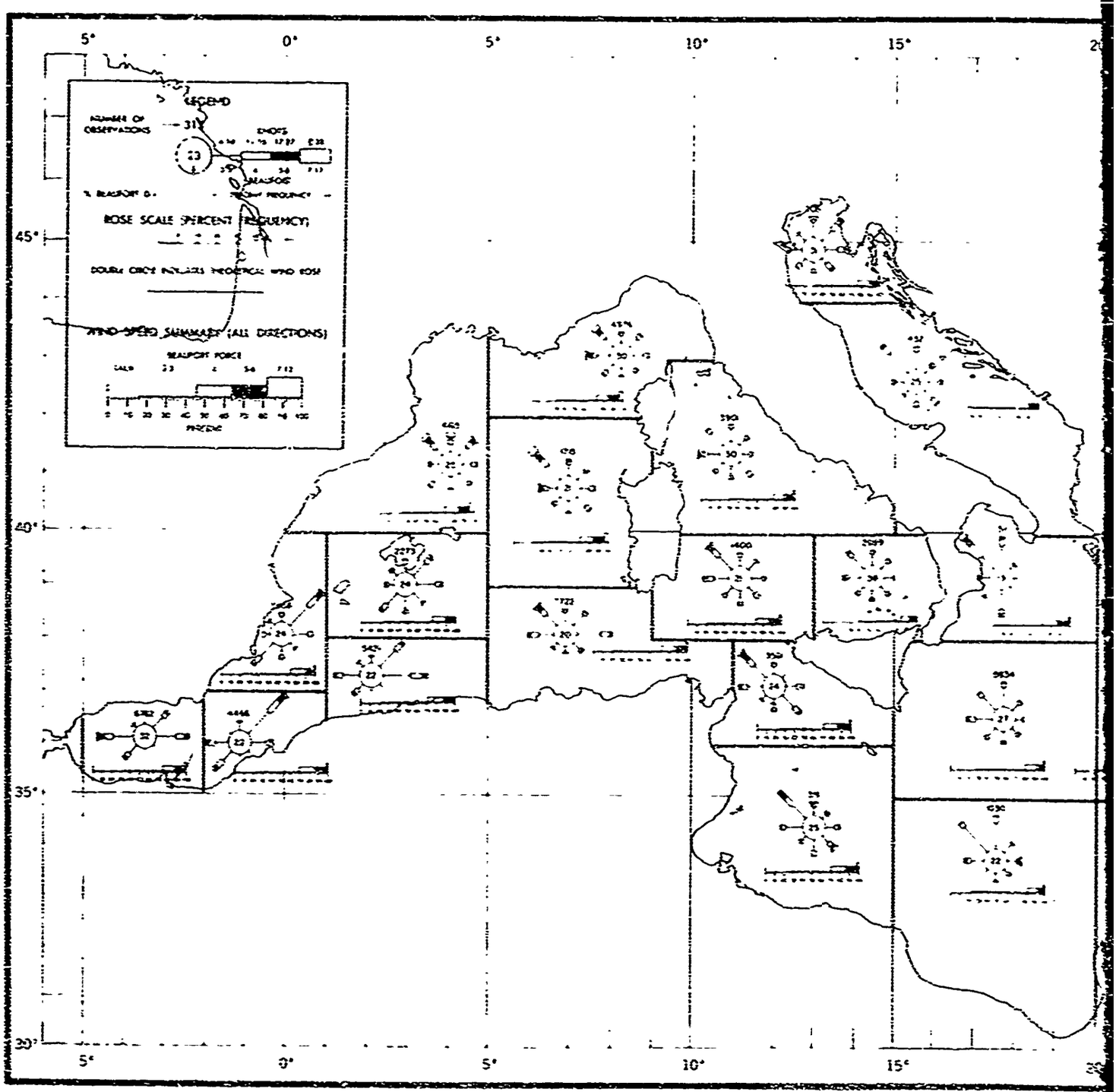

FIGURE 28. SURFACE WIND ROSES, THE MEDITE

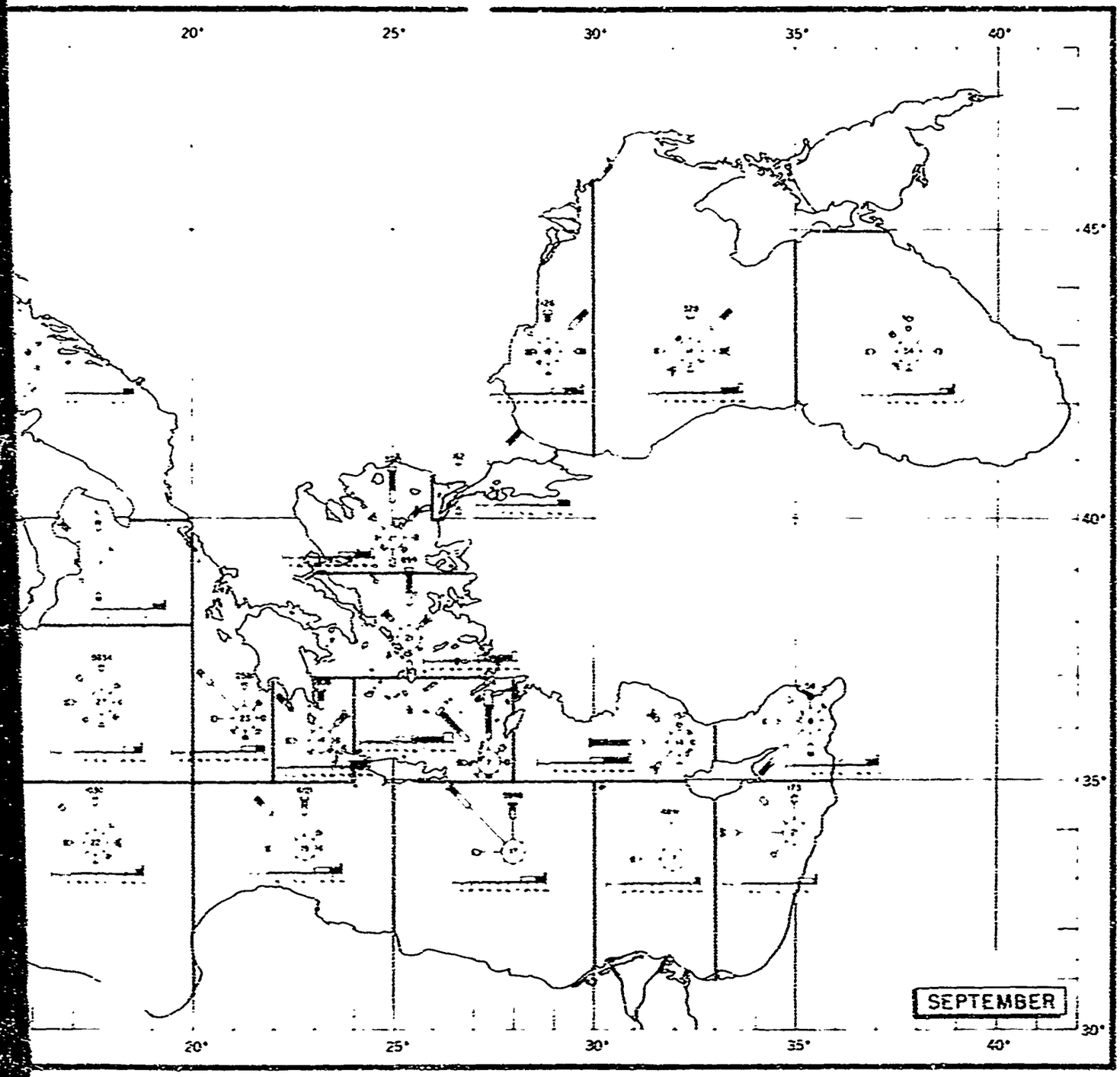

ND ROSES, THE MEDITERRANEAN SEA, SEPTEMBER

FIGURE 28. SURFACE WINDS, SEPTEMBER

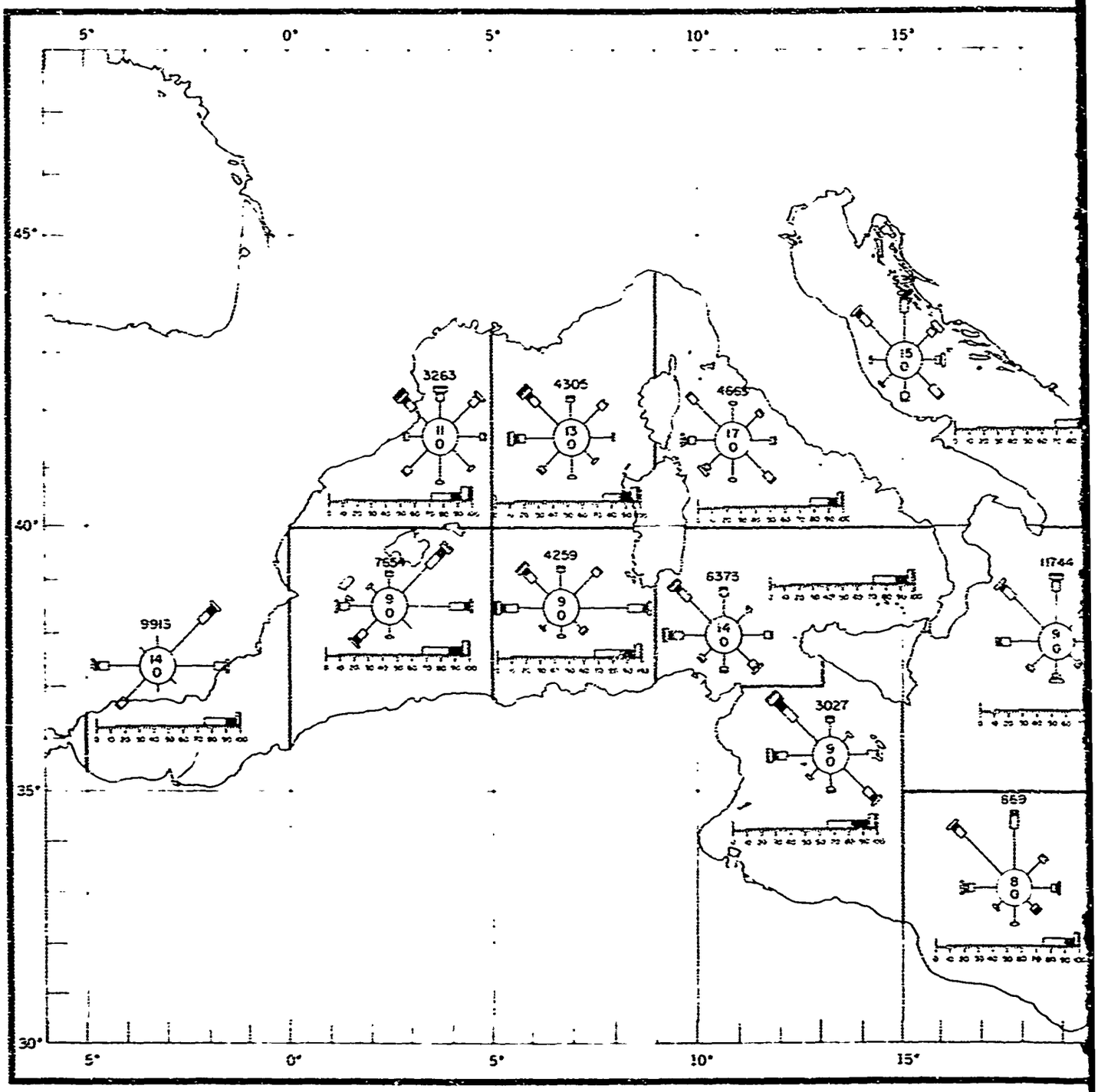

FIGURE 29. STATE OF SEA IN THE MEDITERRAN

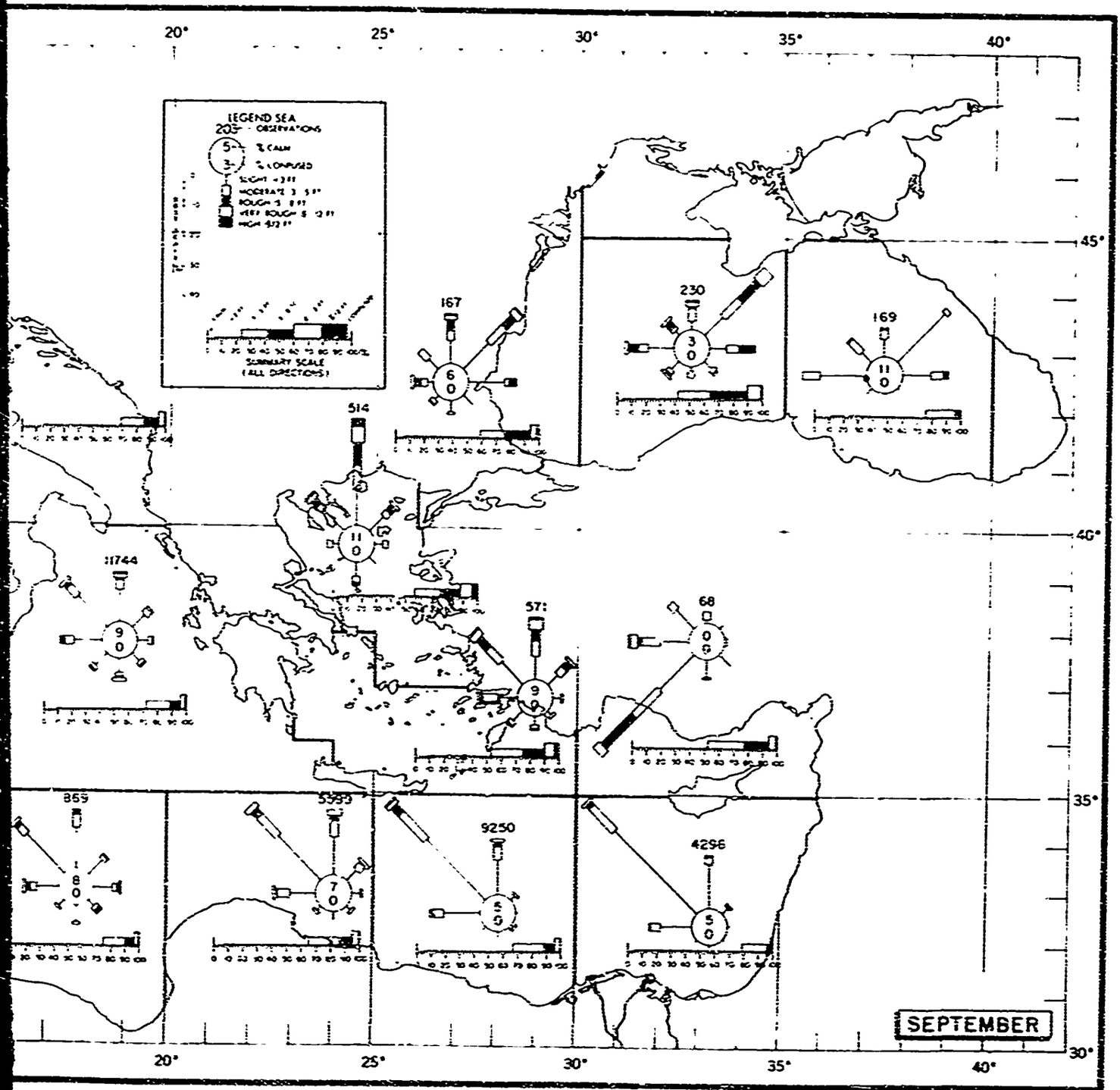

THE MEDITERRANEAN SEA, SEPTEMBER

FIGURE 29. SEA, SEPTEMBER

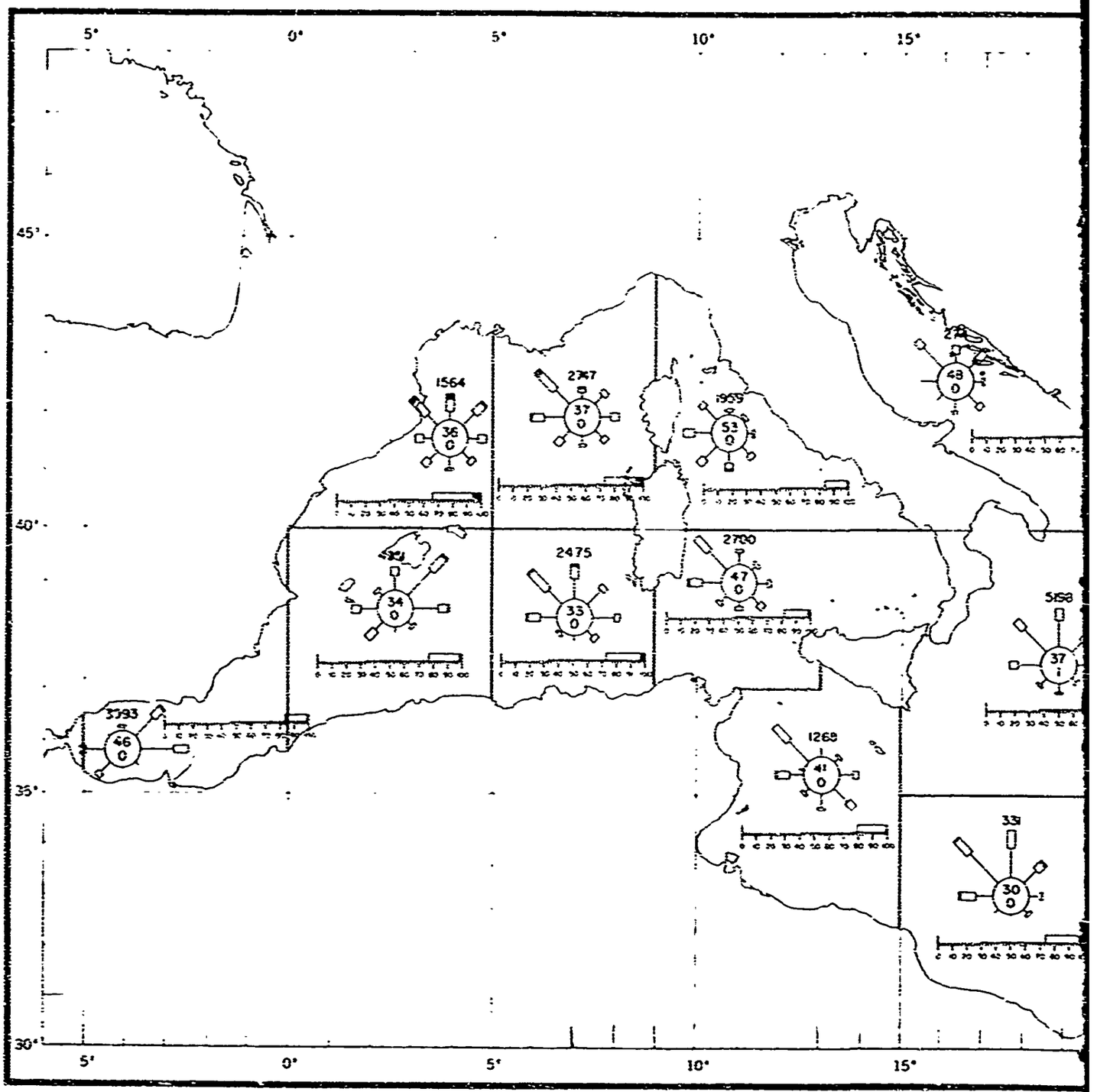

FIGURE 30. SWELL IN THE MEDITERRANEAN

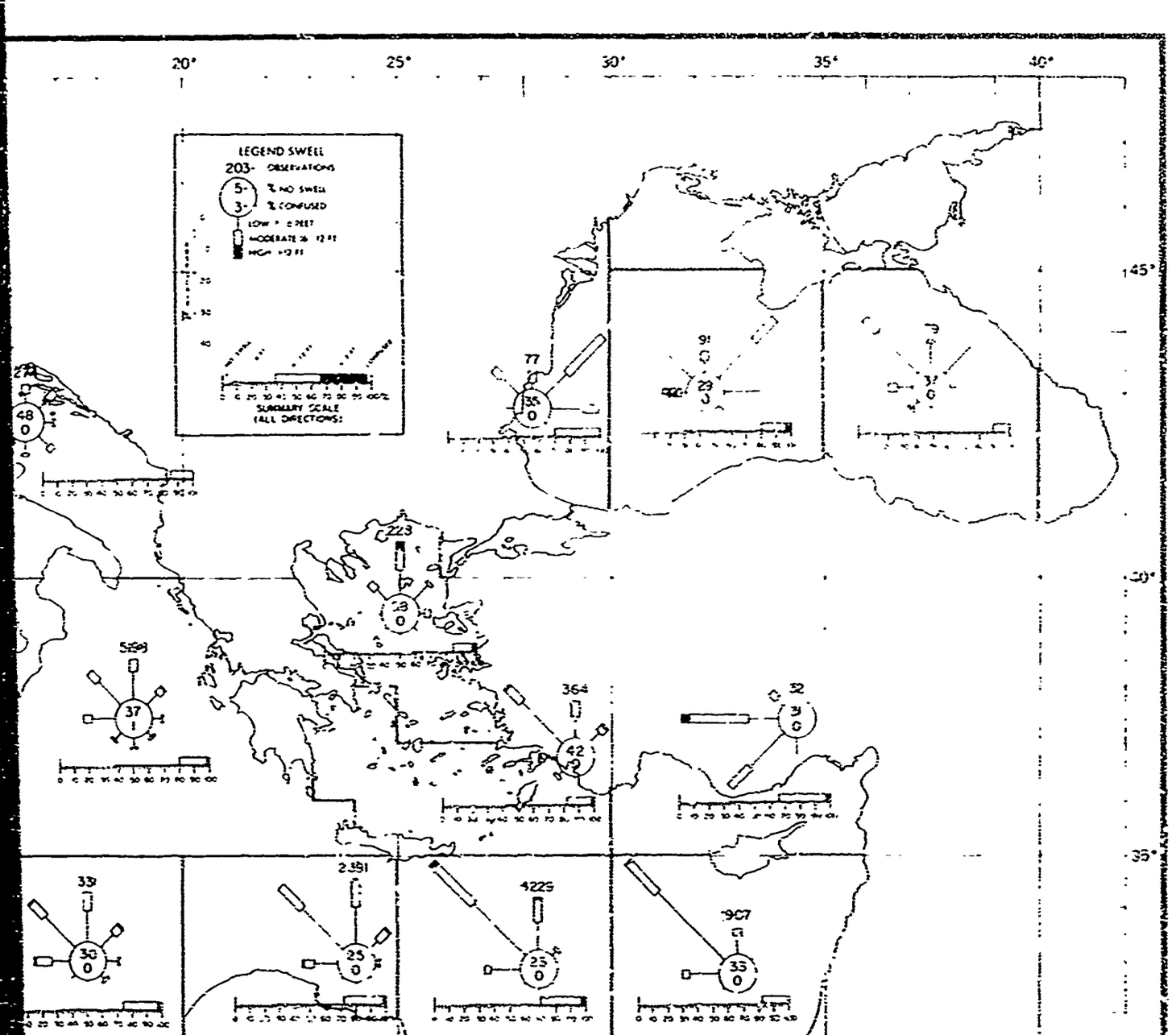

MEDITERRANEAN SEA, SEPTEMBER

FIGURE 30. SWELL, SEPTEMBER

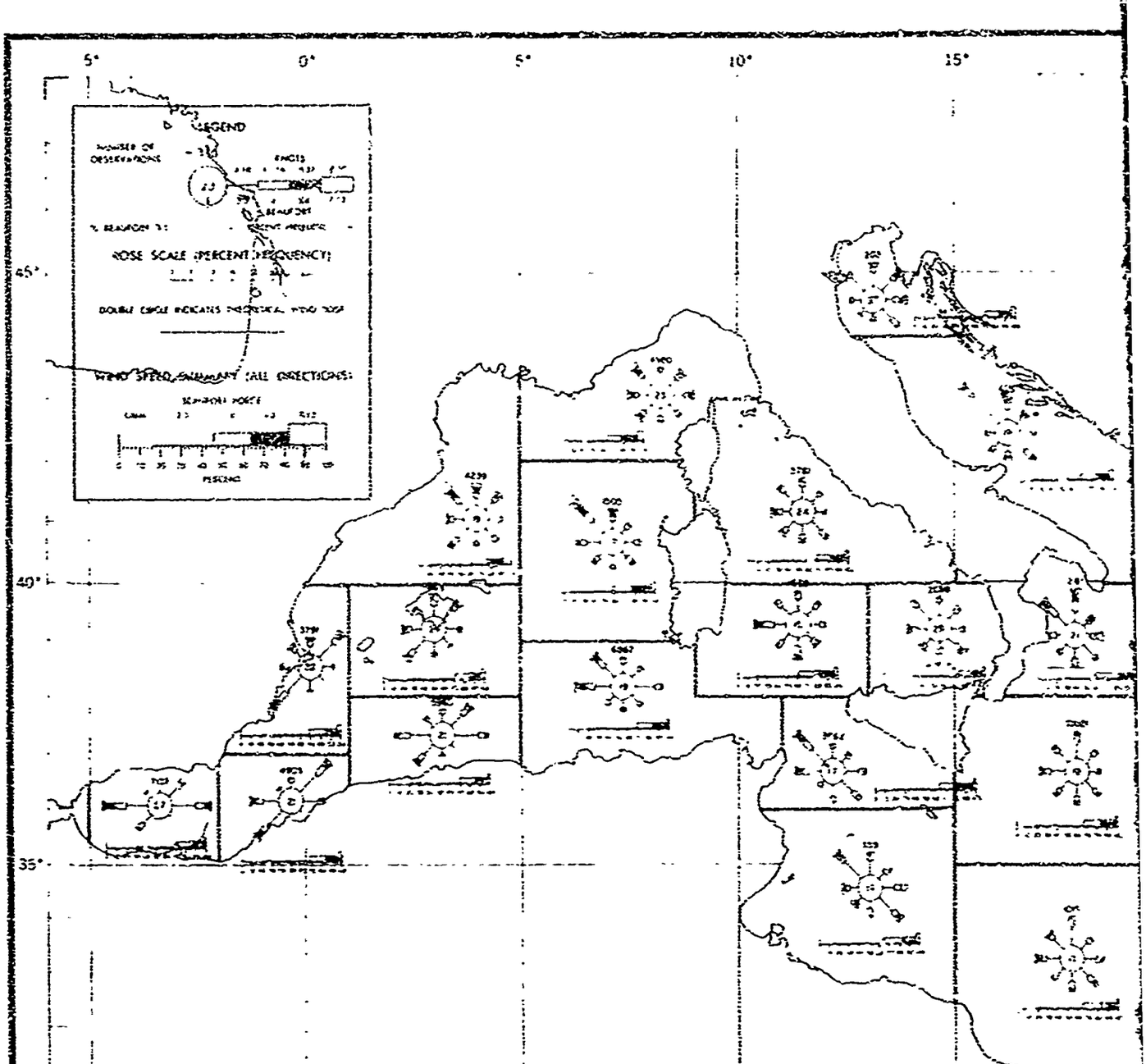

FIGURE 31. SURFACE WIND ROSES THE MEDITE

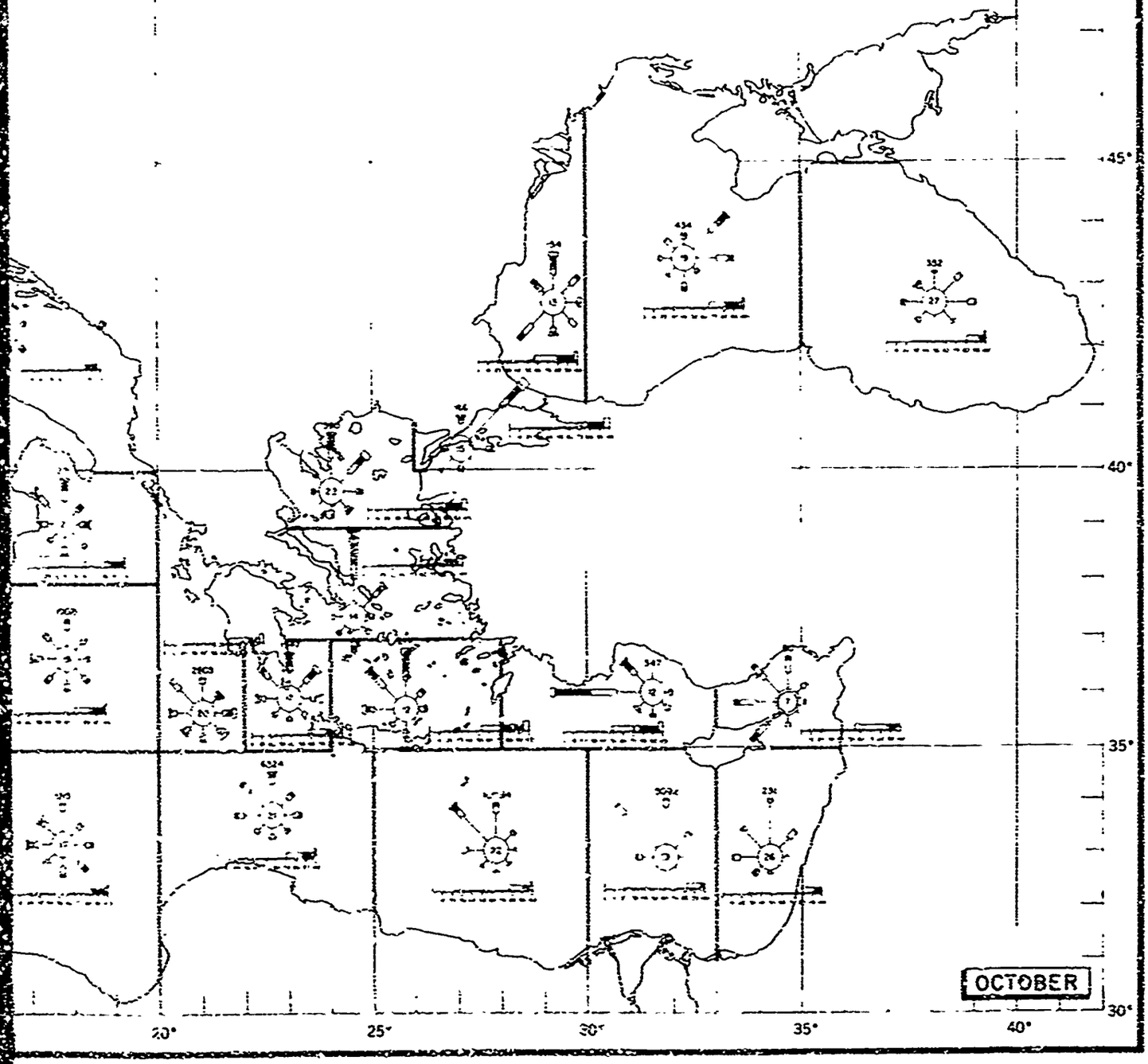

G, THE MEDITERRANEAN SEA, OCTOBER

FIGURE 31. SURFACE WINDS, OCTOBER

2

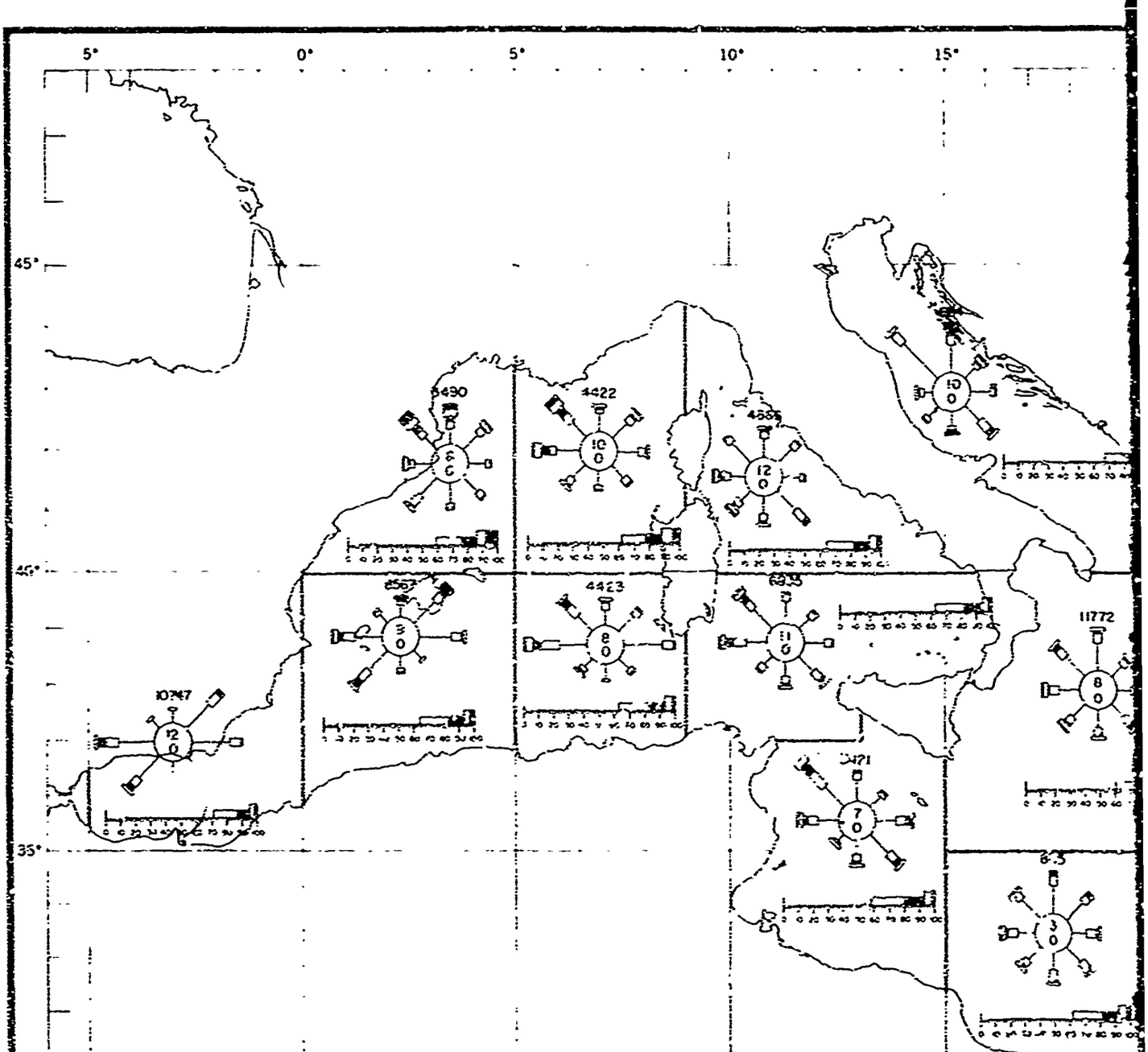

FIGURE 22. STATE OF SEA IN THE MEDITERRANEAN

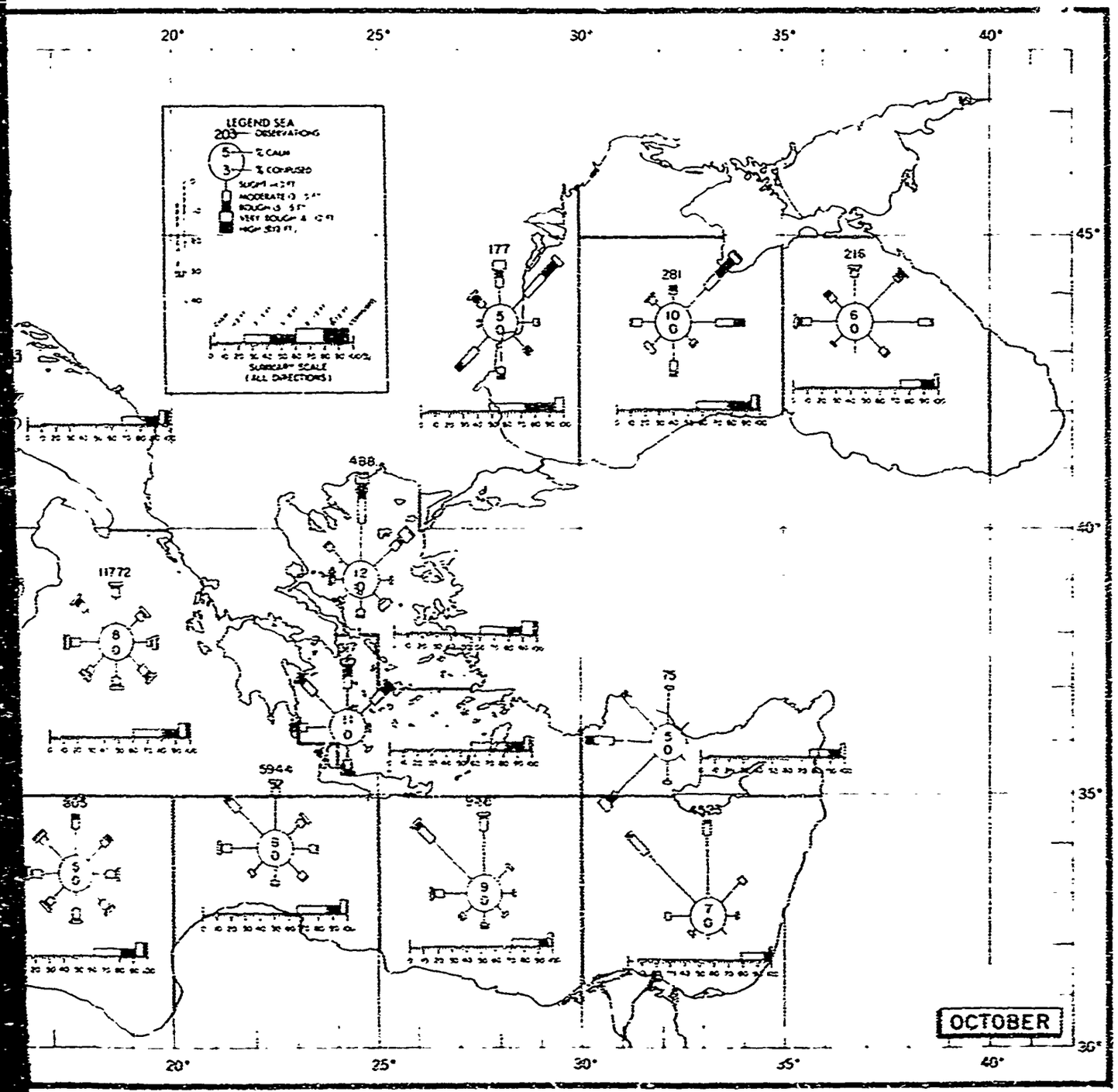

THE MEDITERRANEAN SEA, OCTOBER

FIGURE 32. SEA, OCTOBER

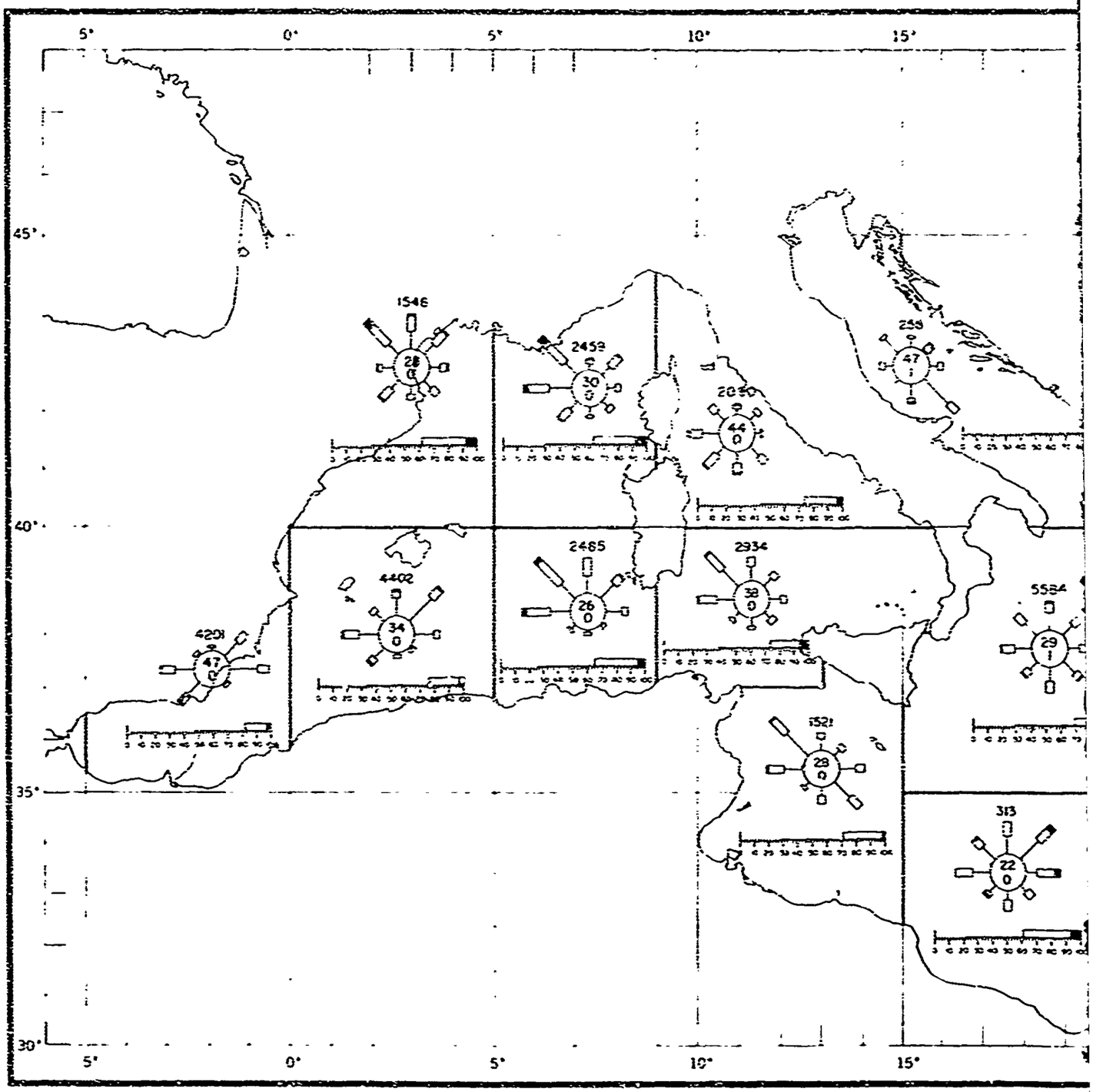

FIGURE 33. SWELL IN THE MEDITERRANEAN

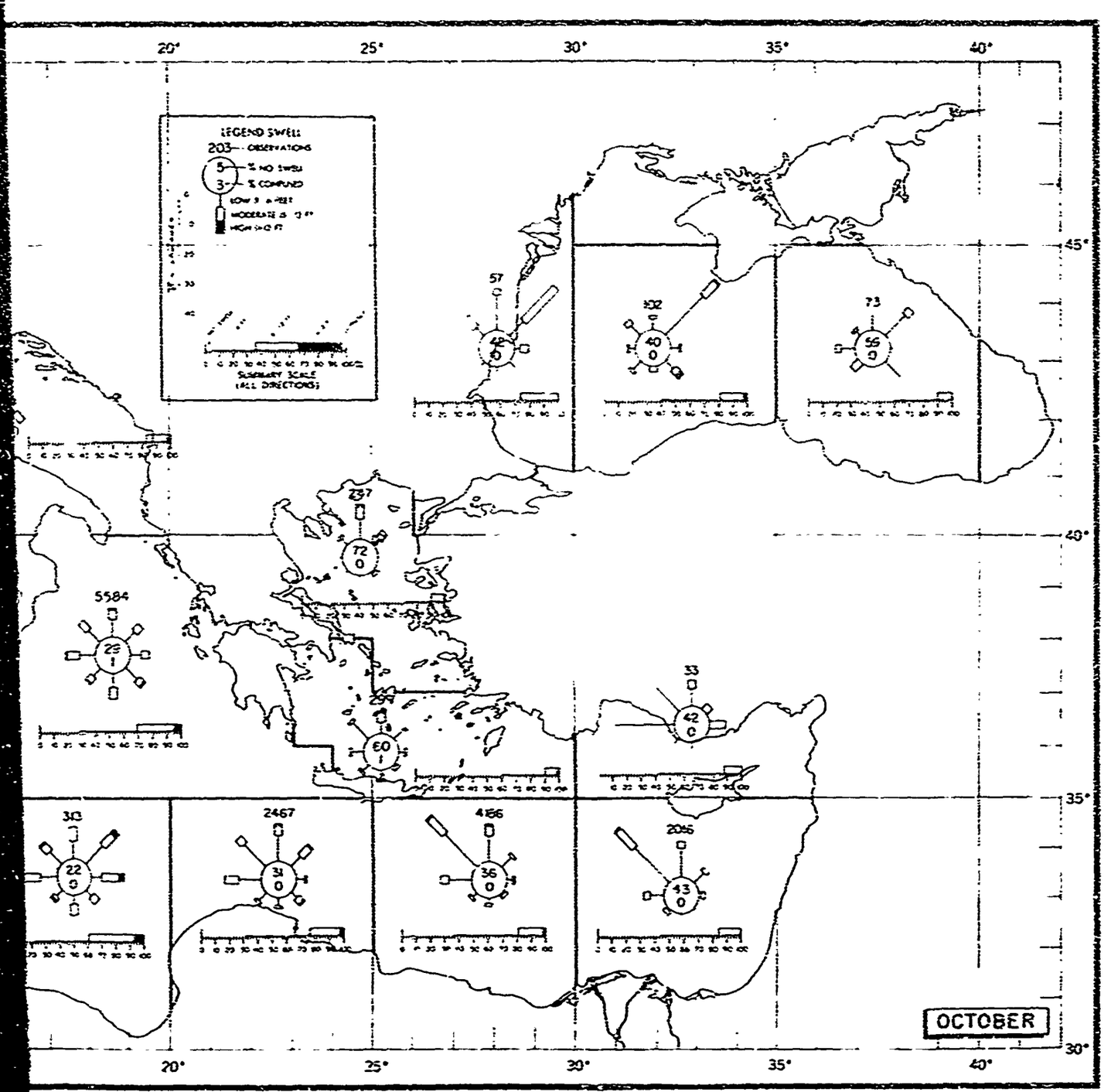

EDITERRANEAN SEA, OCTOBER

FIGURE 33. SWELL, OCTOBER

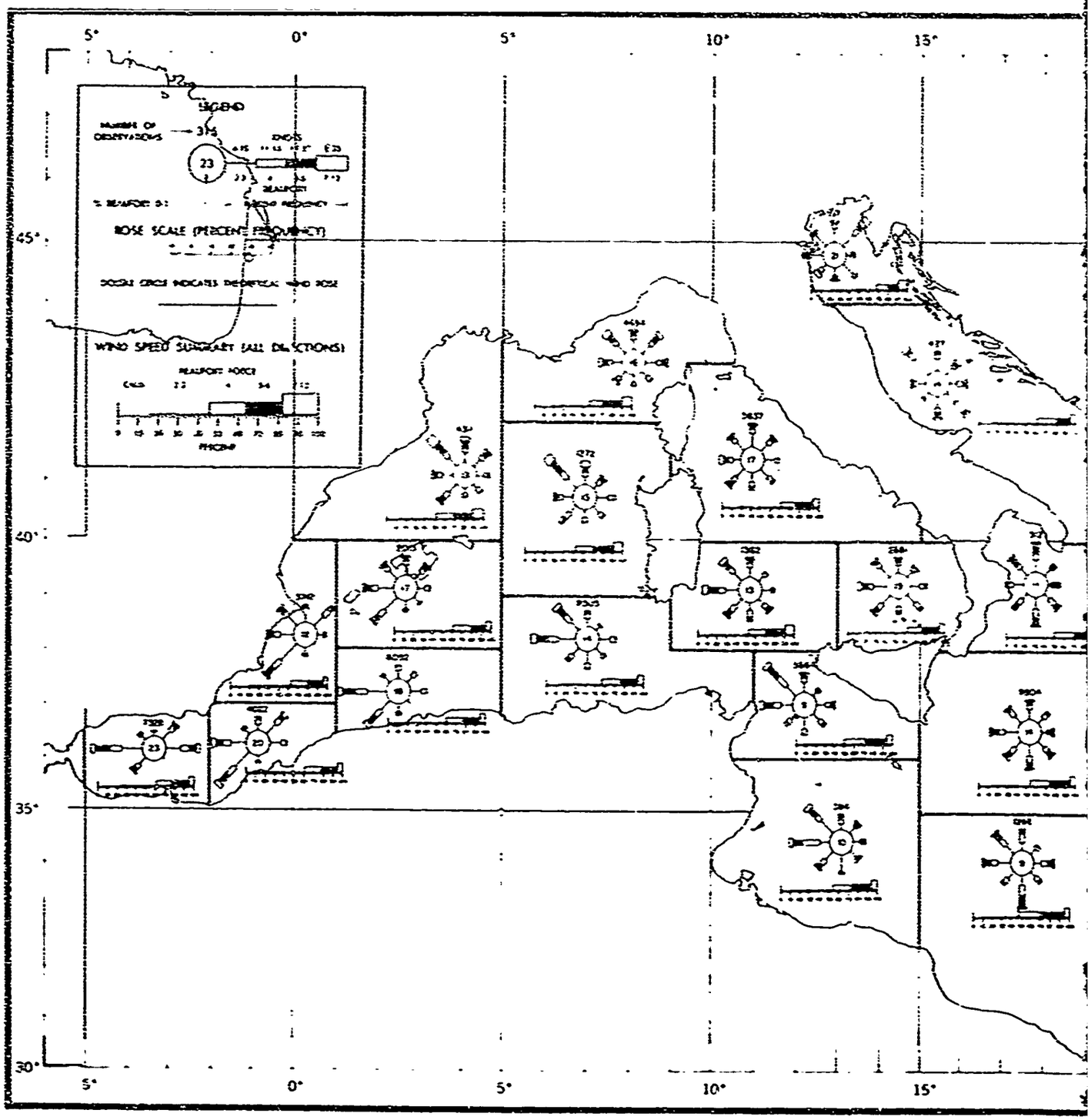

FIGURE 34. SURFACE WIND ROSES, THE MED

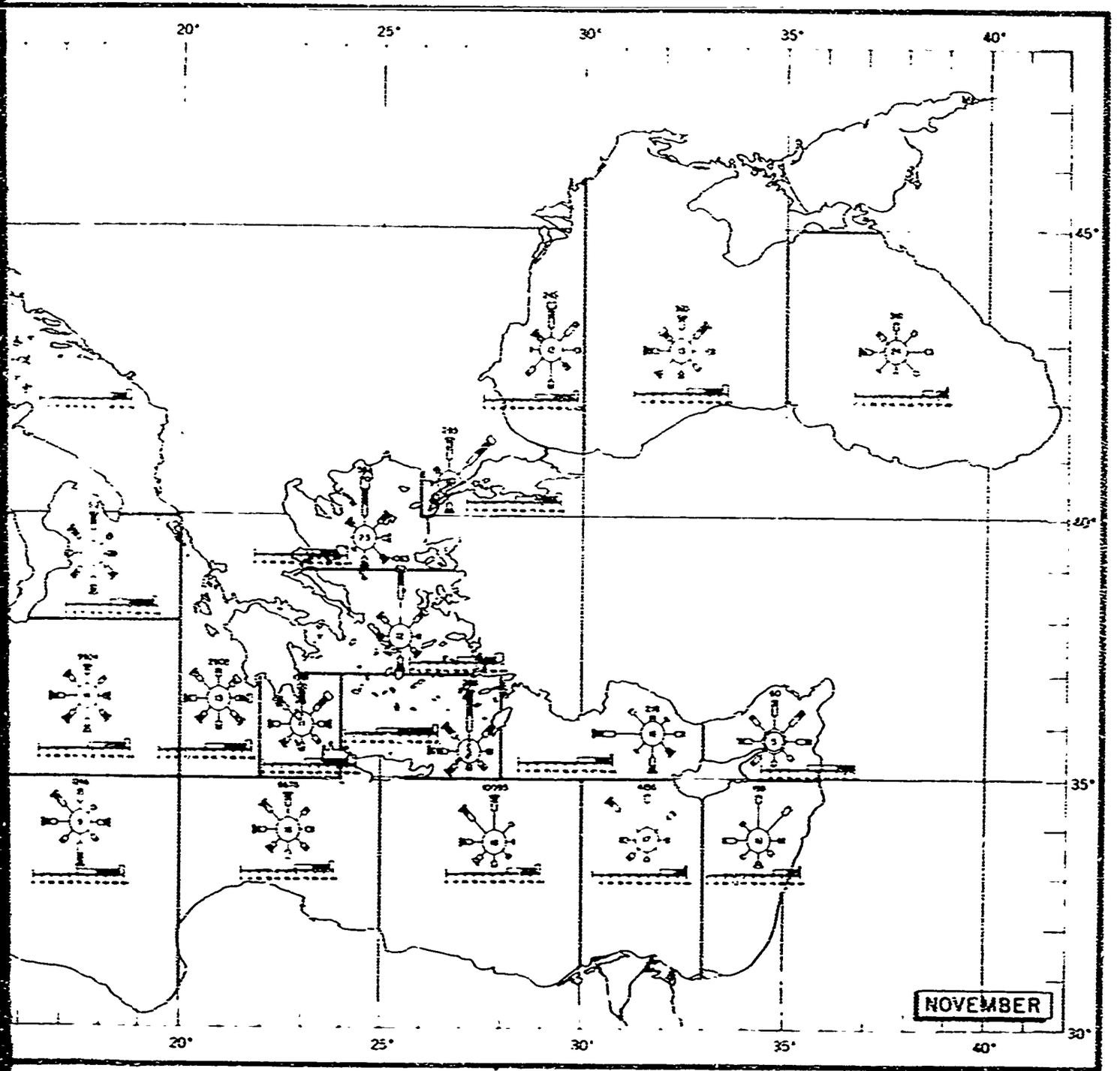

ROSES, THE MEDITERRANEAN SEA, NOVEMBER

FIGURE 34. SURFACE WINDS, NOVEMBER

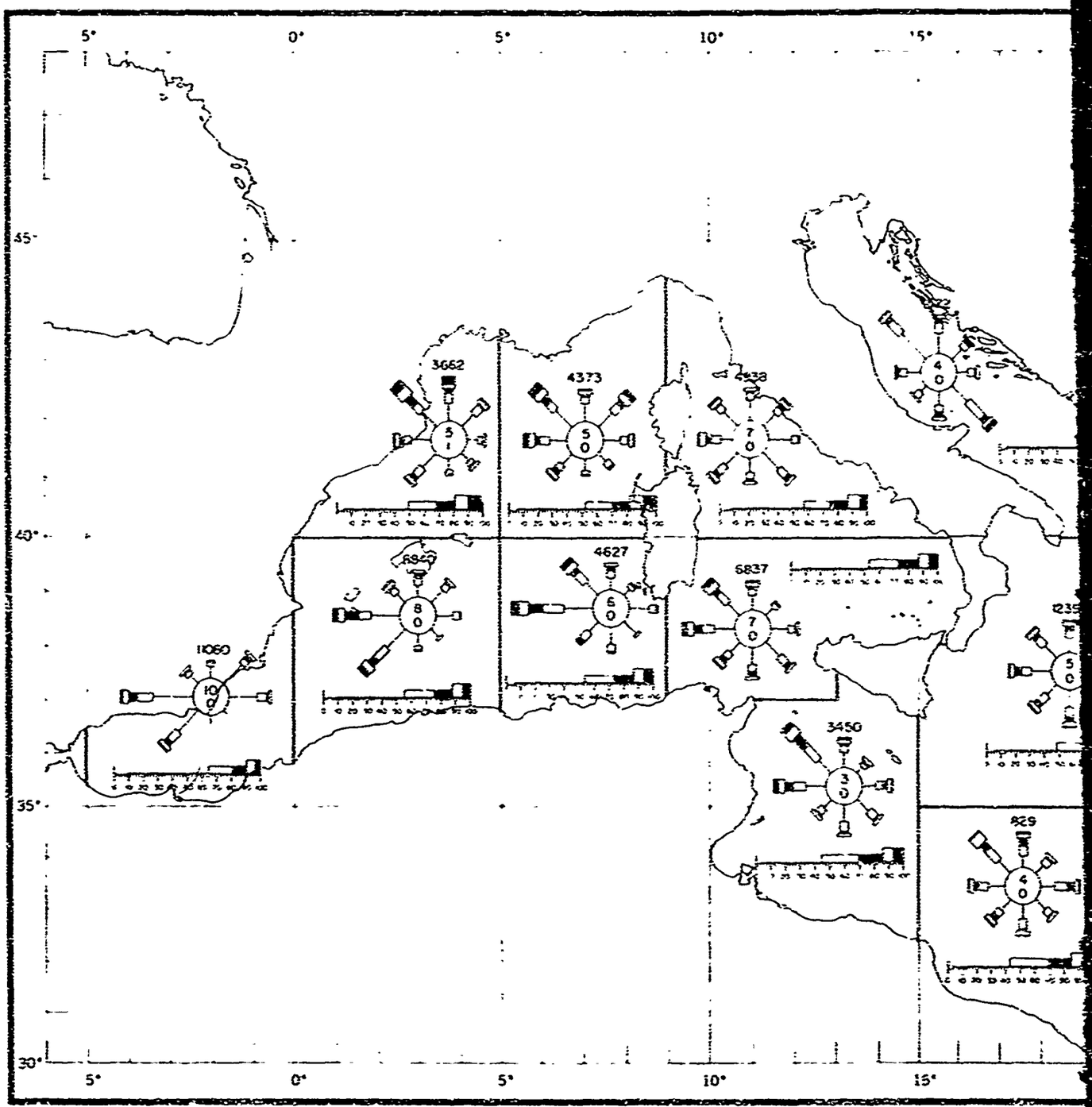

FIGURE 35. STATE OF SEA IN THE MEDITERR

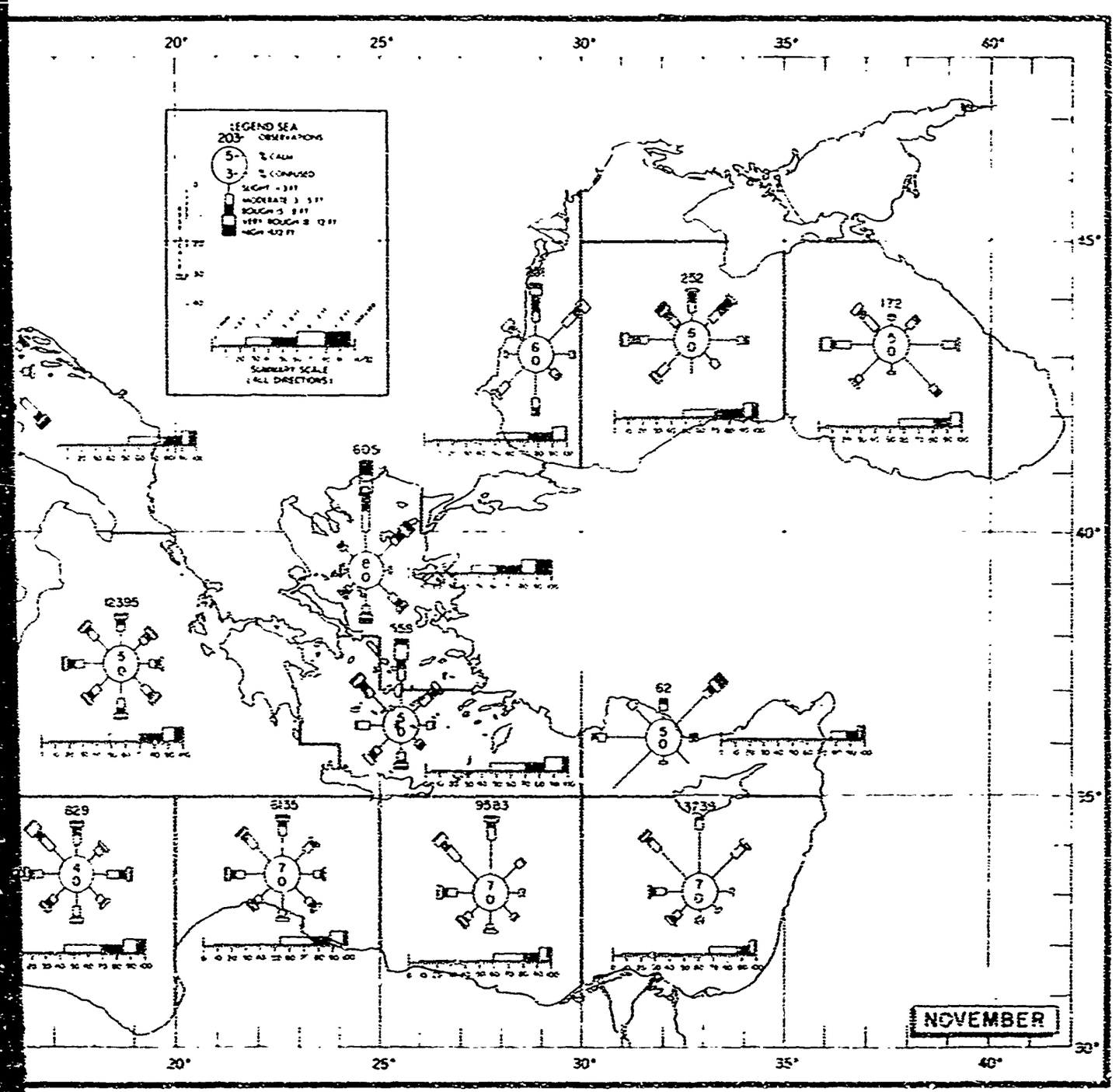

THE MEDITERRANEAN SEA, NOVEMBER

FIGURE 35. SEA, NOVEMBER

2

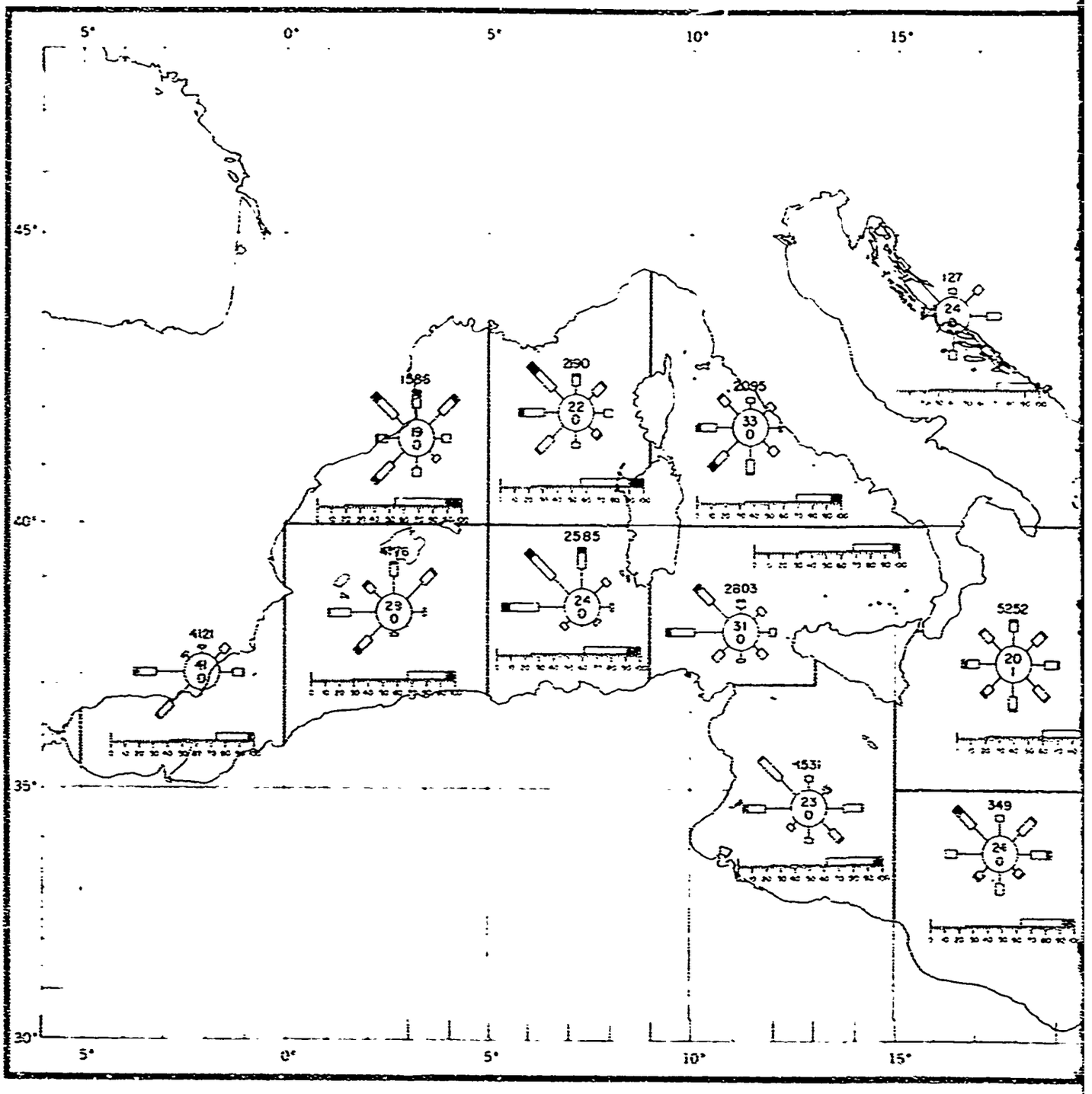

FIGURE 36. SWELL IN THE MEDITERRANE

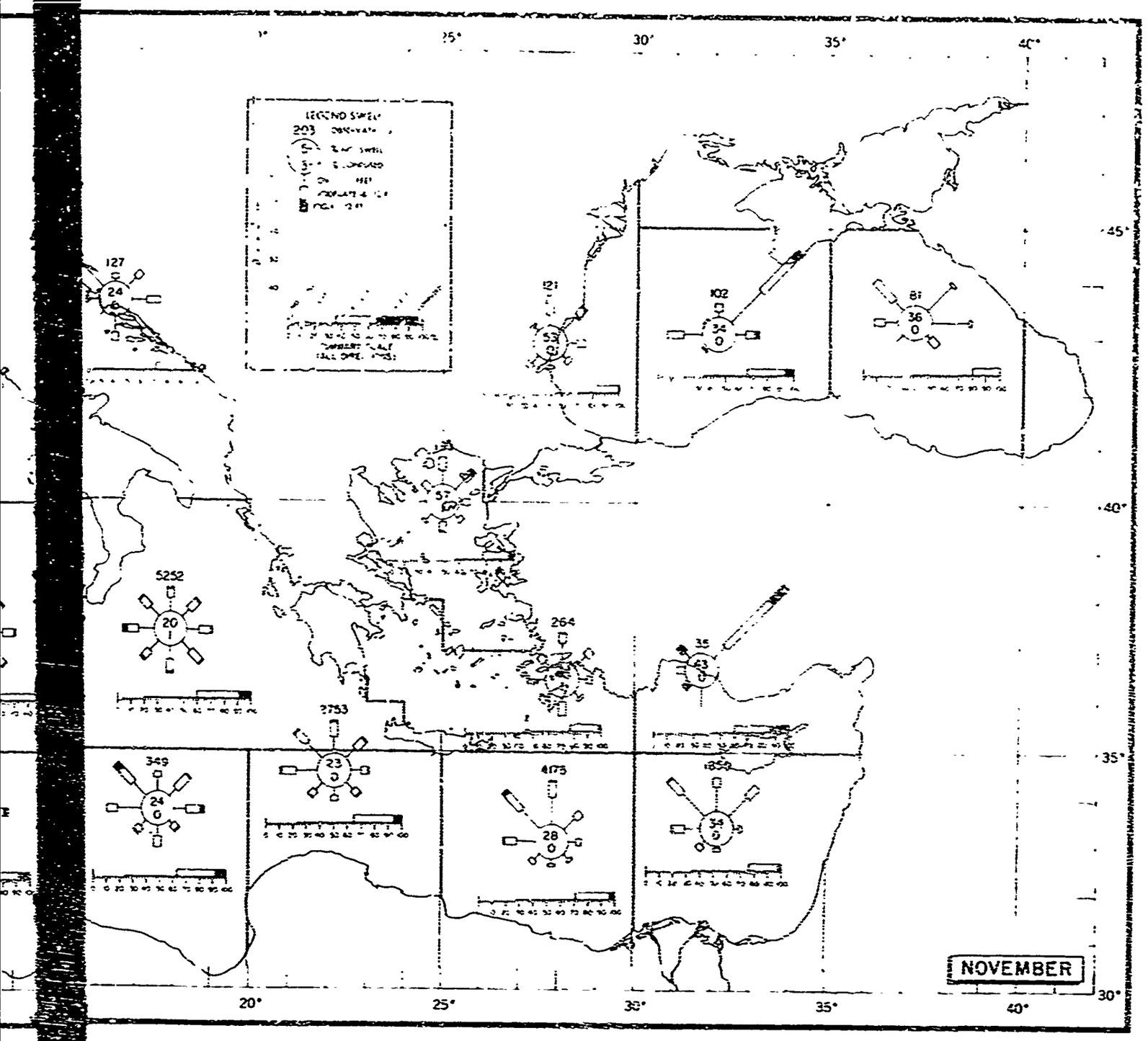

N THE MEDITERRANEAN SEA, NOVEMBER

FIGURE 36. SWELL, NOVEMBER

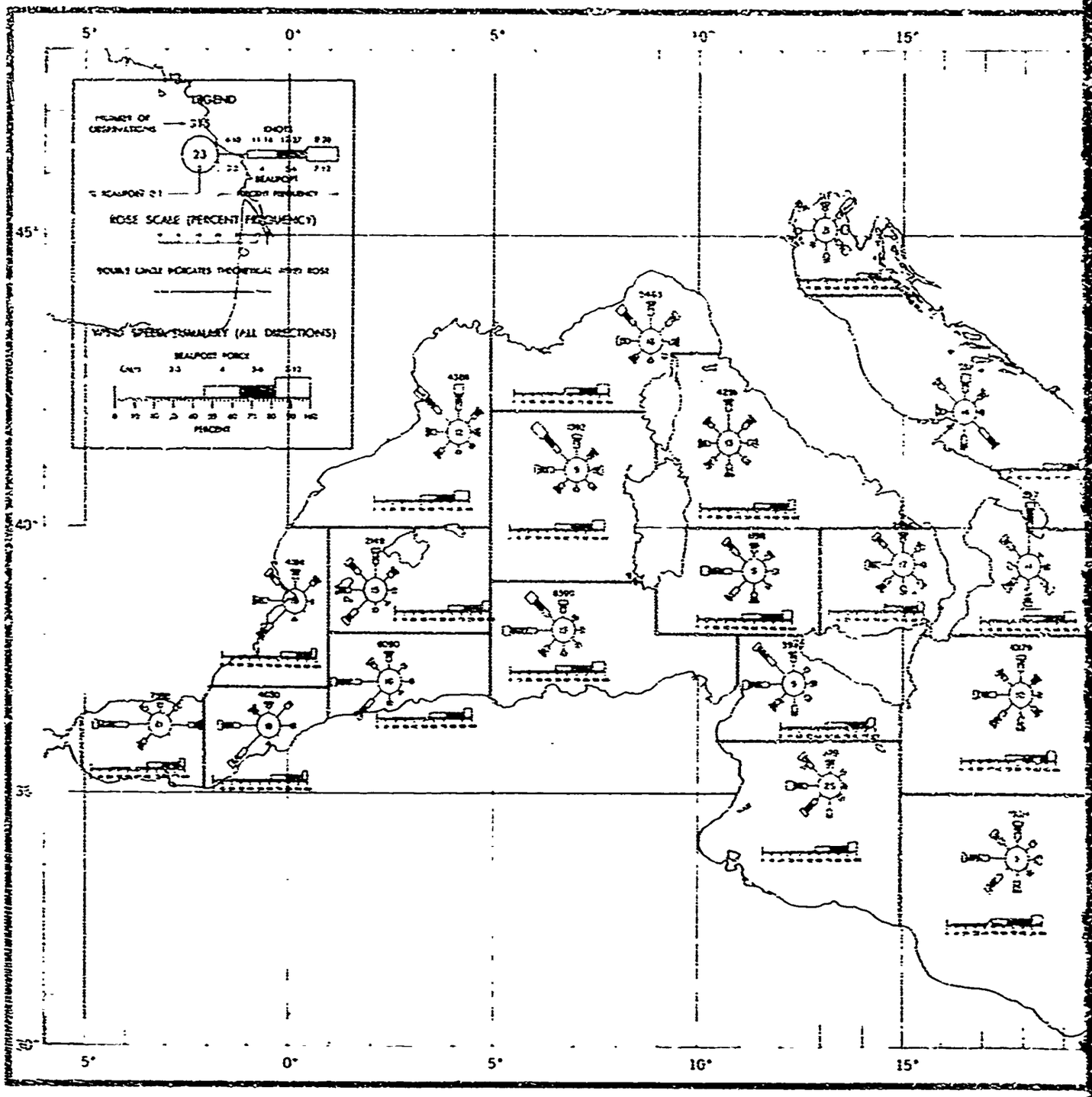

FIGURE 37. SURFACE WIND ROSES, THE MEDITE

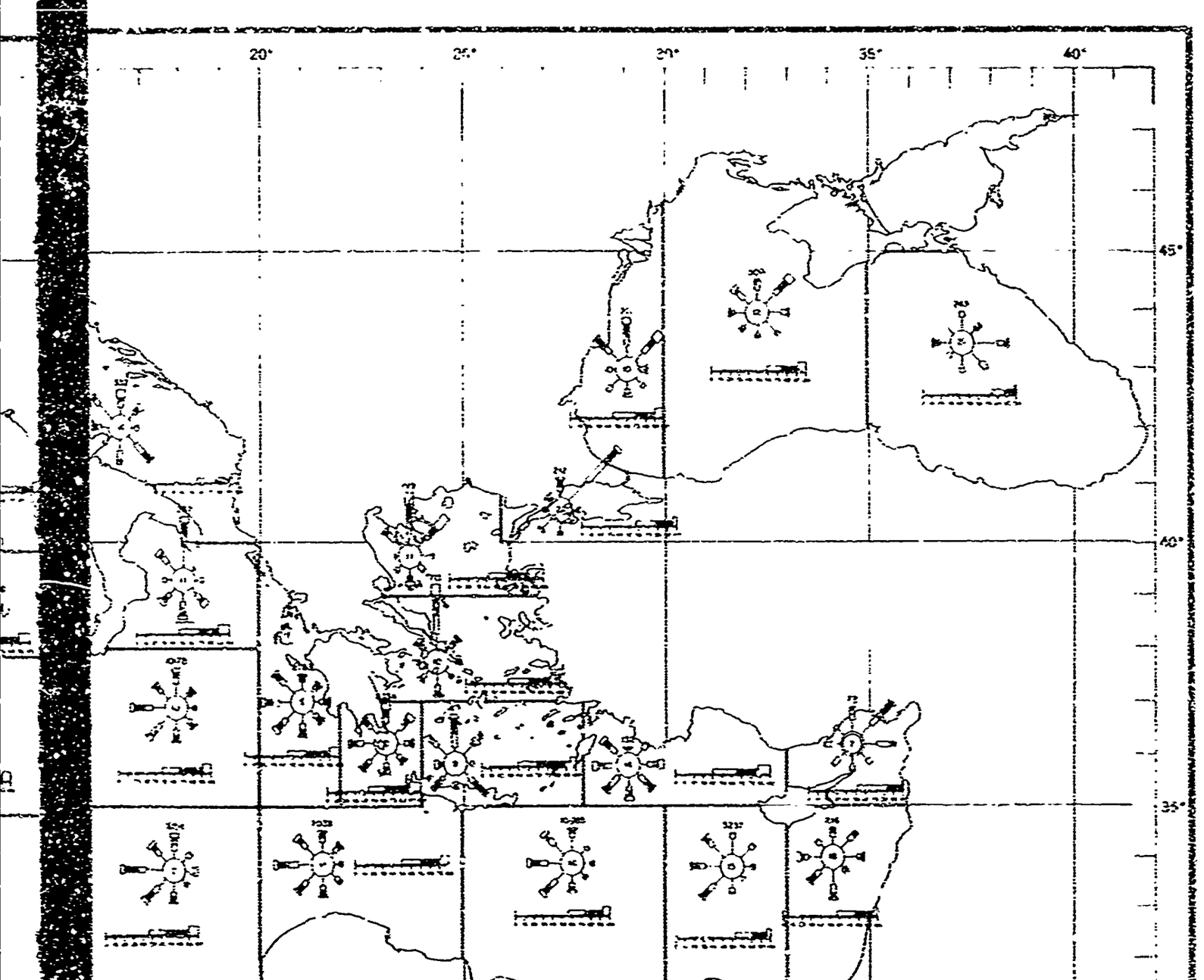

ROSES, THE MEDITERRANEAN SEA, DECEMBER

FIGURE 37. SURFACE WINDS, DECEMBER

2

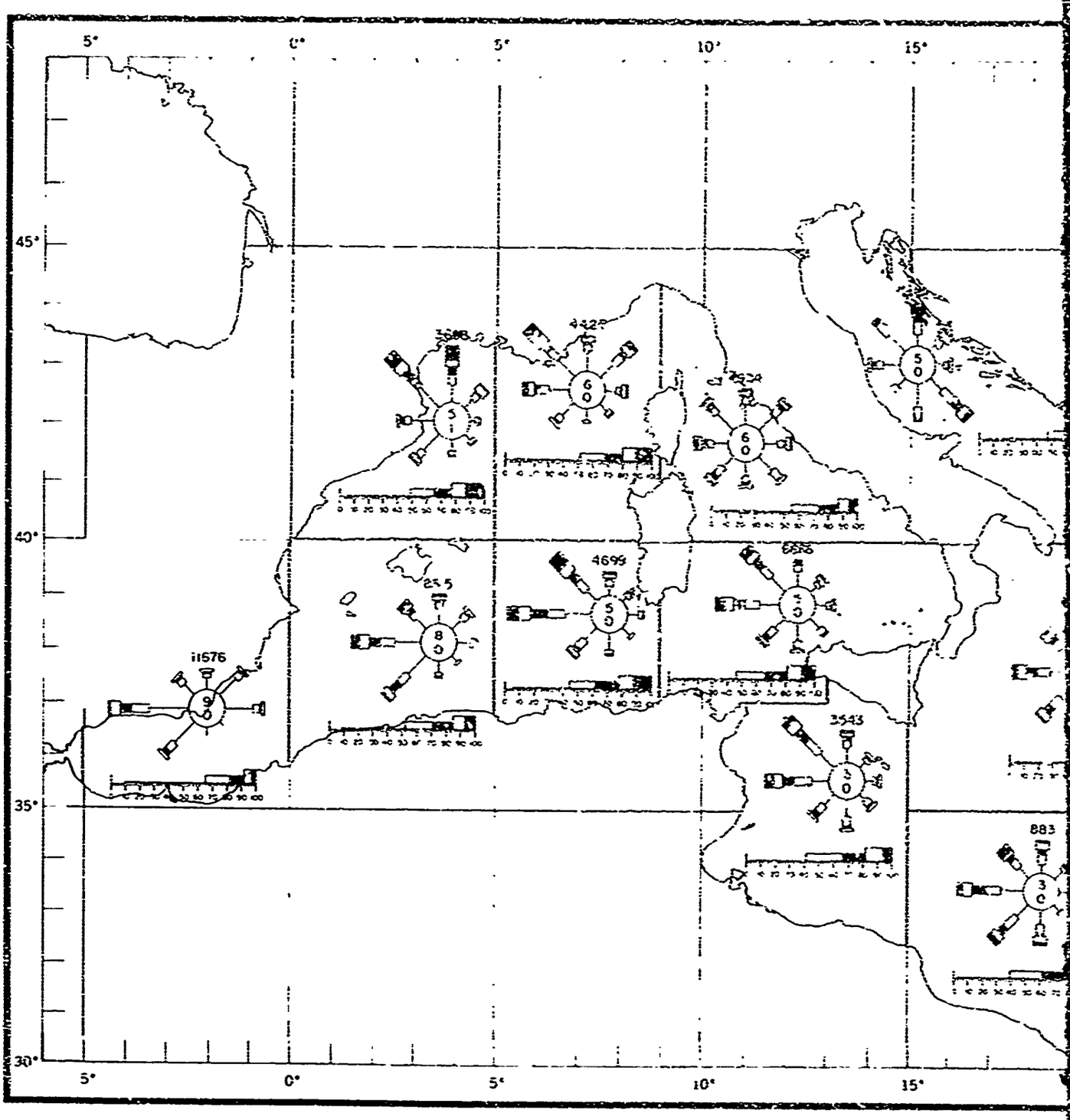

FIGURE 38. STATE OF THE SEA IN THE MEDITE

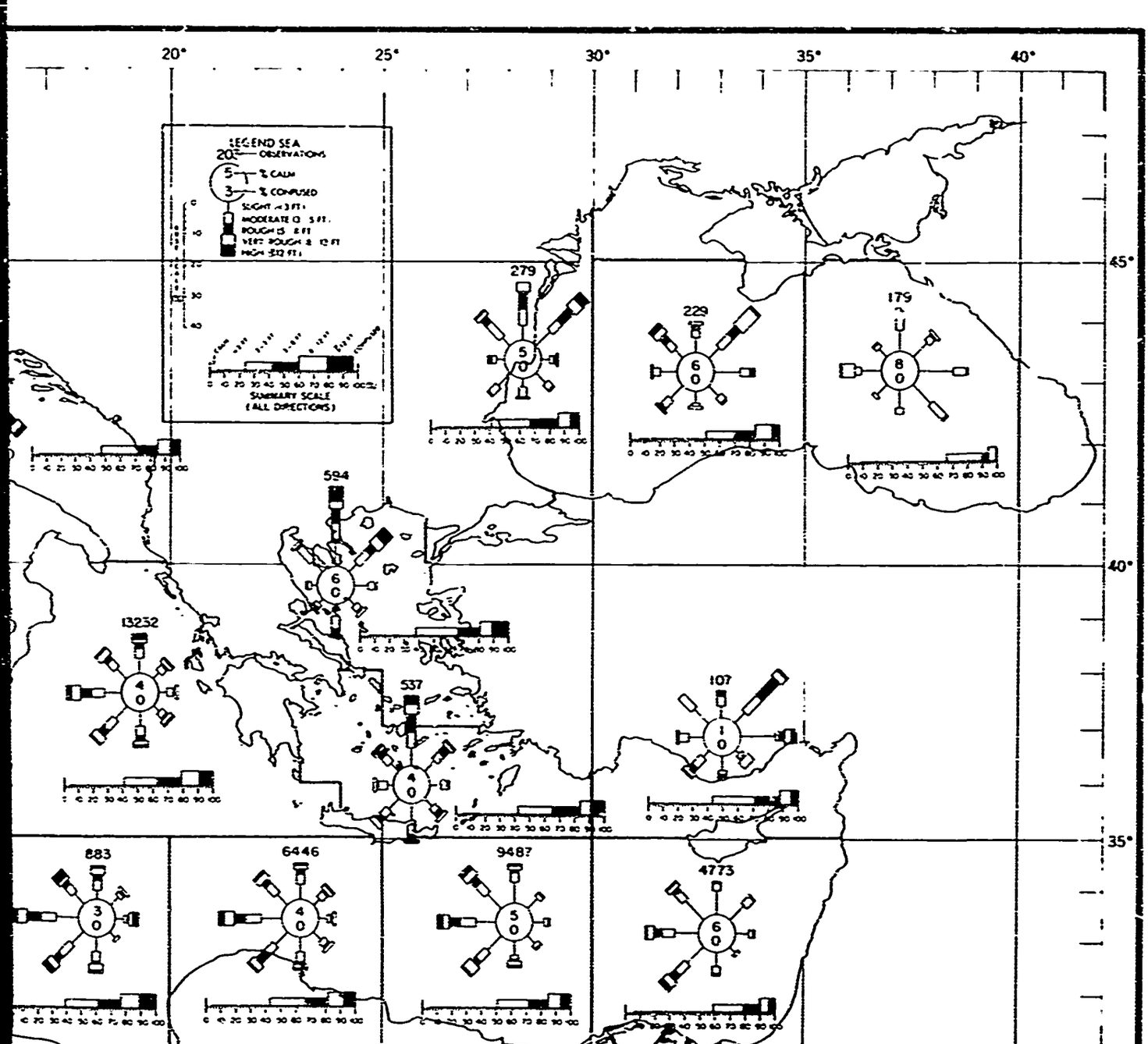

N THE MEDITERRANEAN SEA, DECEMBER

FIGURE 38. SEA, DECEMBER

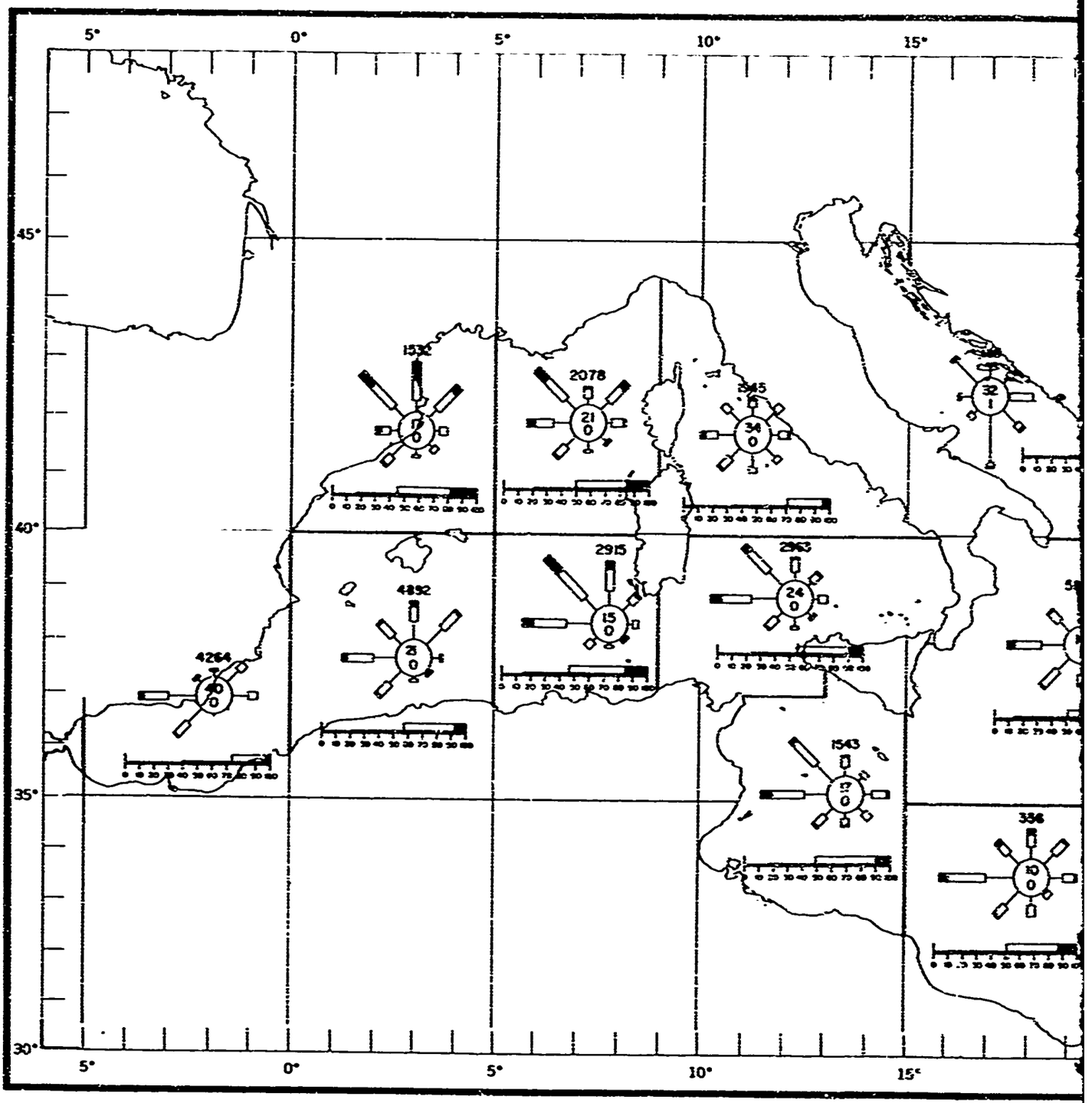

FIGURE 39. SWELL IN THE MEDITERRANEAN SEA,

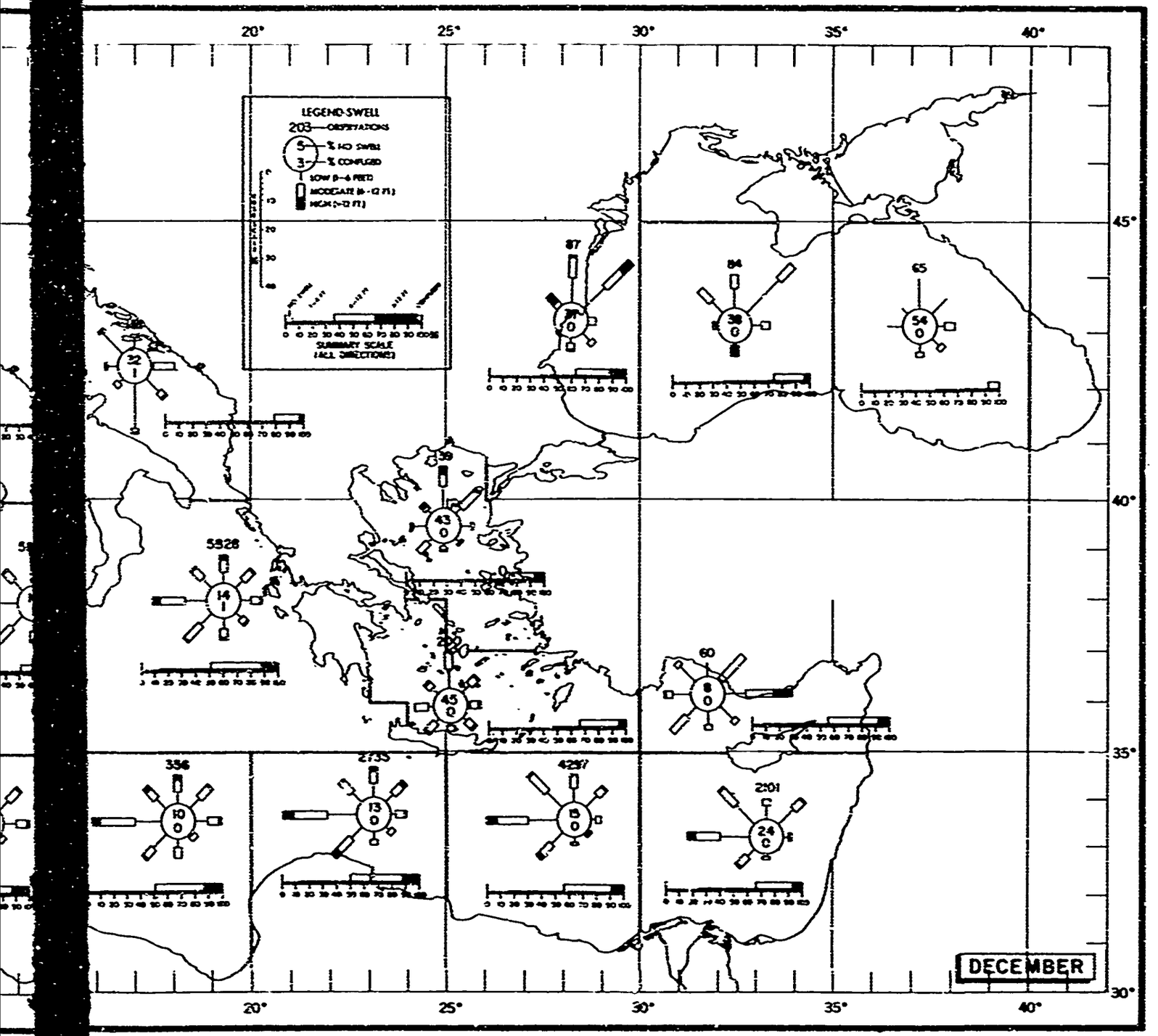

SEA, EDITERRANEAN SEA, DECEMBER

FIGURE 39. SWELL, DECEMBER

2

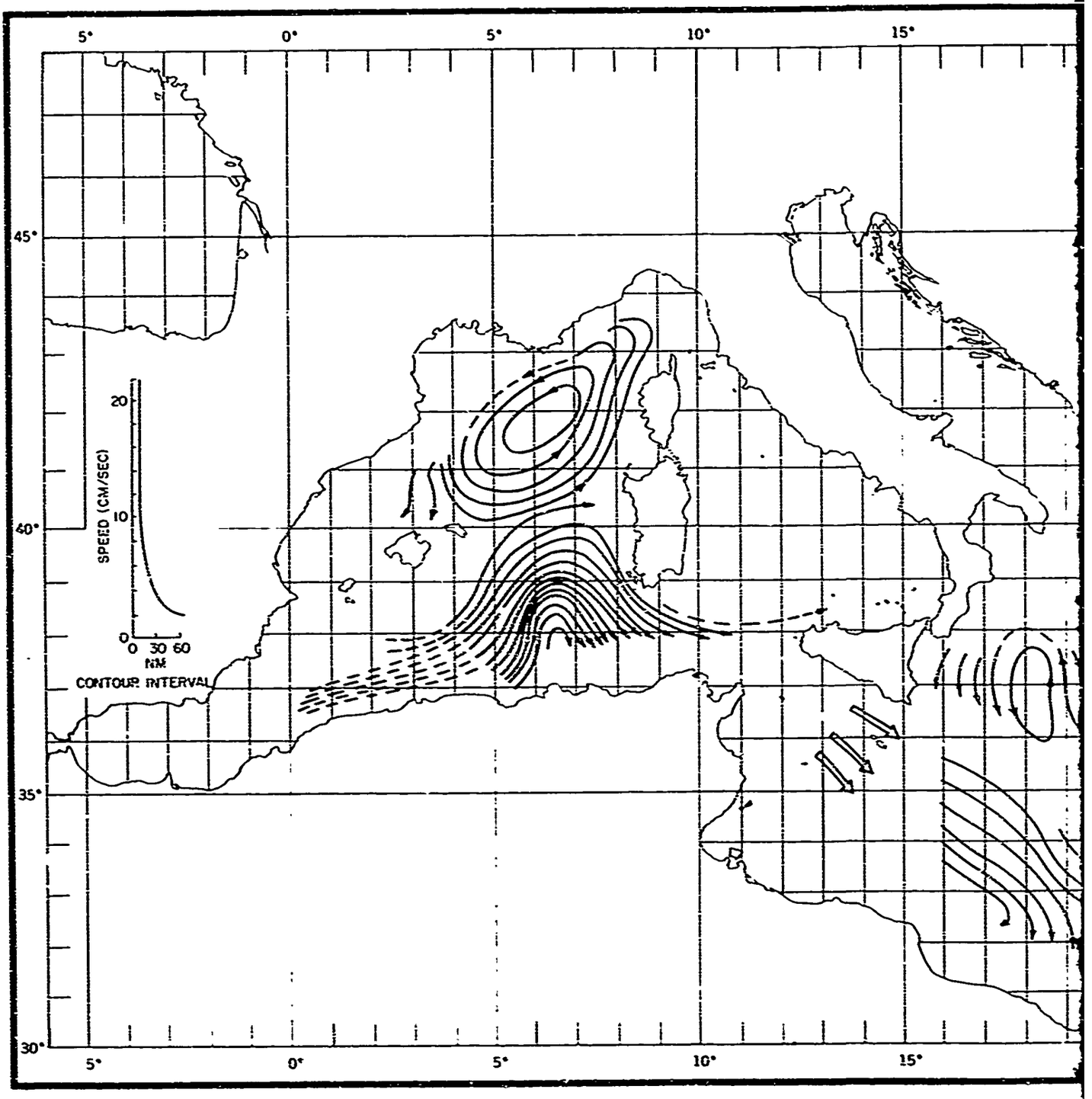

FIGURE 40. SURFACE CURRENT VELOCITY RELATIVE TO THE

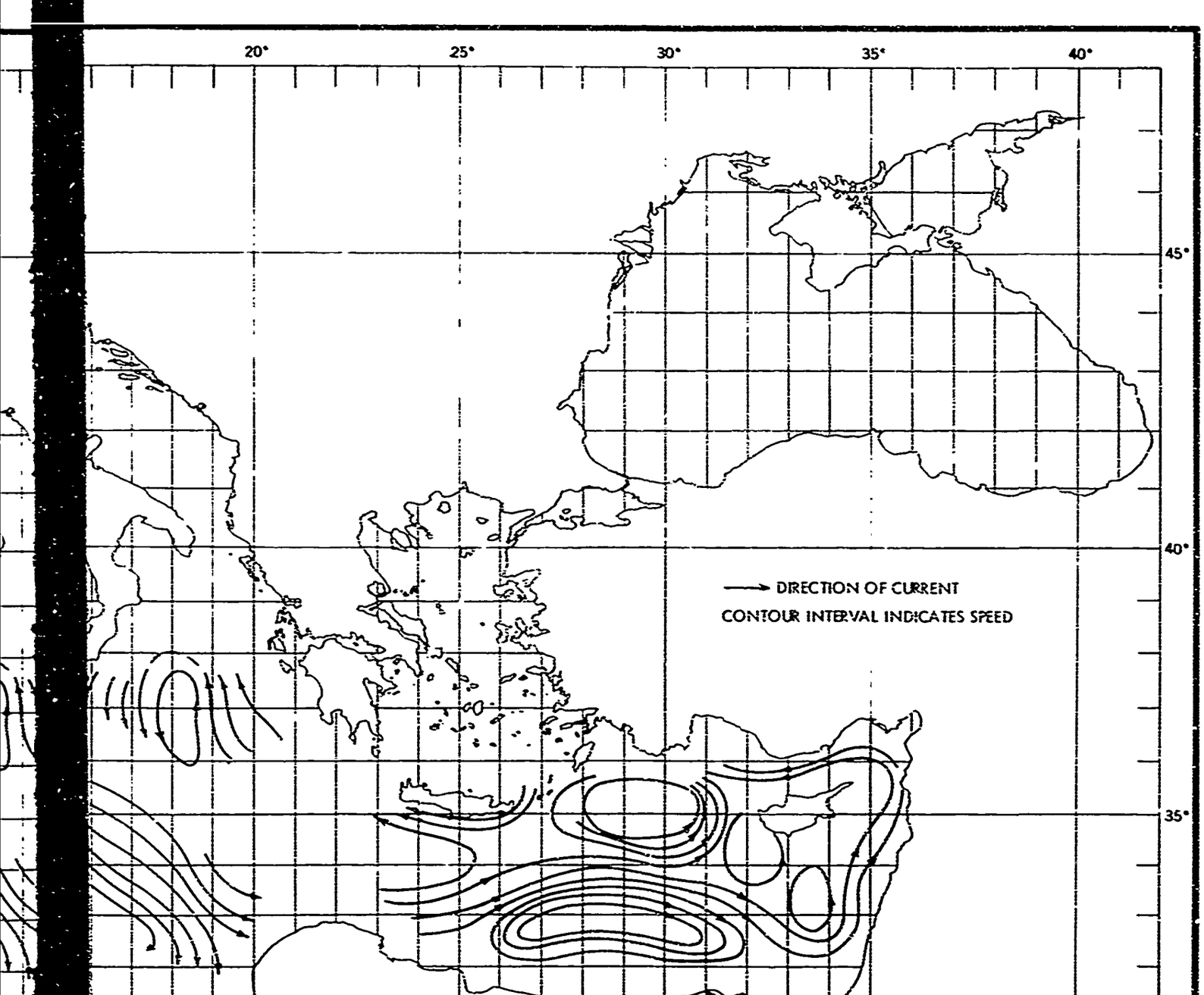

THE RELATIVE TO THE CURRENT VELOCITY AT 1,000 METERS, WINTER

FIGURE 40. SURFACE CURRENT VELOCITY, WINTER

2

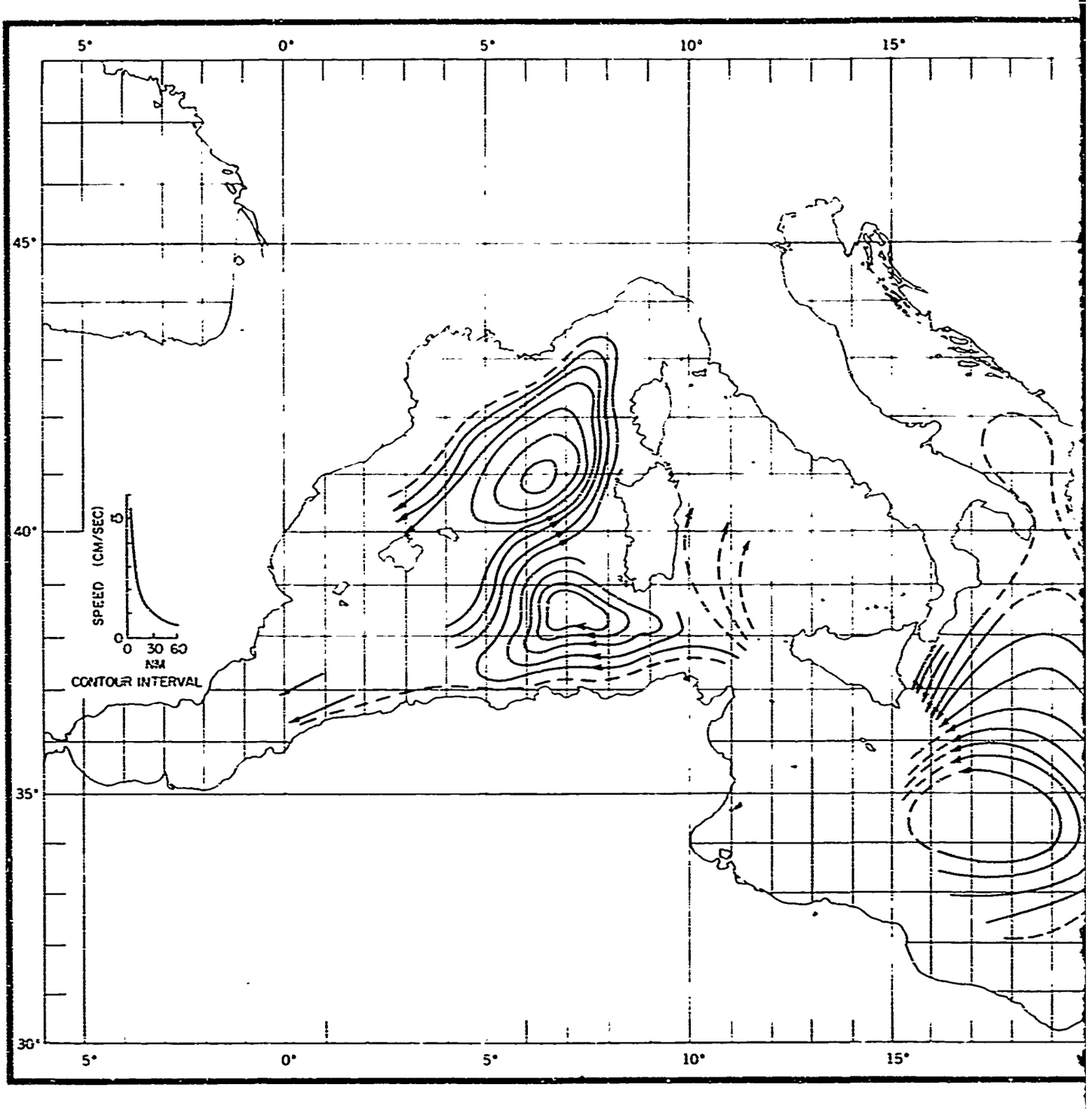

FIGURE 41. CURRENT VELOCITY AT 500 METERS RELATIVE TO THE

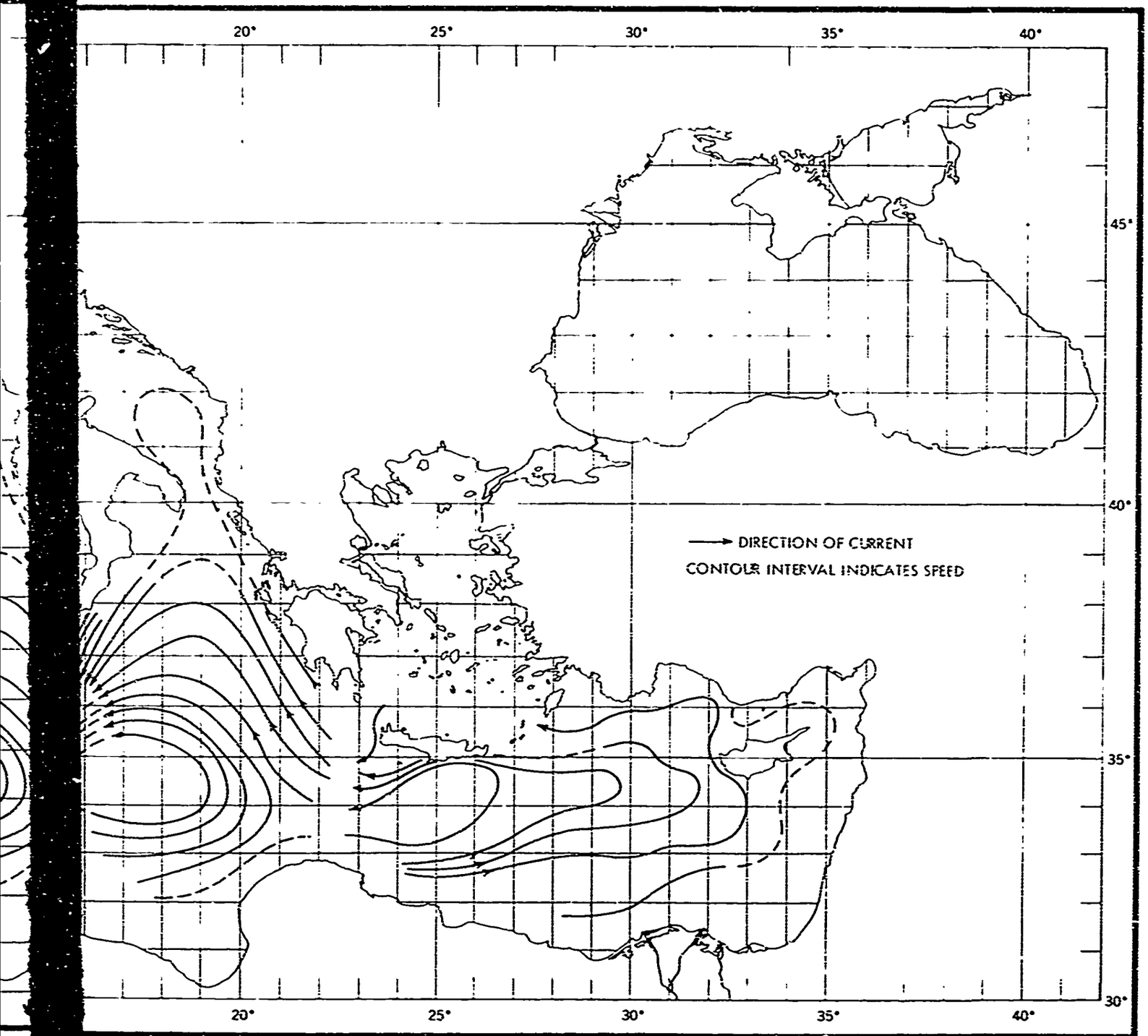

RS RELATIVE TO THE CURRENT VELOCITY AT 1,000 METERS, WINTER

FIGURE 41. CURRENT VELOCITY AT 500 METERS, WINTER

2

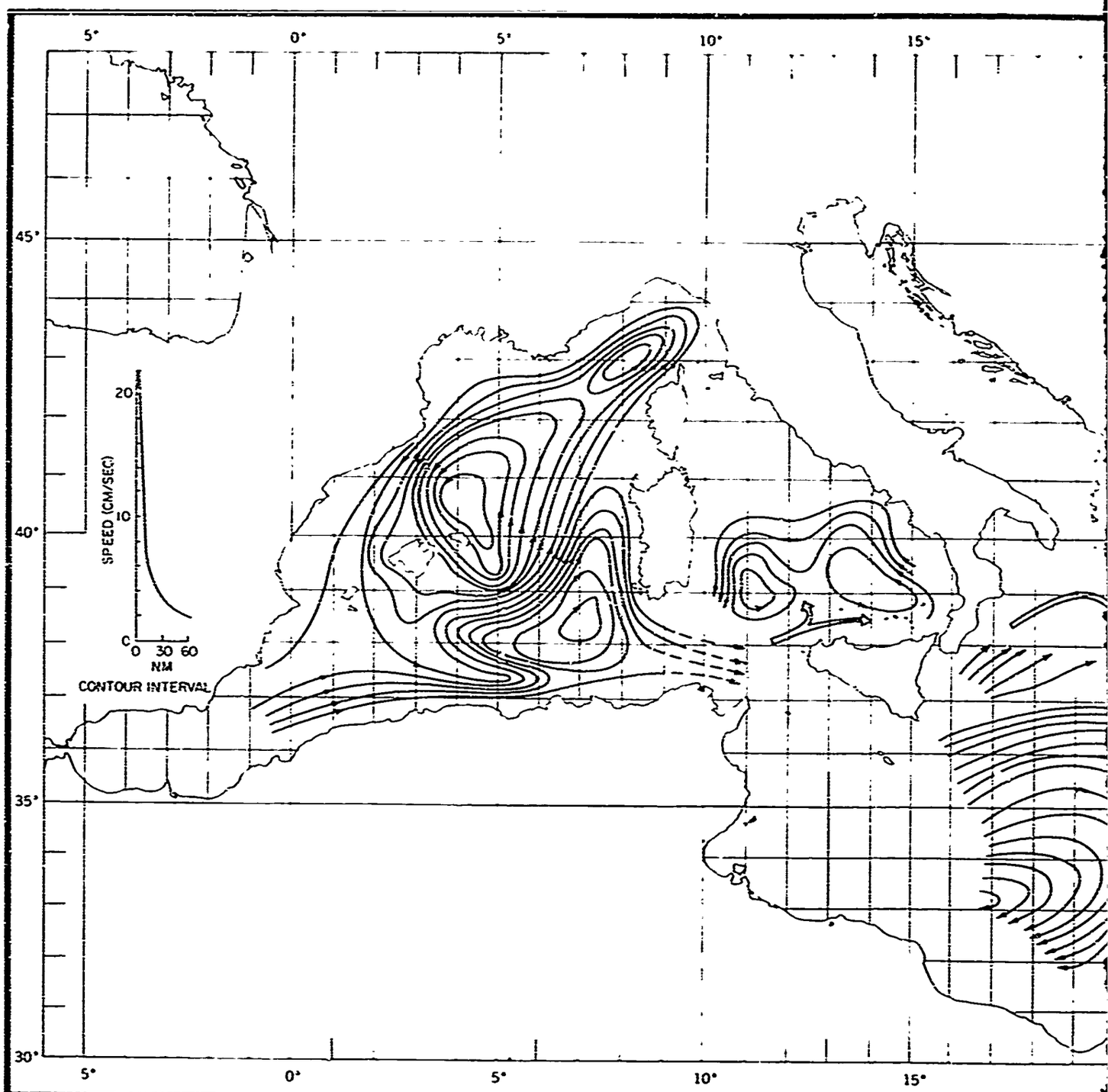

FIGURE 42. SURFACE CURRENT VELOCITY RELATIVE TO THE CUR

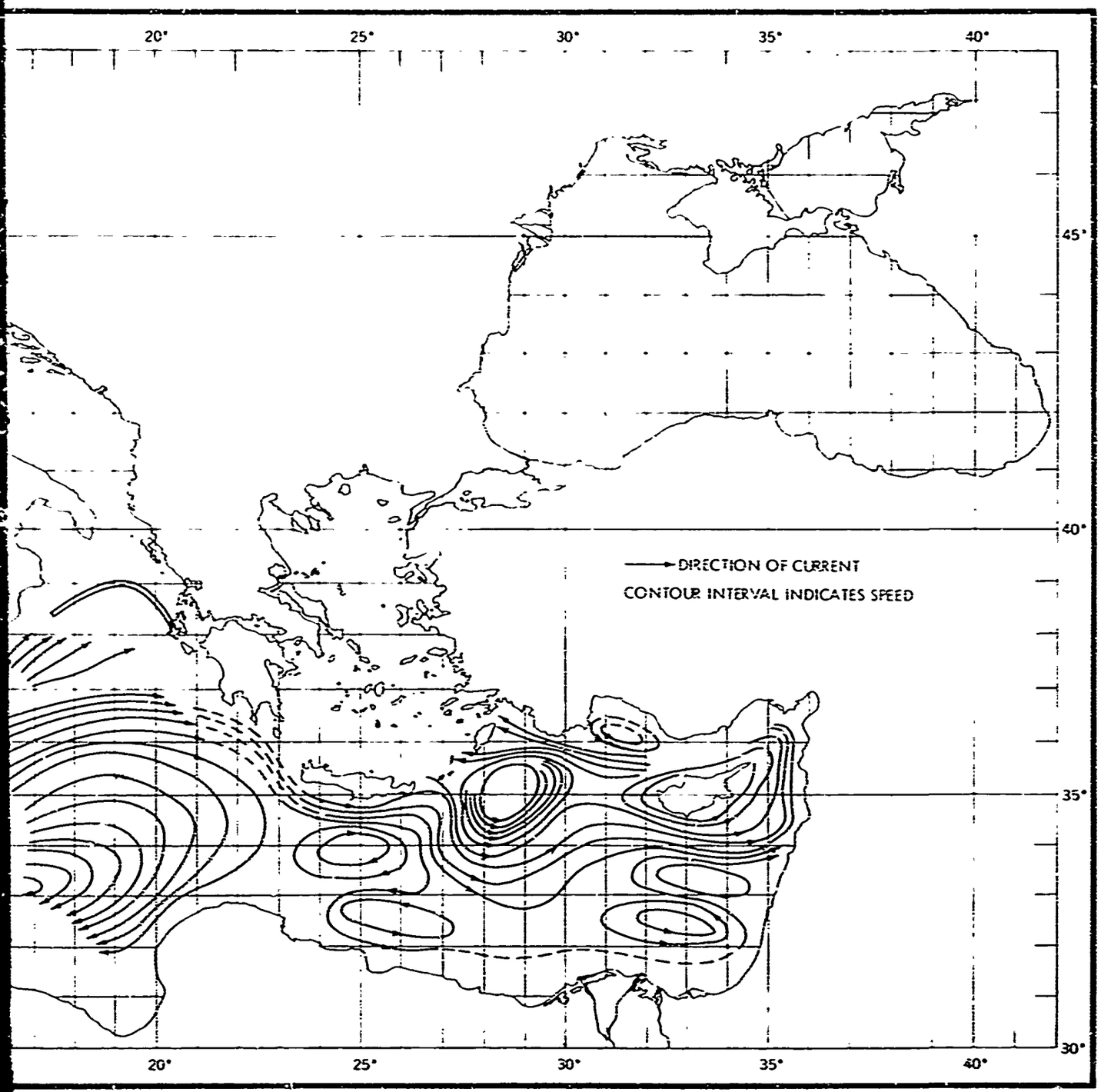

LATIVE TO THE CURRENT VELOCITY AT 1,000 METERS, SUMMER

FIGURE 42. SURFACE CURRENT VELOCITY, SUMMER

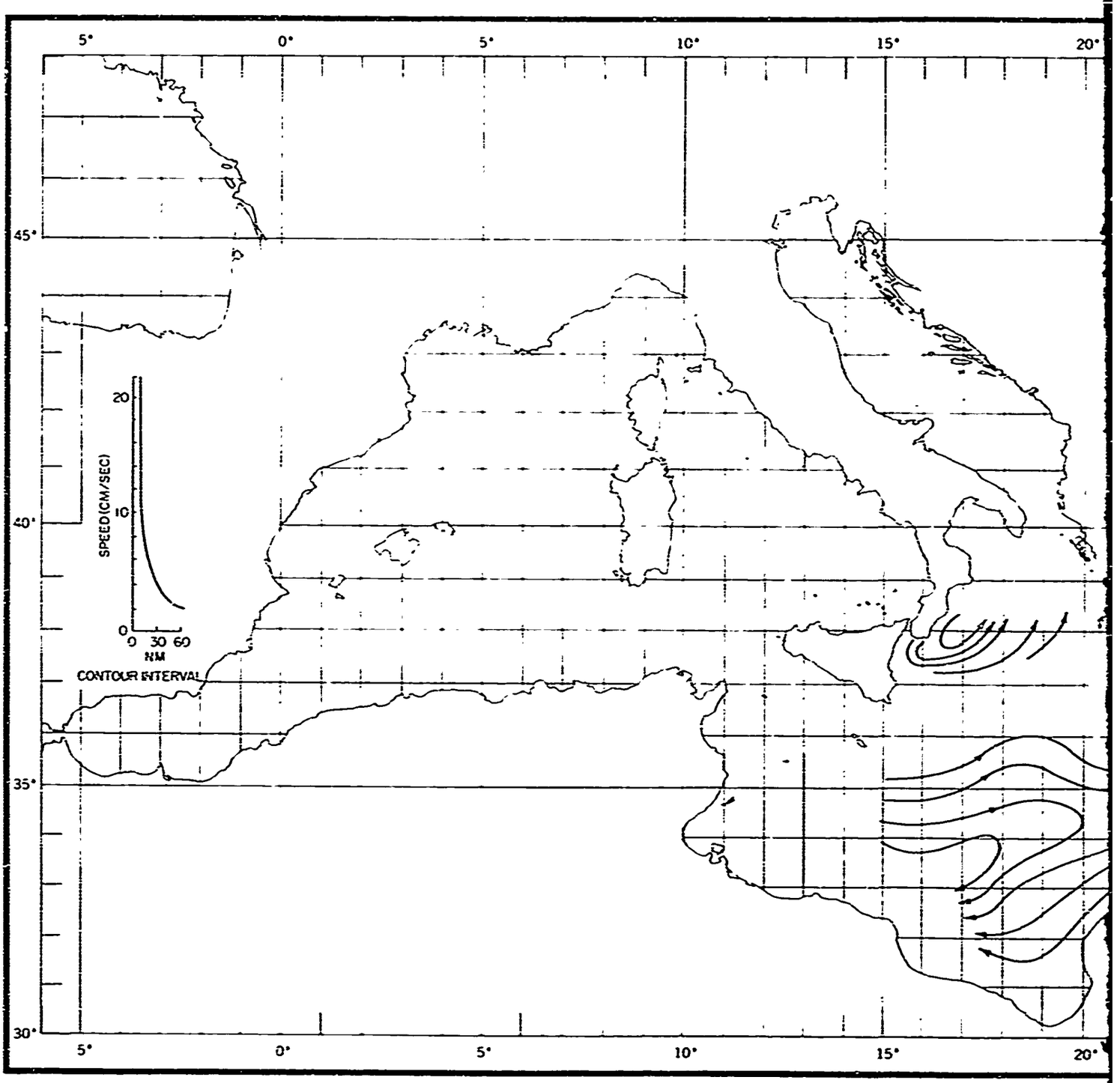

FIGURE 43. CURRENT VELOCITY AT 250 METERS RELATIVE TO THE CUR

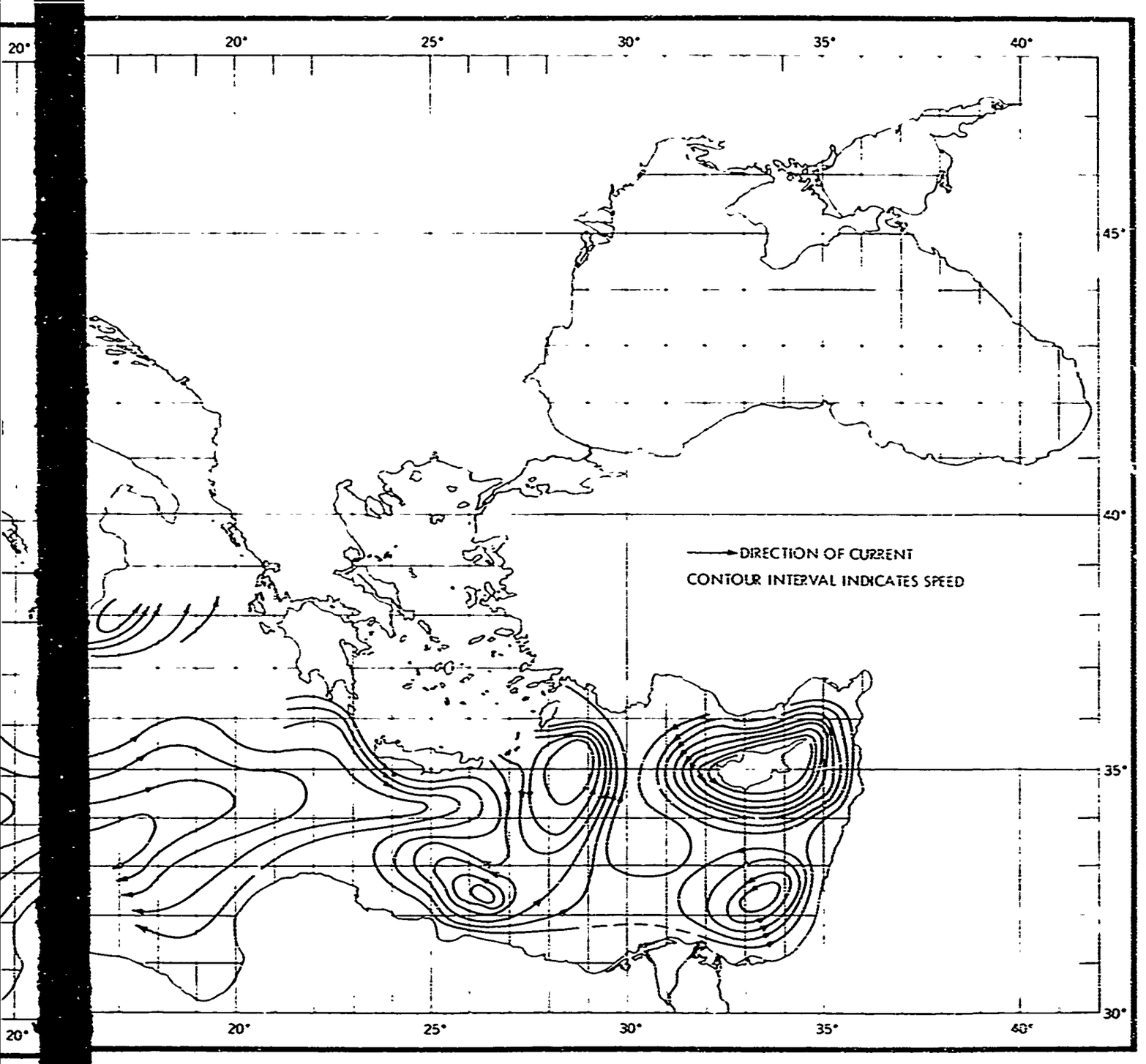

S RELATIVE TO THE CURRENT VELOCITY AT 1,000 METERS, SUMMER

FIGURE 43. CURRENT VELOCITY AT 250 METERS, SUMMER

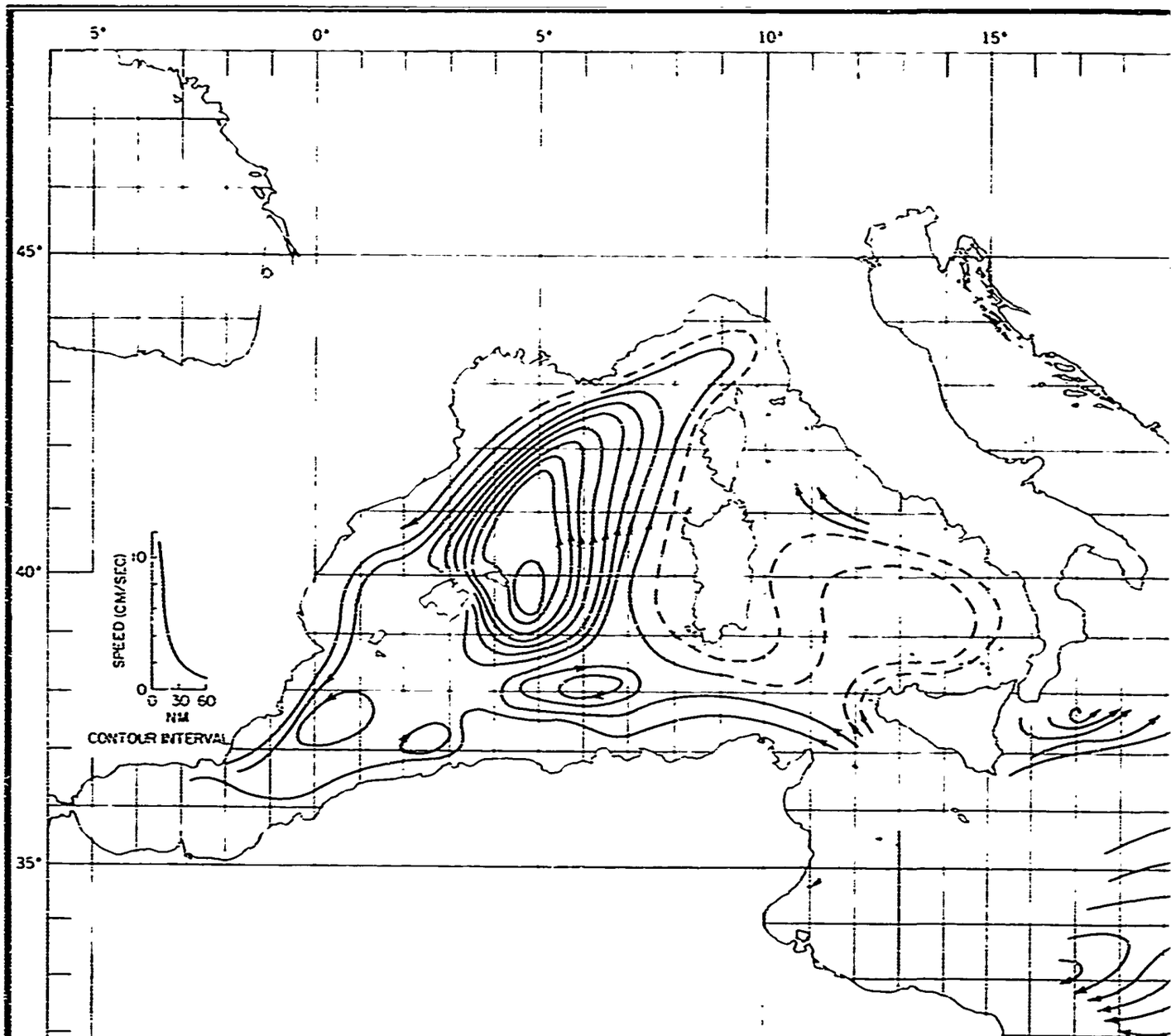

FIGURE 44. CURRENT VELOCITY AT 500 METERS RELATIVE TO TH

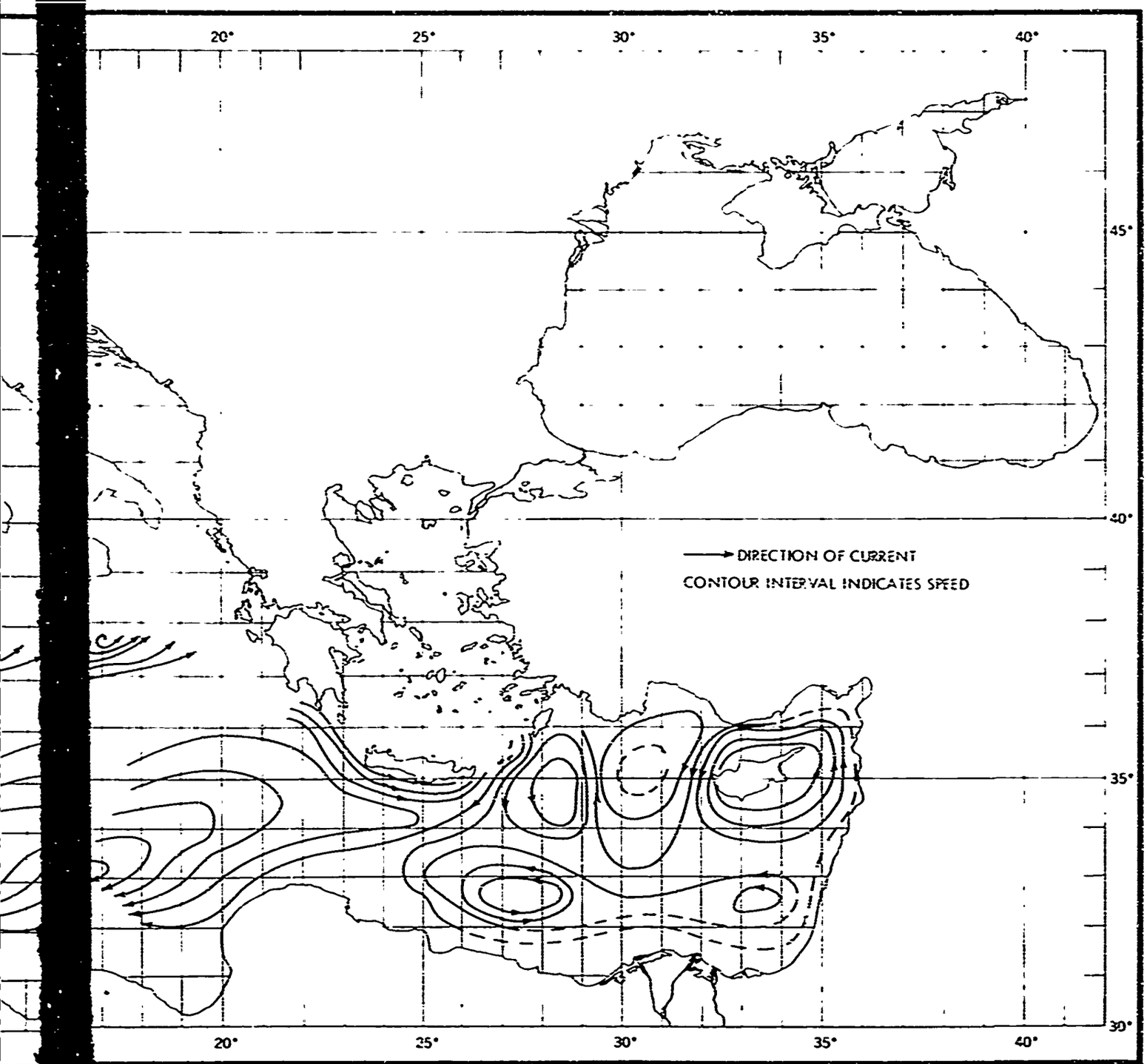

TO TH ELATIVE TO THE CURRENT VELOCITY AT 1,000 METERS, SUMMER

FIGURE 44. CURRENT VELOCITY AT 500 METERS, SUMMER

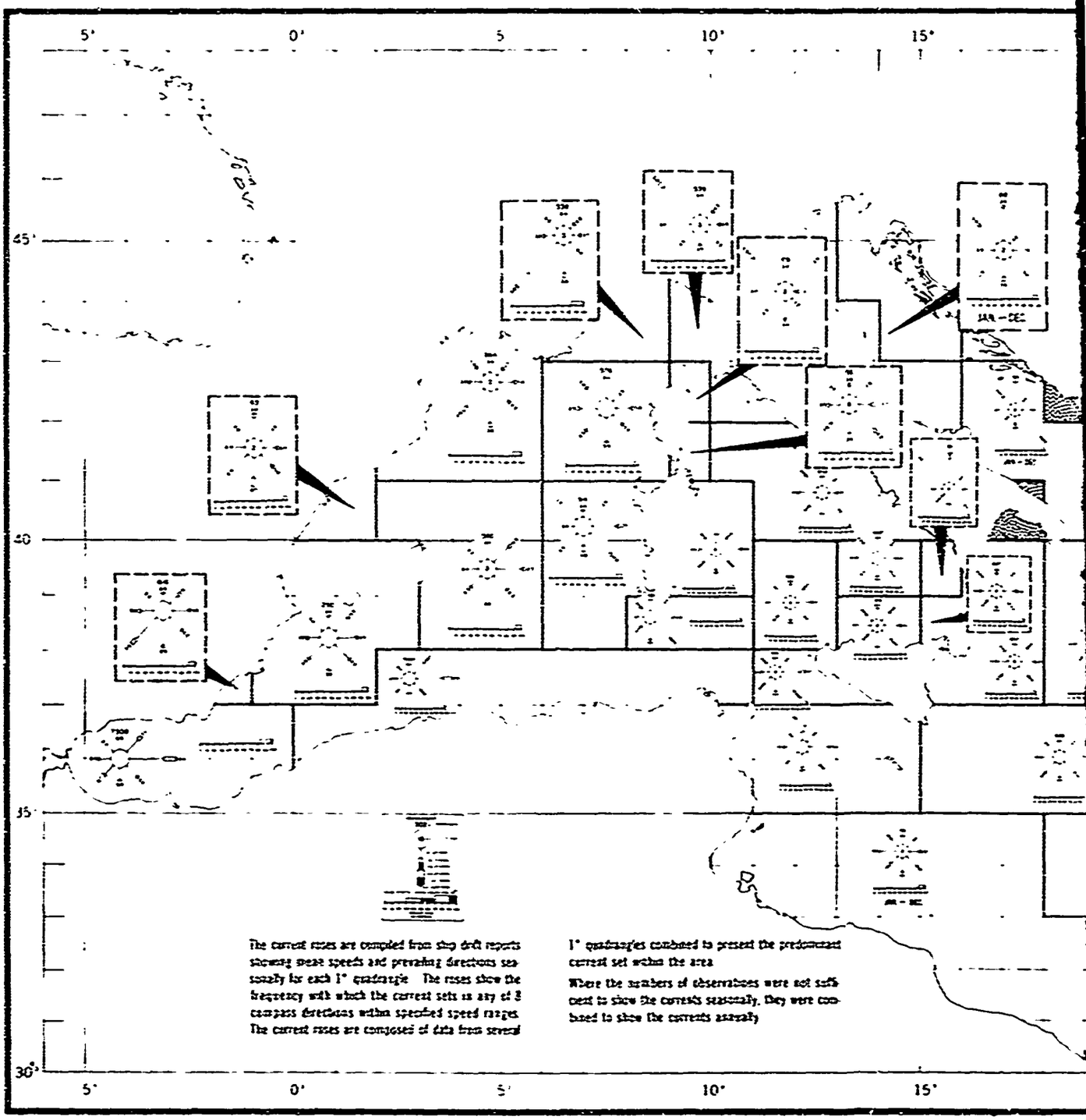

FIGURE 45. SURFACE CURRENT ROSES IN THE

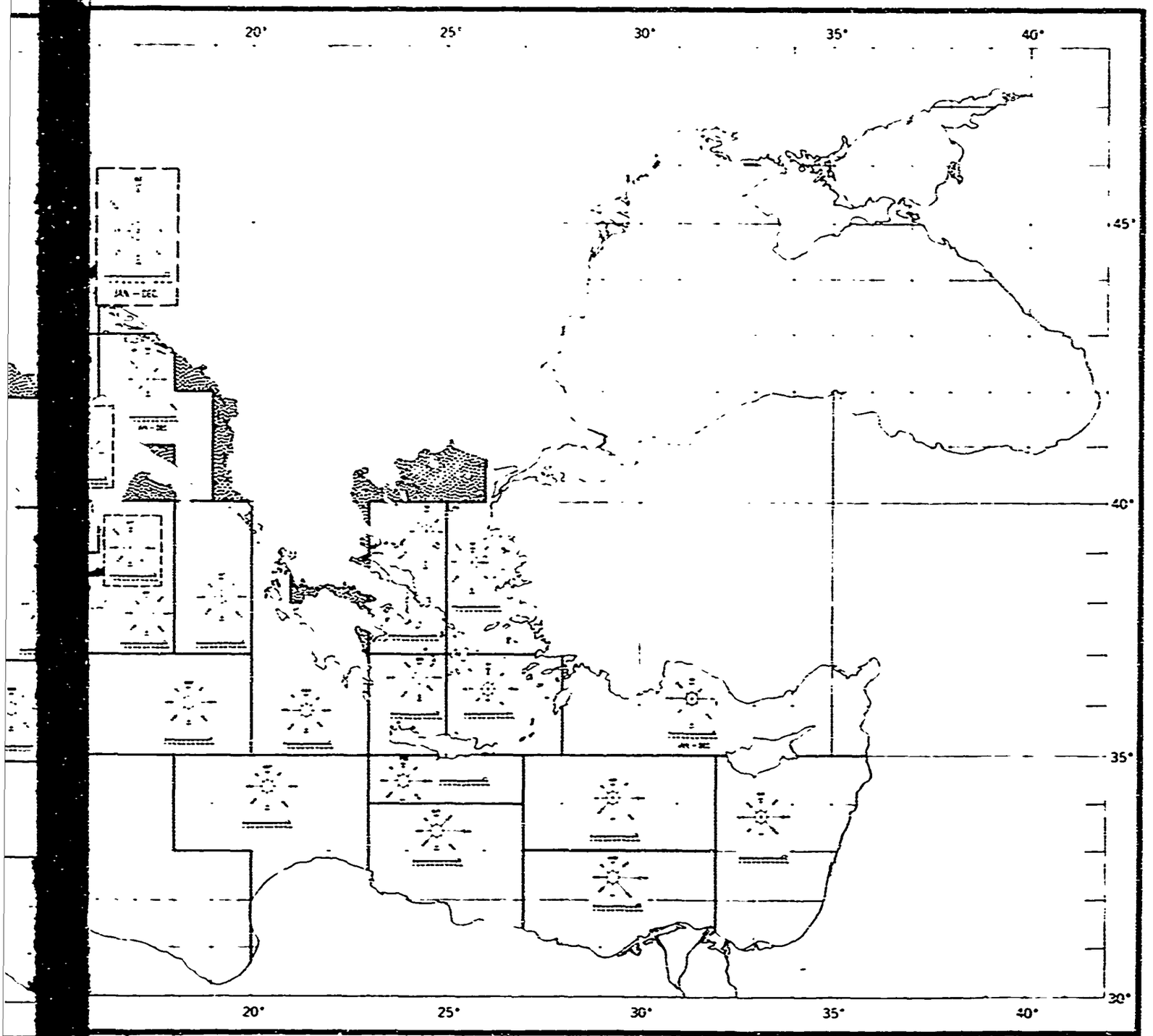

THE ENT ROSES IN THE MEDITERRANEAN SEA, WINTER

FIGURE 45. SURFACE CURRENTS, WINTER

2

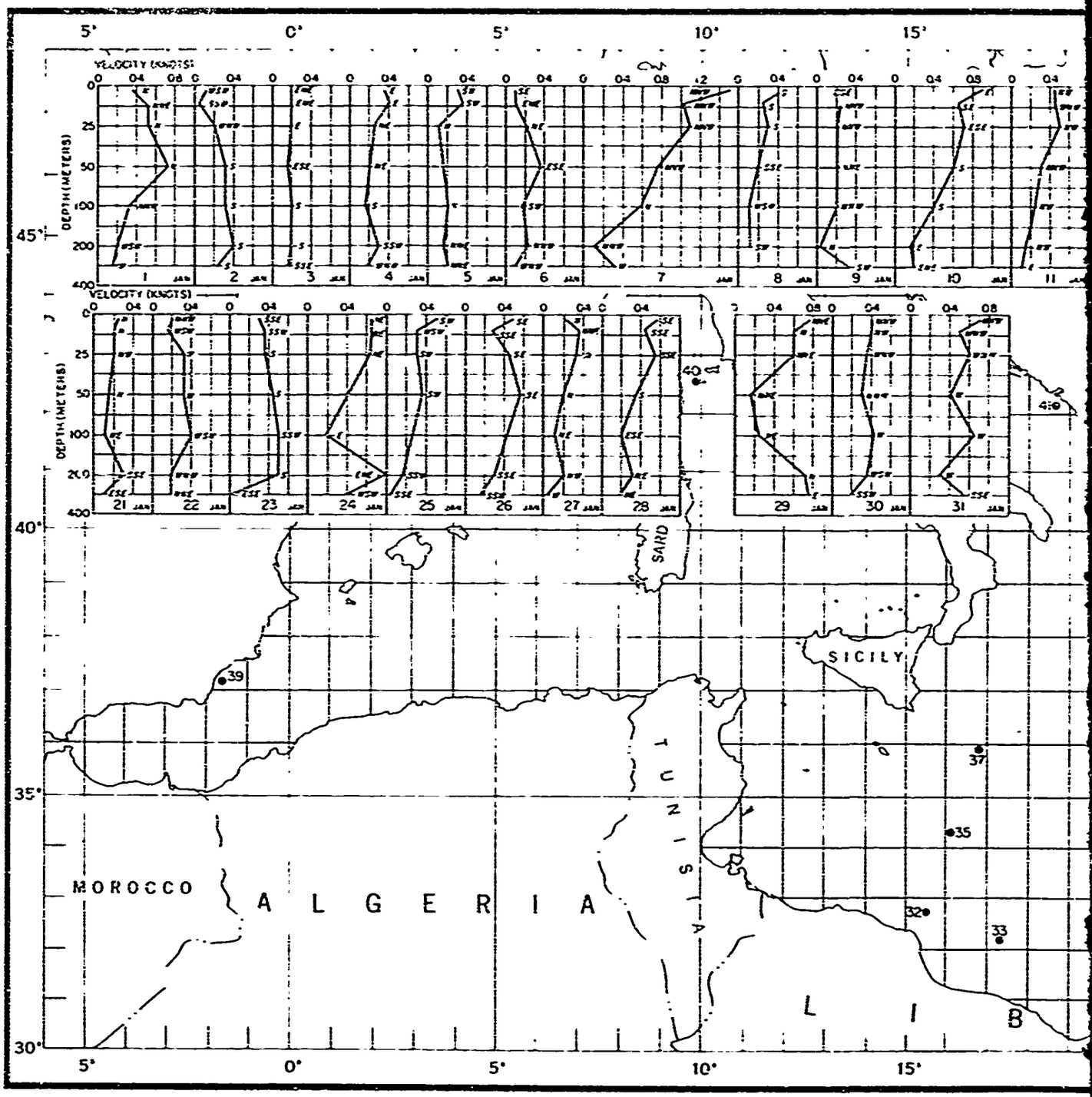

FIGURE 46. SUBSURFACE CURRENTS IN THE

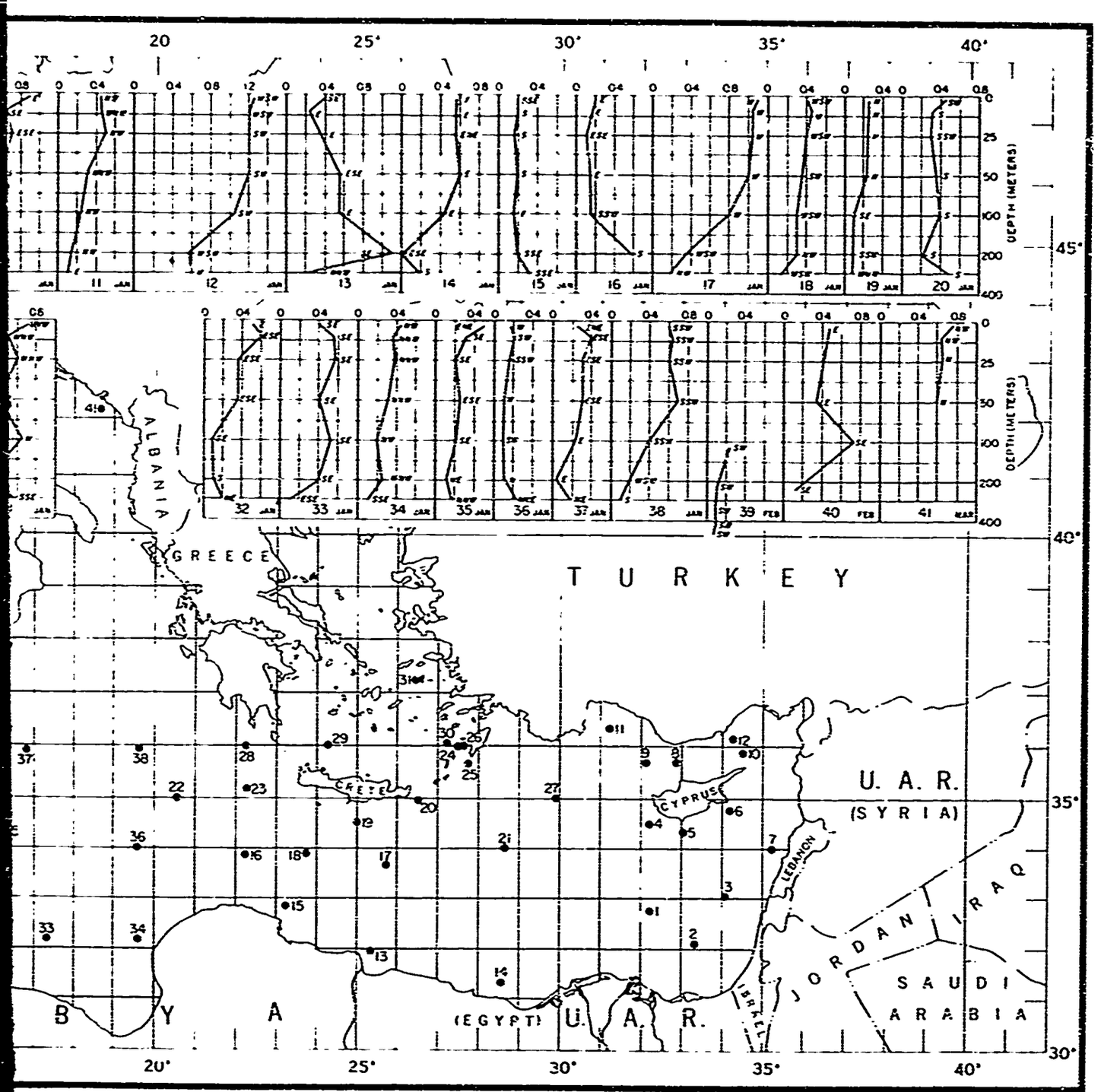

RRENTS IN THE MEDITERRANEAN SEA, WINTER

FIGURE 46. SUBSURFACE CURRENTS, WINTER

2

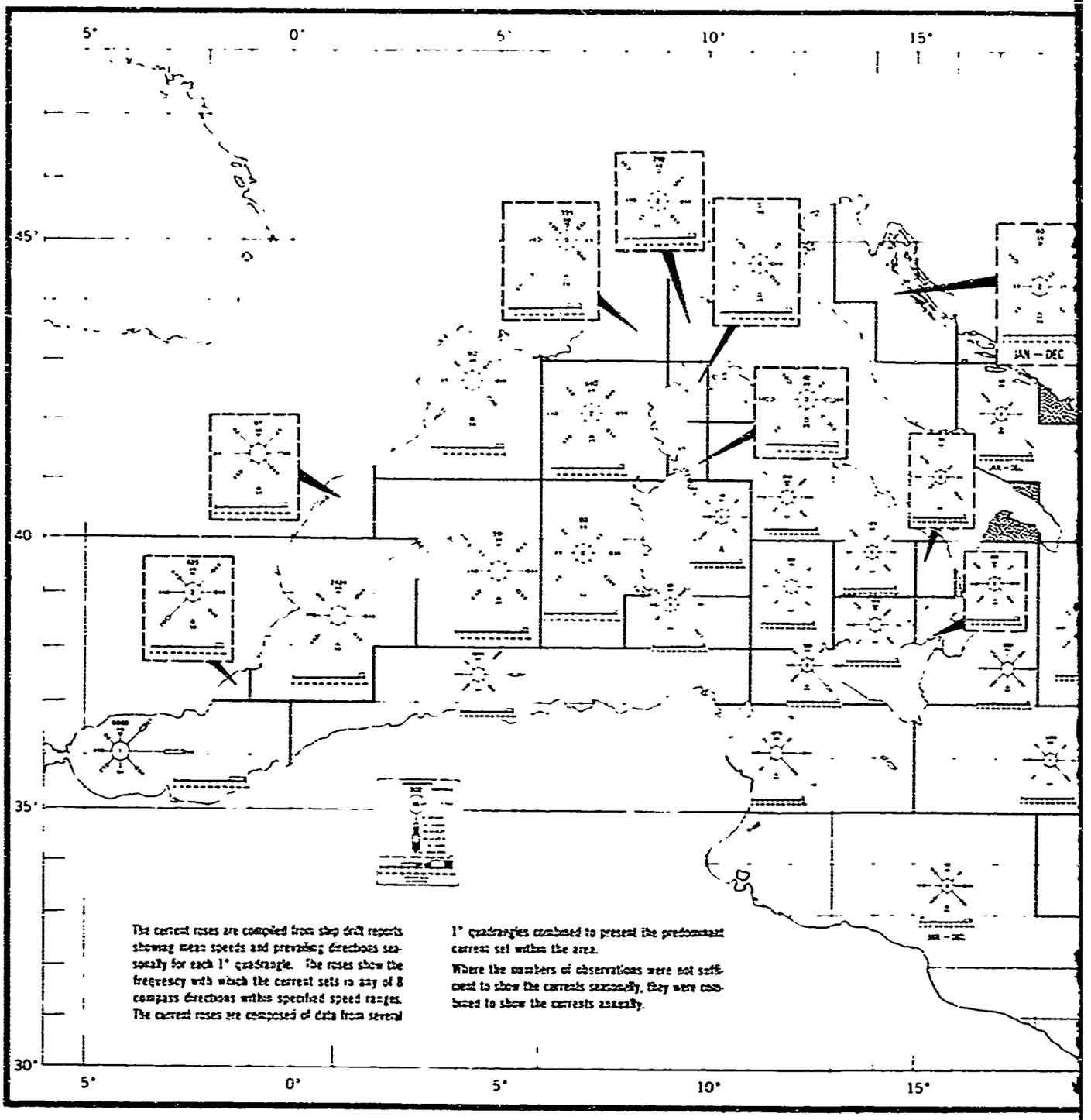

FIGURE 47. SURFACE CURRENT ROSES IN TH

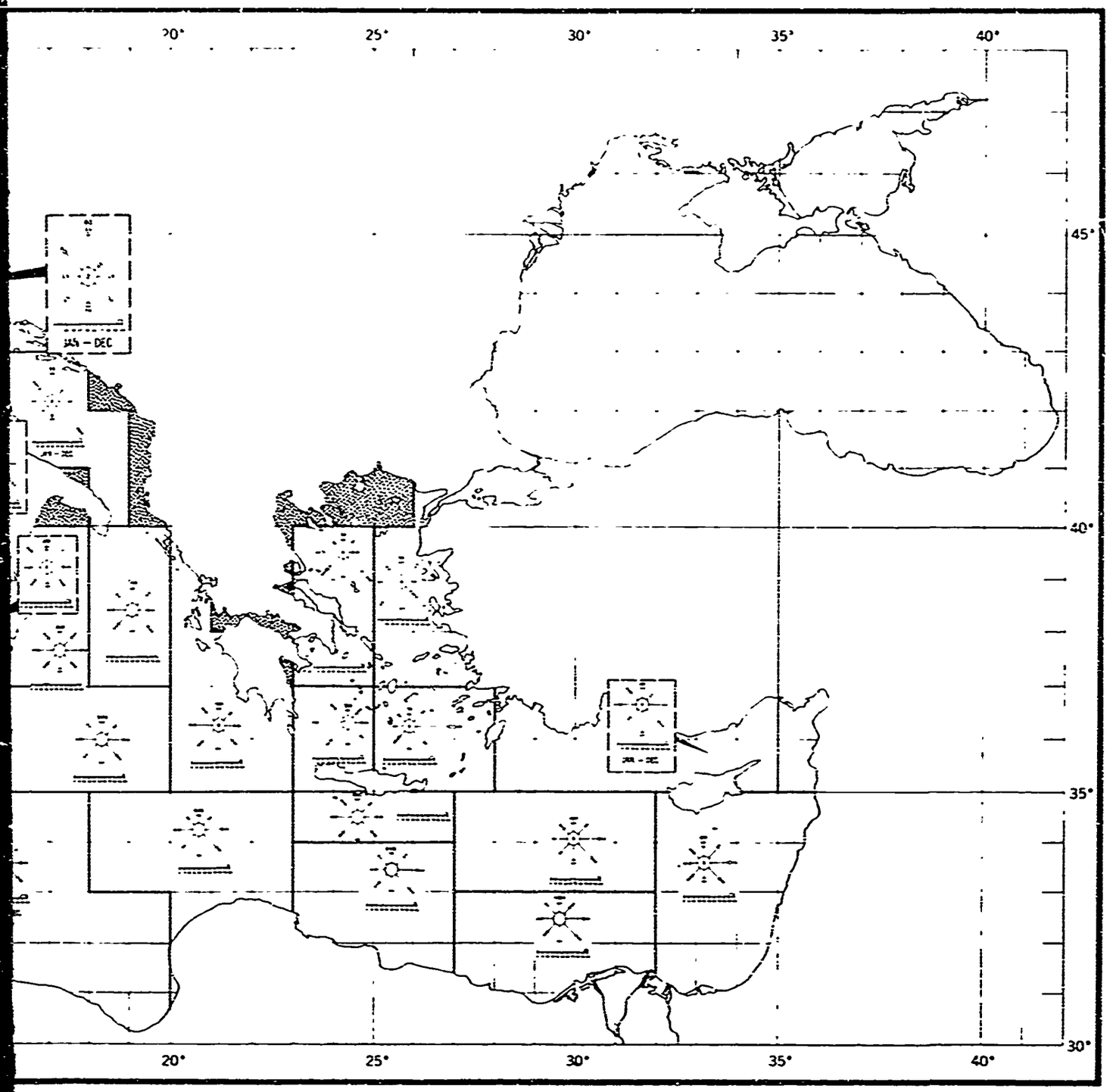

IN TH ENT ROSES IN THE MEDITERRANEAN SEA, SPRING

FIGURE 47. SURFACE CURRENTS, SPRING

2

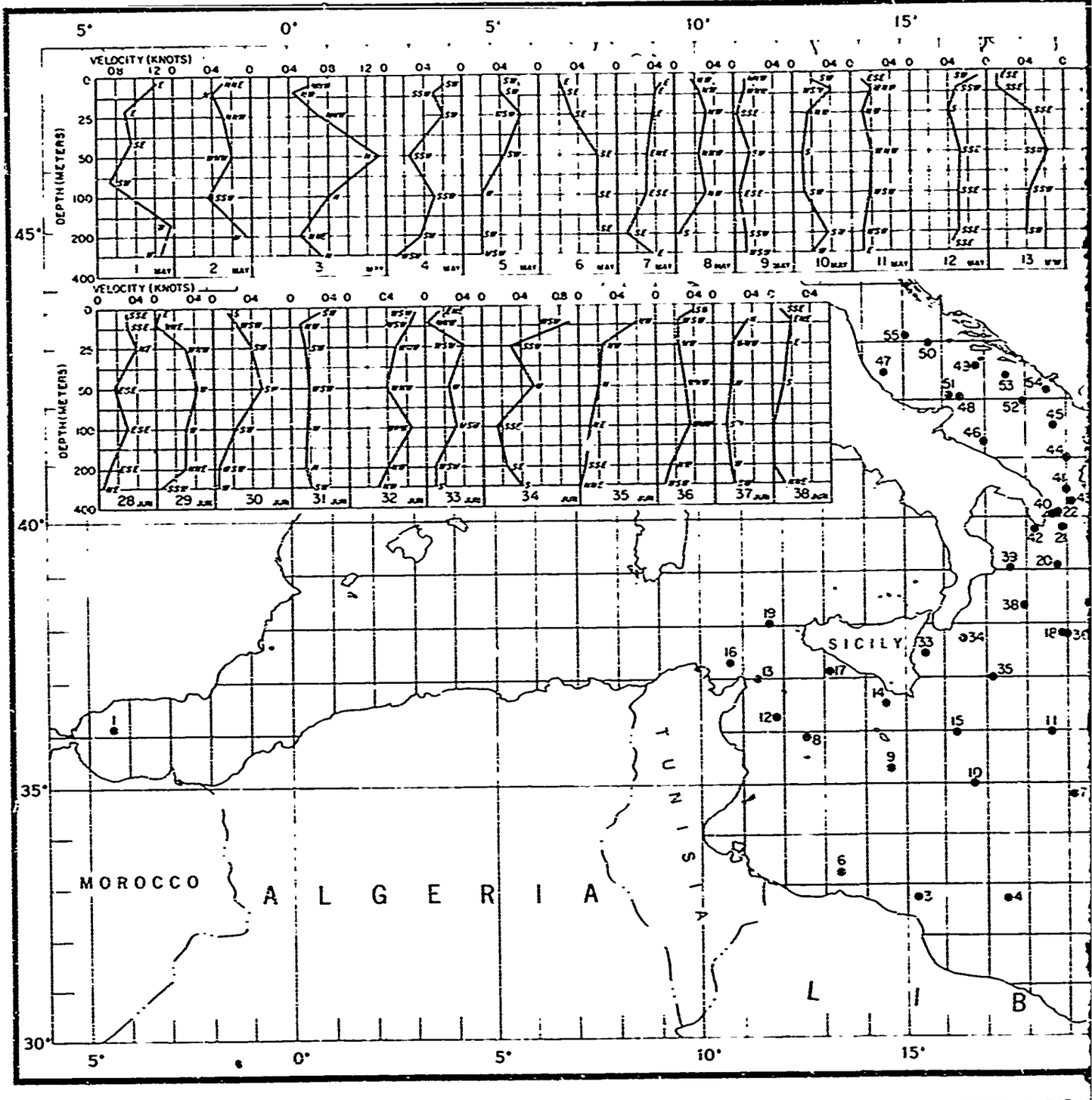

FIGURE 48. SUBSURFACE CURRENTS IN THE M

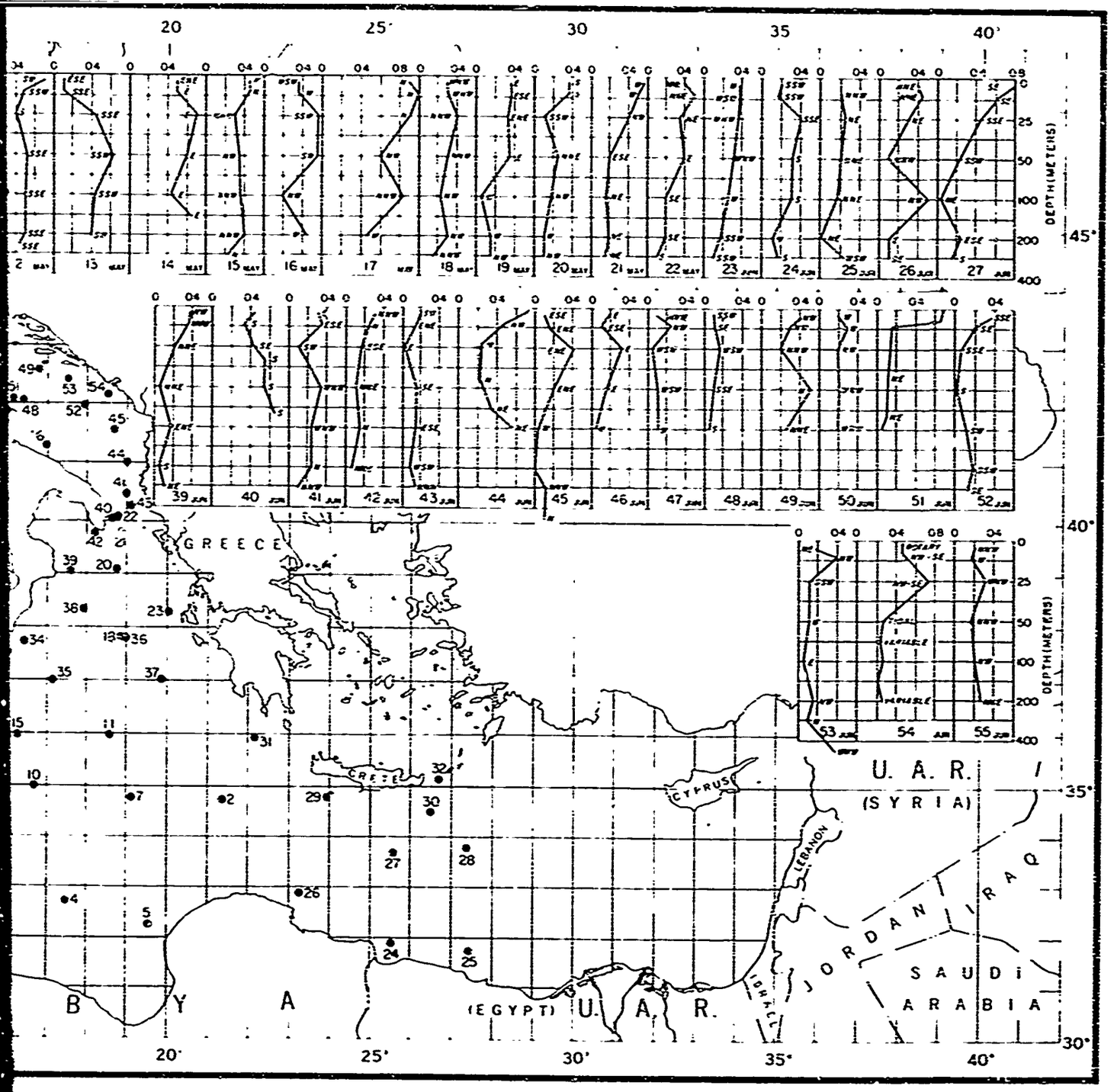

RRENTS IN THE MEDITERRANEAN SEA, SPRING

FIGURE 48. SUBSURFACE CURRENTS, SPRING

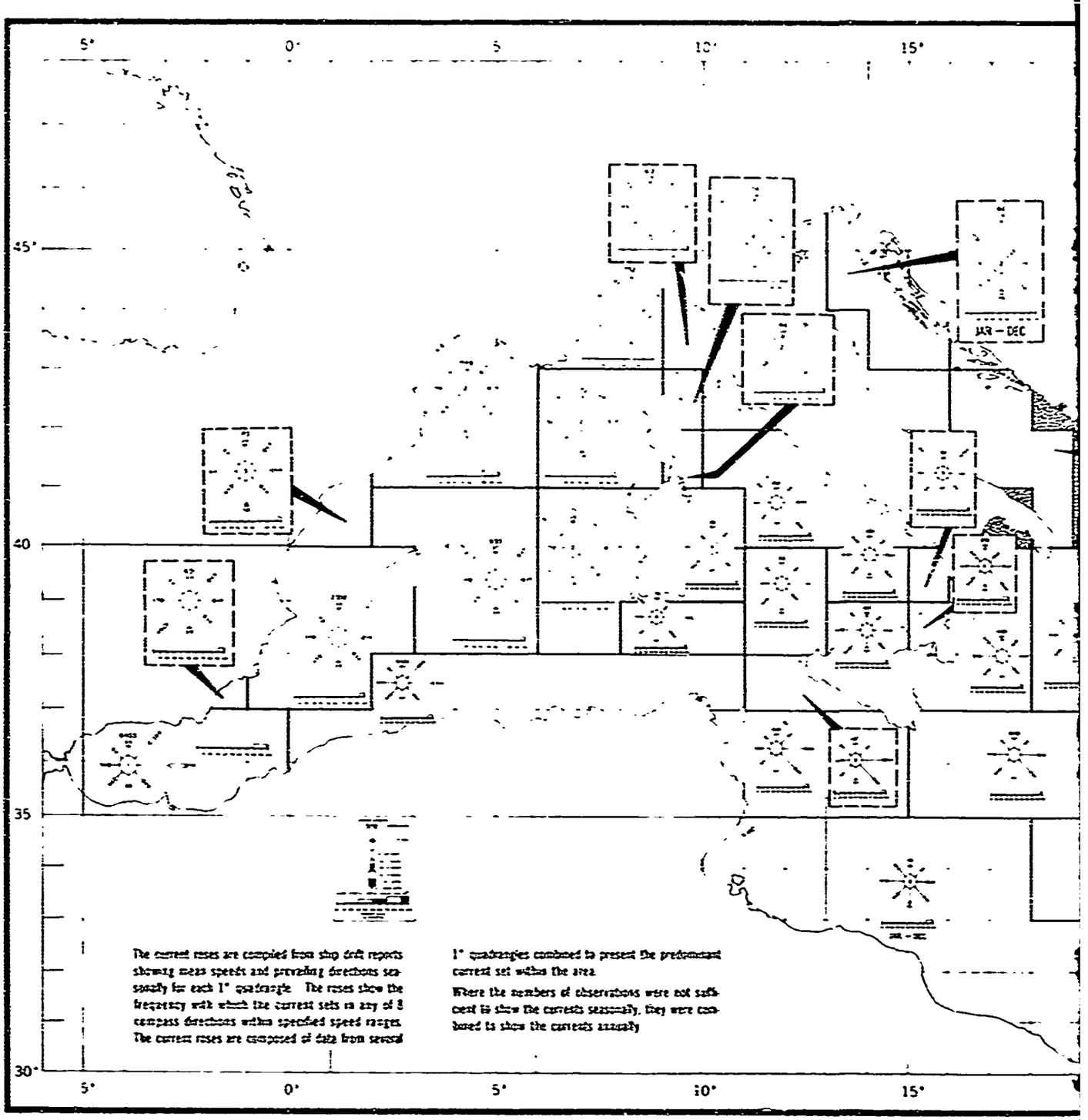

FIGURE 49. SURFACE CURRENT ROSES IN TH

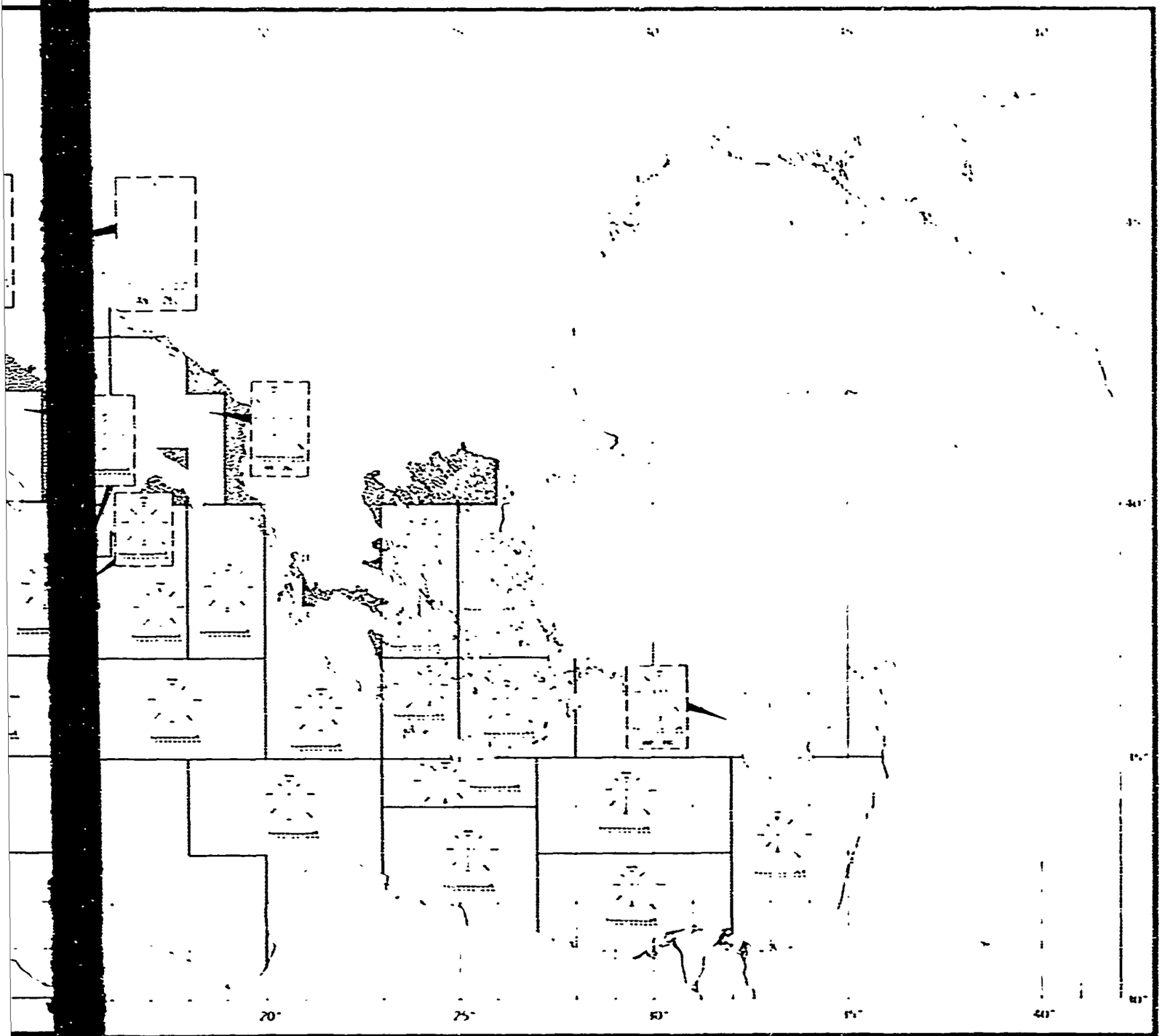

IN TH RRENT ROSES IN THE MEDITERRANEAN SEA, SUMMER

FIGURE 49. SURFACE CURRENTS, SUMMER

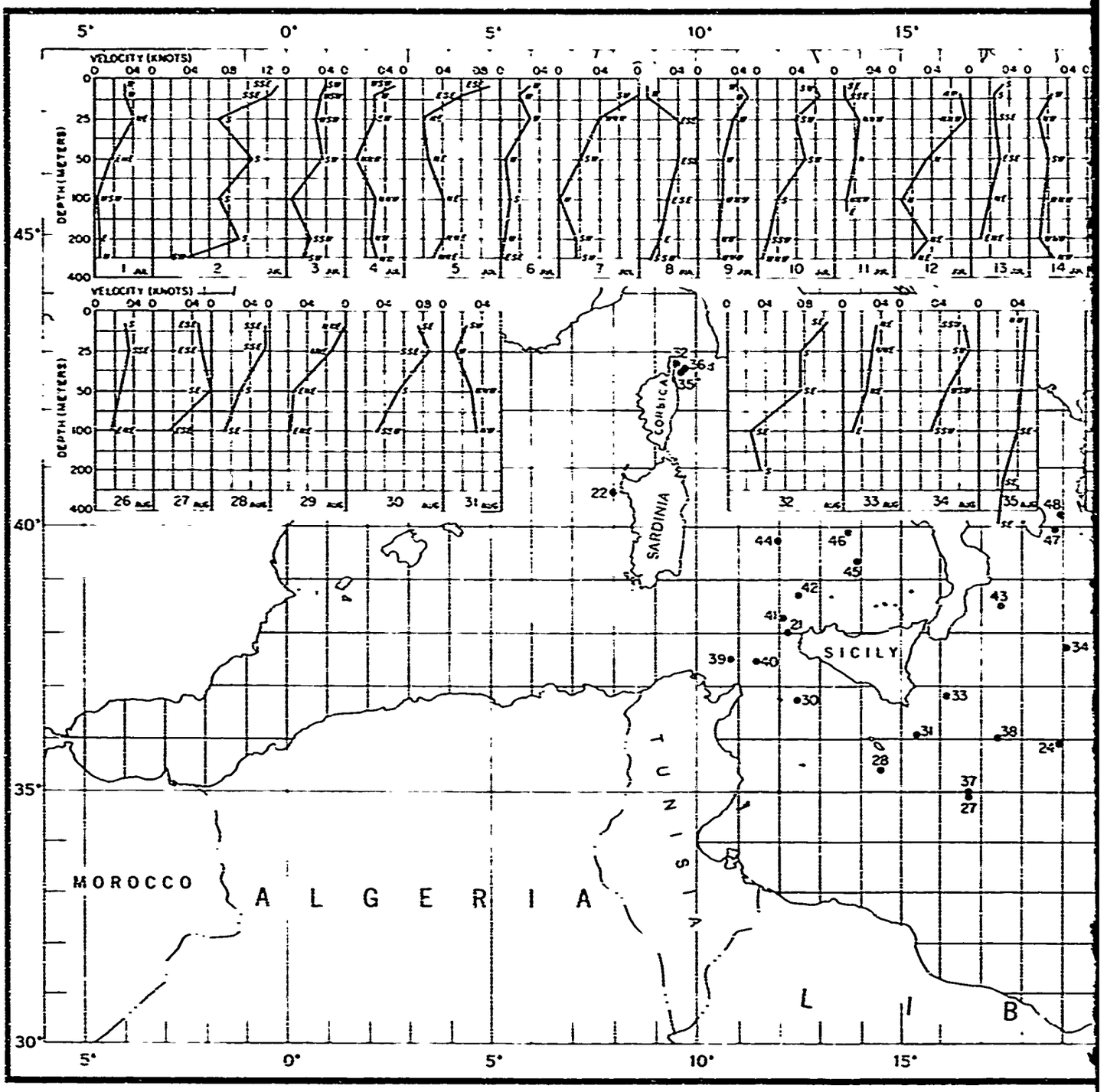

FIGURE 50. SUBSURFACE CURRENTS IN THE ME

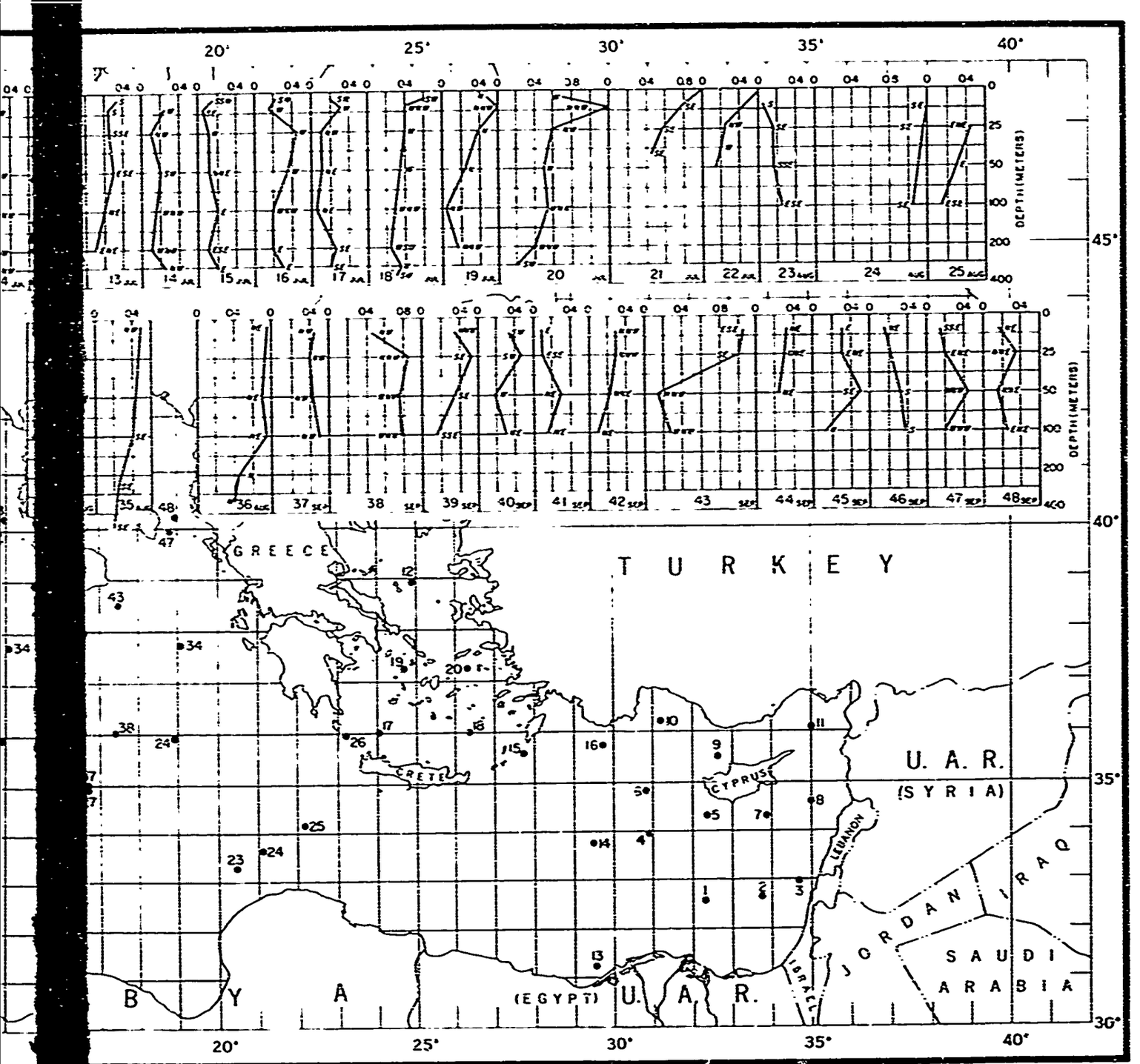

RENTS IN THE MEDITERRANEAN SEA, SUMMER

FIGURE 50. SUBSURFACE CURRENTS, SUMMER

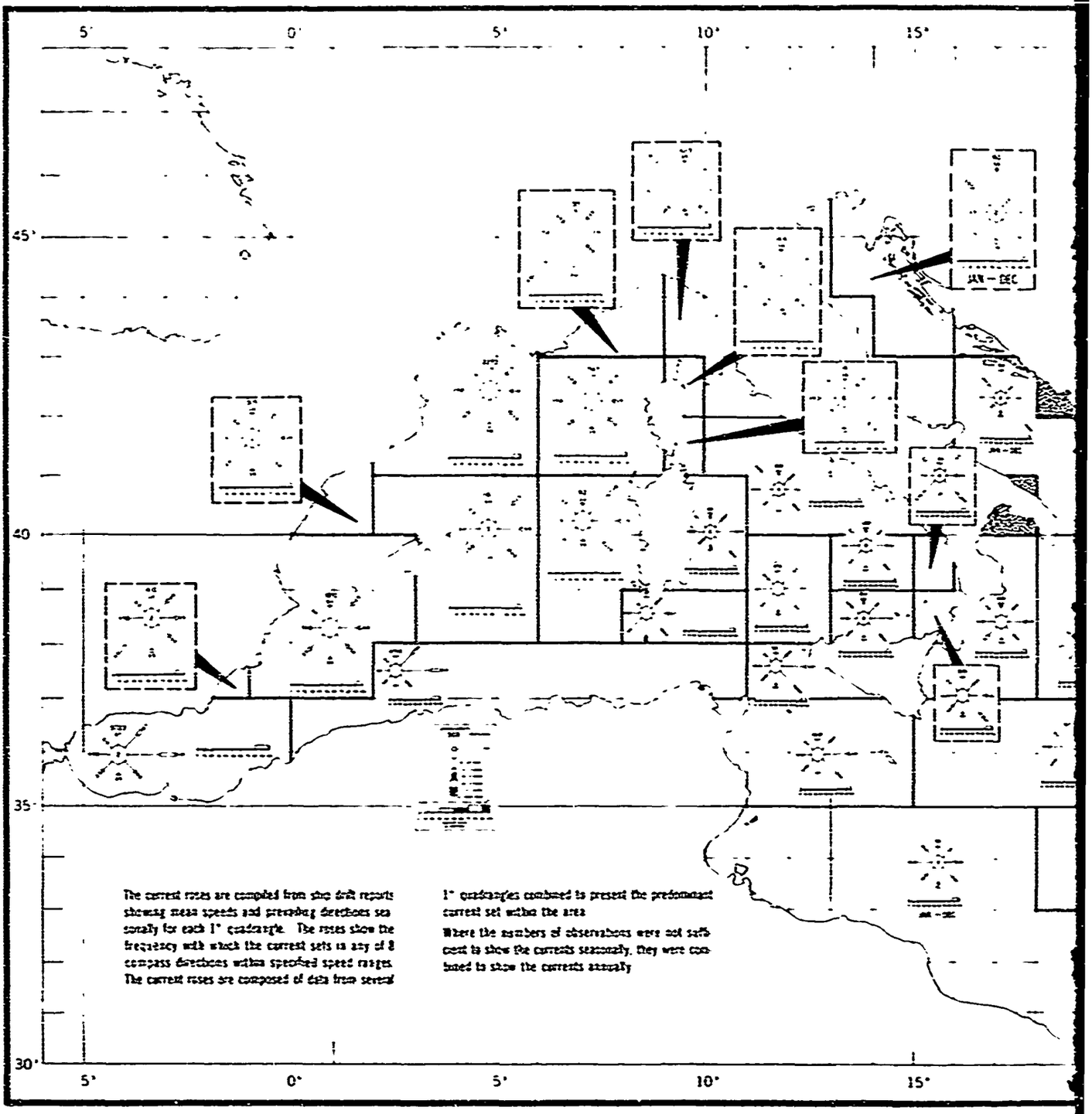

FIGURE 51. SURFACE CURRENT ROSES IN

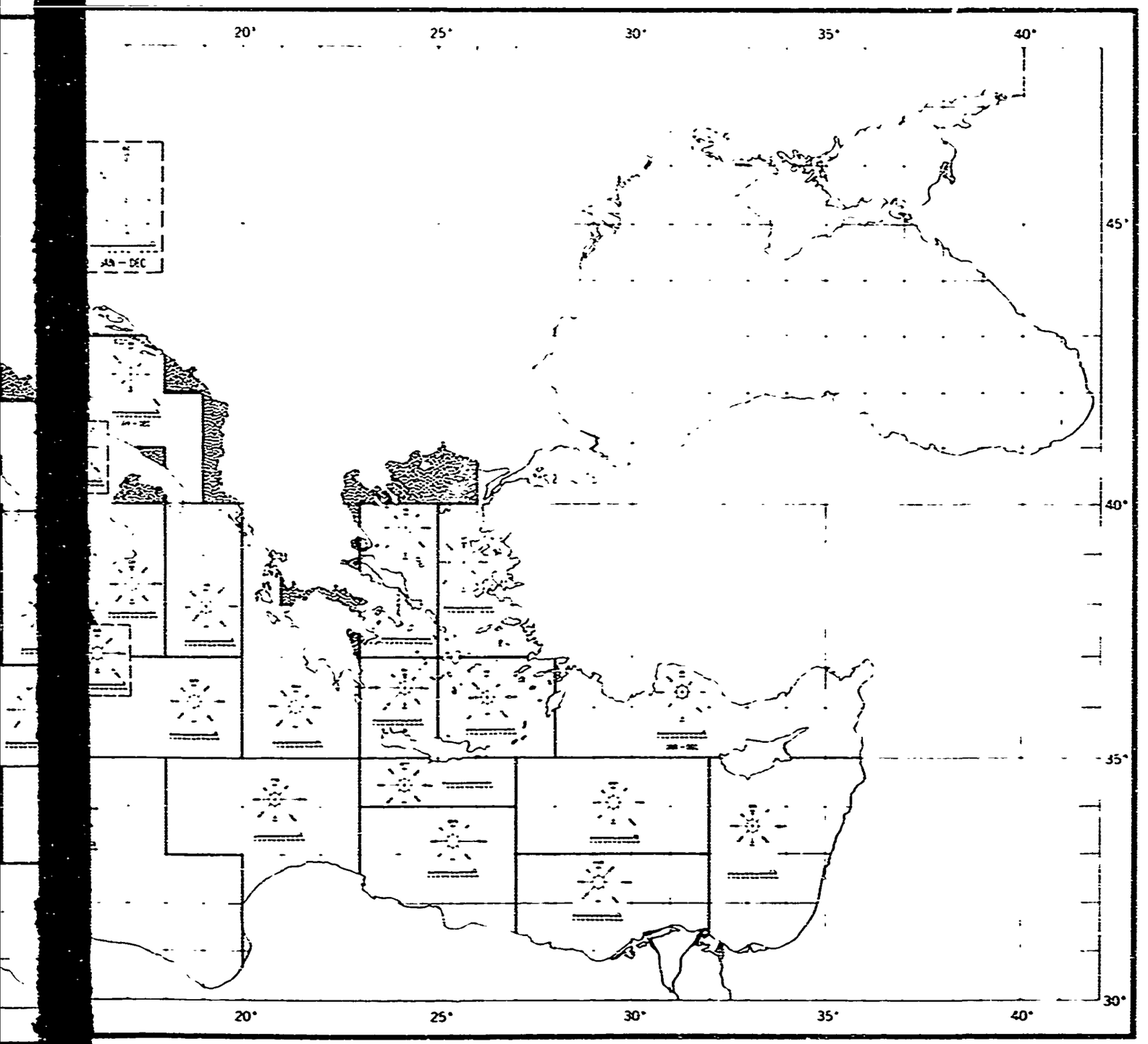

ES IN RRENT ROSES IN THE MEDITERRANEAN SEA, FALL

FIGURE 51. SURFACE CURRENTS, FALL

2

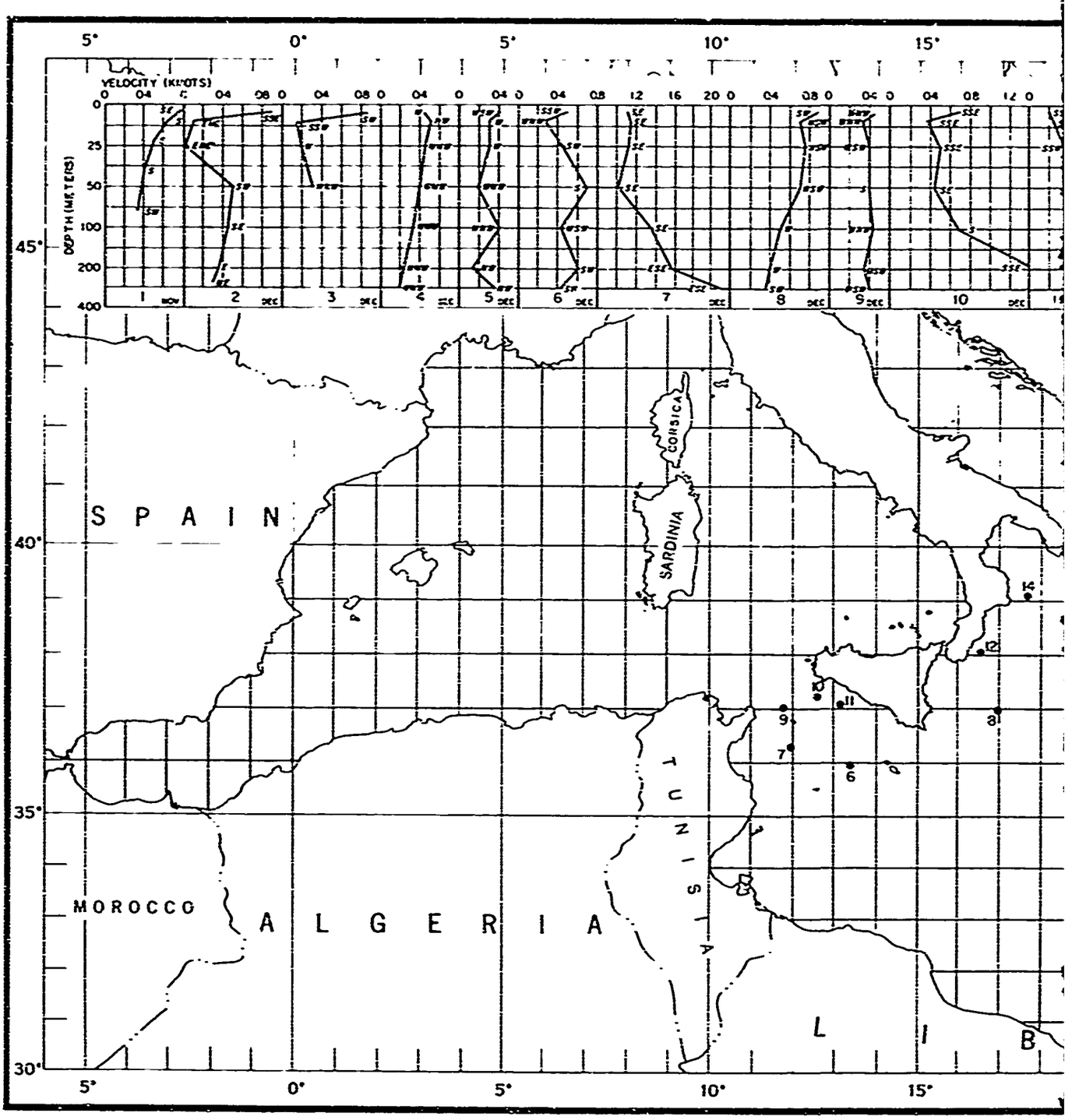

FIGURE 52. SUBSURFACE CURRENTS IN

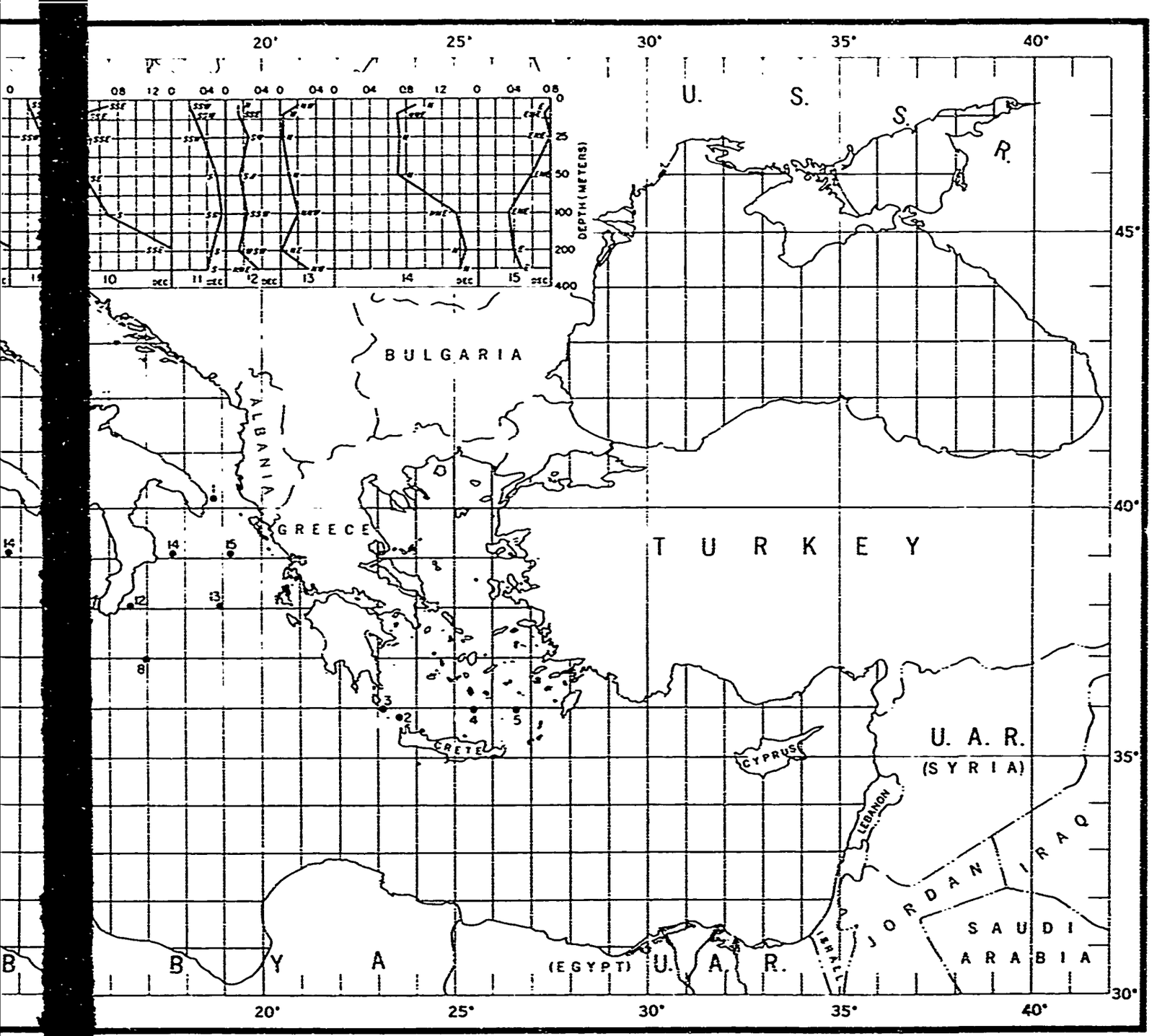

NTS IN ACE CURRENTS IN THE MEDITERRANEAN SEA, FALL

FIGURE 52. SUBSURFACE CURRENTS, FALL

2

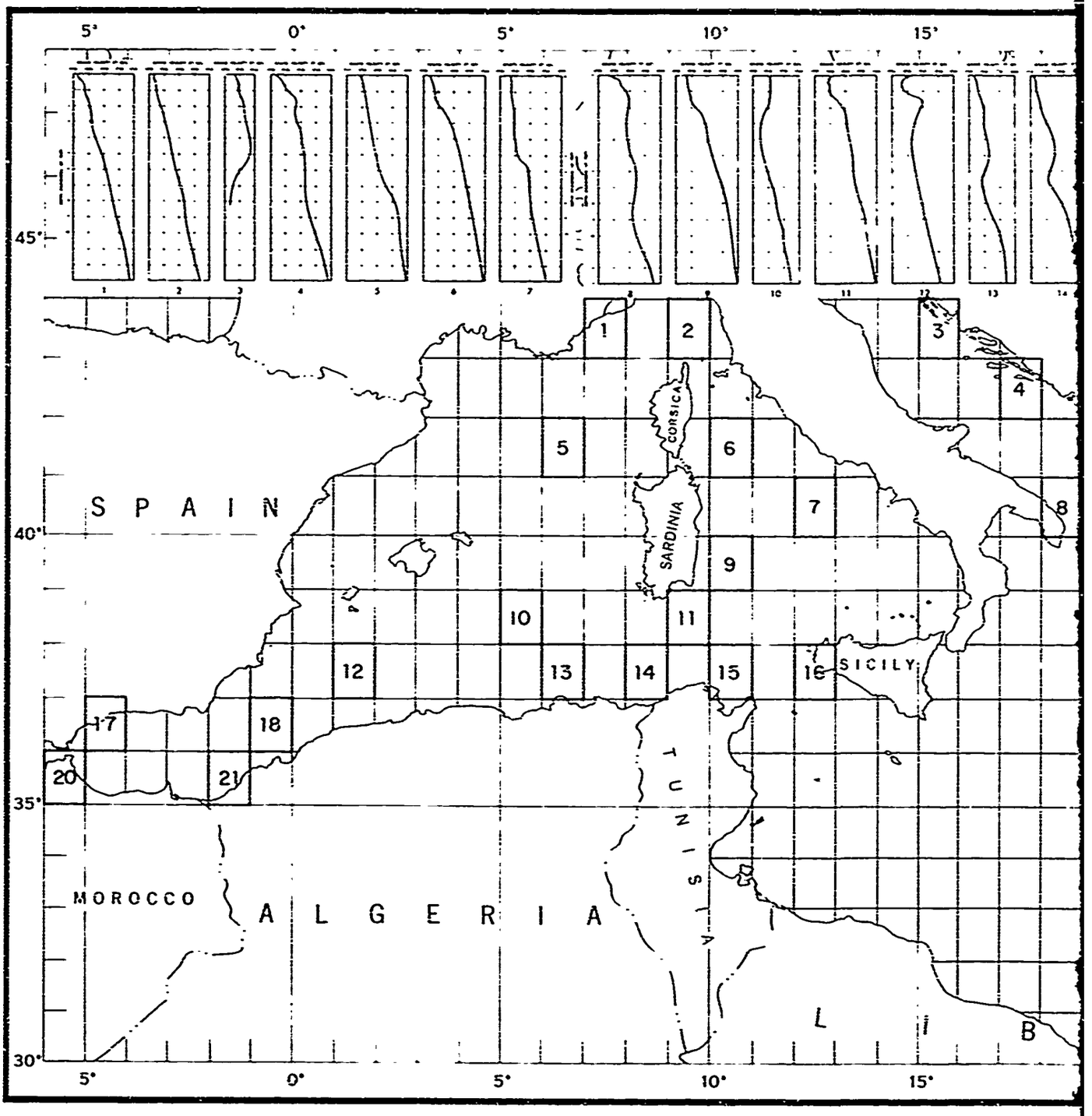

FIGURE 53. MEAN SOUND VELOCITY PROFIL

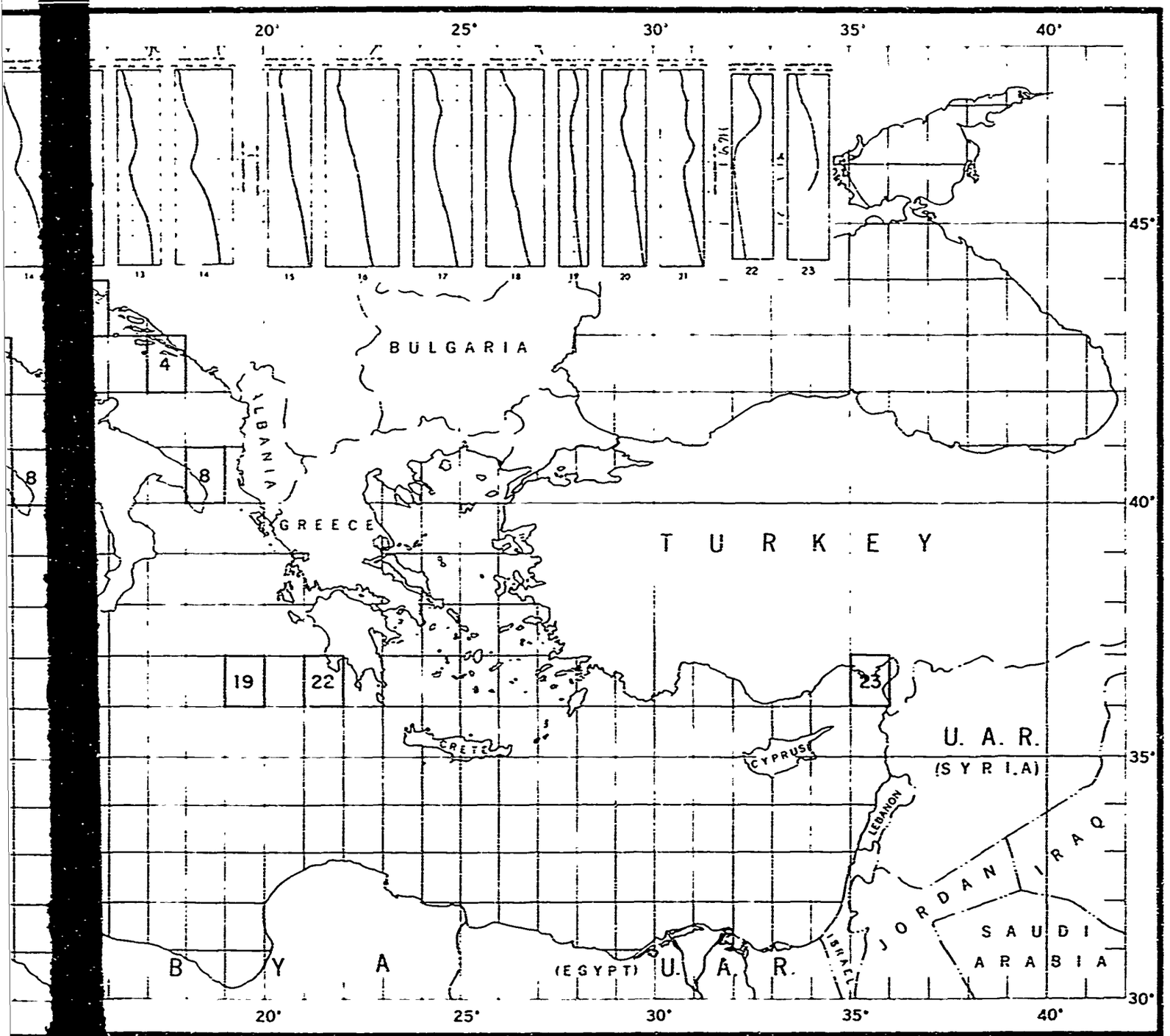

ROFIL ELOCITY PROFILES IN THE MEDITERRANEAN SEA, WINTER

FIGURE 53. SOUND VELOCITY PROFILES, WINTER

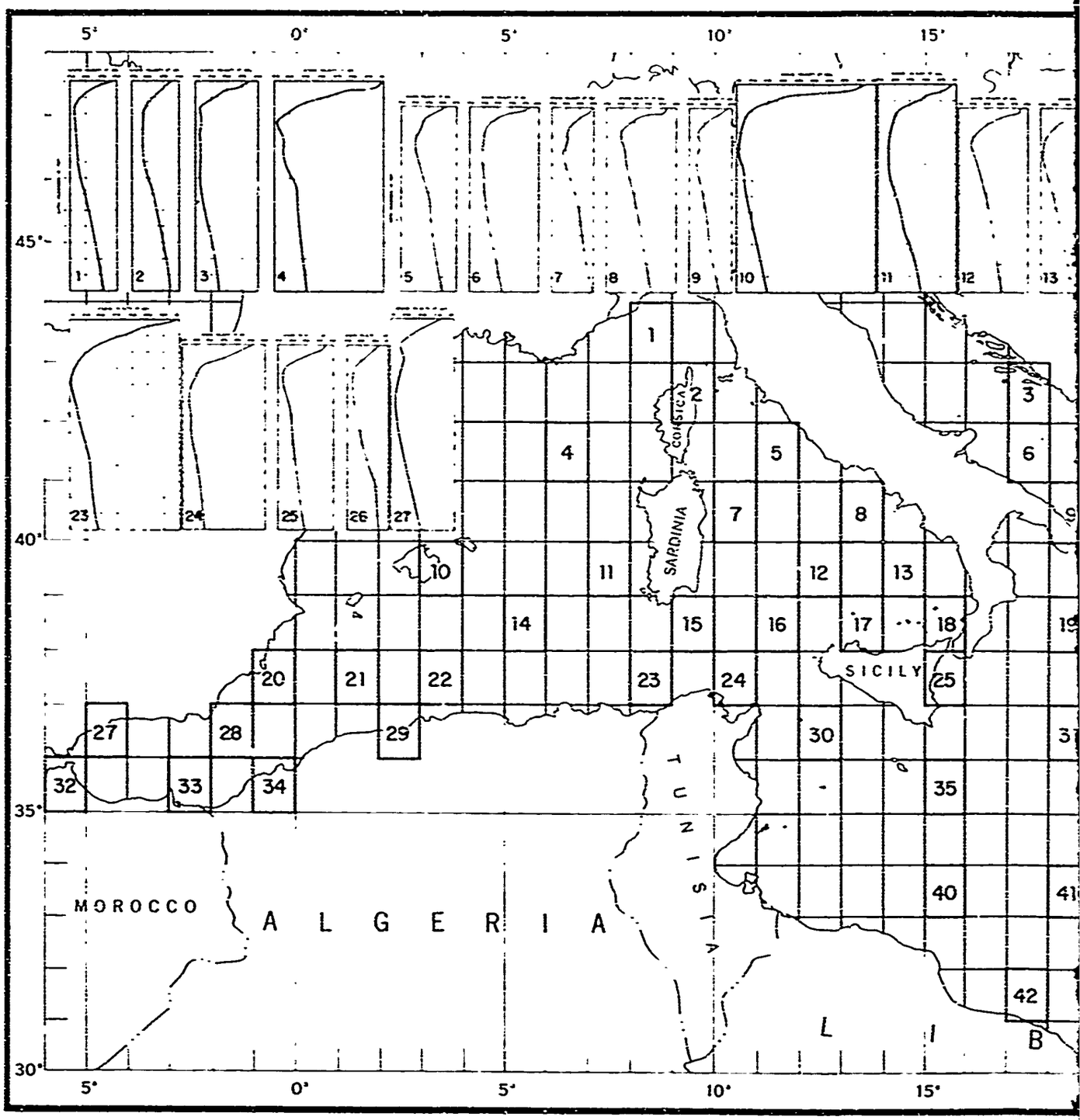

FIGURE 54. MEAN SOUND VELOCITY PROFIL

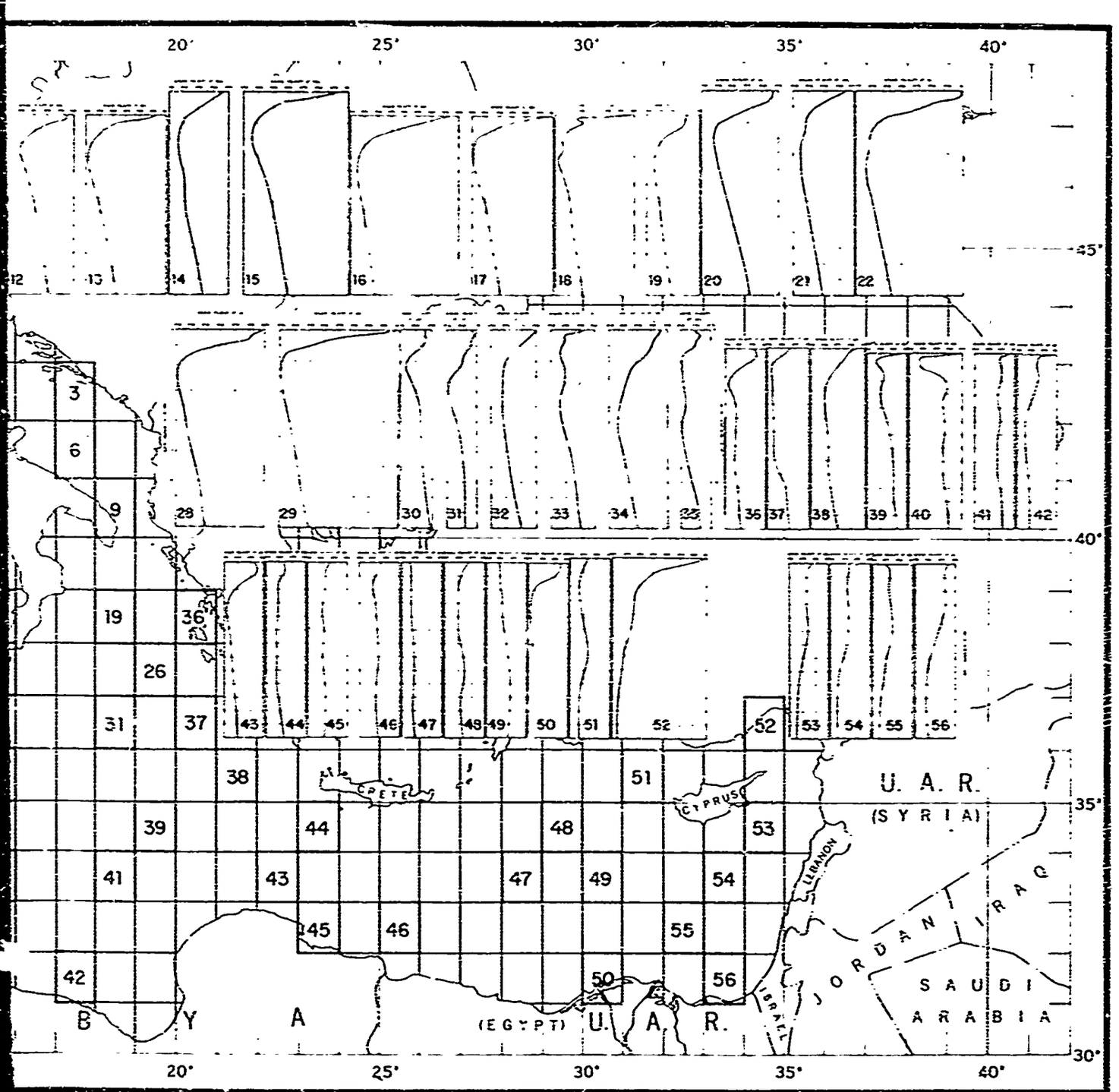

LOCITY PROFILES IN THE MEDITERRANEAN SEA, SPRING

FIGURE 54. SOUND VELOCITY PROFILES, SPRING

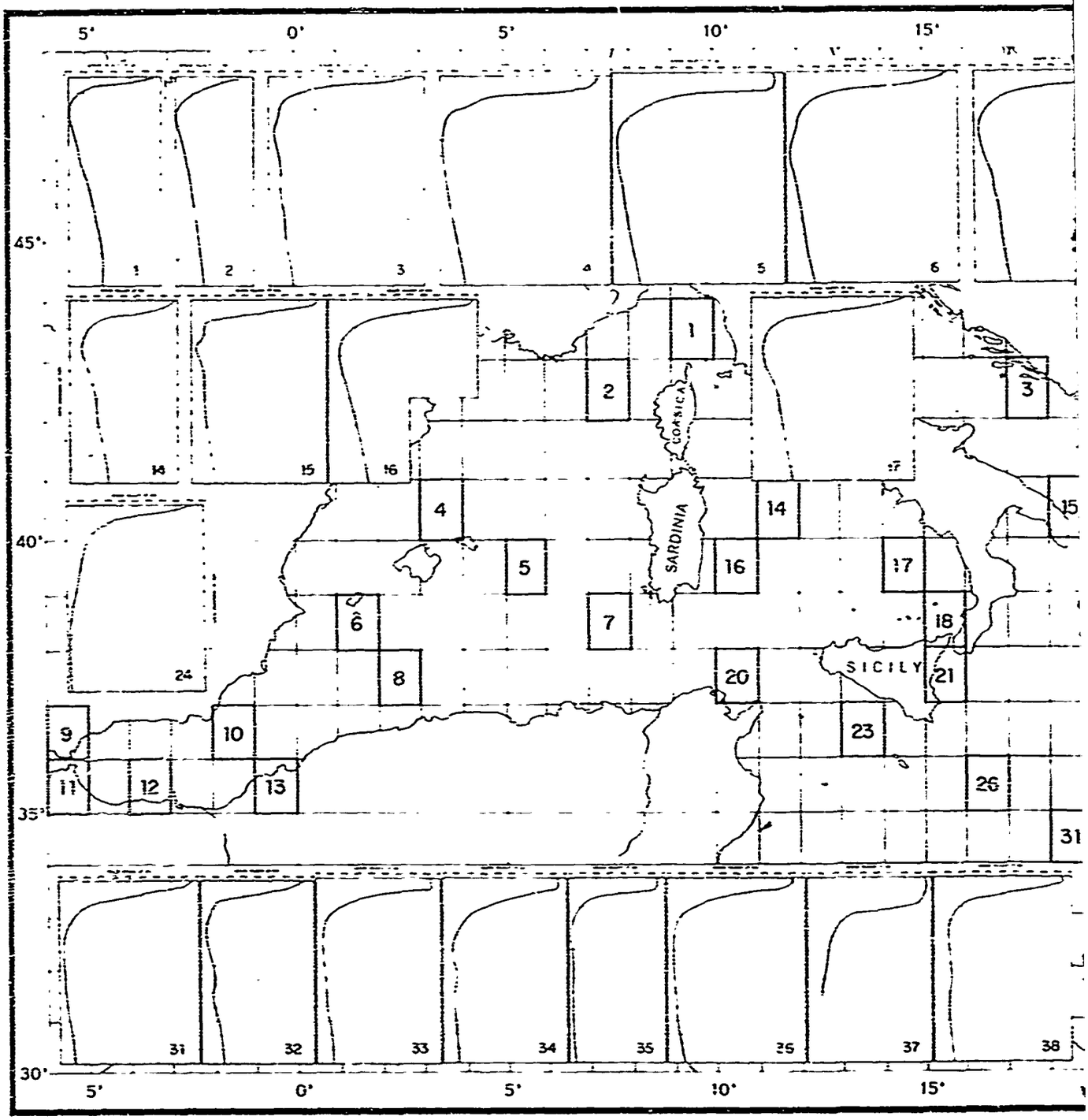

FIGURE 55. MEAN SOUND VELOCITY PROFILE

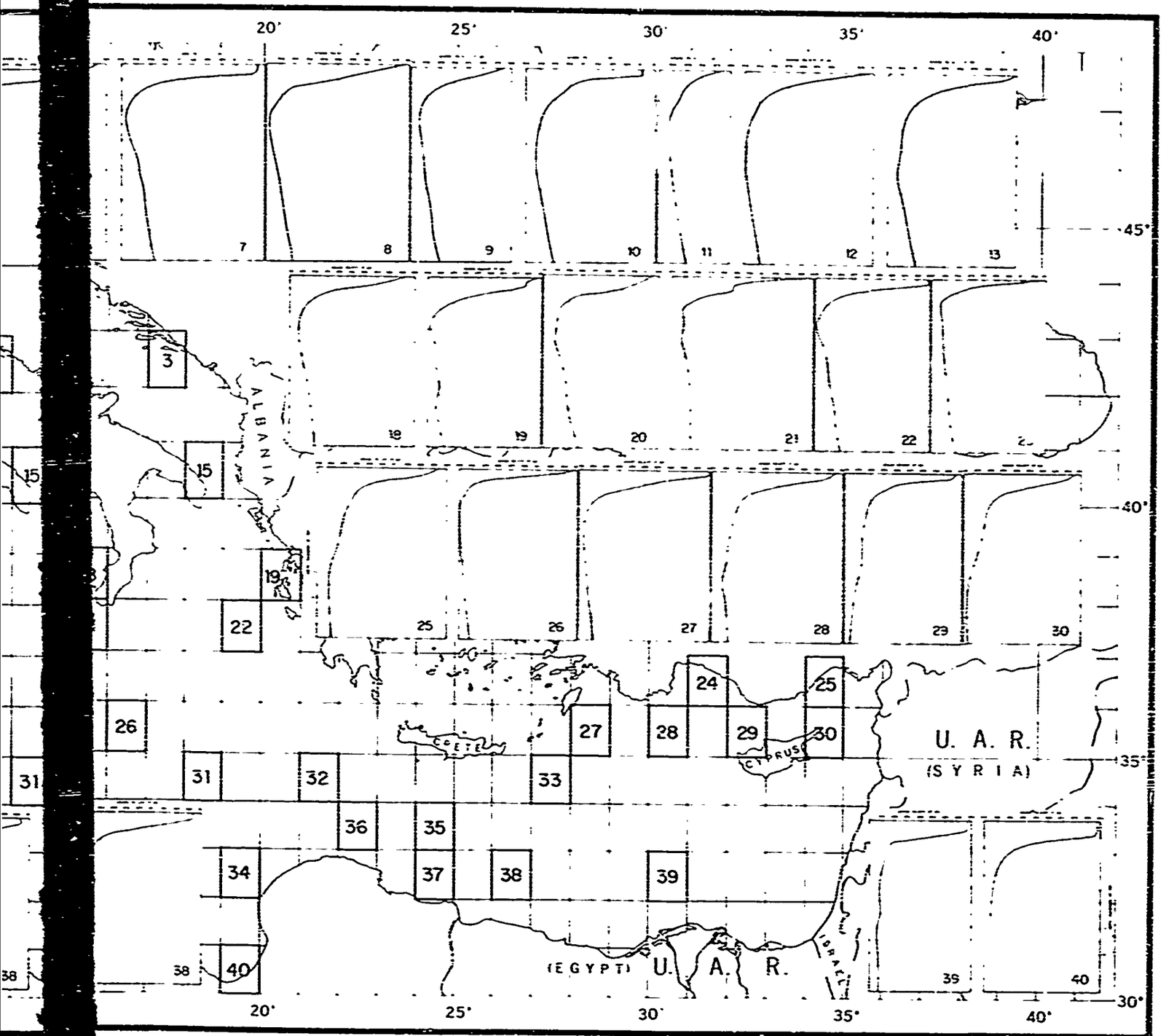

OFILES ELOCITY PROFILES IN THE MEDITERRANEAN SEA, SUMMER

FIGURE 55. SOUND VELOCITY PROFILES, SUMMER

2

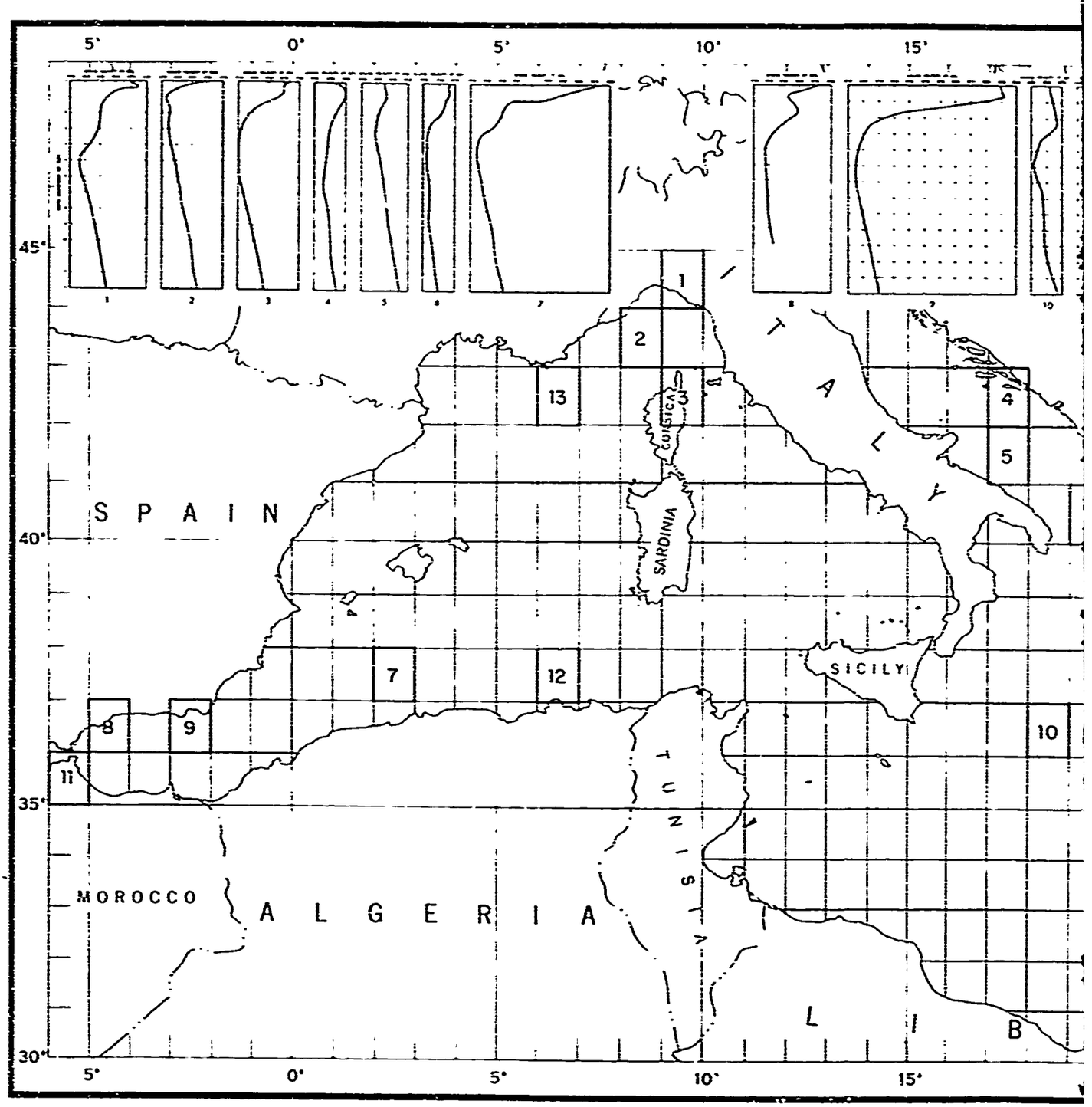

FIGURE 56. MEAN SOUND VELOCITY PROFILES

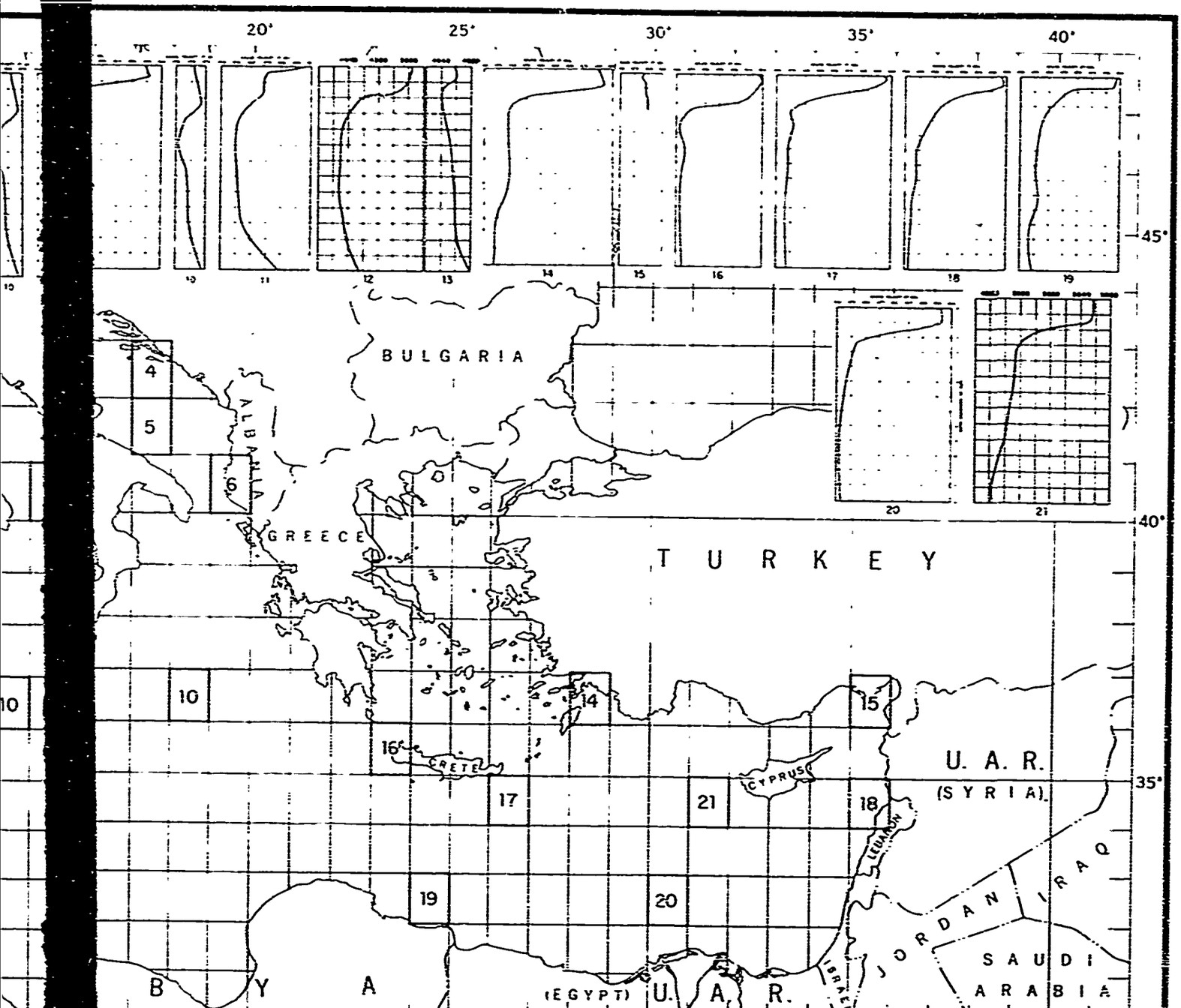

OFILES LOCITY PROFILES IN THE MEDITERRANEAN SEA, FALL

FIGURE 56. SOUND VELOCITY PROFILES, FALL

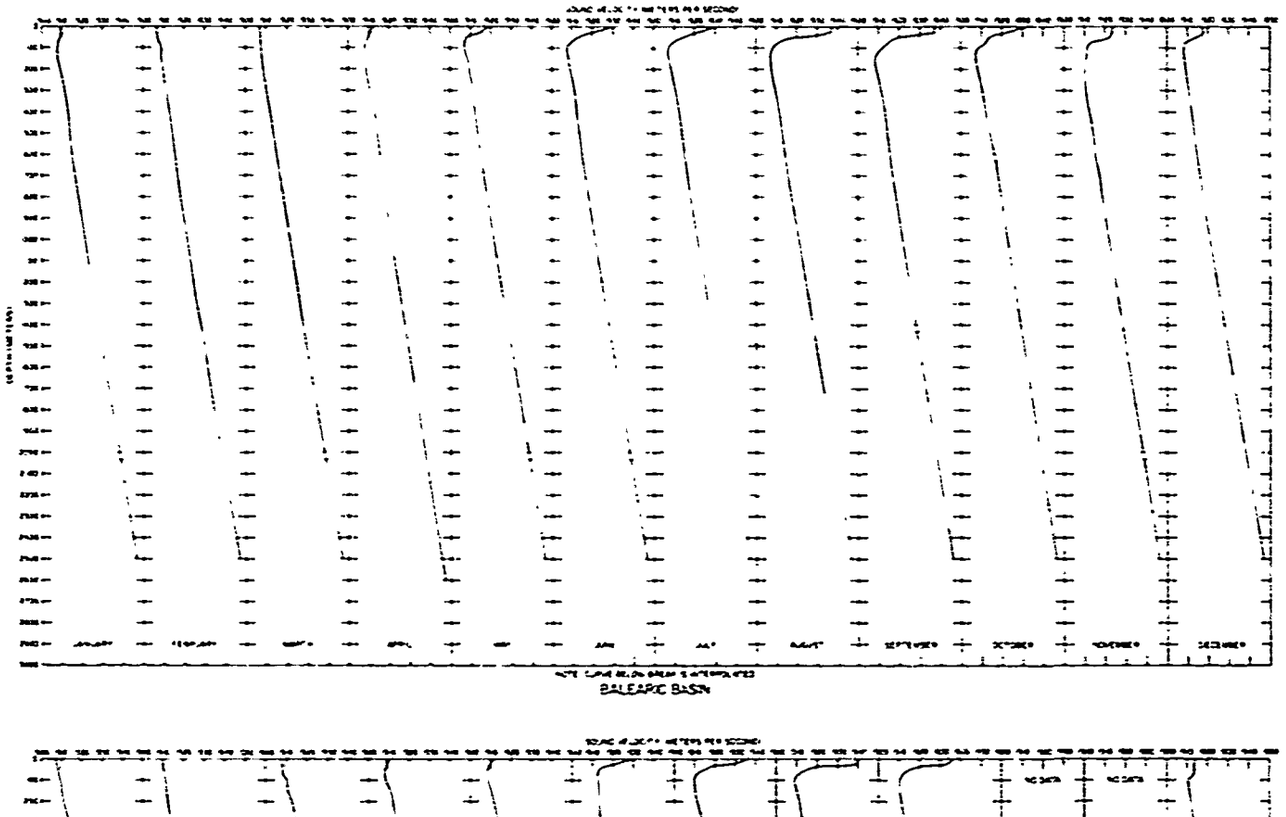

FIGURE 57. TYPICAL MONTHLY SOUND VELOCITY PROFILES

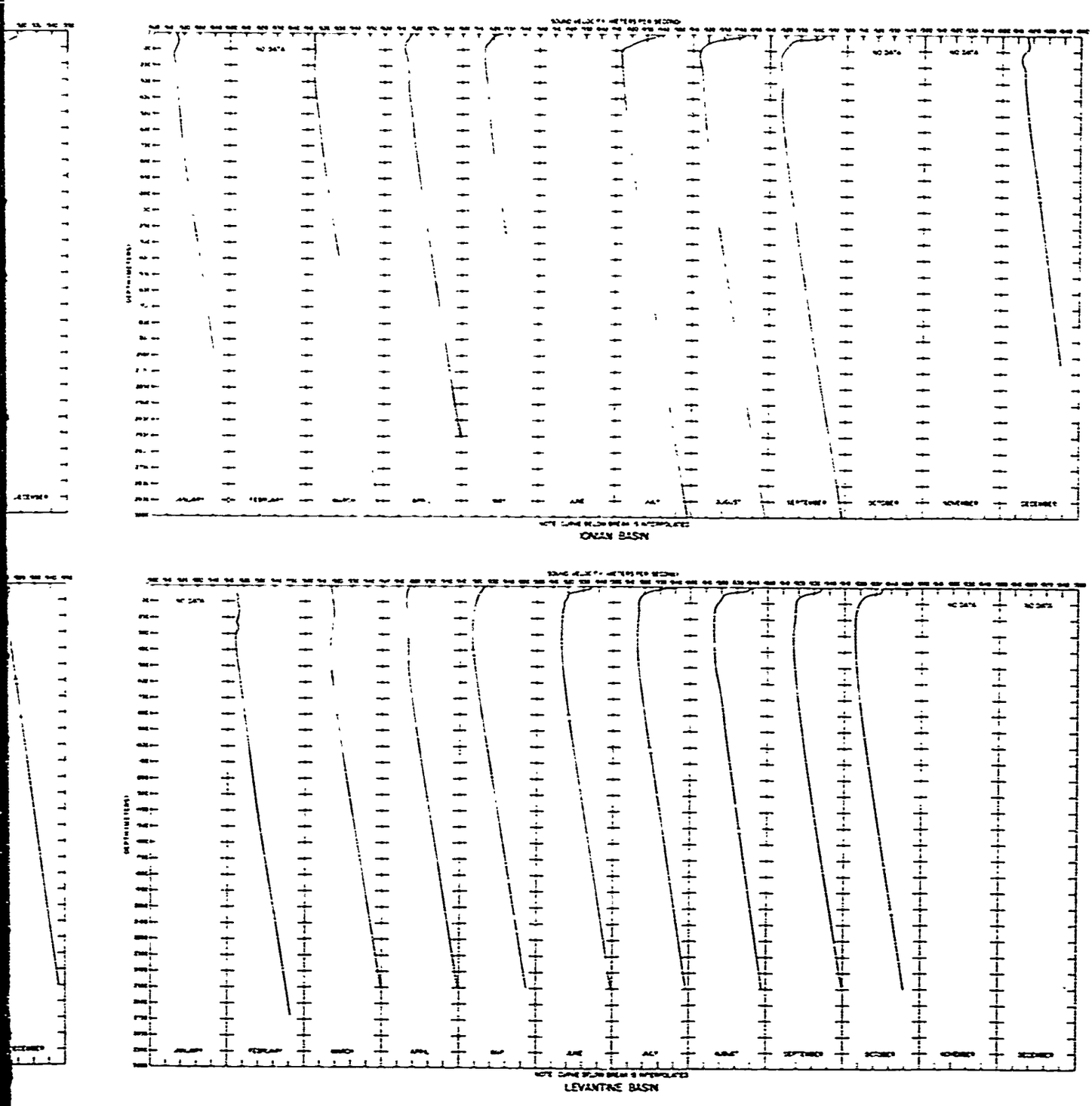

LOCITY PROFILES FOR MAJOR BASINS IN THE MEDITERRANEAN SEA

FIGURE 57. SOUND VELOCITY PROFILES FOR MAJOR BASINS

2

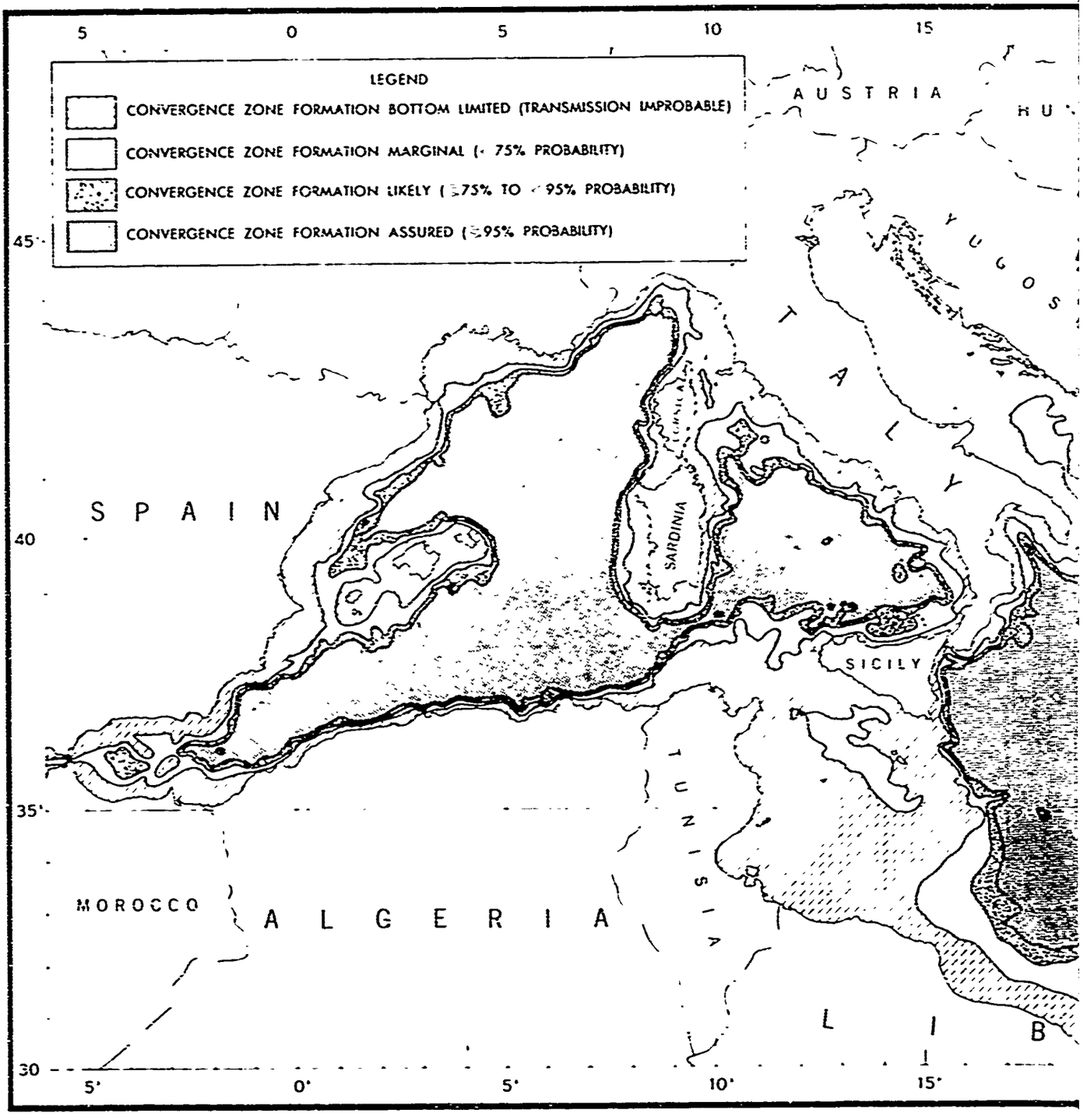

FIGURE 58. PERCENT PROBABILITY OF CONVERGENCE ZONE FORMATION

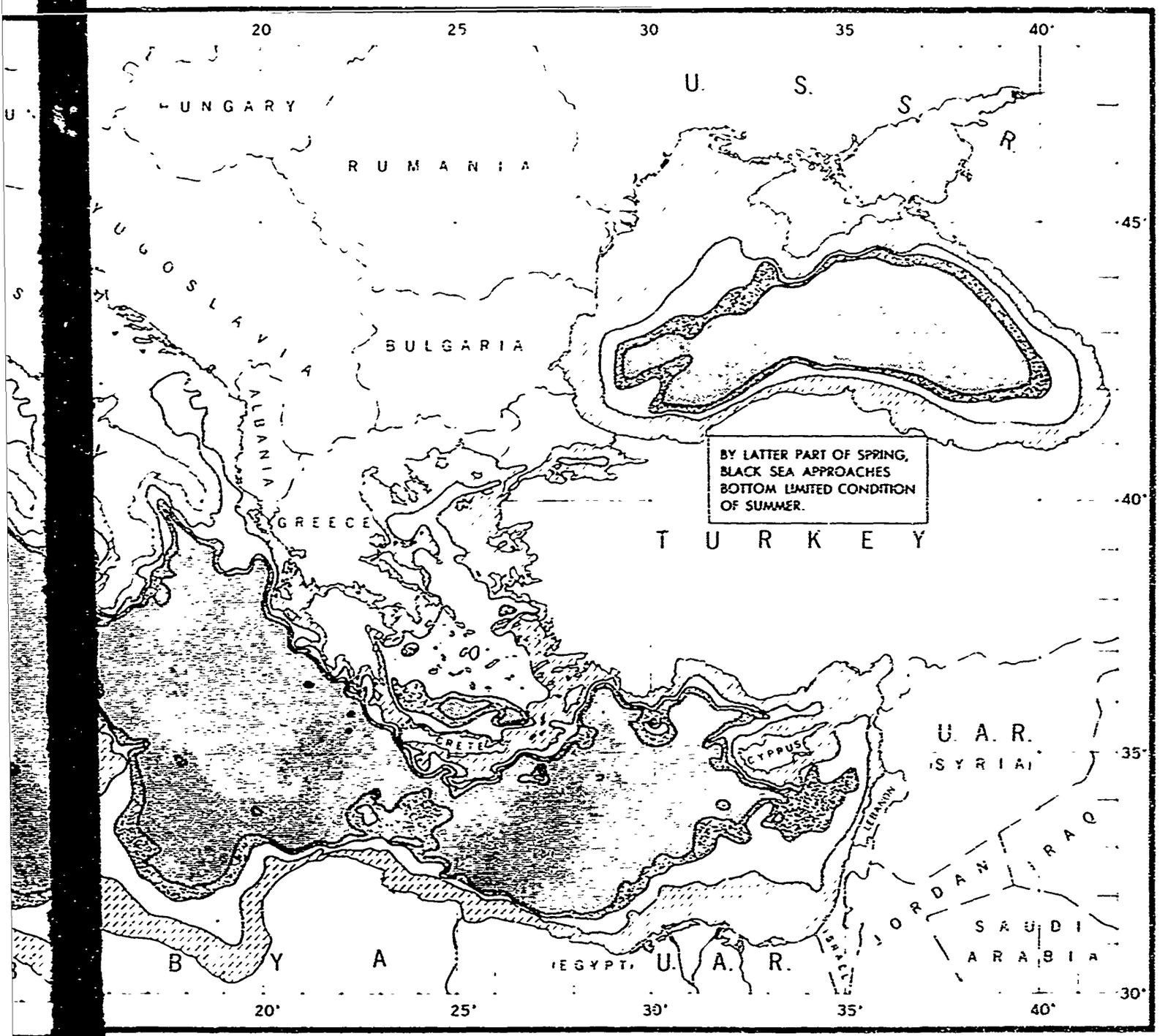

ONE FORMATION IN THE MEDITERRANEAN SEA, SPRING

FIGURE 58. CONVERGENCE ZONE FORMATION, SPRING

CONFIDENTIAL

2

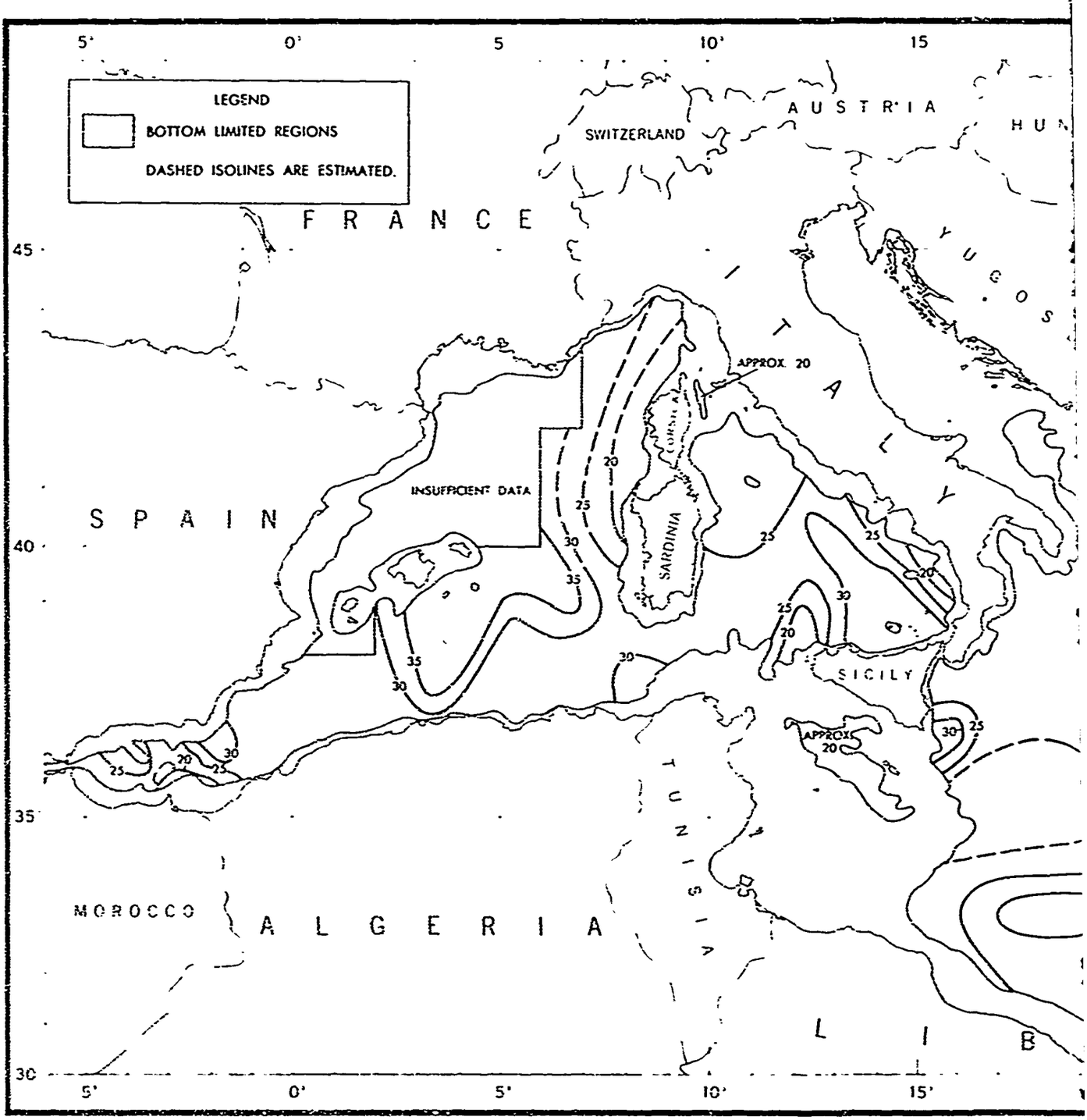

FIGURE 59. CONVERGENCE ZONE RANGE (KILOYARDS) IN THE

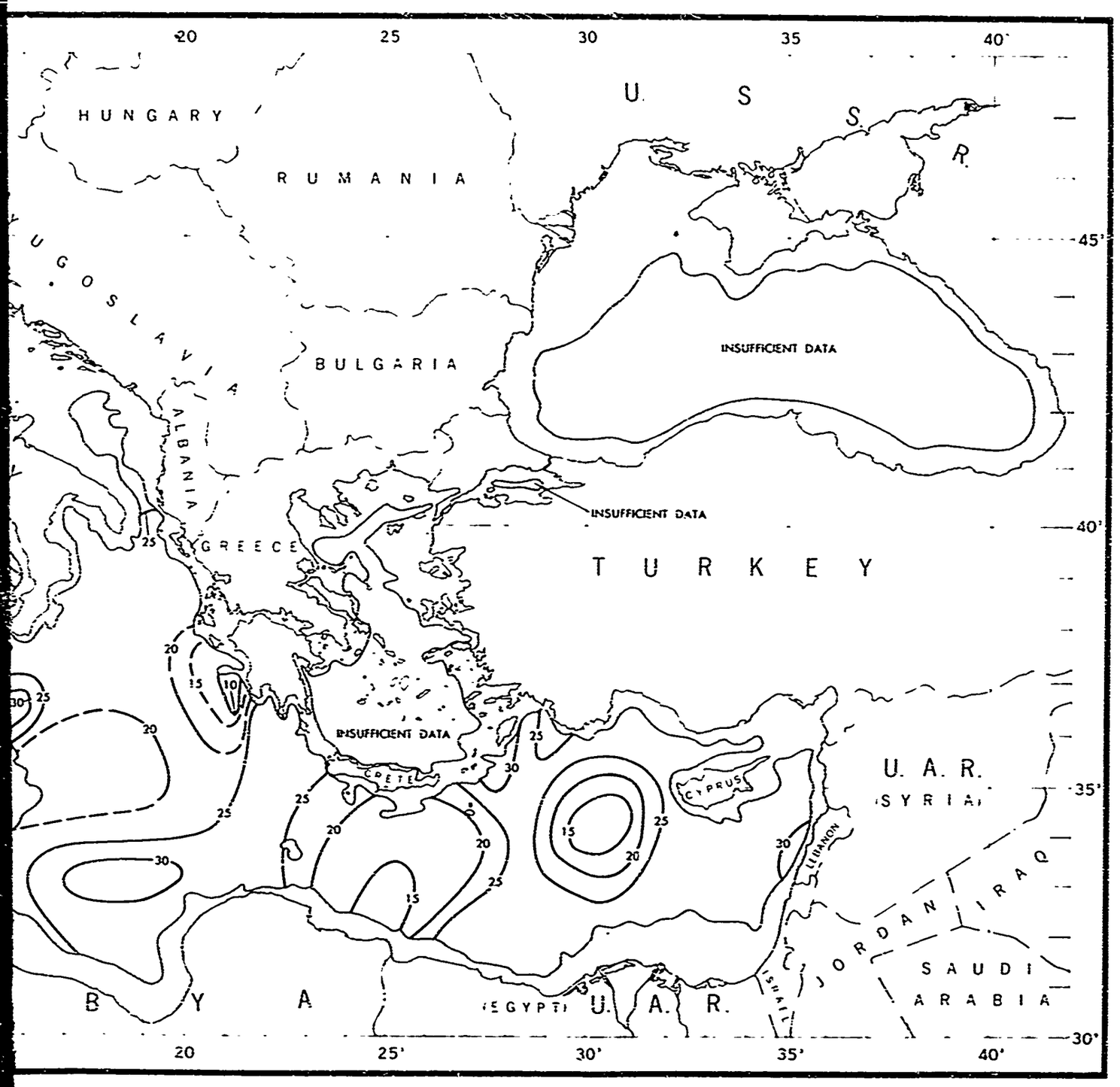

THE ... LOYARDS) IN THE MEDITERRANEAN SEA, SPRING

FIGURE 59. CONVERGENCE ZONE RANGE, SPRING CONFIDENTIAL

2

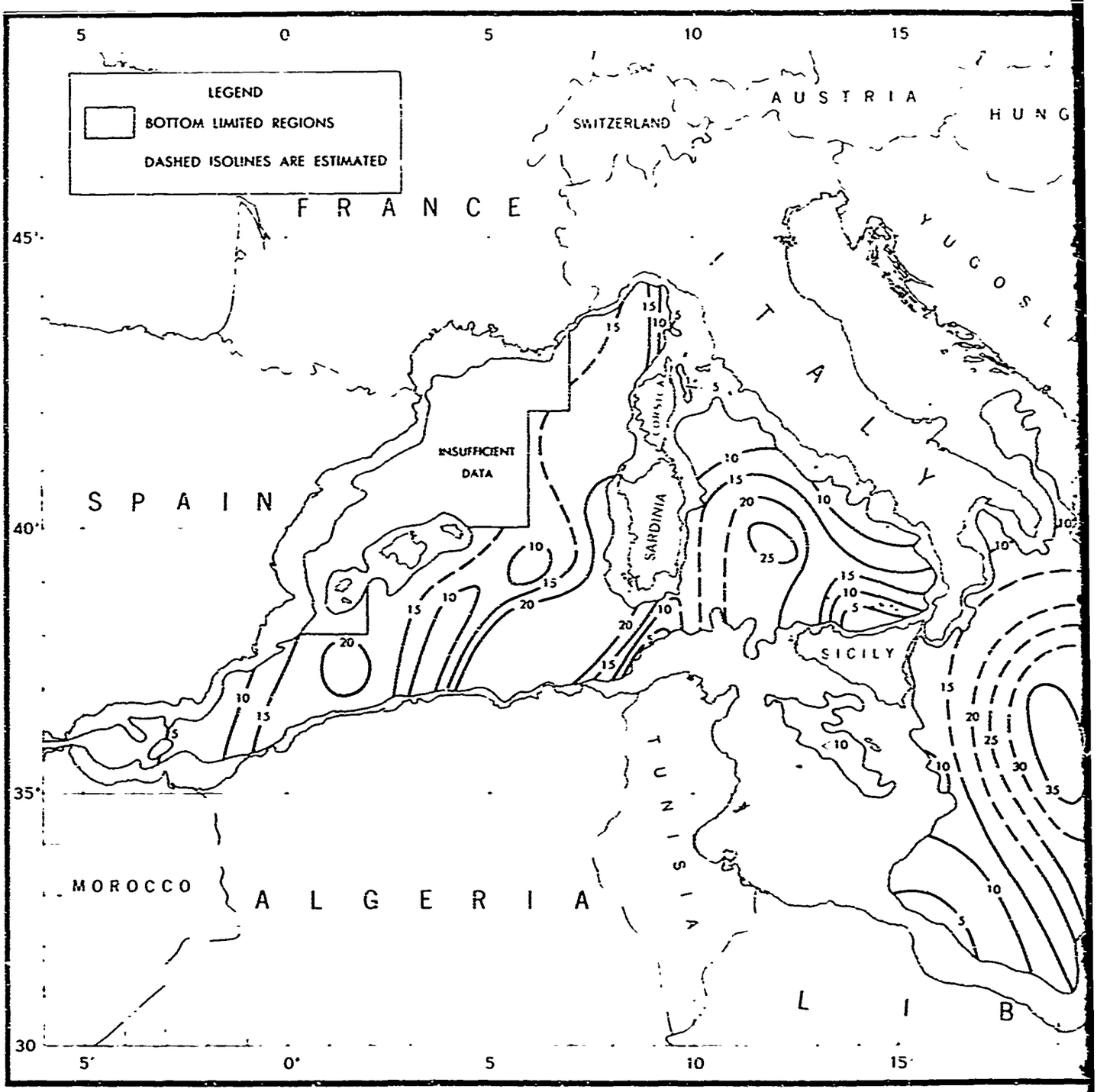

FIGURE 60. SURFACE INSONIFICATION INTERVAL (KILOYARDS) IN THE A

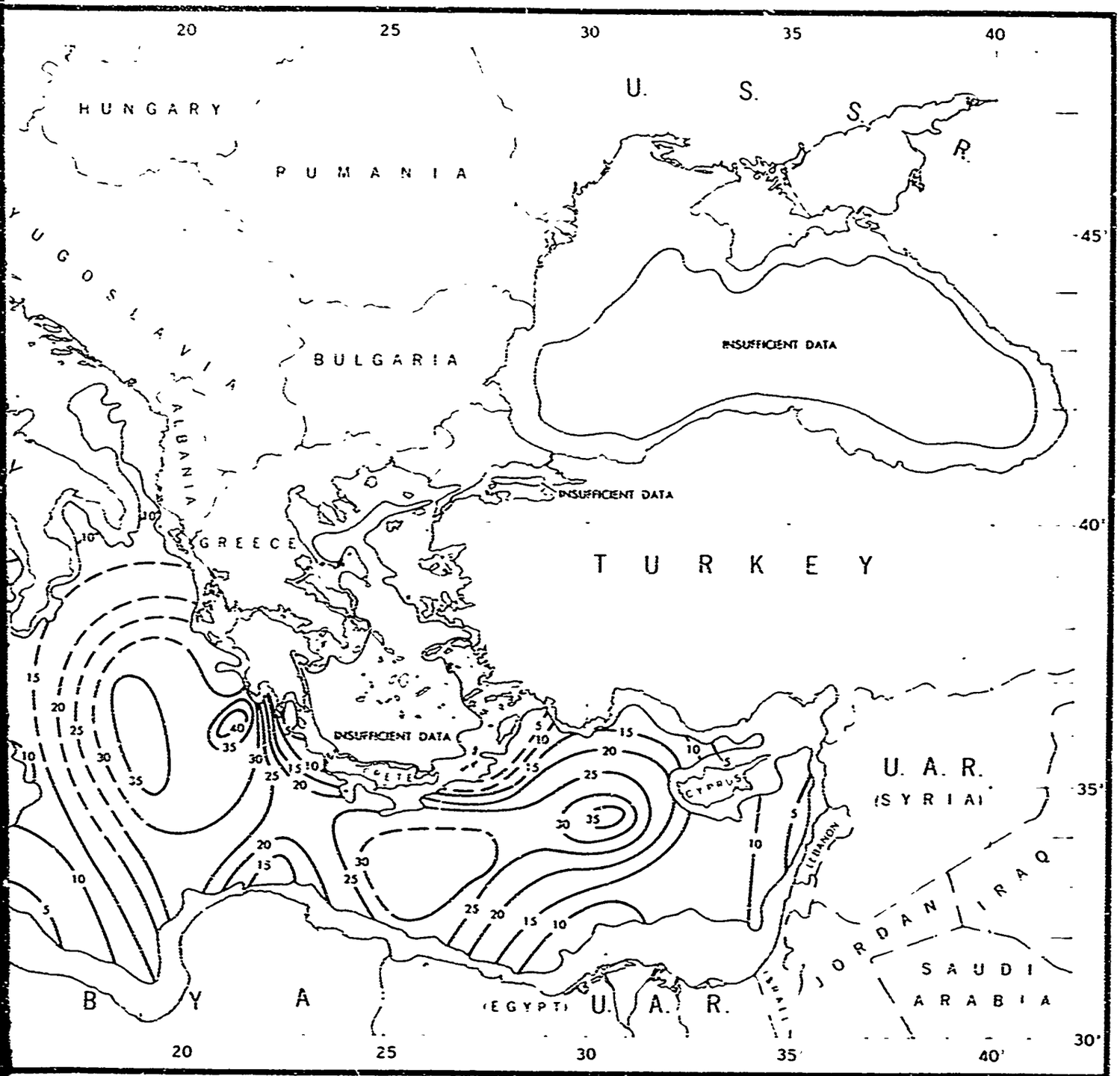

KILOYARDS) IN THE MEDITERRANEAN SEA, SPRING

FIGURE 60. SURFACE INSONIFICATION INTERVAL, SPRING

CONFIDENTIAL

2

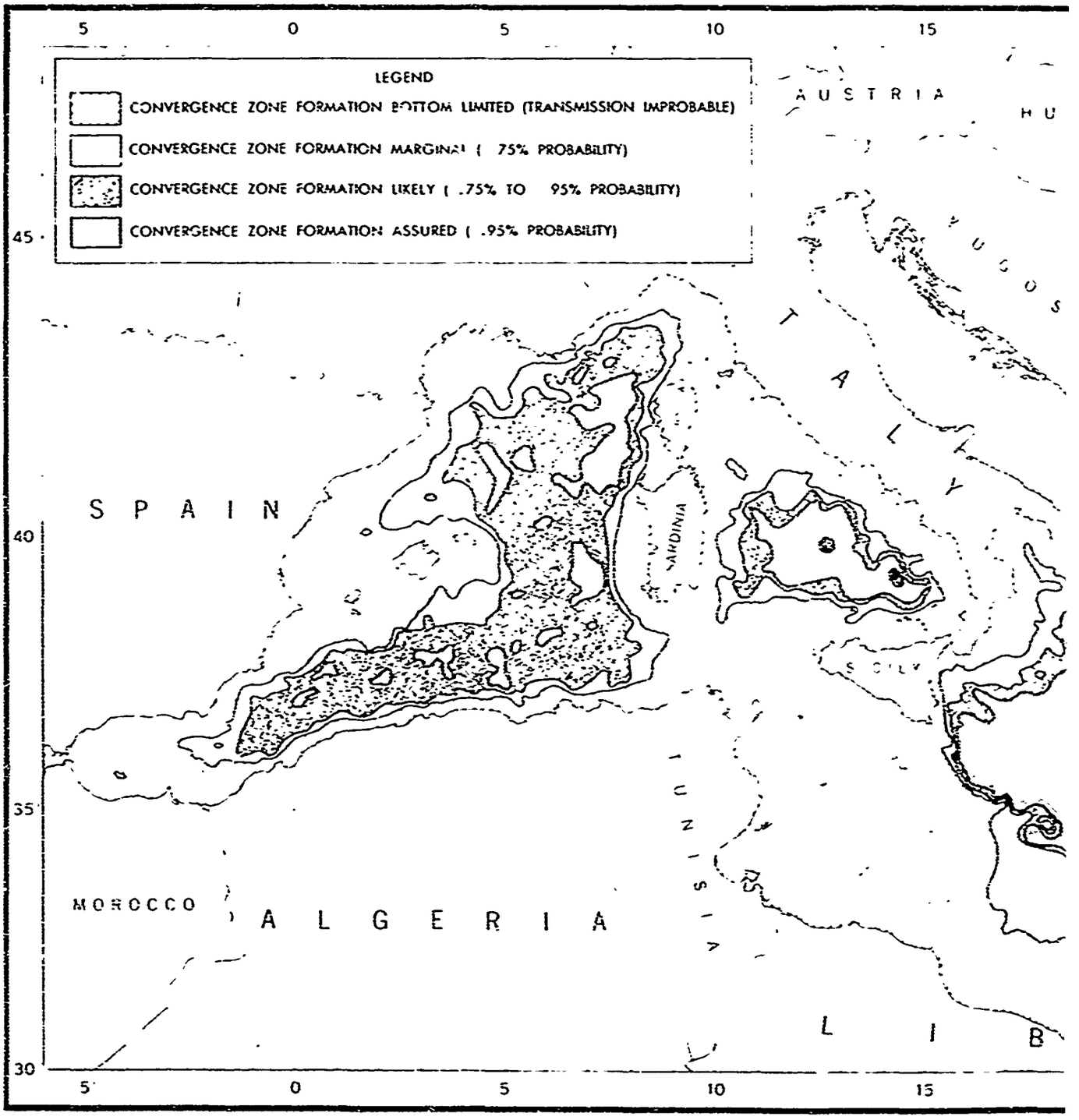

FIGURE 61. PERCENT PROBABILITY OF CONVERGENCE ZONE FORMATION

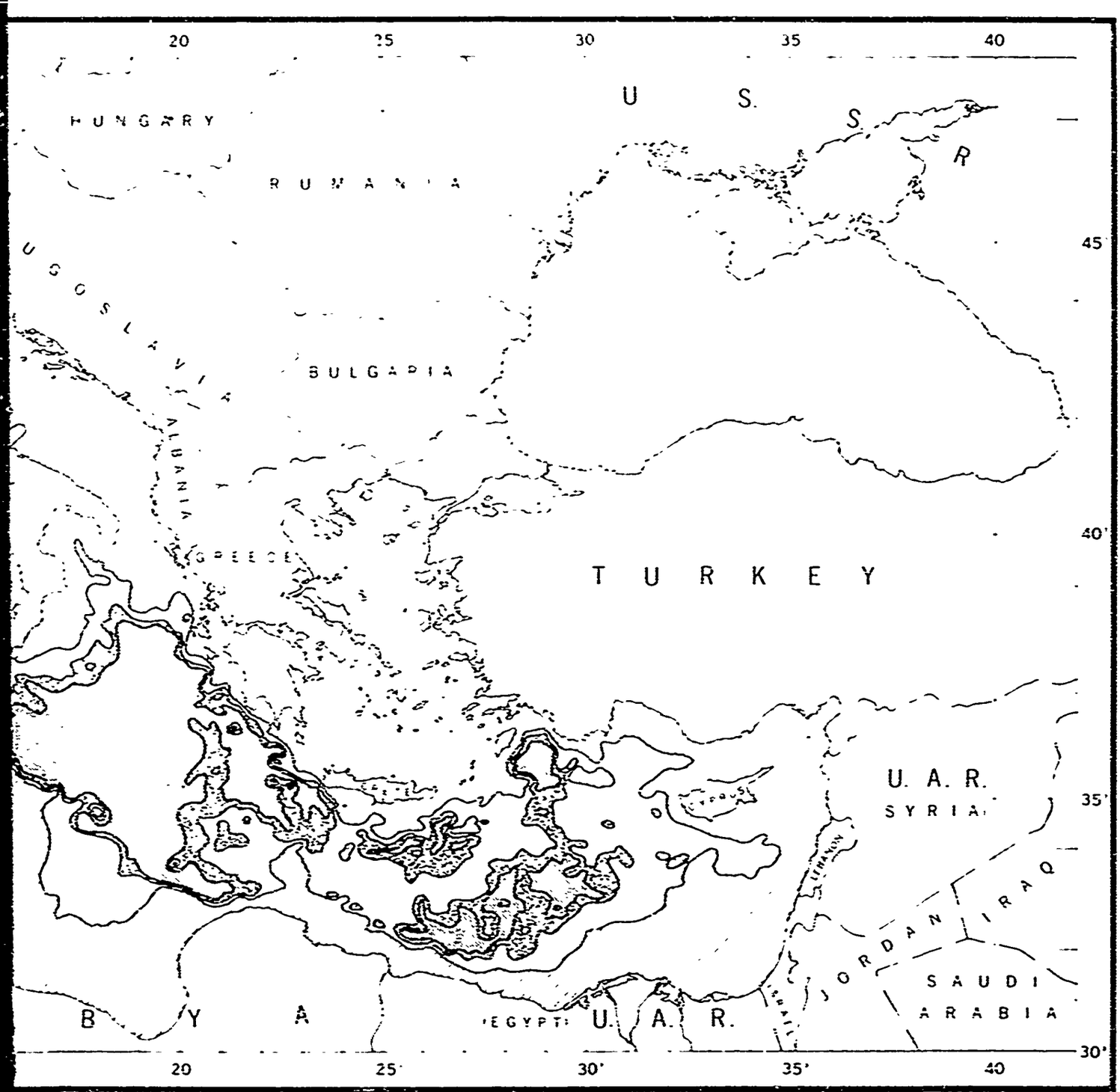

E FORMATION IN THE MEDITERRANEAN SEA, SUMMER

FIGURE 61. CONVERGENCE ZONE FORMATION, SUMMER

CONFIDENTIAL

2

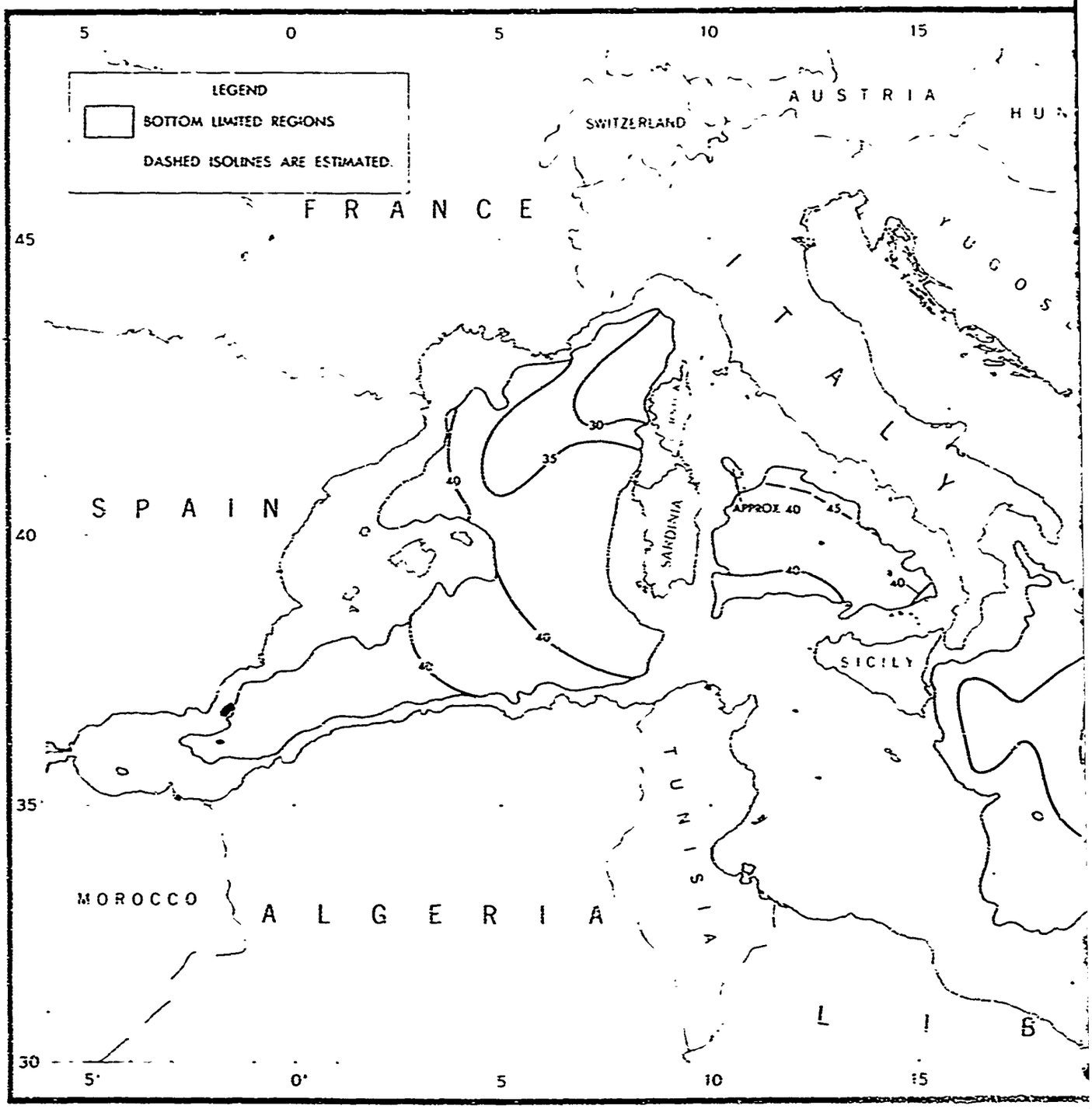

FIGURE 62. CONVERGENCE ZONE RANGE (KILOYARDS) IN THE

YARDS) IN THE MEDITERRANEAN SEA, SUMMER

FIGURE 62. CONVERGENCE ZONE RANGE, SUMMER

CONFIDENTIAL

2

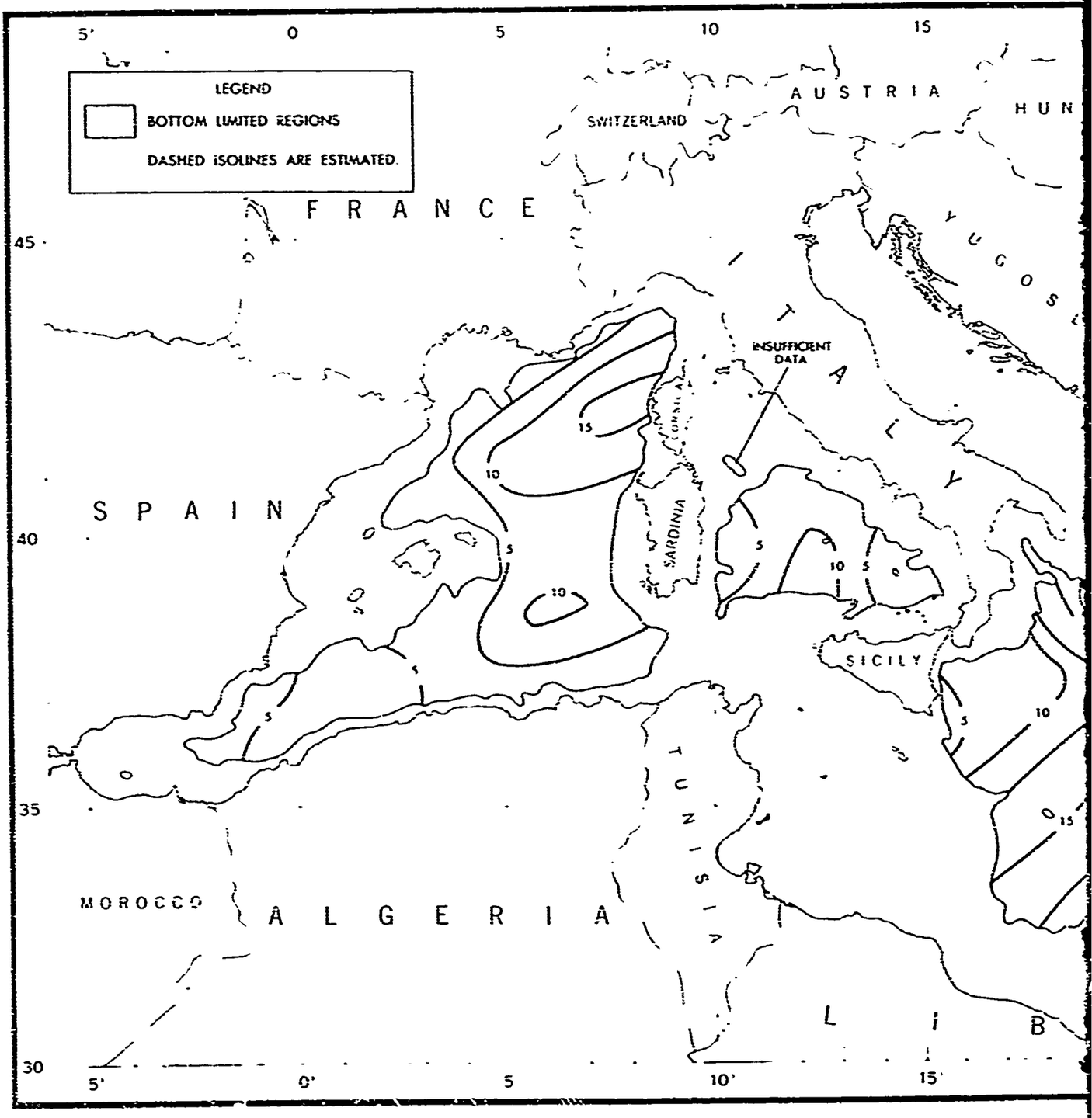

FIGURE 63. SURFACE INSONIFICATION INTERVAL (KILOYARDS) IN TH

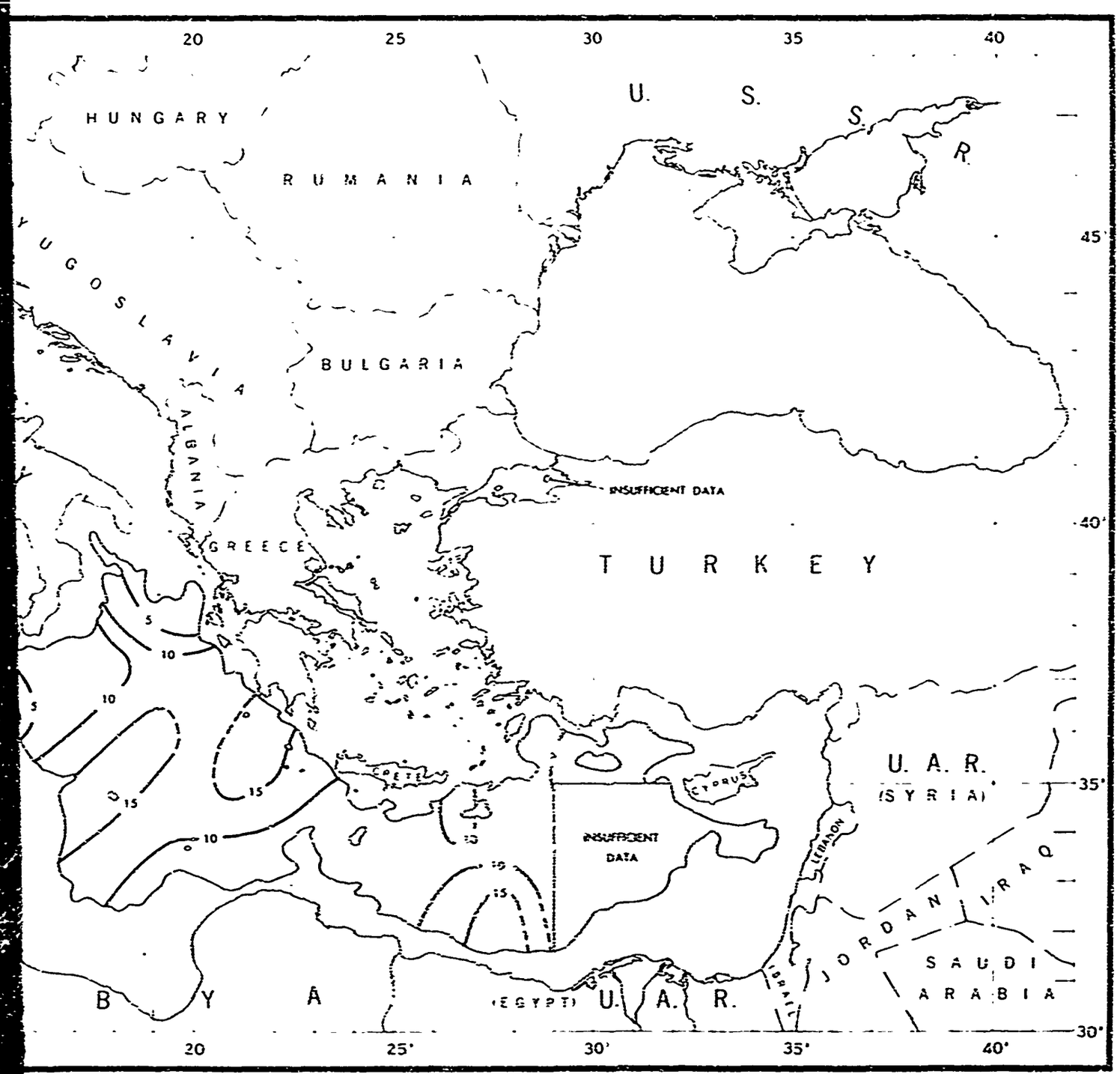

IN TH KILOYARDS) IN THE MEDITERRANEAN SEA, SUMMER

FIGURE 63. SURFACE INSONIFICATION INTERVAL, SUMMER

2

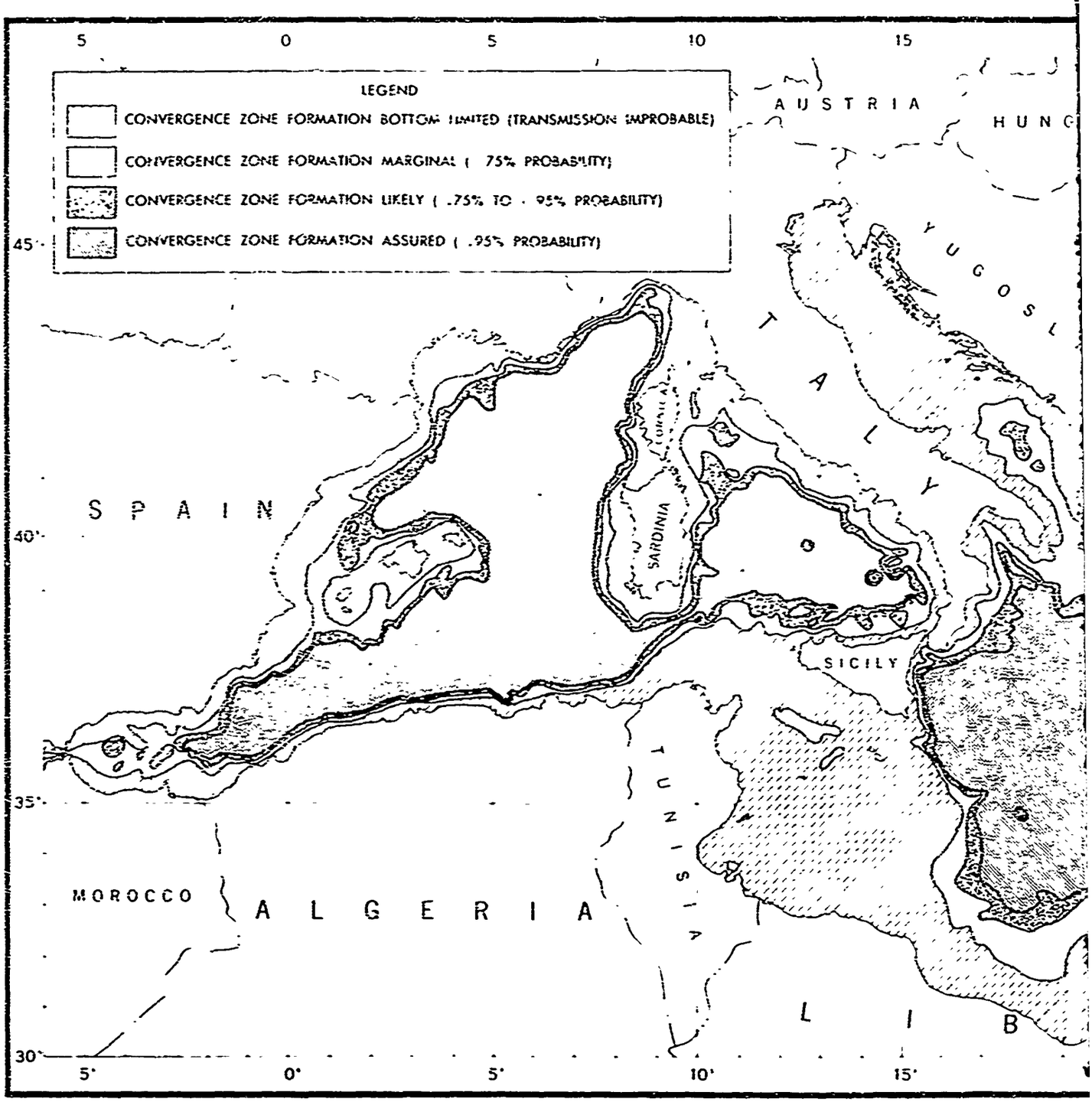

FIGURE 64. PERCENT PROBABILITY OF CONVERGENCE ZONE FORMATION IN

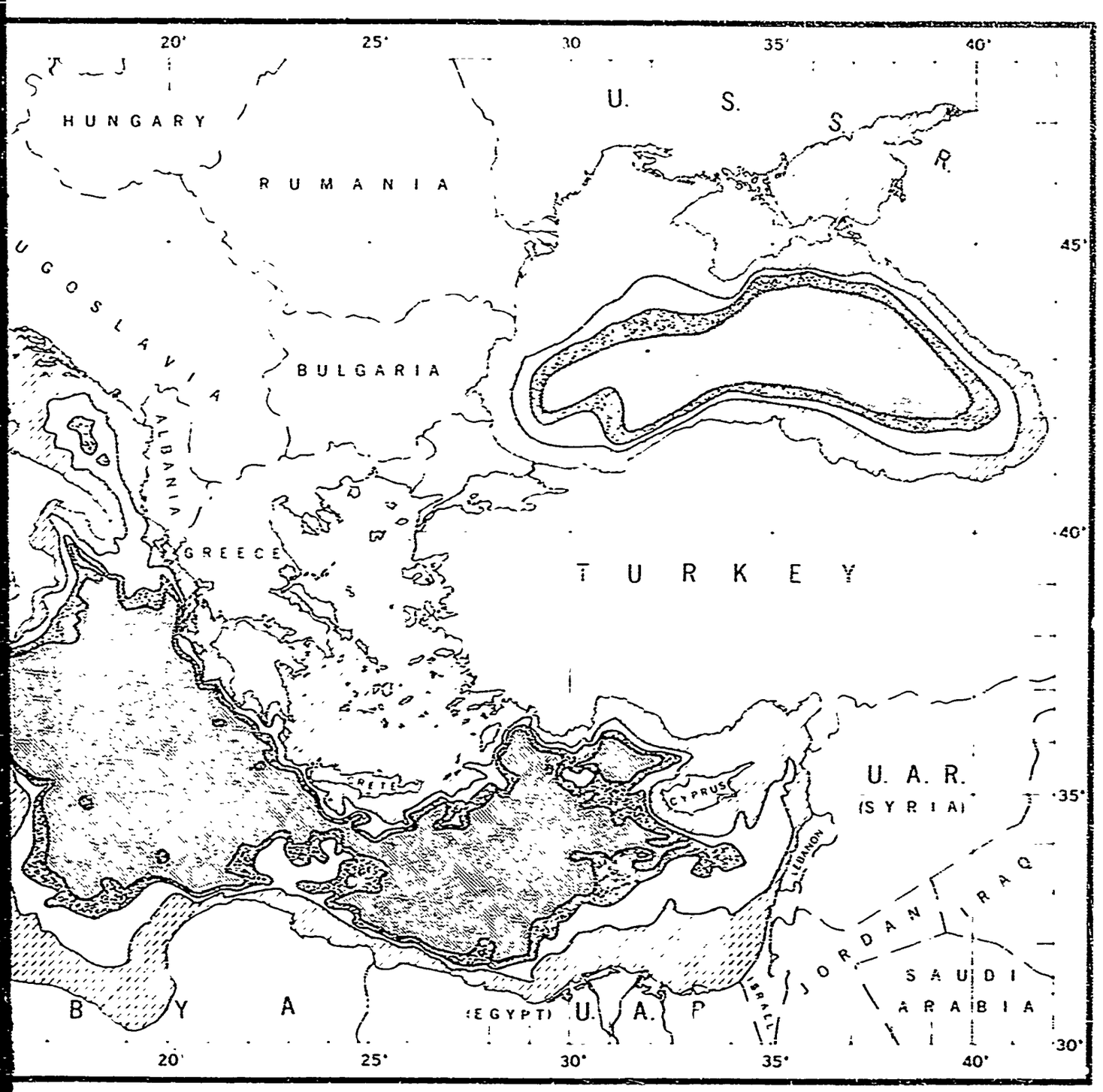

NE FORMATION IN THE MEDITERRANEAN SEA, FALL

FIGURE 64. CONVERGENCE ZONE FORMATION, FALL

CONFIDENTIAL

2

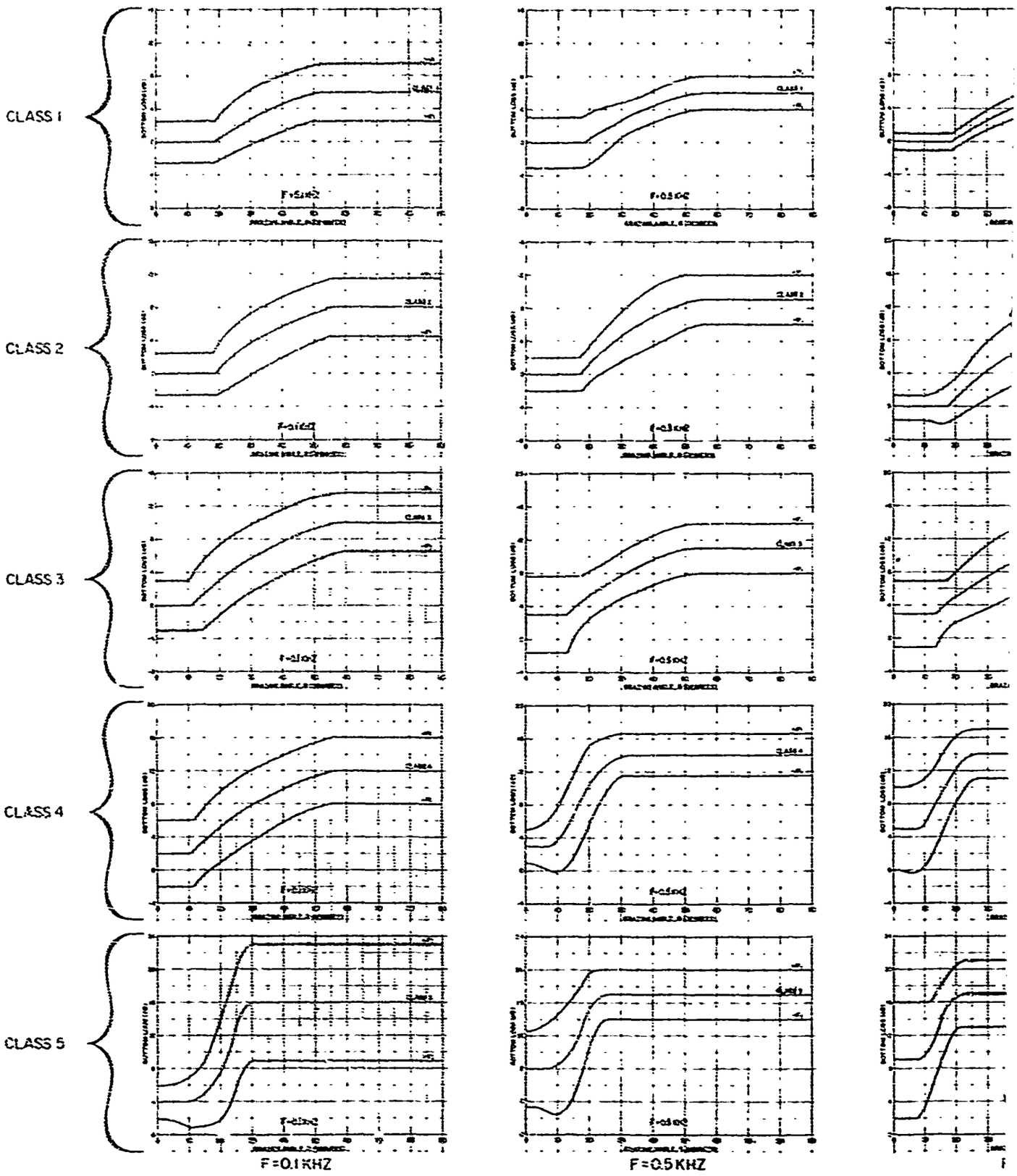

FIGURE 65. ACOUSTIC BOTTOM LOSS IN

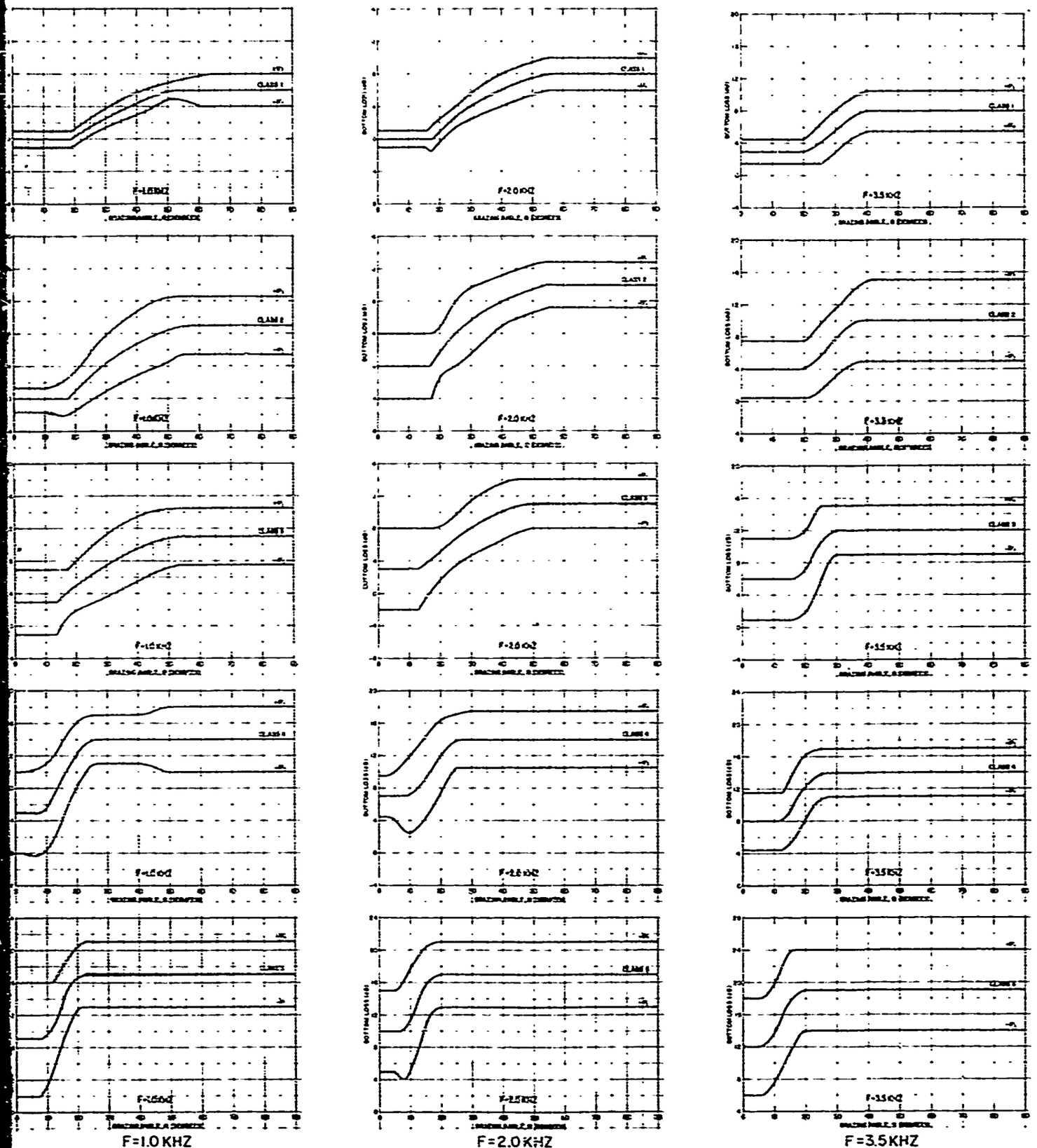

TTOM LOSS IN THE MEDITERRANEAN SEA

FIGURE 65. BOTTOM LOSS

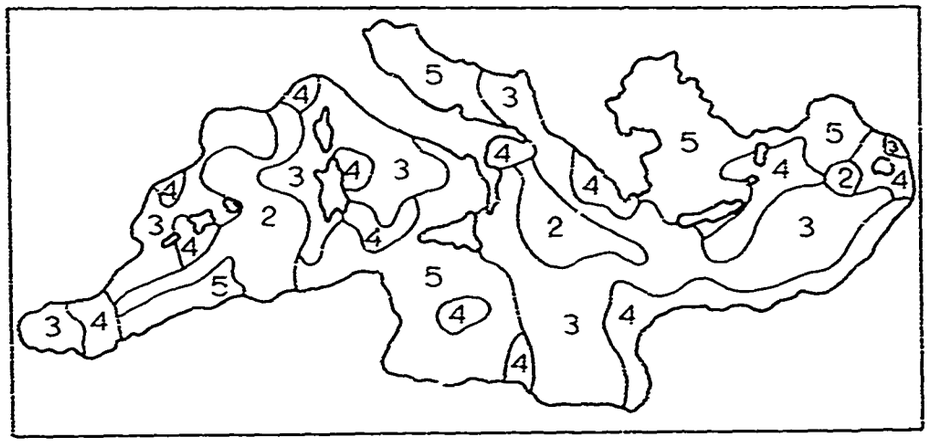

BOTTOM LOSS CLASSES

1 Very Low Loss
2 Relatively Low Loss
3 Intermediate Loss
4 Relatively High Loss
5 Very High Loss

Figure 66 Bottom Loss Regions of the Mediterranean Sea

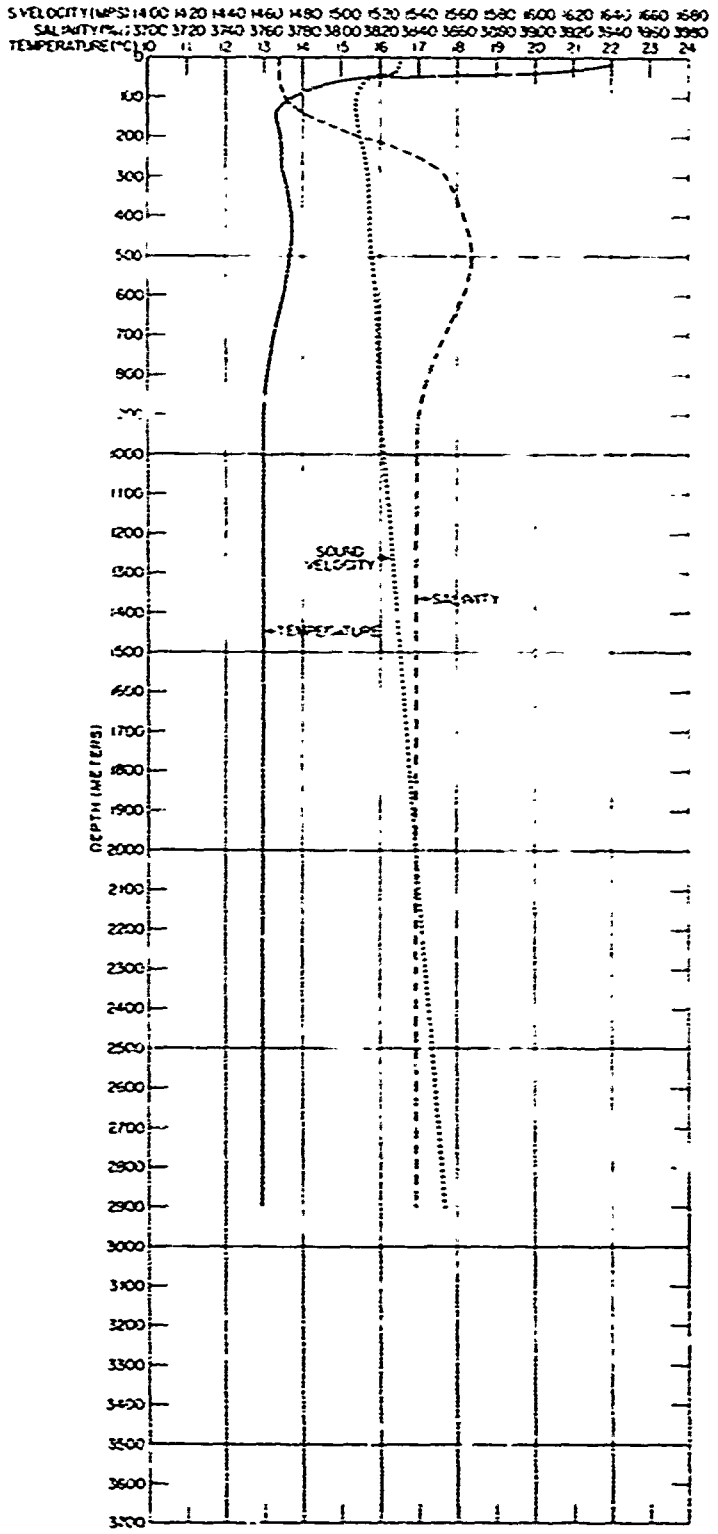

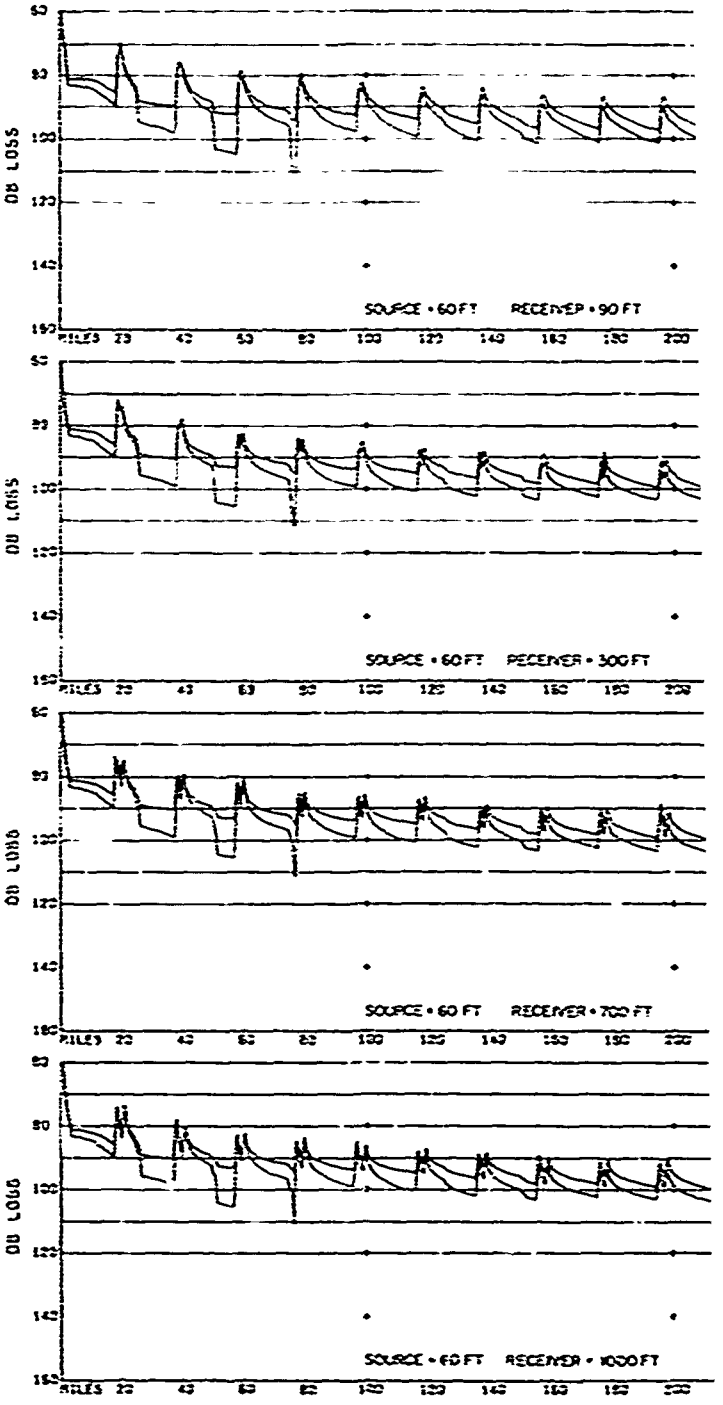

FIGURE 67. ACOUSTIC PROPAGATION LOSS, WESTERN MEDITERRAN

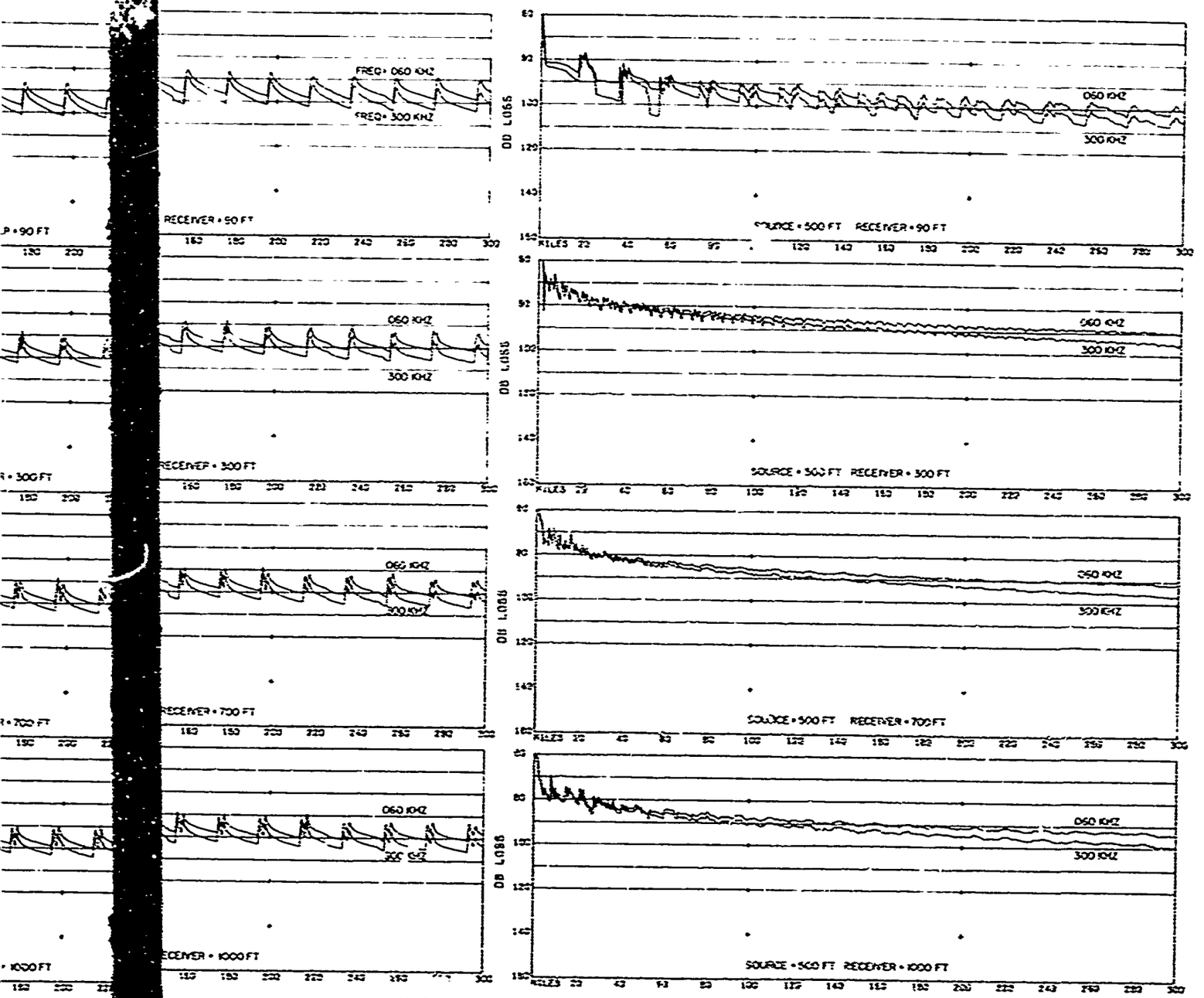

NOTE: BOTTOM CLASS 3

FIGURE 67 PROPAGATION LOSS, WESTERN MEDITERRANEAN, SUMMER

STERN MEDITERRANEAN SEA, SUMMER

MEDITERRANEA

CONFIDENTIAL

1

2

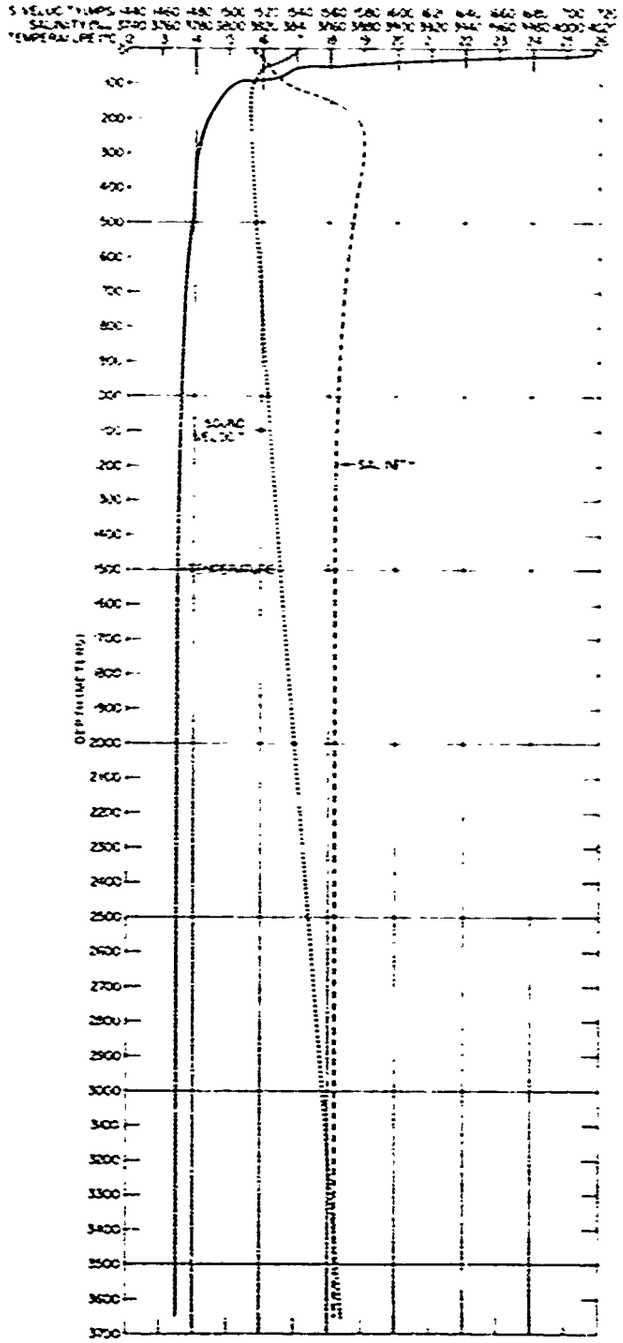

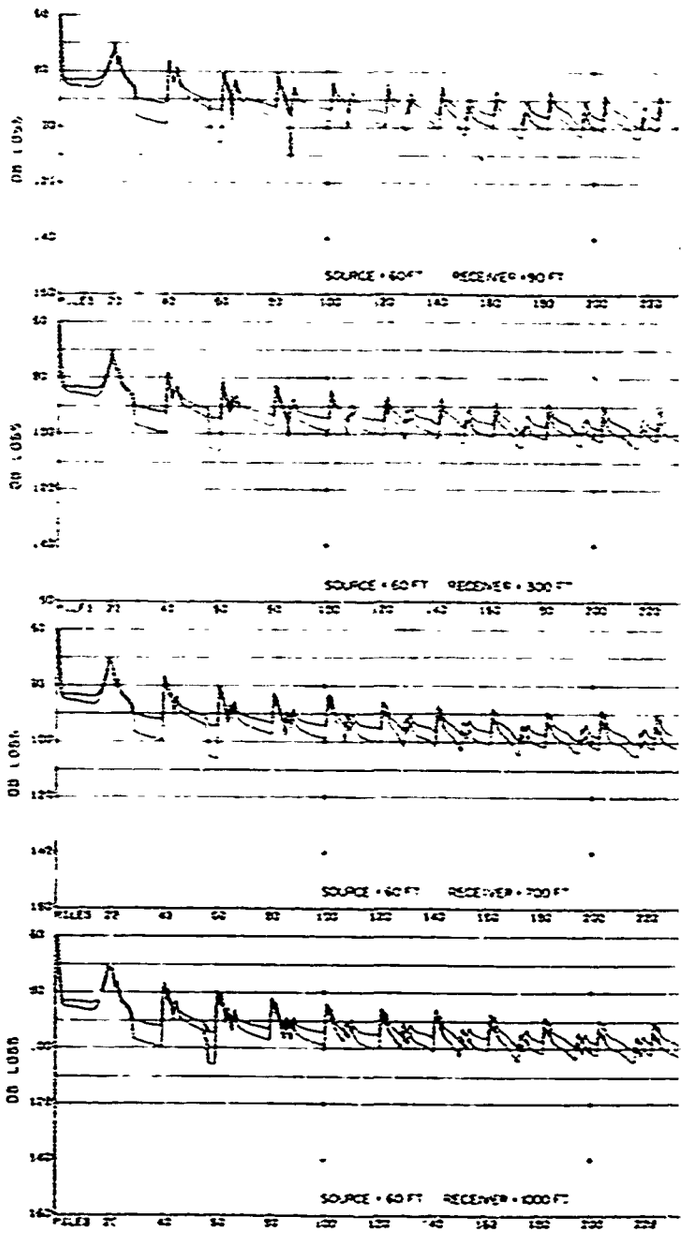

FIGURE 68. ACOUSTIC PROPAGATION LOSS, CENTRAL MEDITERRANEAN SEA, SUM

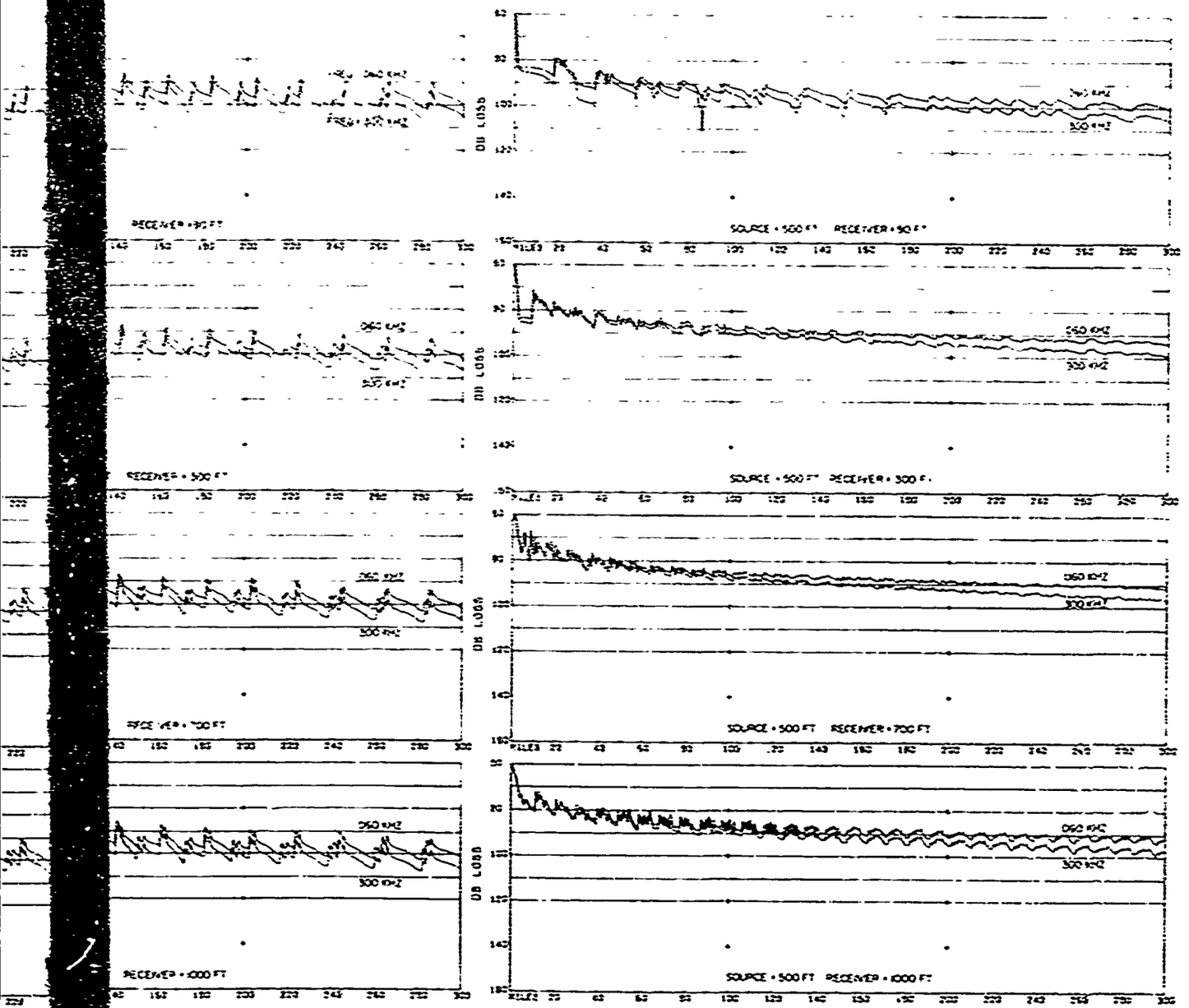

NOTE: BOTTOM CLASS 3

MEDITERRANEAN SEA, SUMMER

FIGURE 68. PROPAGATION LOSS, CENTRAL MEDITERRANEAN, SUMMER

CONFIDENTIAL

2

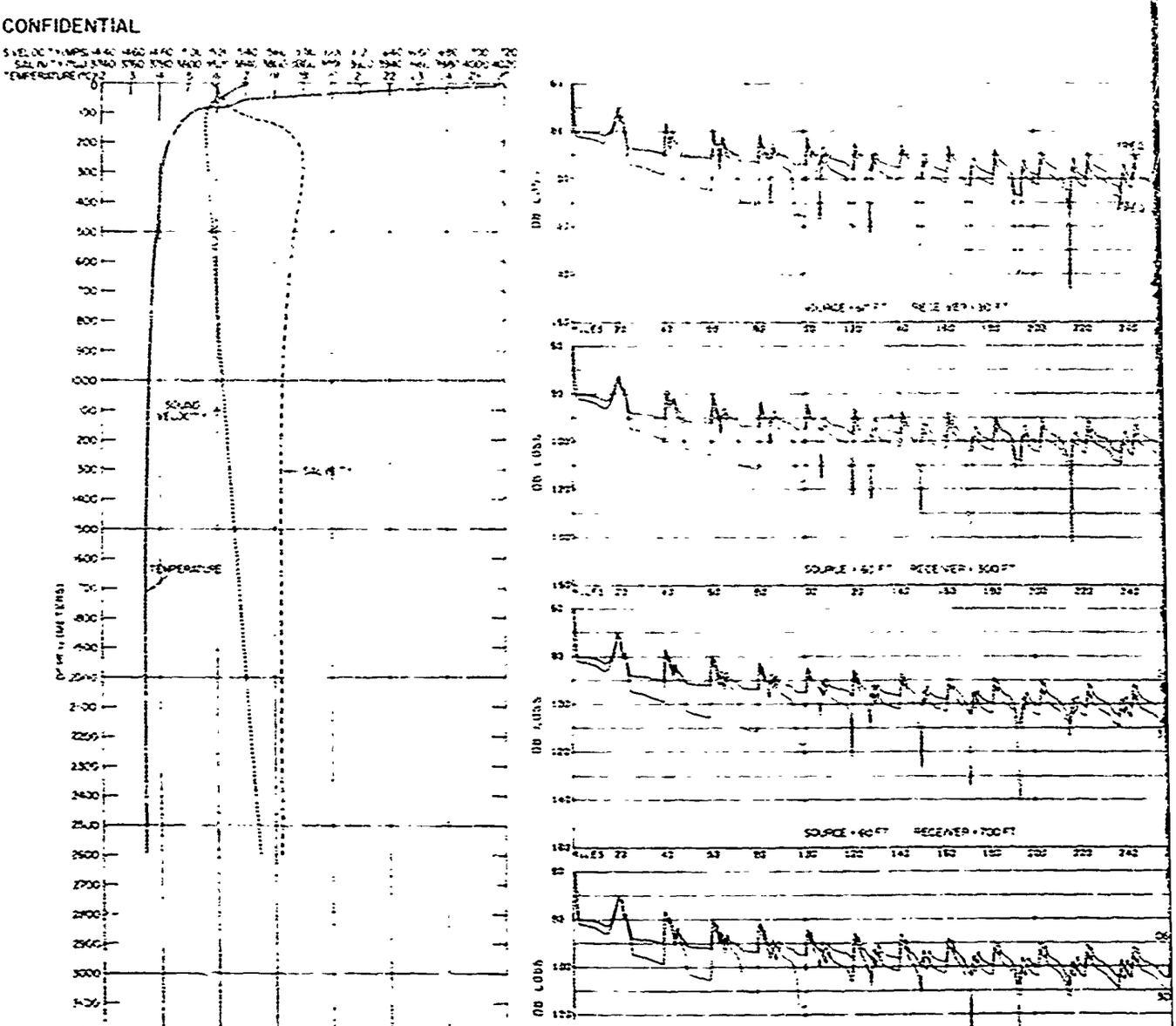

FIGURE 69. ACOUSTIC PROPAGATION LOSS, EASTERN MEDITERRANEAN SEA, SUMMER

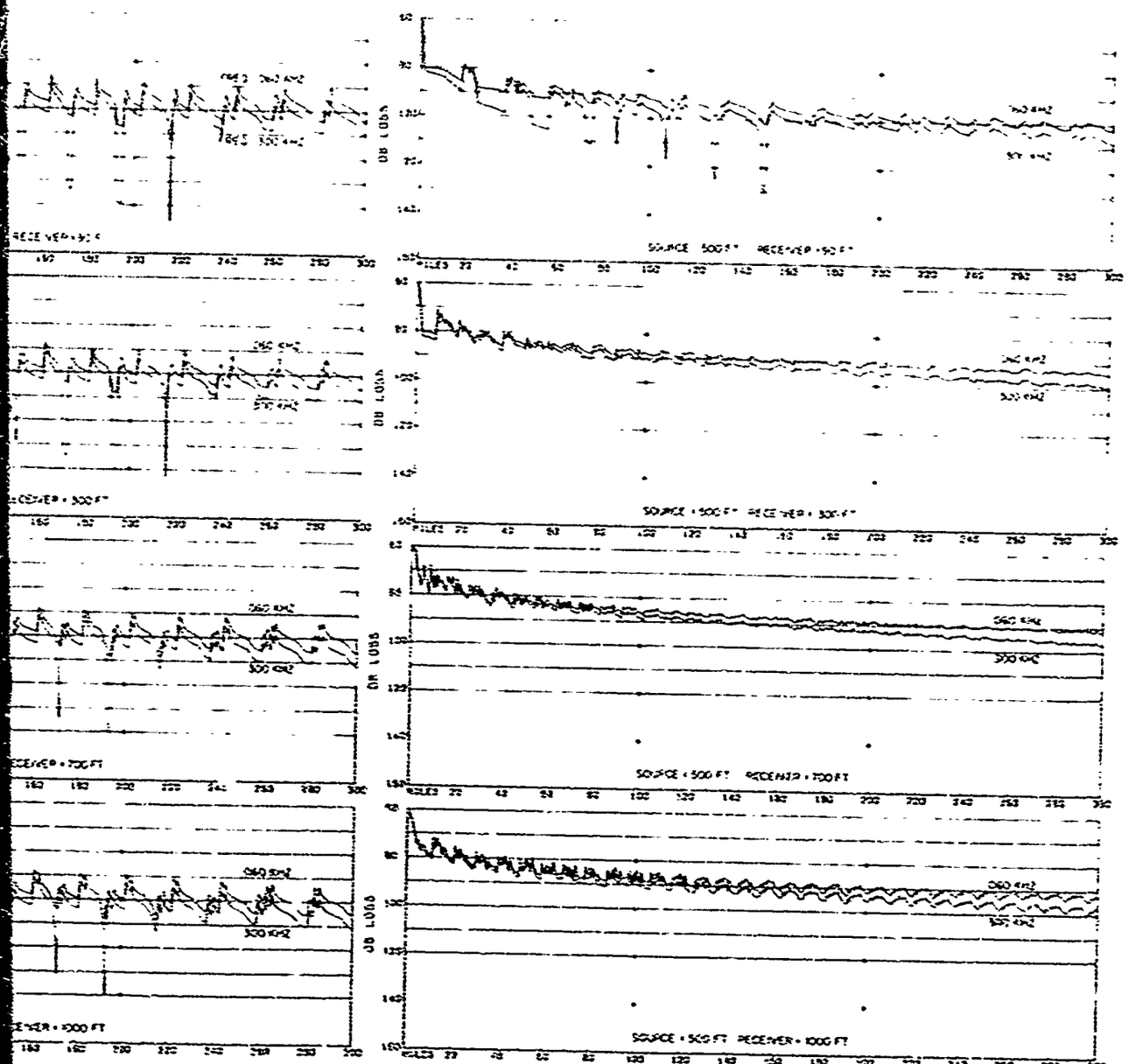

NOTE: BOTTOM CLASS 3

ERRANEAN SEA, SUMMER

FIGURE 69. PROPAGATION LOSS, EASTERN MEDITERRANEAN, SUMMER

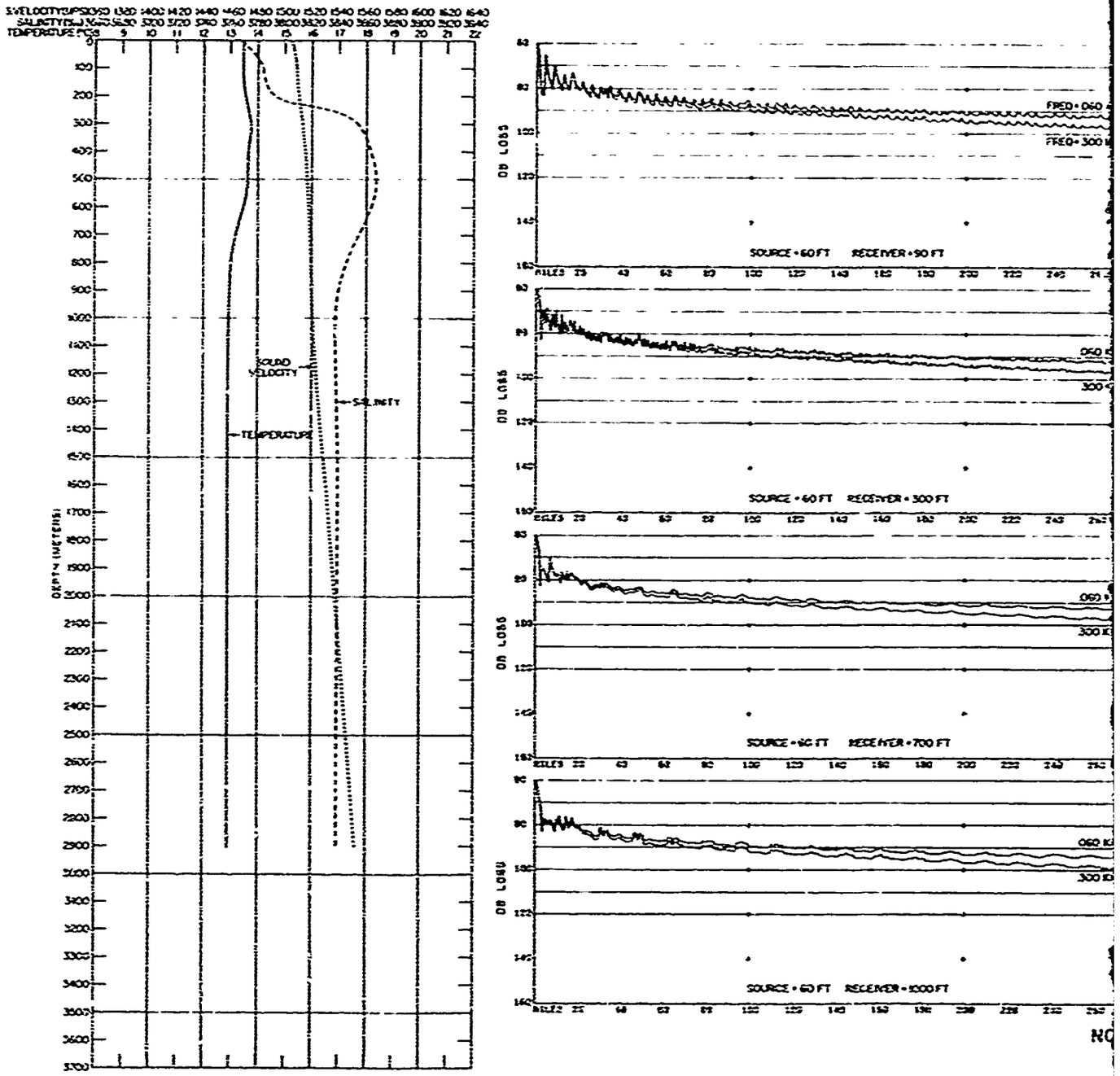

FIGURE 70. ACOUSTIC PROPAGATION LOSS, WESTERN MEDITERRANEAN SEA, WINTER

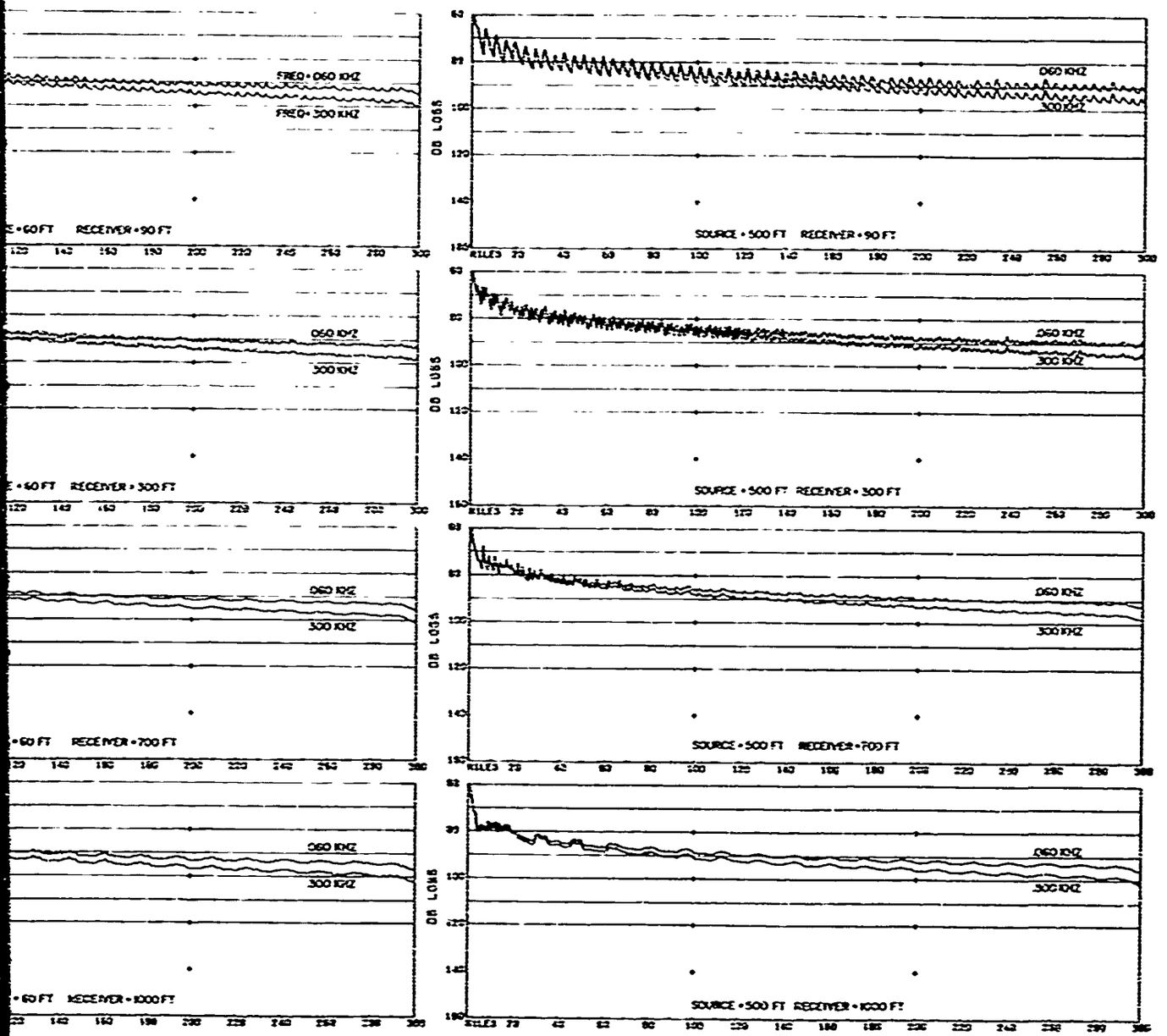

NOTE: BOTTOM CLASS 3

STERN MEDITERRANEAN SEA, WINTER

FIGURE 70. PROPAGATION LOSS, WESTERN MEDITERRANEAN, WINTER

CONFIDENTIAL

2

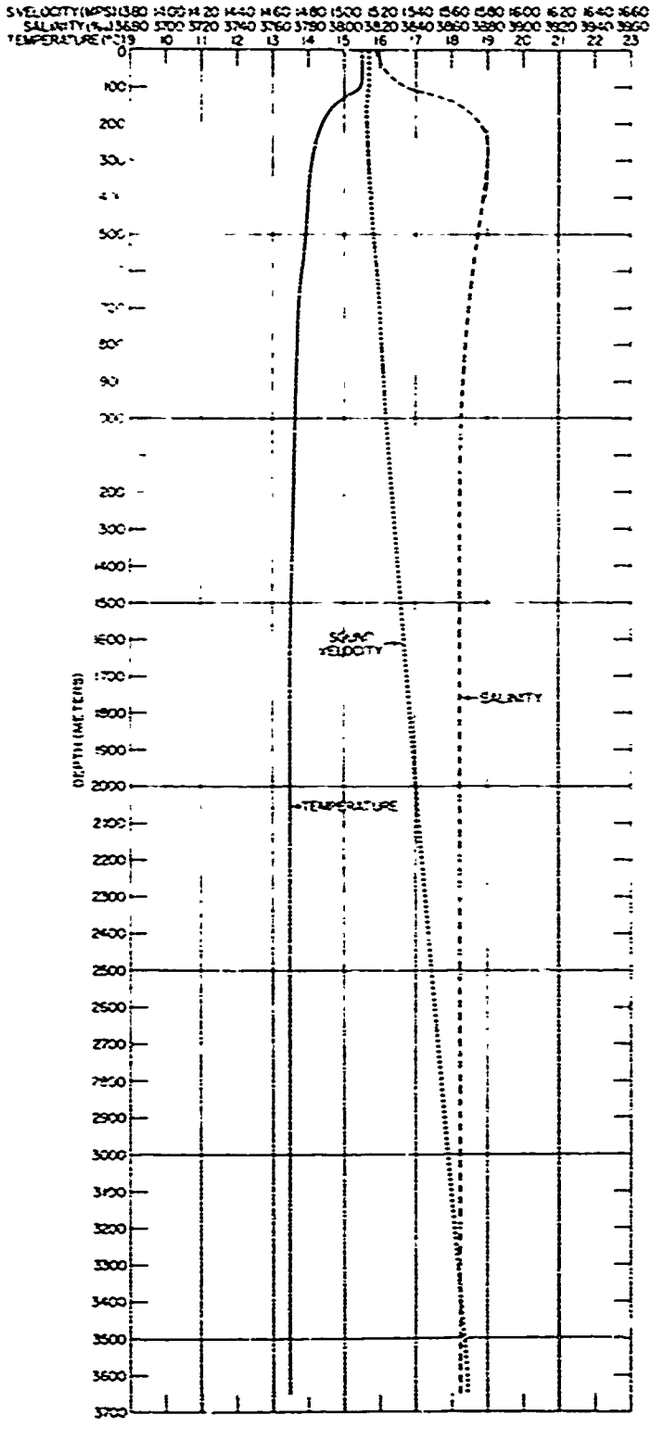

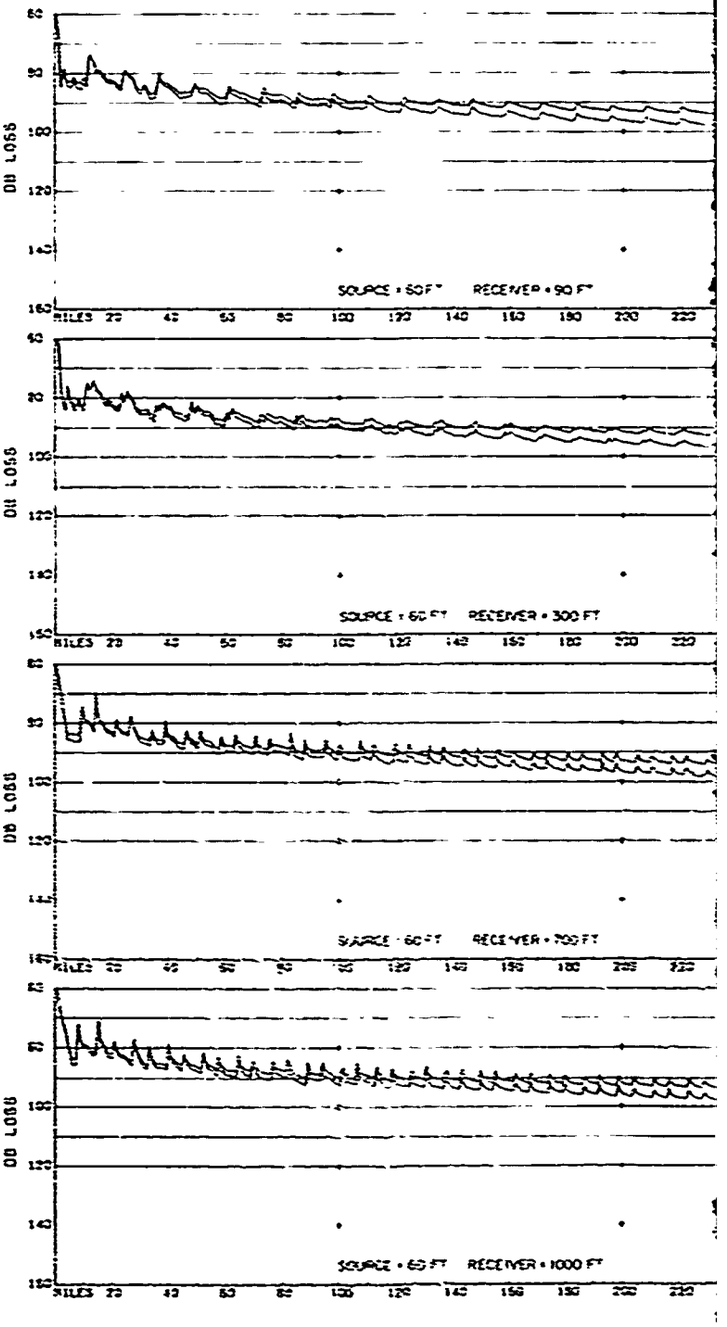

FIGURE 71. ACOUSTIC PROPAGATION LOSS, CENTRAL MEDITERRANEAN SEA, WIN

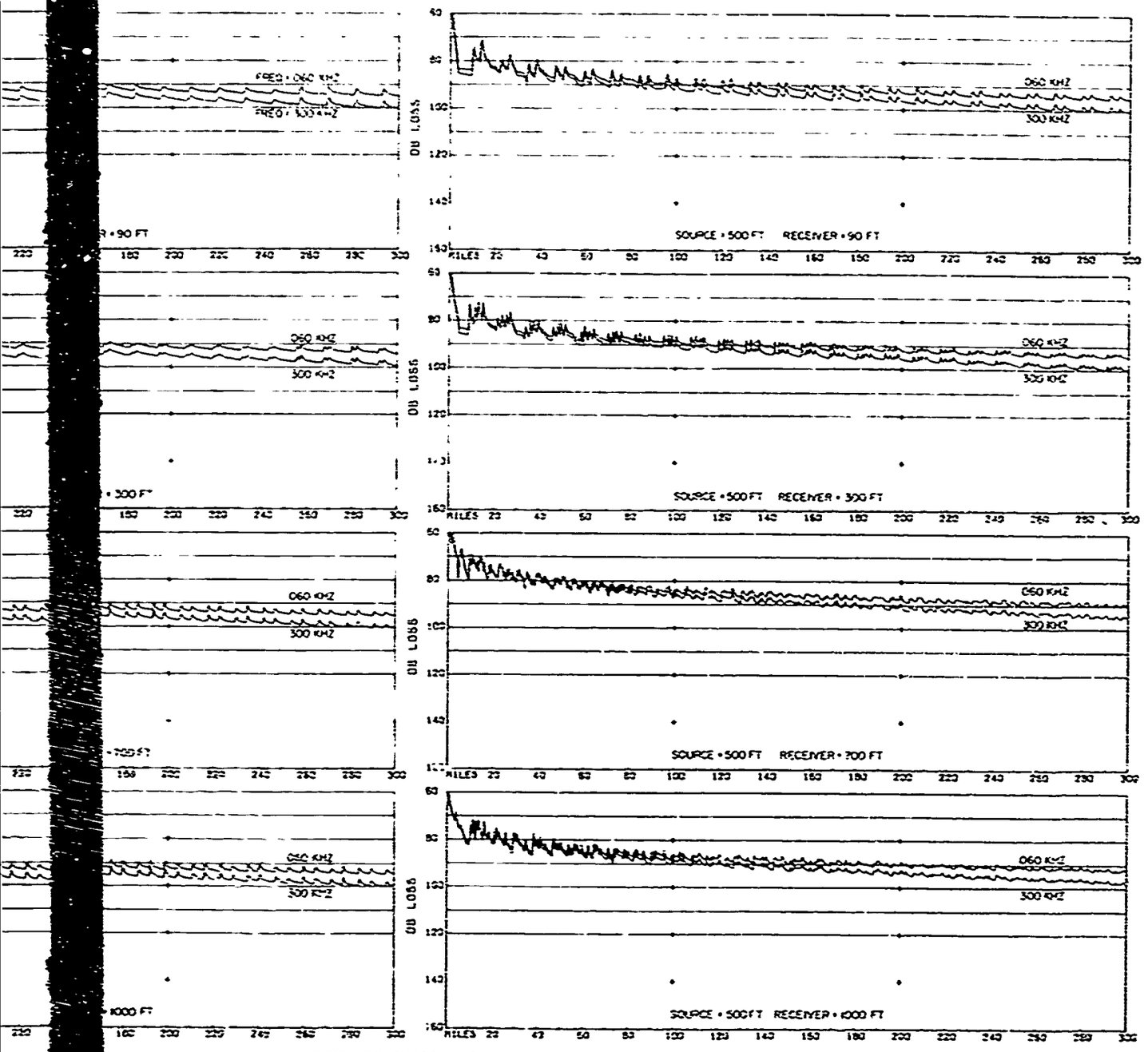

NOTE: BOTTOM CLASS 3

. WIN ANEAN SEA, WINTER

FIGURE 71. PROPAGATION LOSS, CENTRAL MEDITERRANEAN, WINTER

CONFIDENTIAL

2

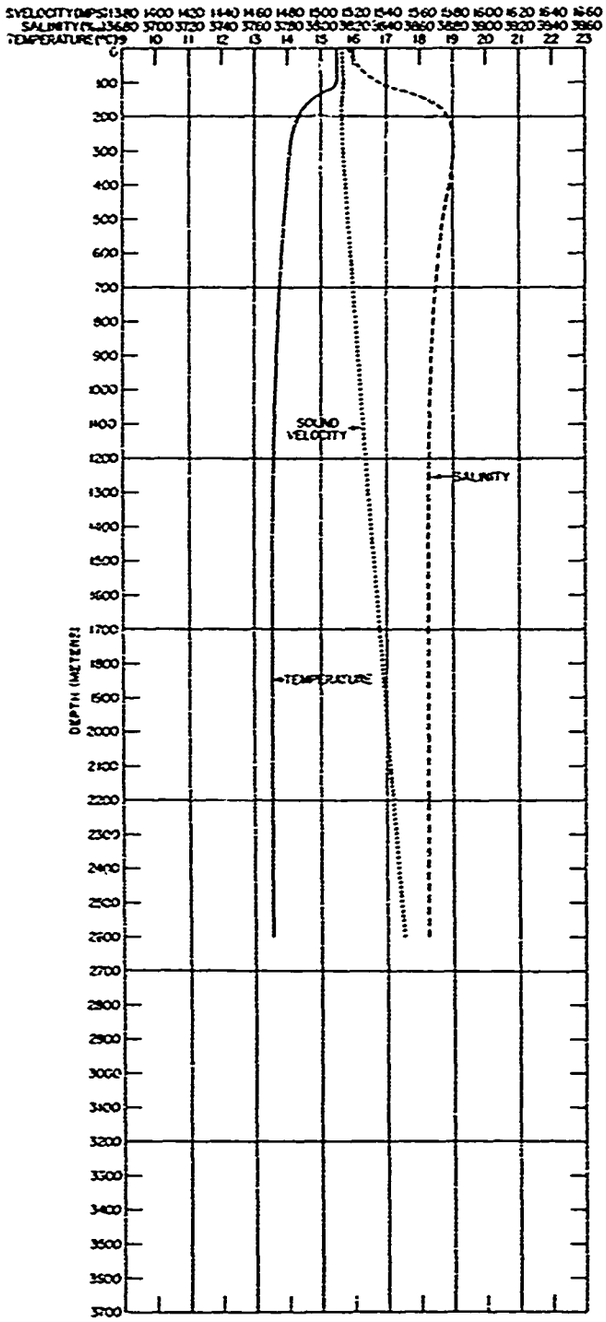

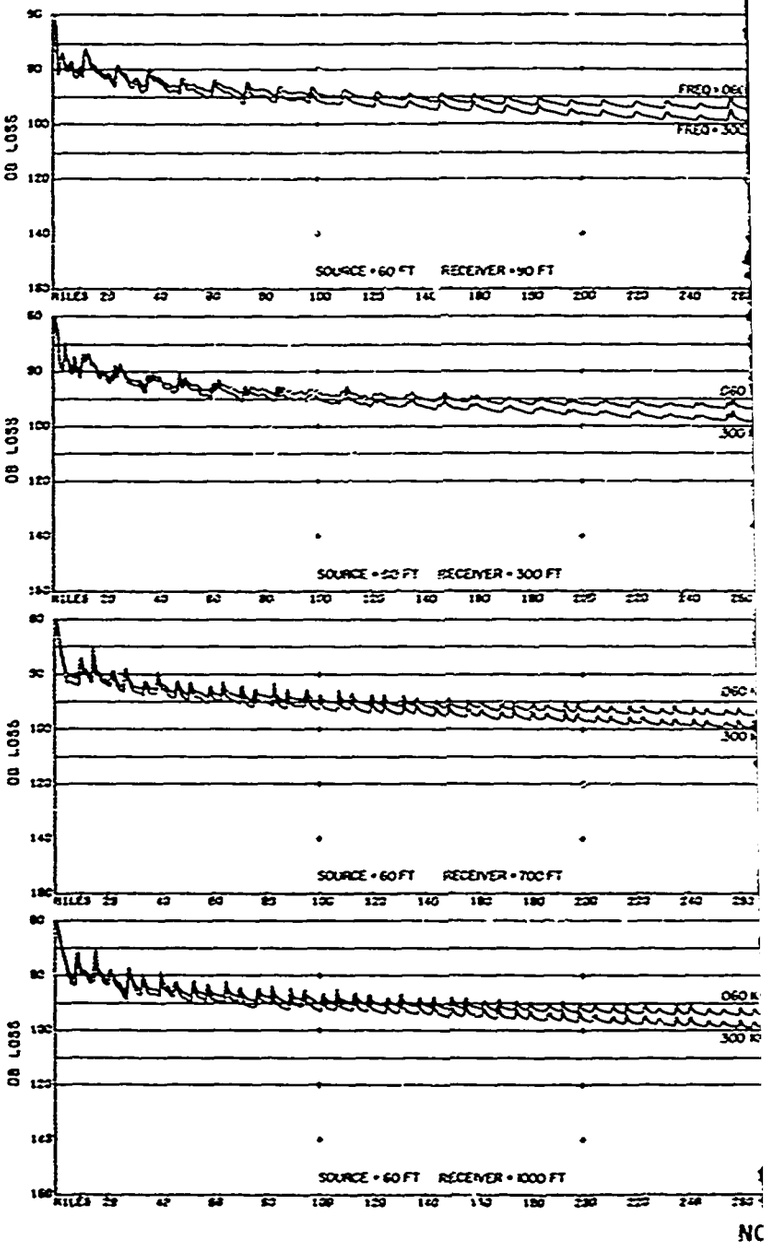

FIGURE 72. ACOUSTIC PROPAGATION LOSS, EASTERN MEDITERRANEAN SEA, WINTER

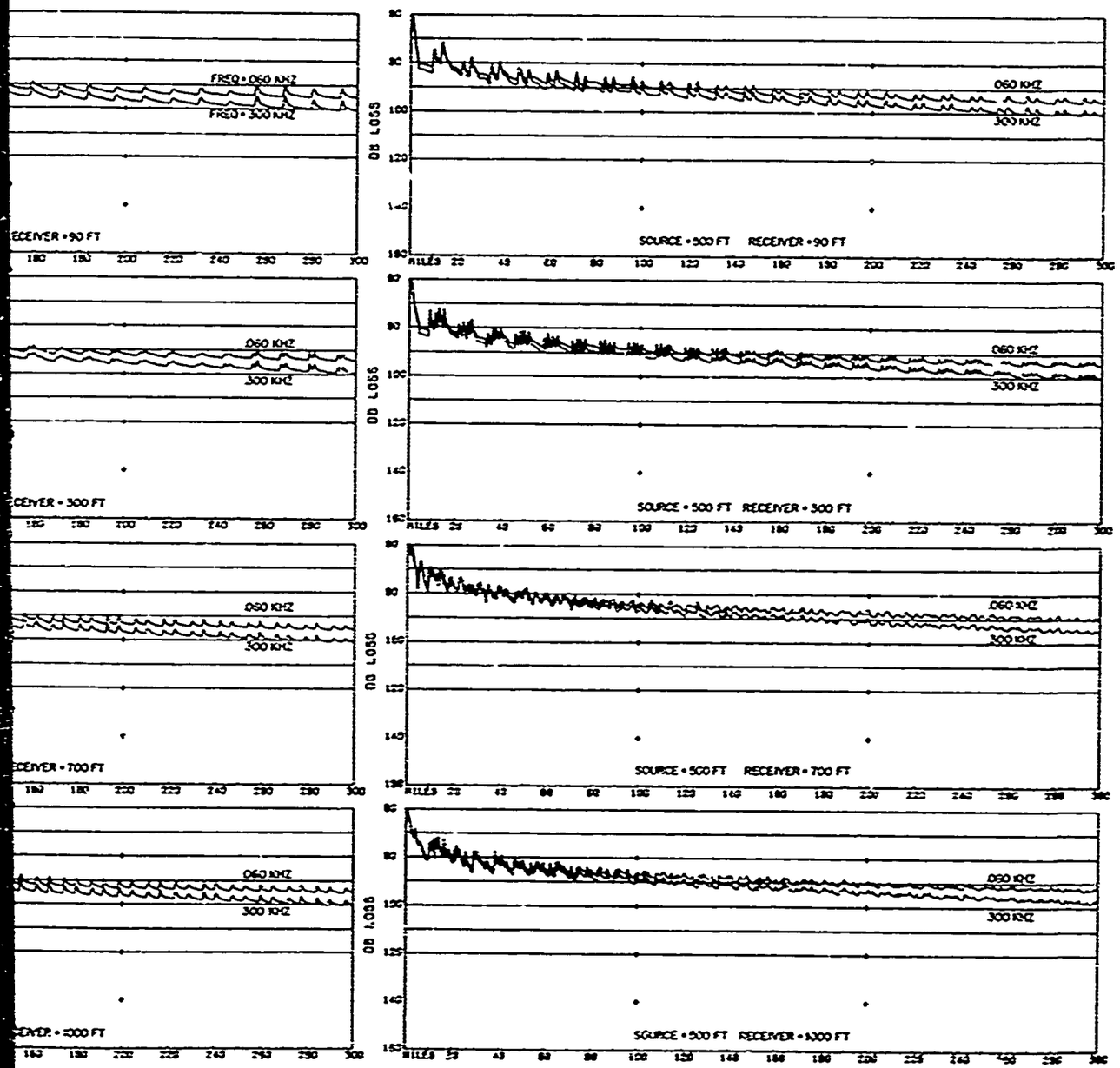

NOTE: BOTTOM CLASS 3

DITERRANEAN SEA, WINTER

FIGURE 72. PROPAGATION LOSS, EASTERN MEDITERRANEAN, WINTER

CONFIDENTIAL

2

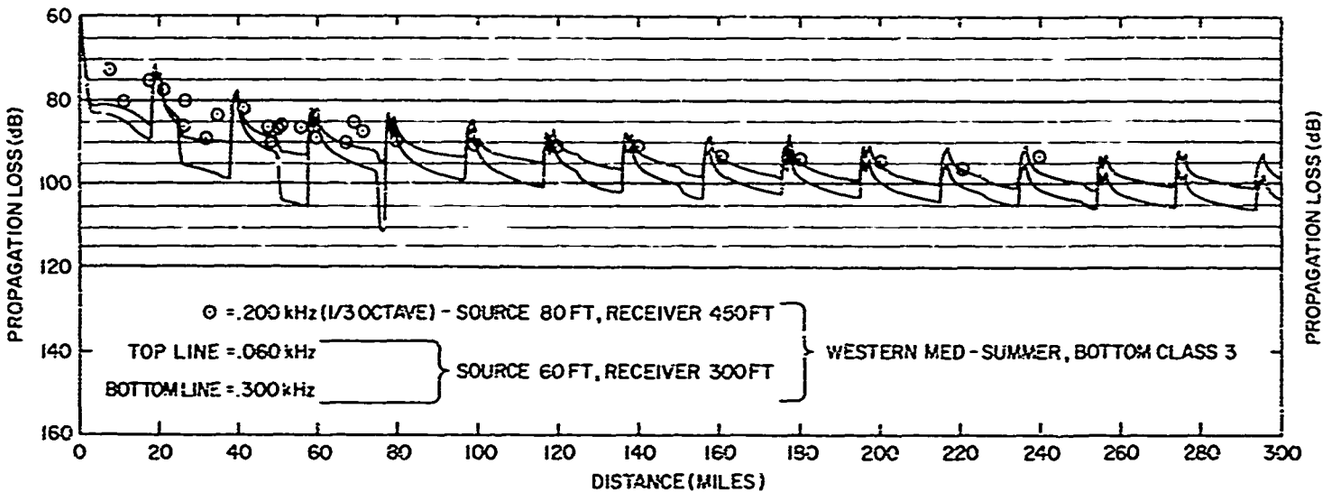

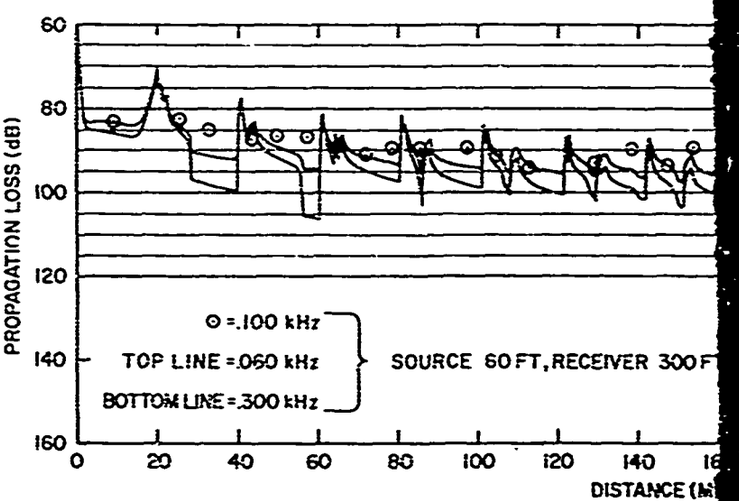

FIGURE 73. ACOUSTIC PROPAGATION LOSS (COMPARISON OF MEASU

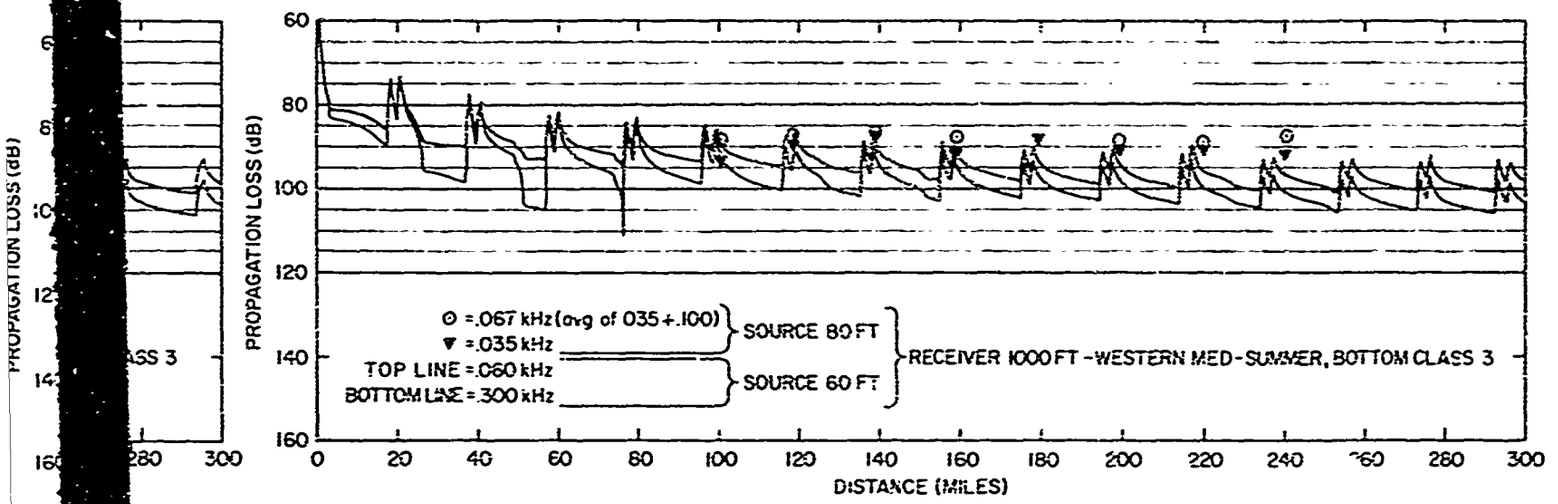

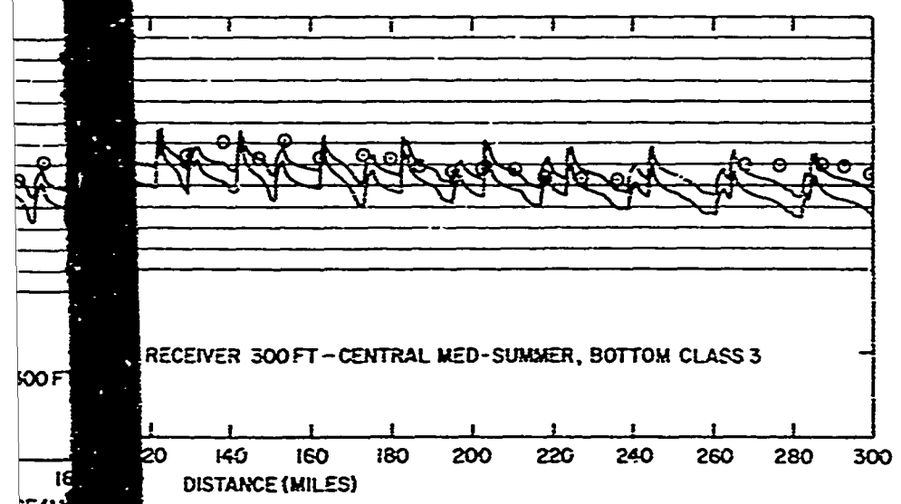

RISON OF MEASUREMENTS WITH FNWC MODEL PREDICTIONS)

FIGURE 73. PROPAGATION LOSS

CONFIDENTIAL

2

A
B

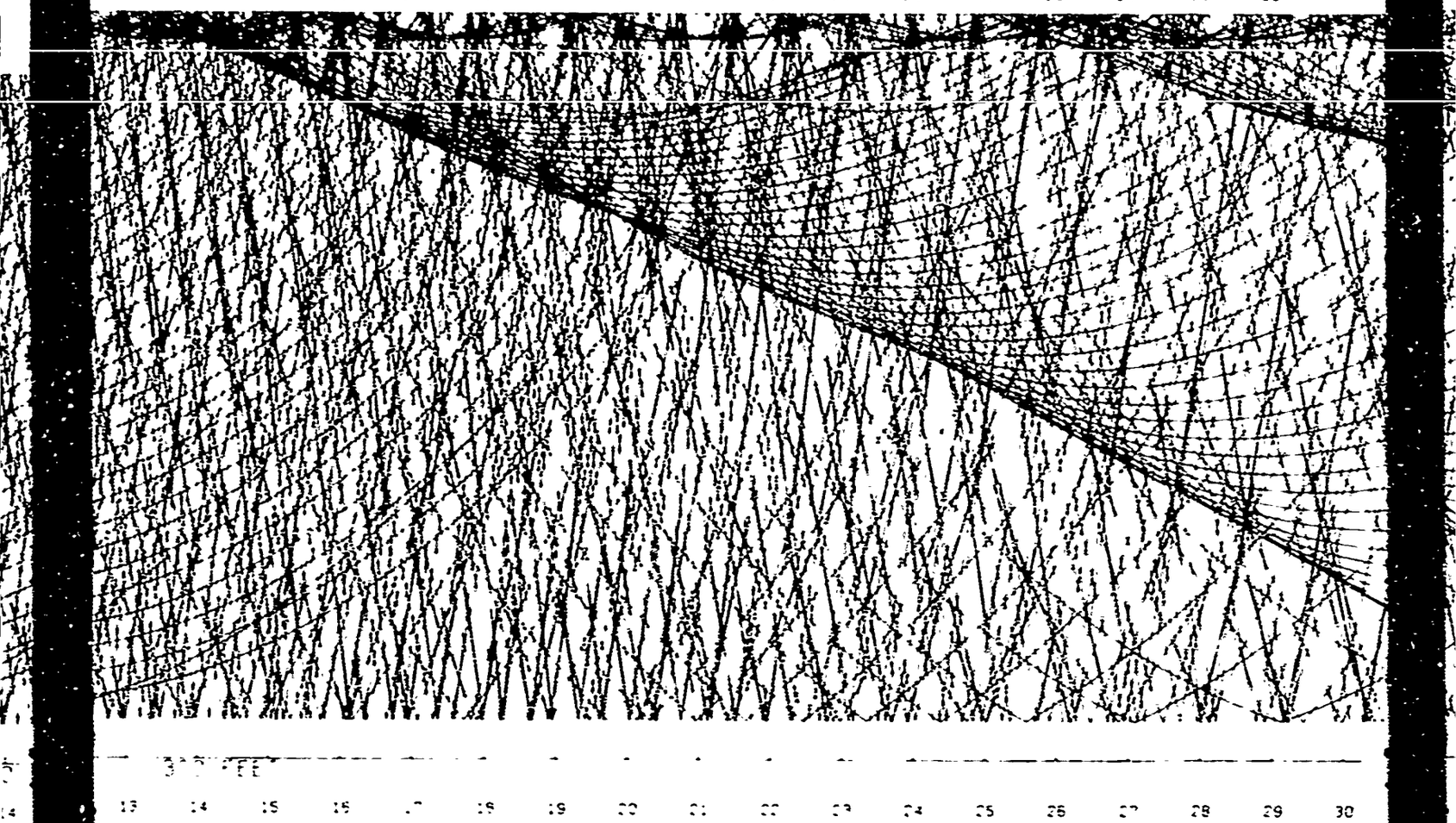

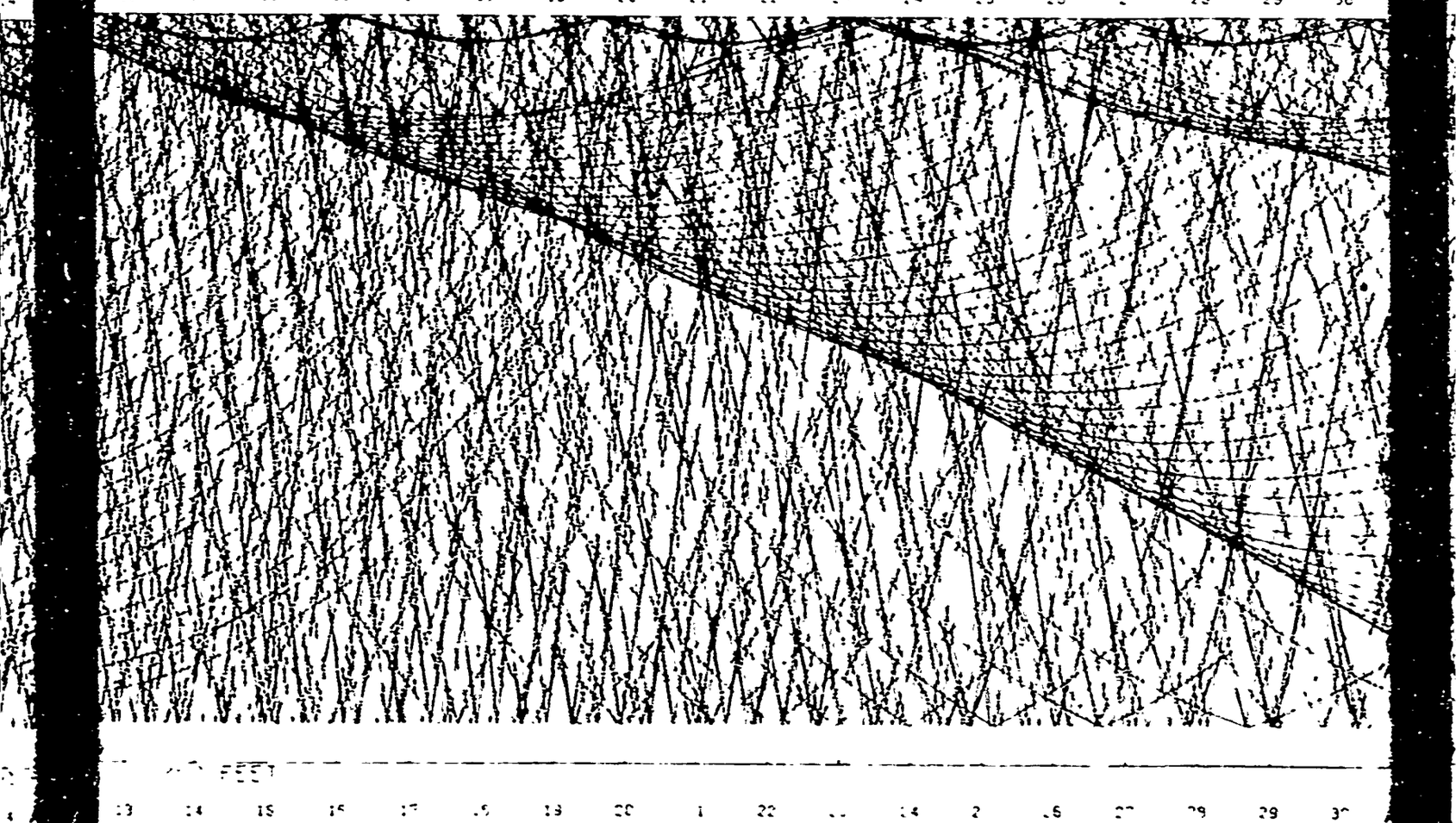

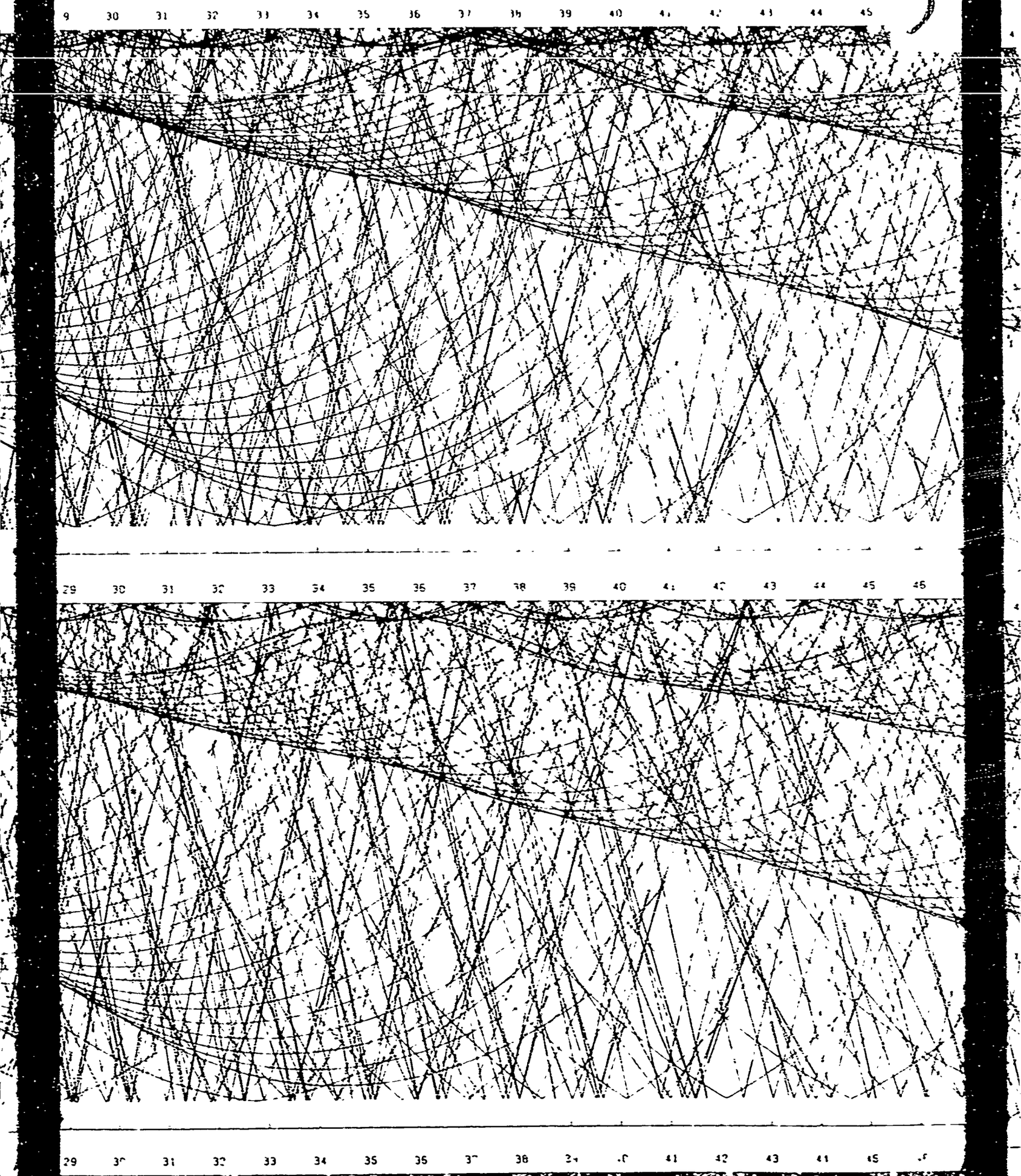
29 30 31 32 33 34 35 36 37 38 39 40 41 42 43 44 45
29 30 31 32 33 34 35 36 37 38 39 40 41 42 43 44 45

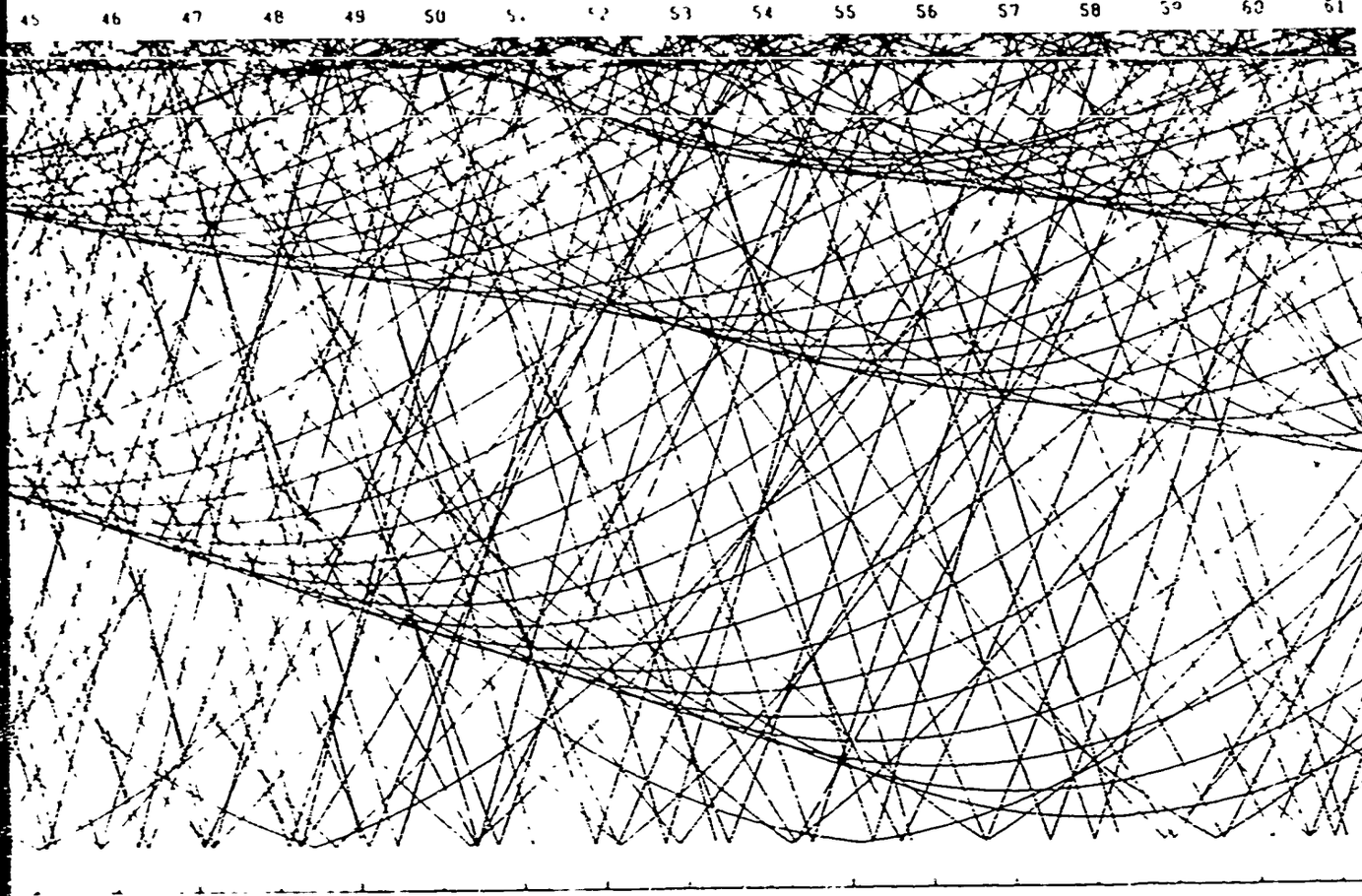
45 46 47 48 49 50 53 54 55 56 57 58 60 61

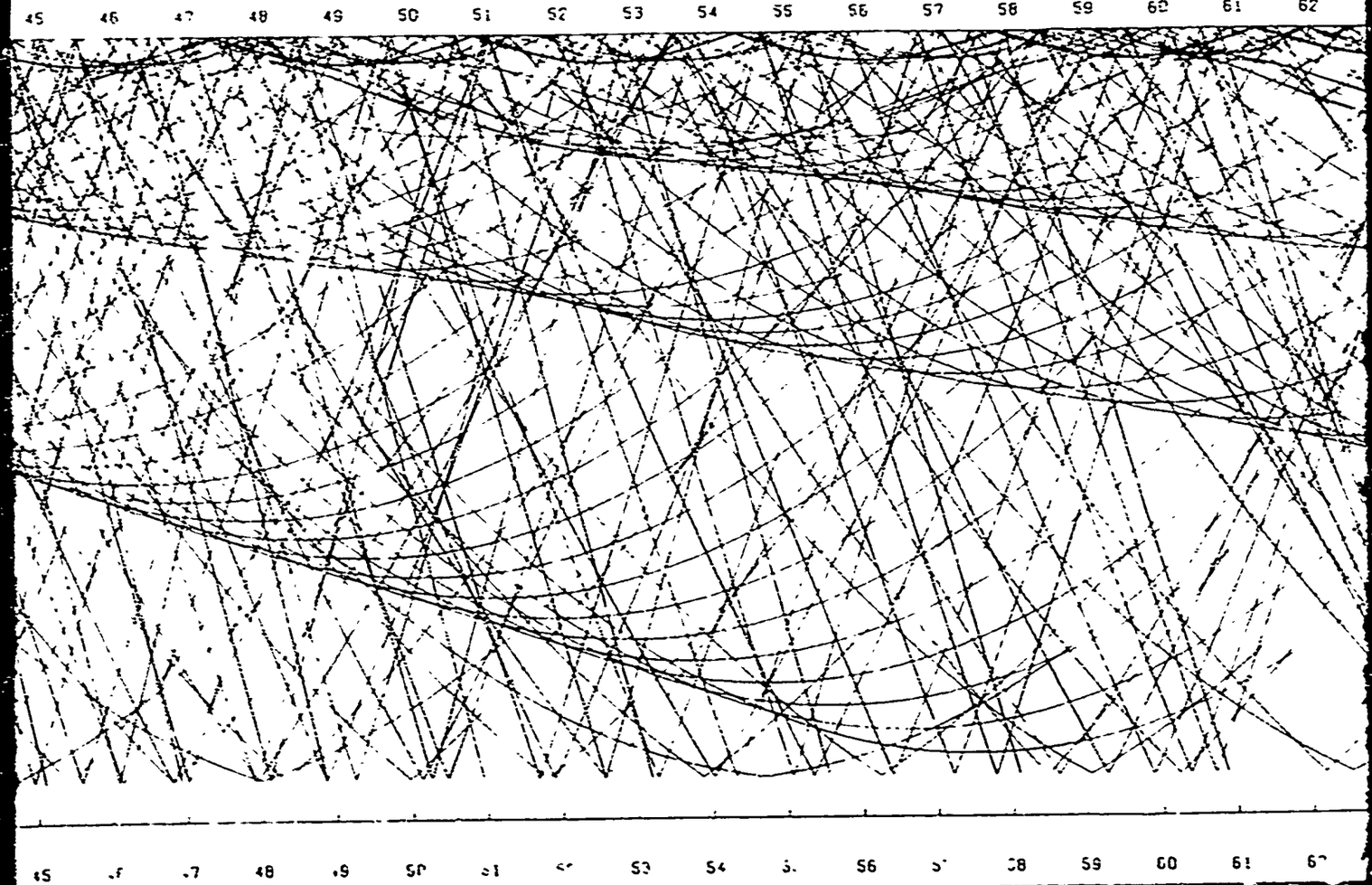
45 46 48 49 50 51 52 53 54 55 56 57 58 59 60 61 62

48 53 54 56 58 59 60 61

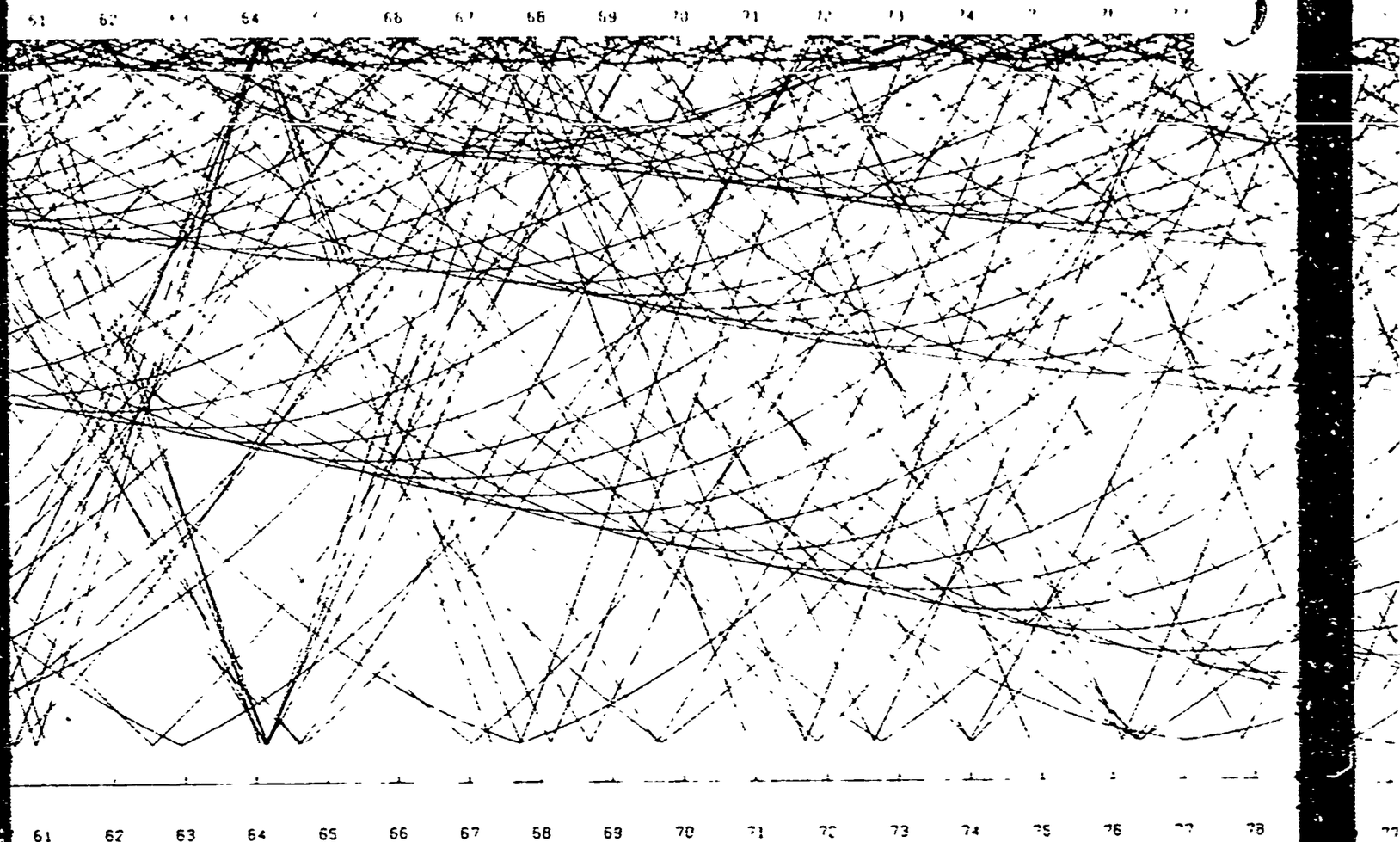
61 62 63 64 65 66 67 68 69 70 71 72 73 74 75 76 77 78

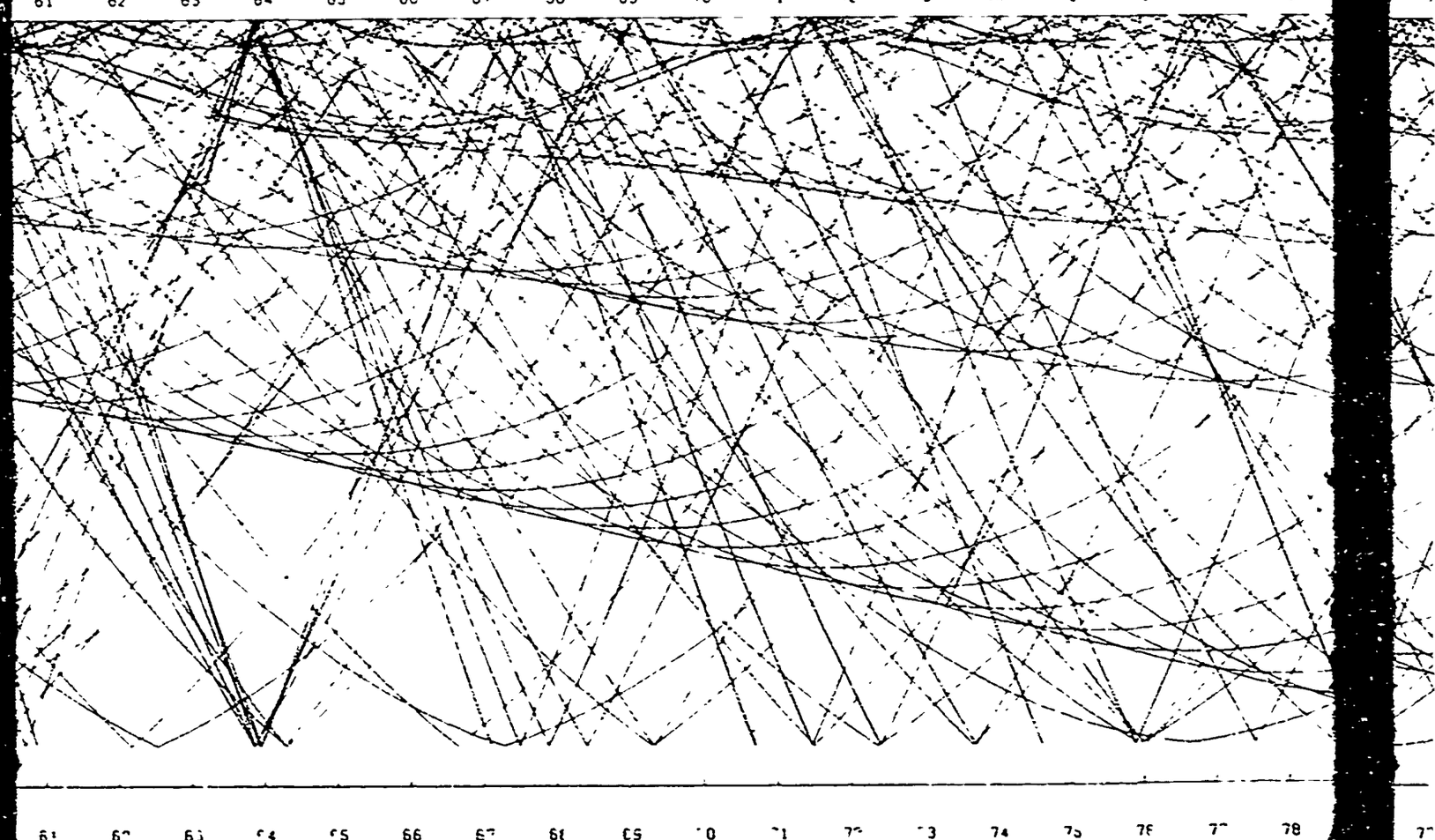
61 62 63 64 65 66 67 68 69 70 71 72 73 74 75 76 77 78

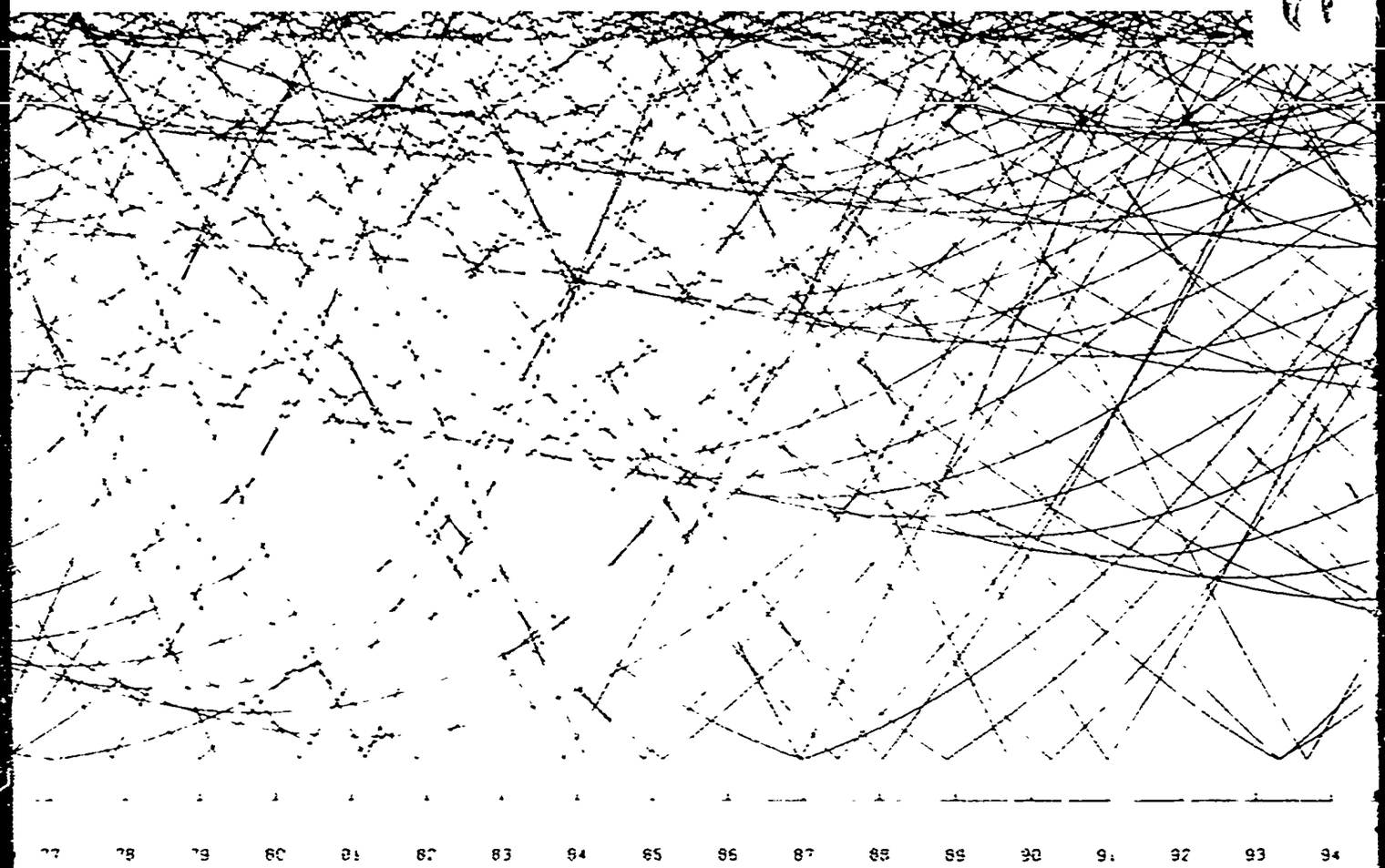

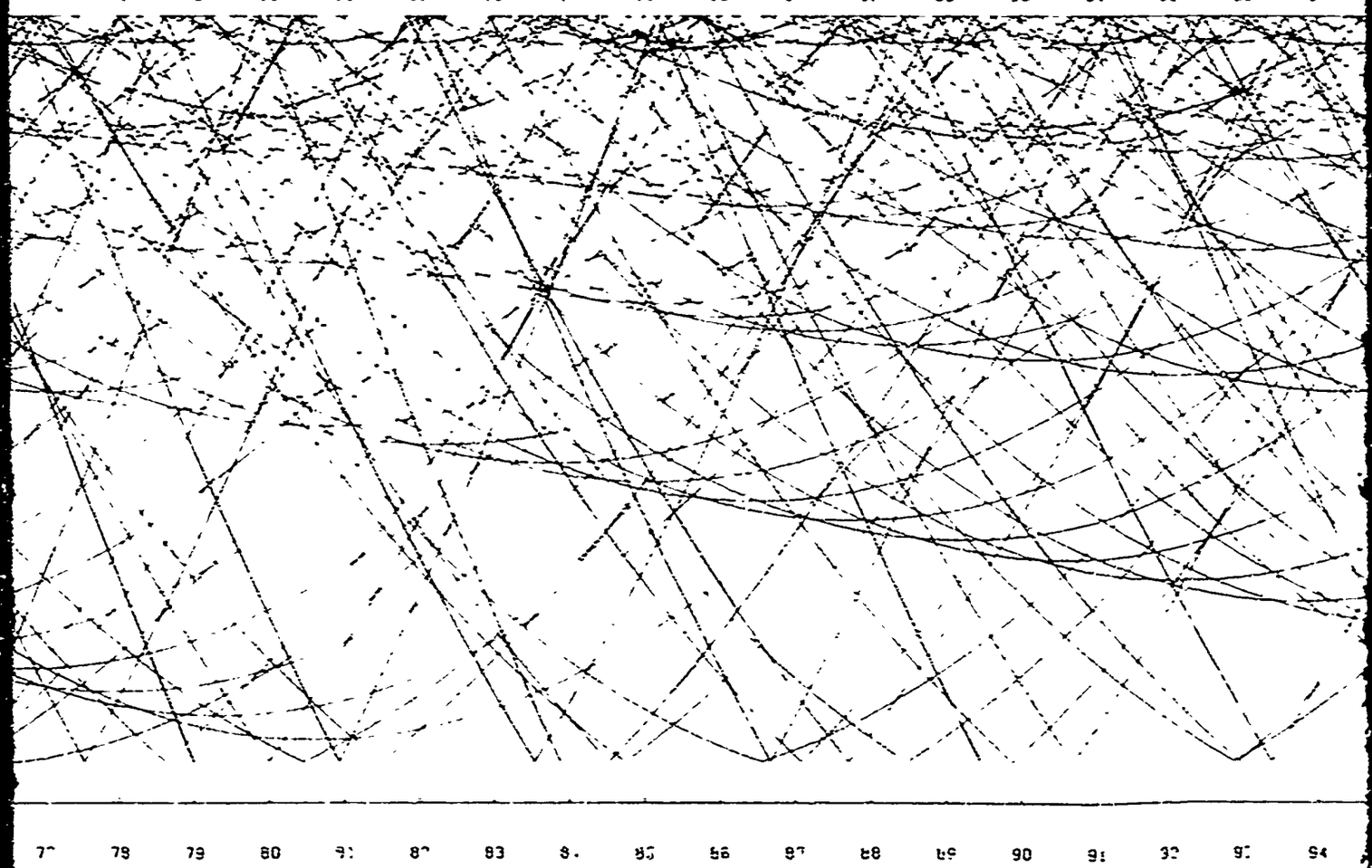

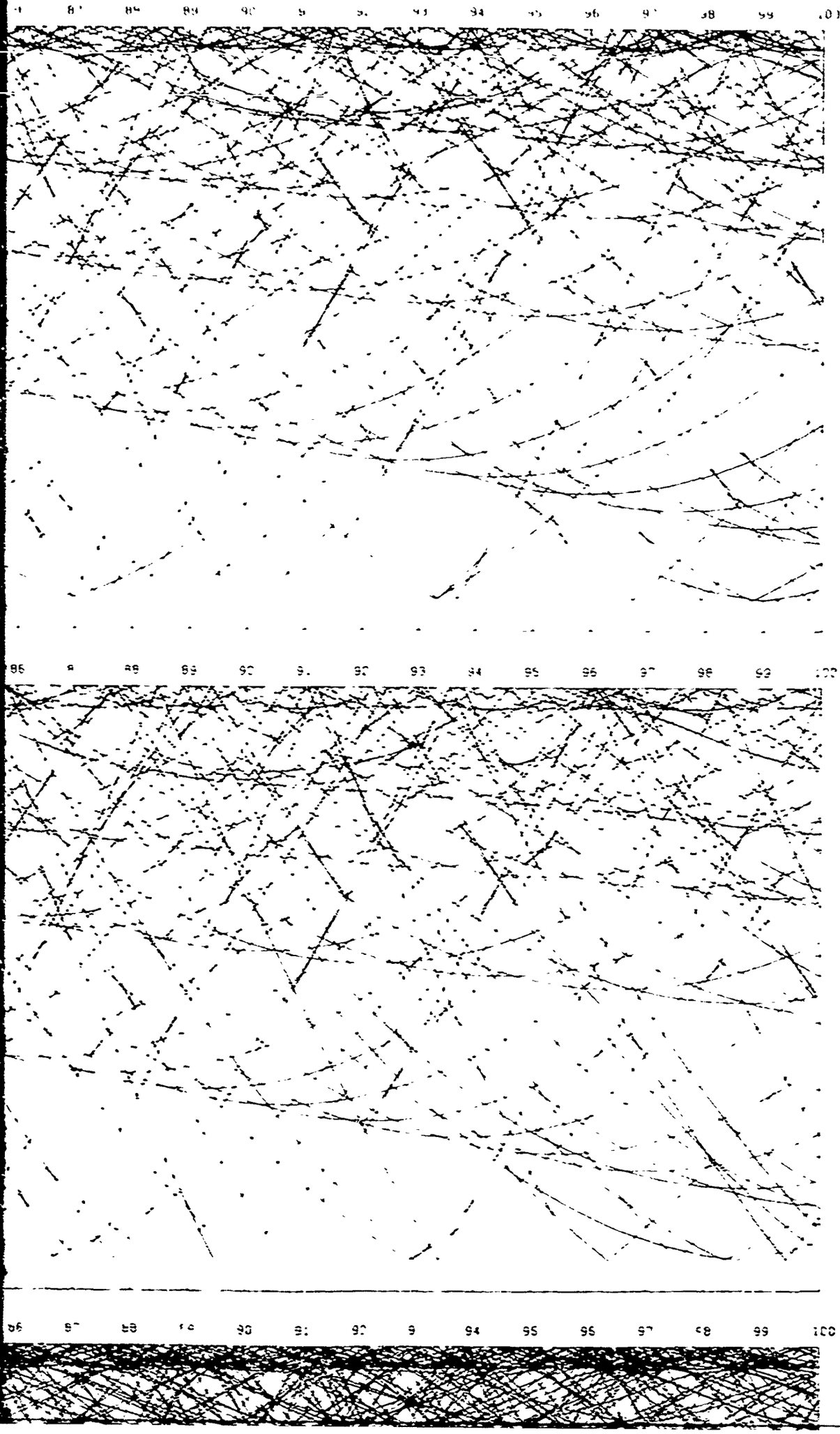

7

C

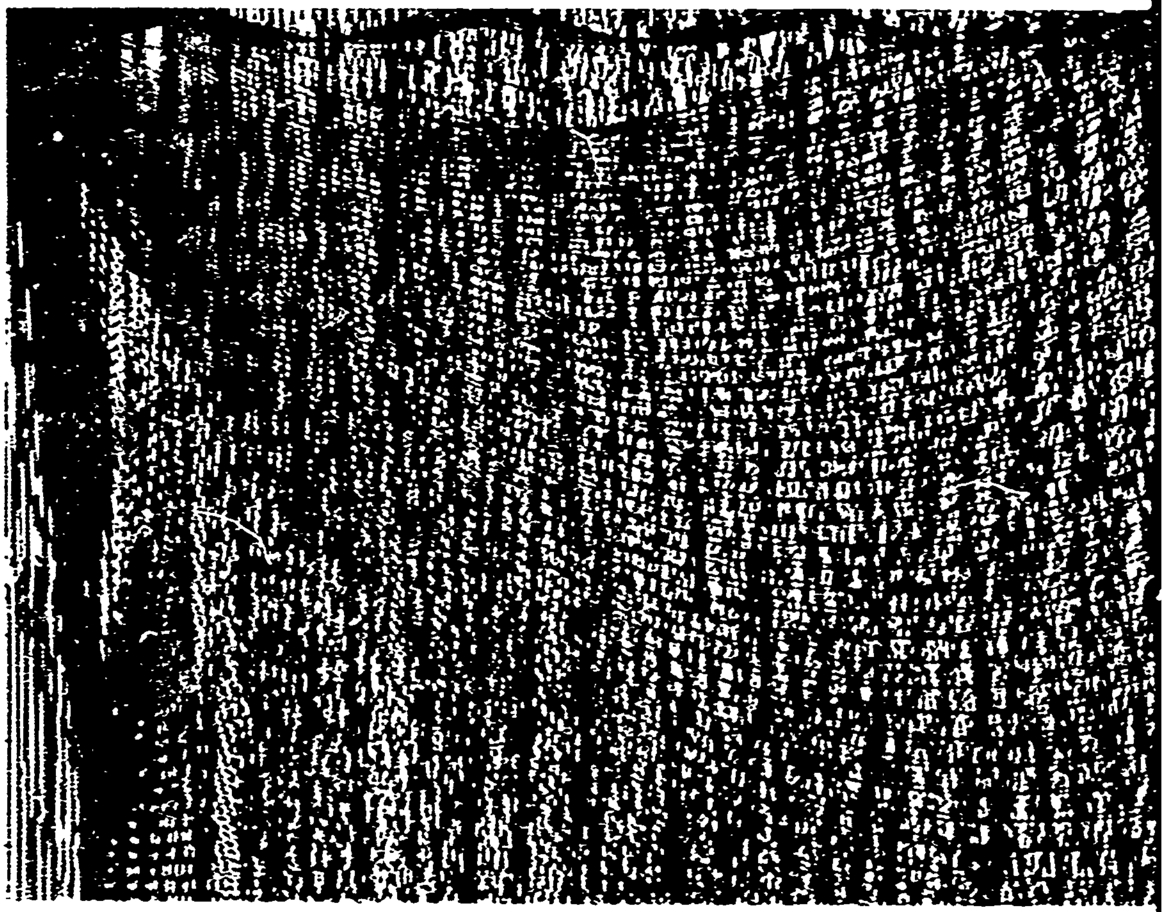

D

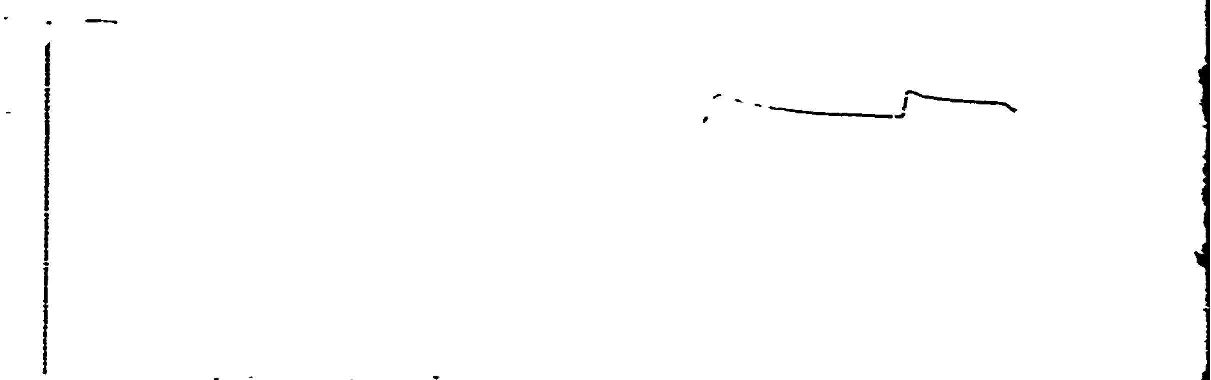

11

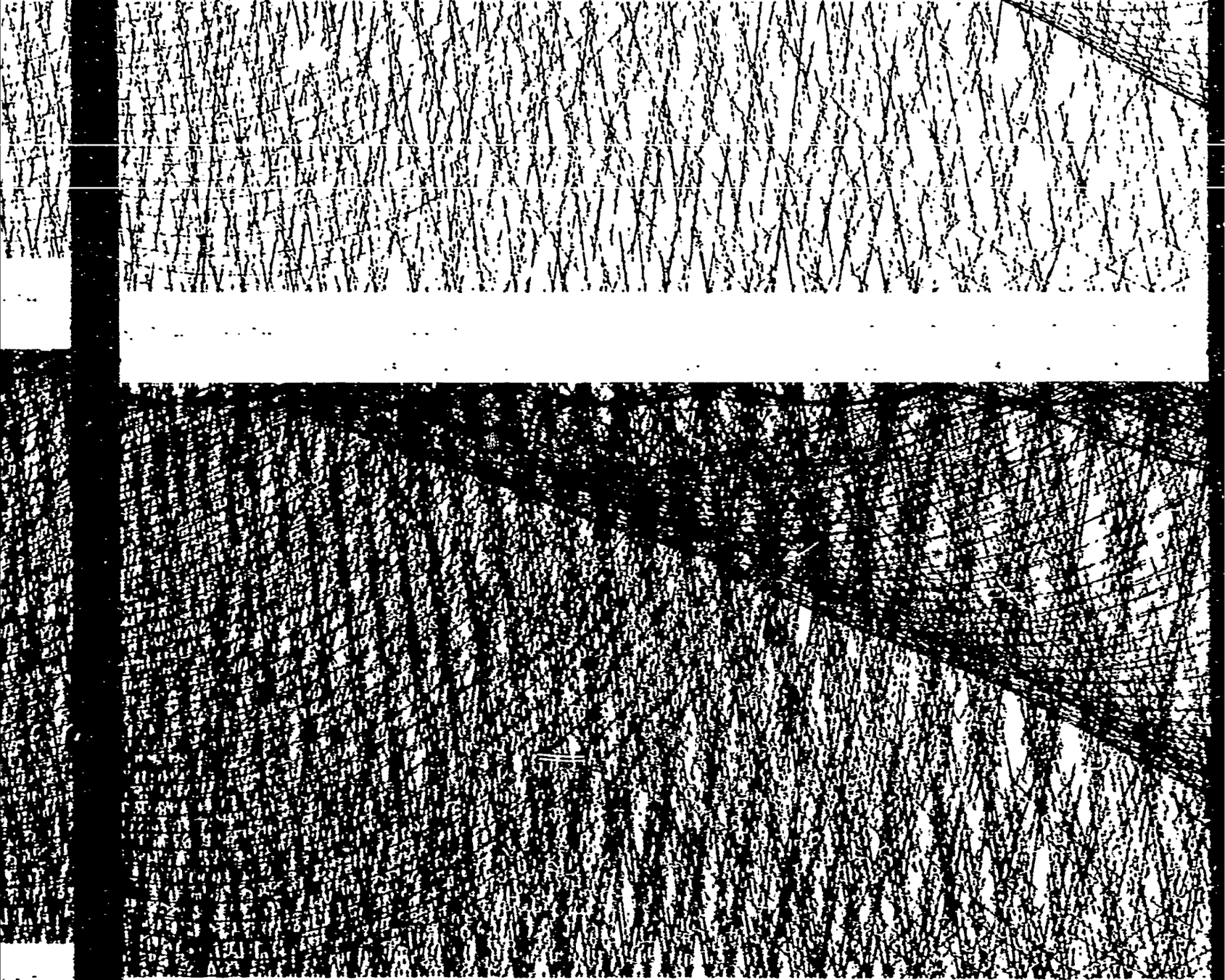

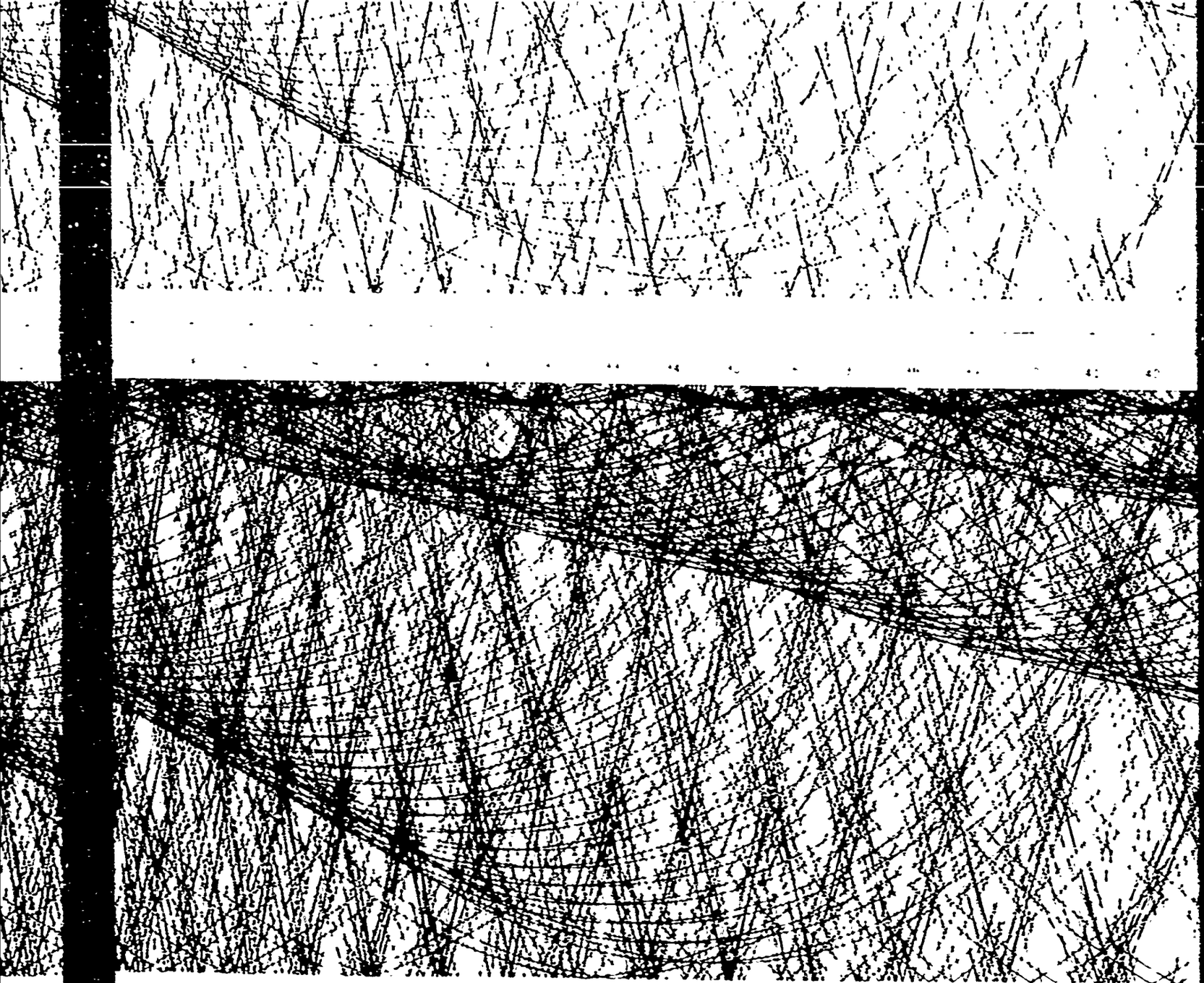

60 65 70 75 80

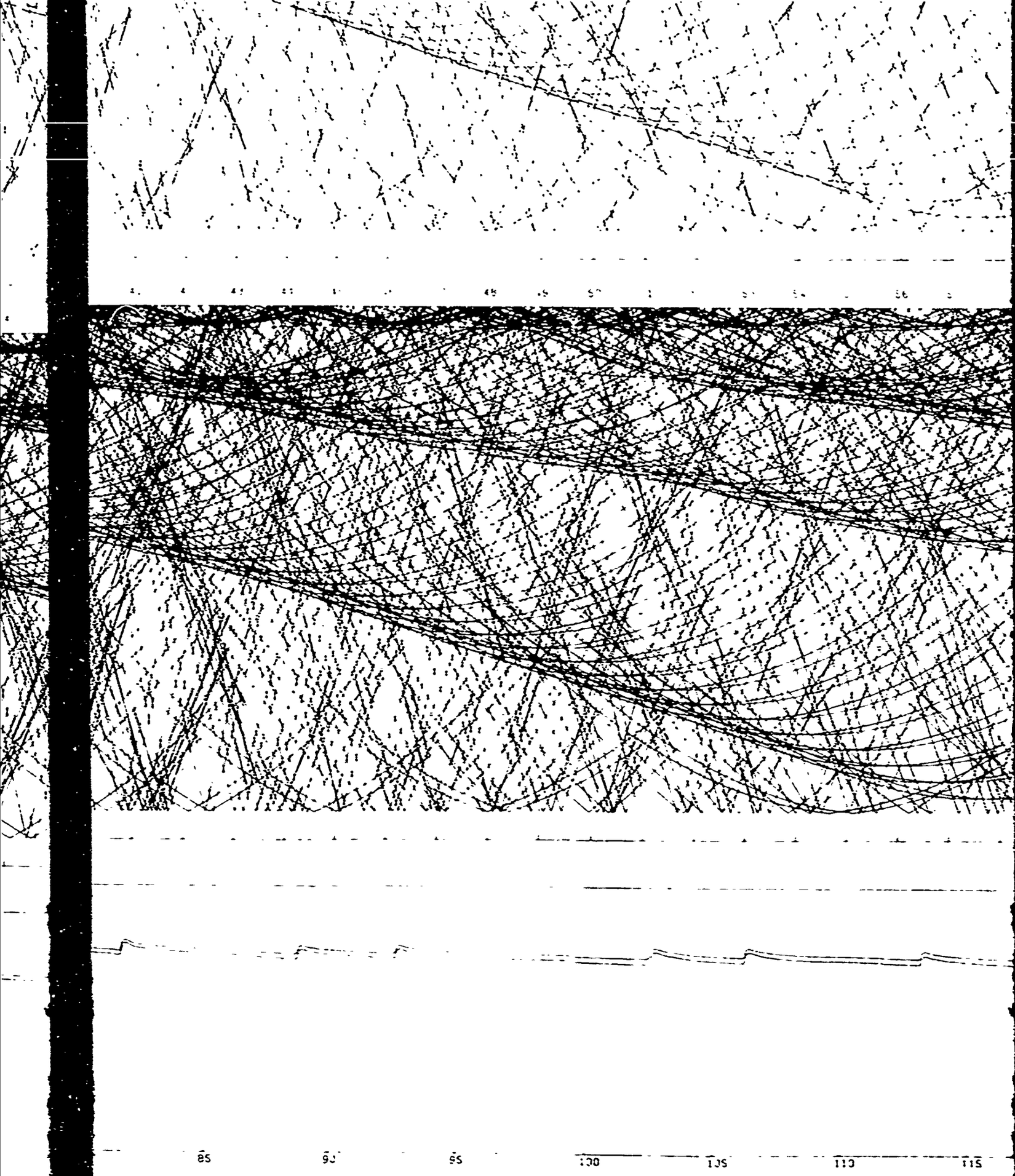

FIGURE 74. RAY PATHS AND TRANSMISSION LOSS -- EASTERN MEDITERRANEAN WINTER

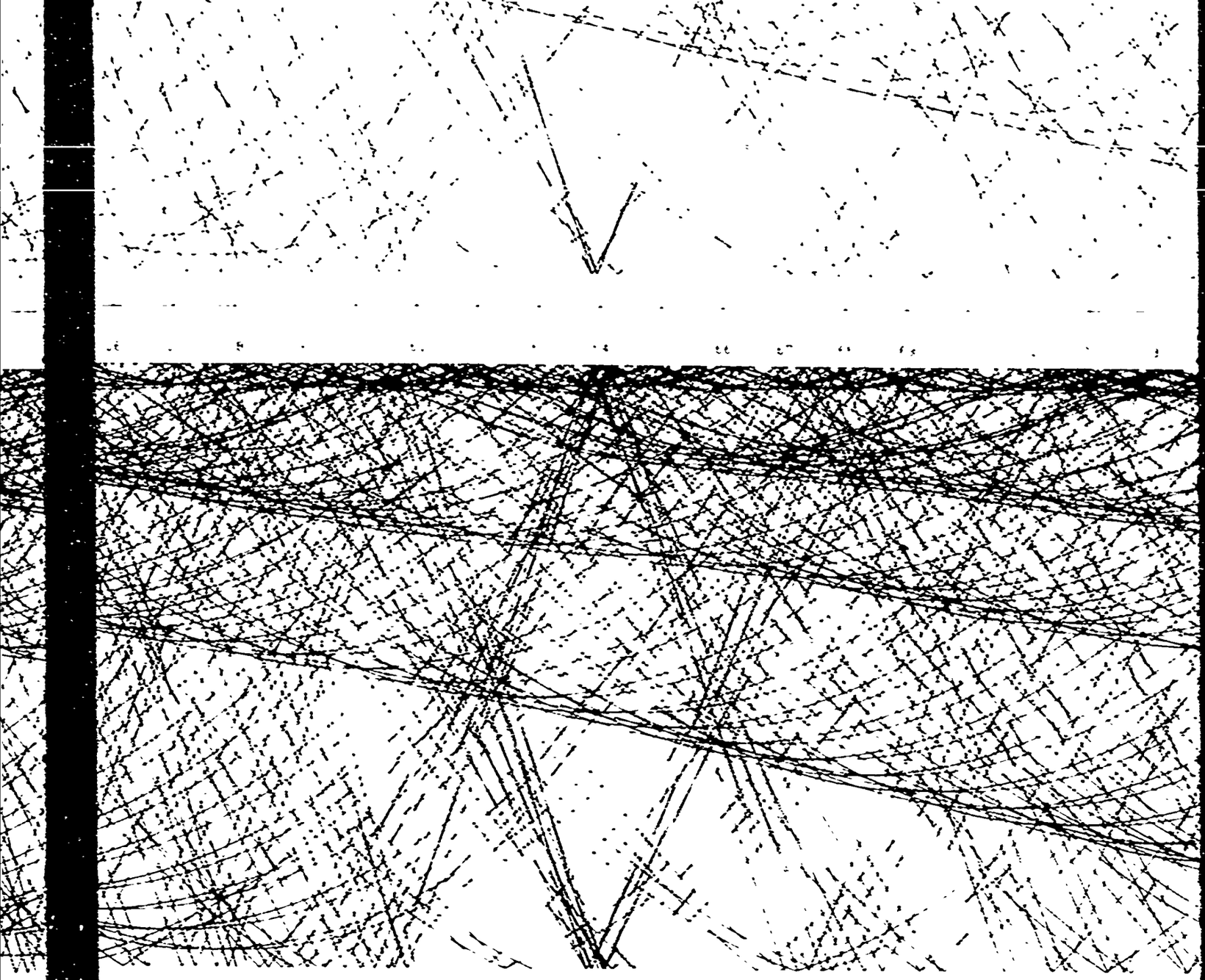

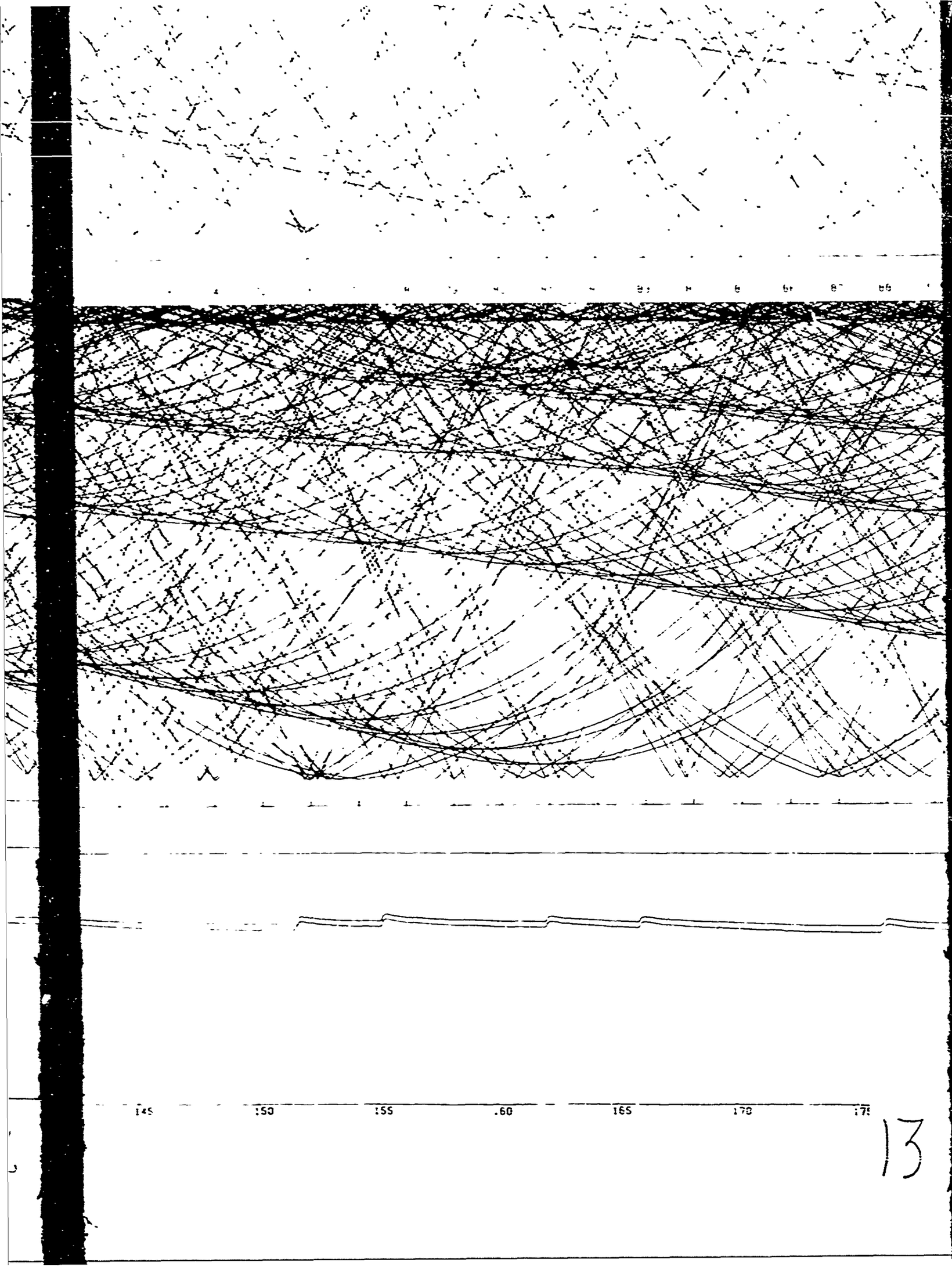
145
150
155
160
165
170
175

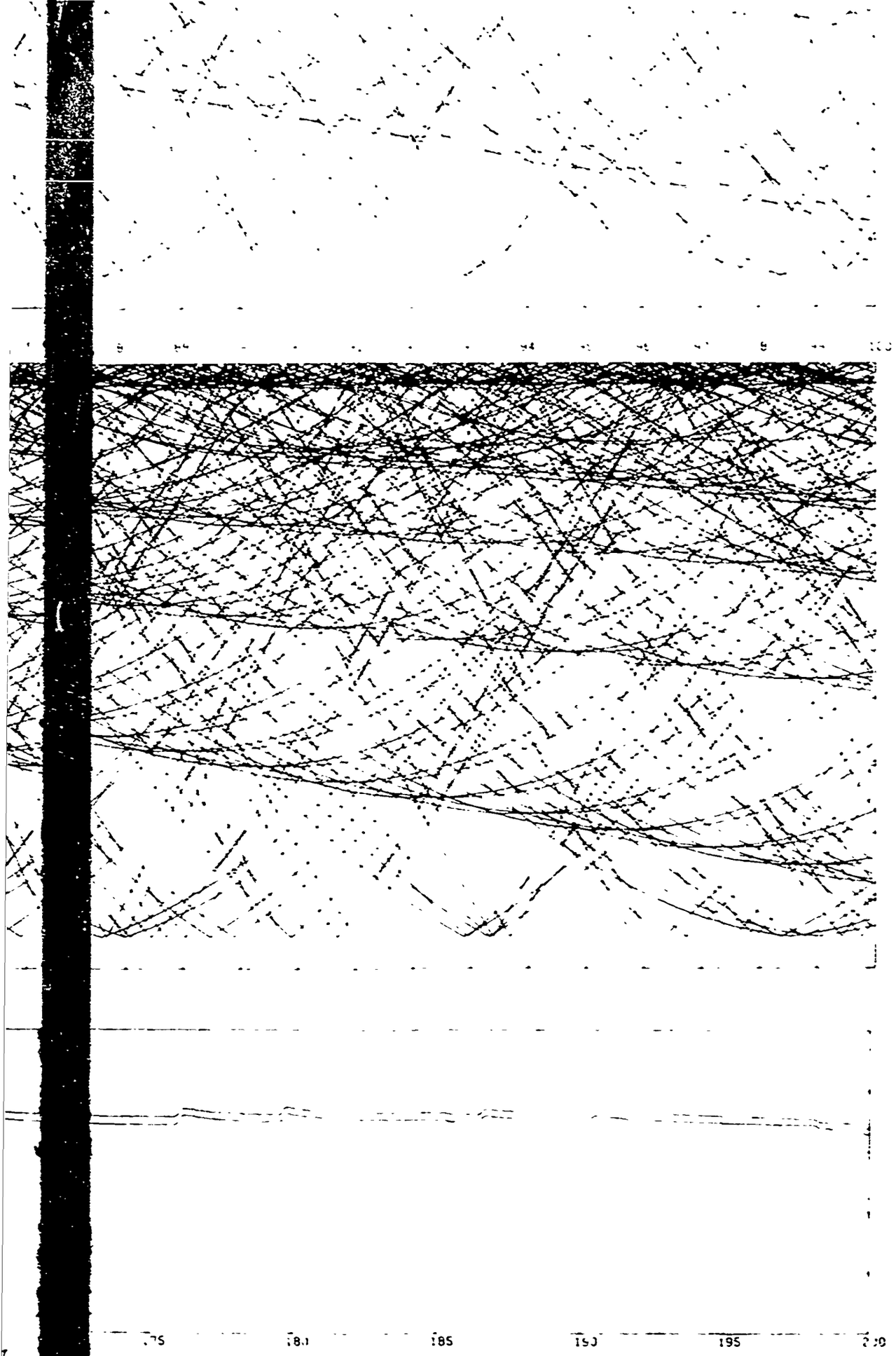

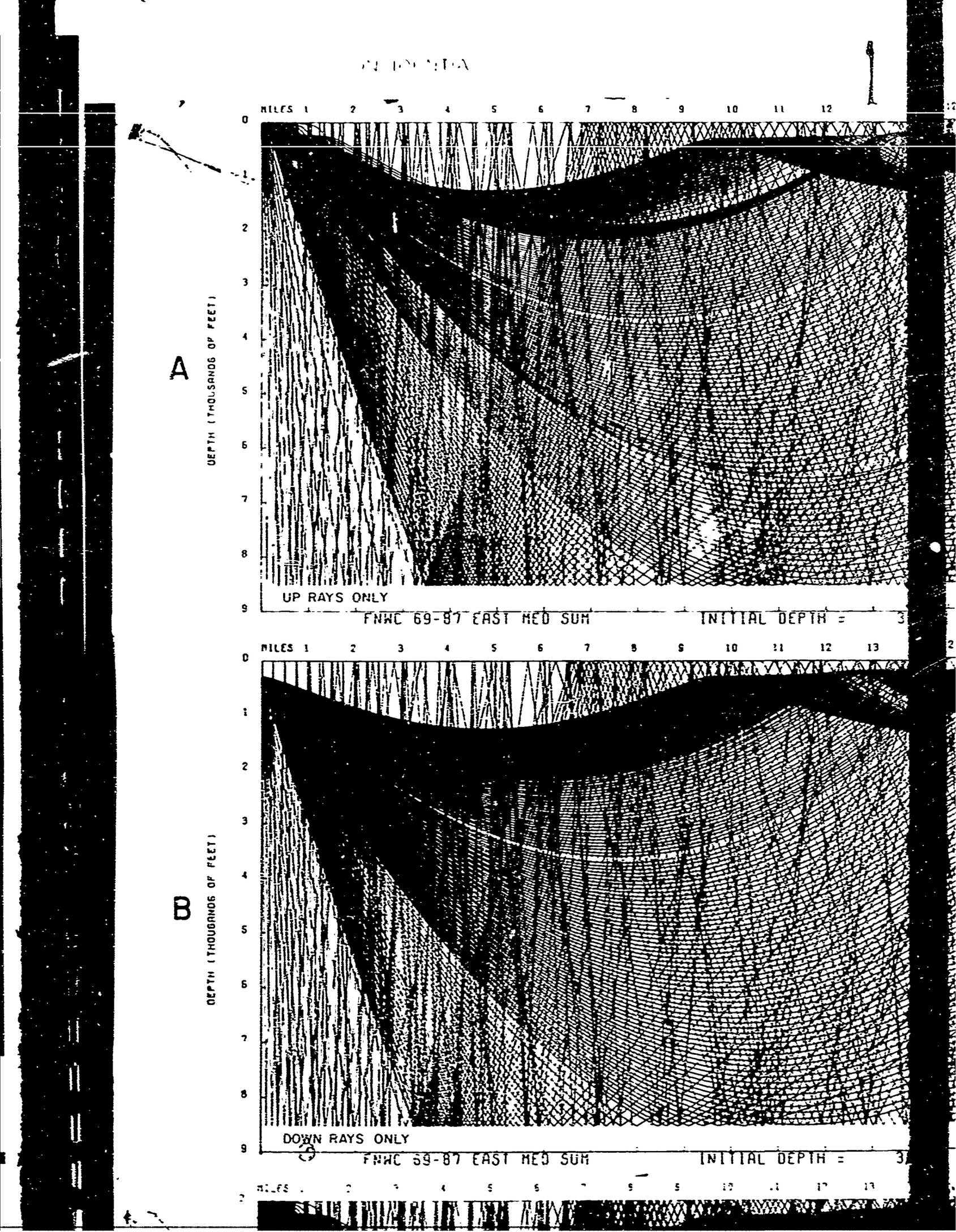
A
MILES 1 2 3 4 5 6 7 8 9 10 11 12
DEPTH (THOUSANDS OF FEET)
0 1 2 3 4 5 6 7 8 9
UP RAYS ONLY
FNWC 69-87 EAST MED SUM
INITIAL DEPTH =
B
MILES 1 2 3 4 5 6 7 8 9 10 11 12 13
DEPTH (THOUSANDS OF FEET)
0 1 2 3 4 5 6 7 8 9
DOWN RAYS ONLY
FNWC 69-87 EAST MED SUM
INITIAL DEPTH =

2

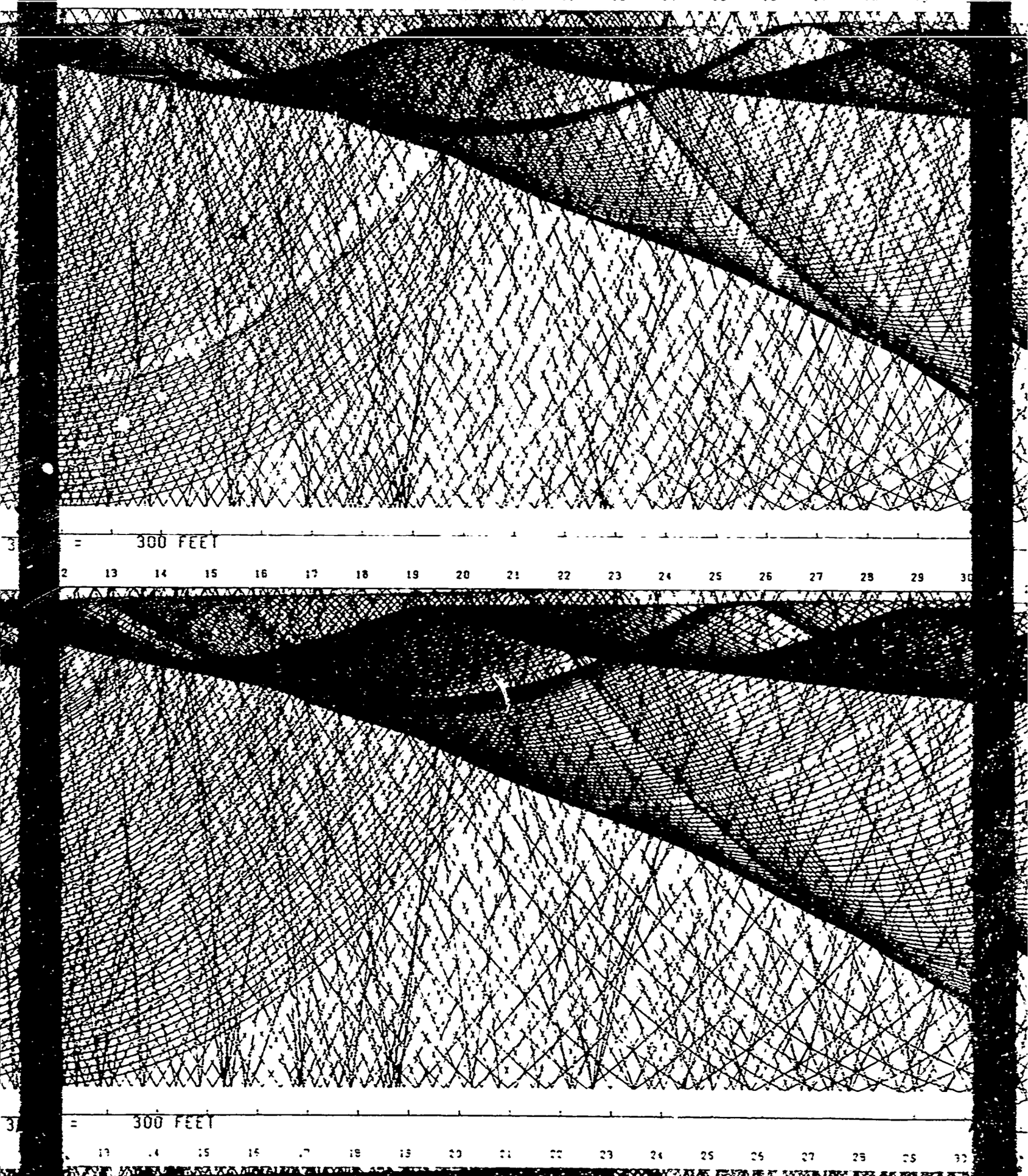
12 13 14 15 16 17 18 19 20 21 22 23 24 25 26 27 28
= 300 FEET
12 13 14 15 16 17 18 19 20 21 22 23 24 25 26 27 28 29 30
= 300 FEET

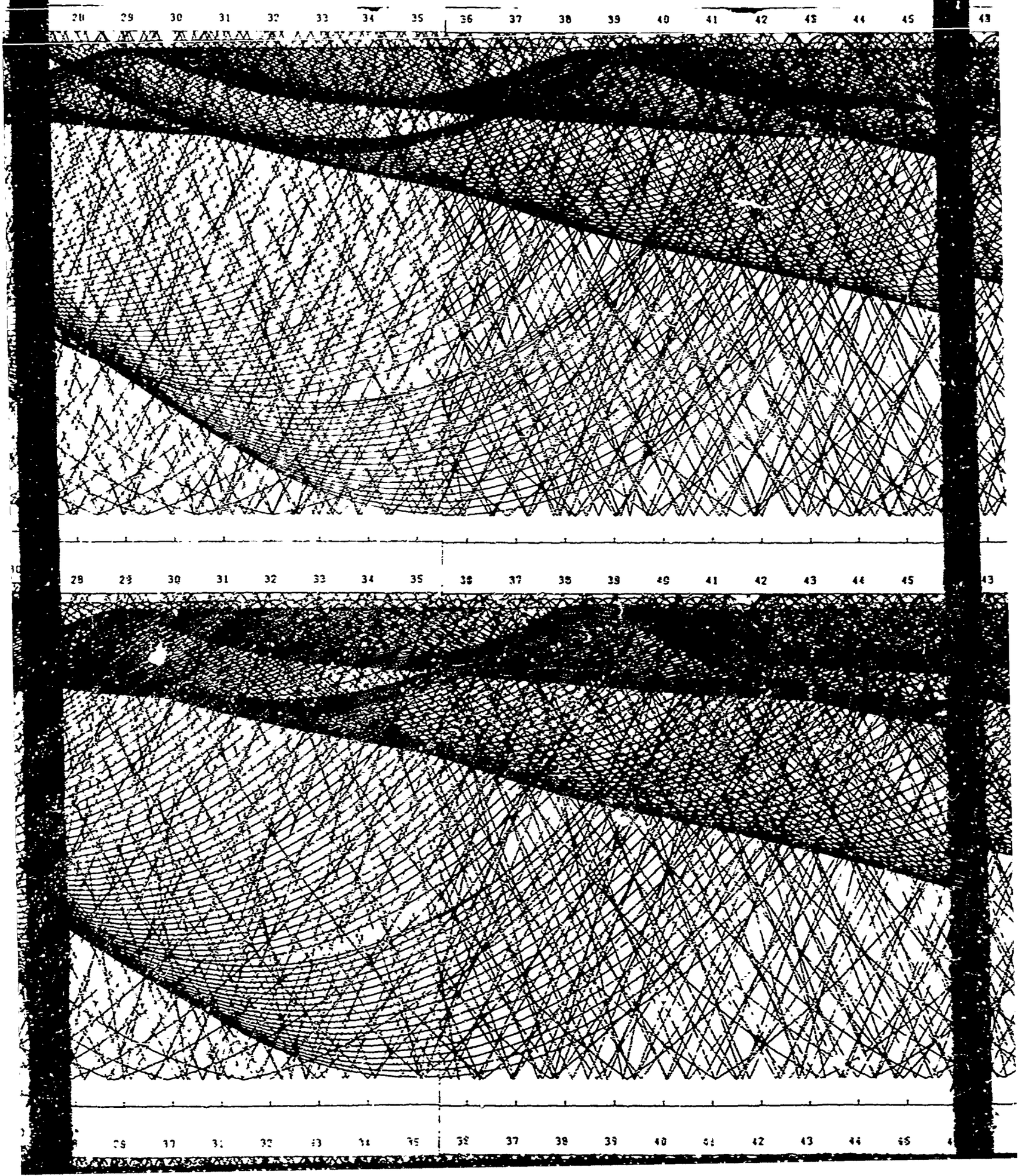
28 29 30 31 32 33 34 35 36 37 38 39 40 41 42 43 44 45 46
28 29 30 31 32 33 34 35 36 37 38 39 40 41 42 43 44 45 46

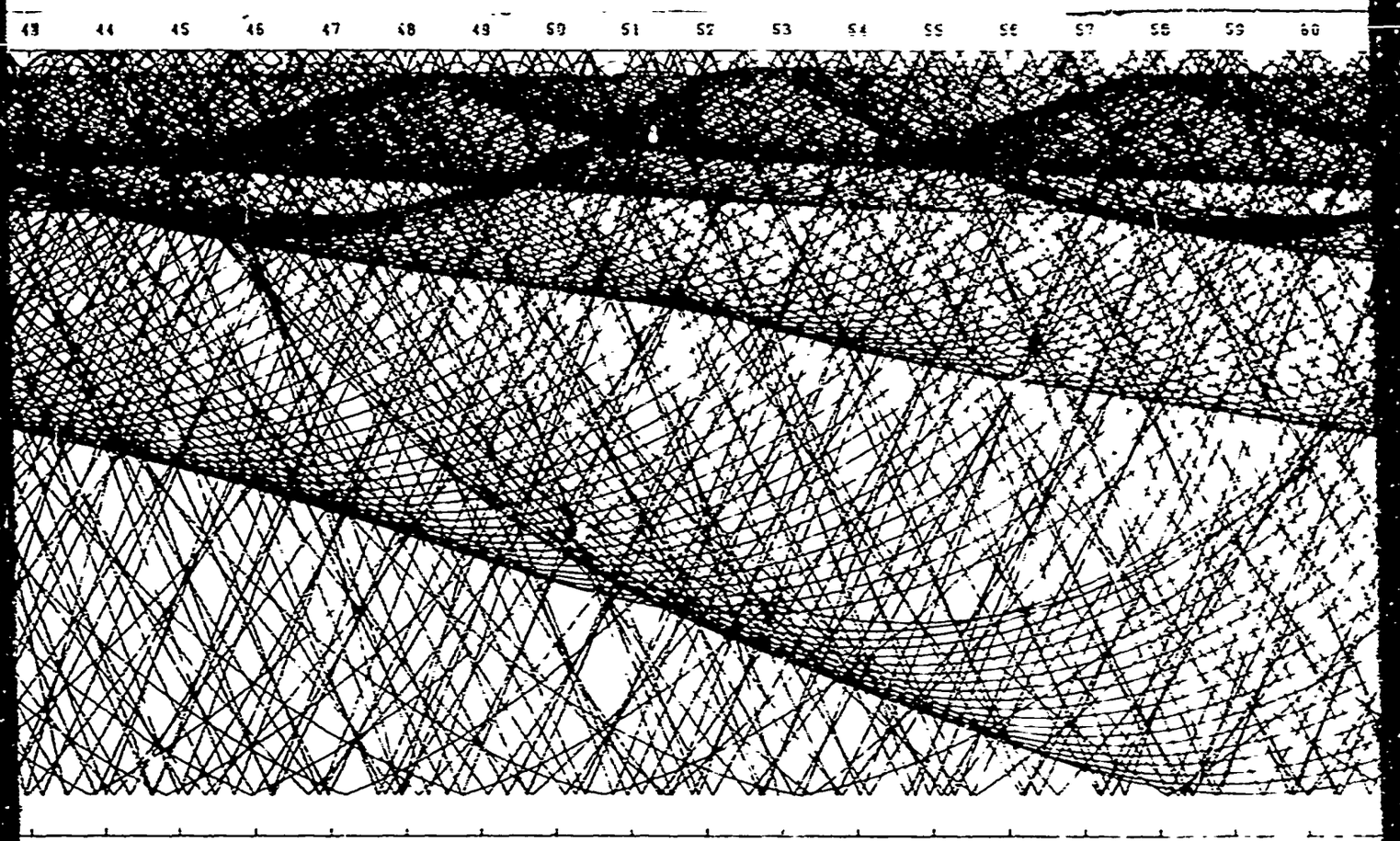
43 44 45 46 47 48 49 50 51 52 53 54 55 56 57 58 59 60

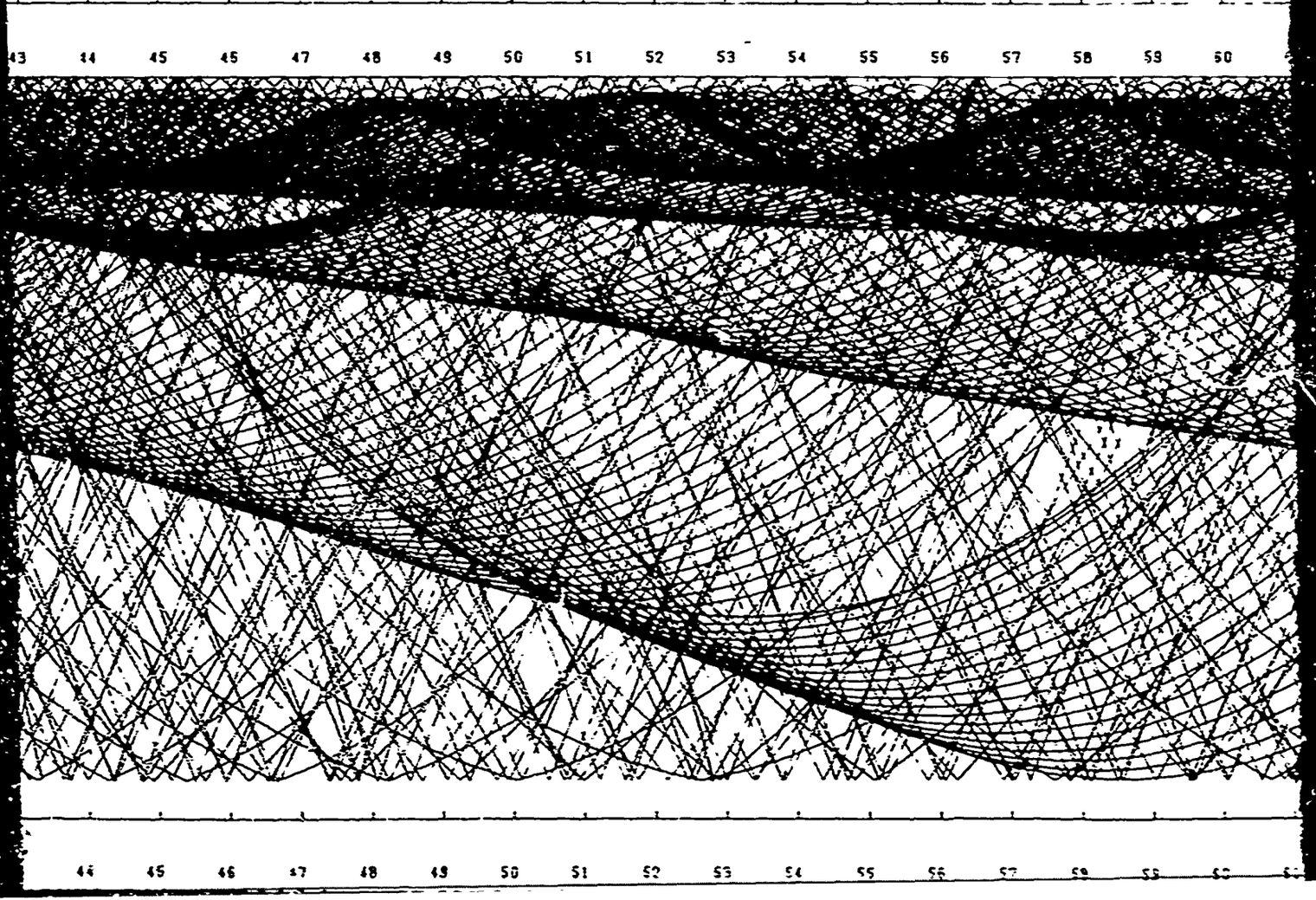
43 44 45 46 47 48 49 50 51 52 53 54 55 56 57 58 59 60
44 45 46 47 48 49 50 51 52 53 54 55 56 57 58 59 60

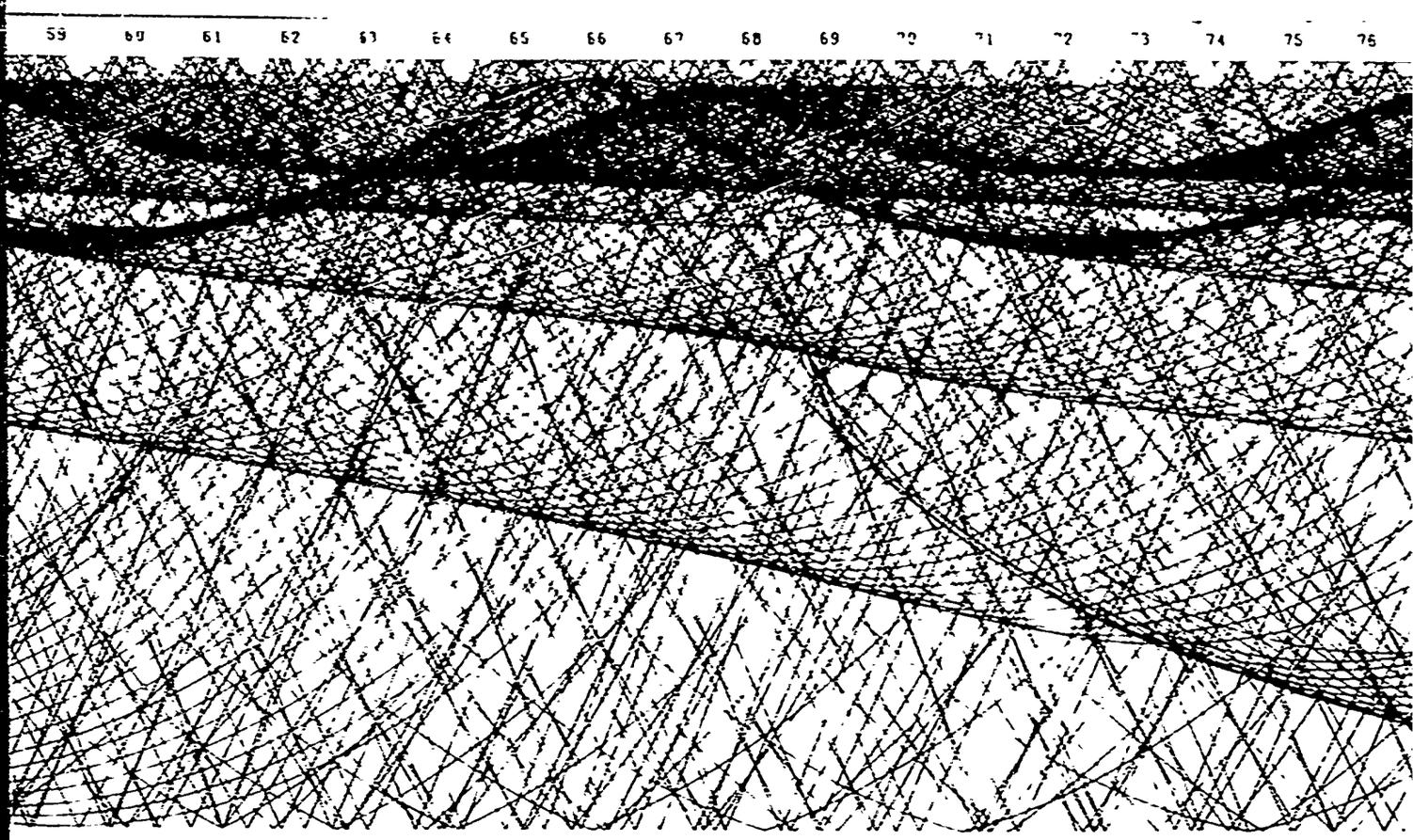
59 60 61 62 63 64 65 66 67 68 69 70 71 72 73 74 75 76

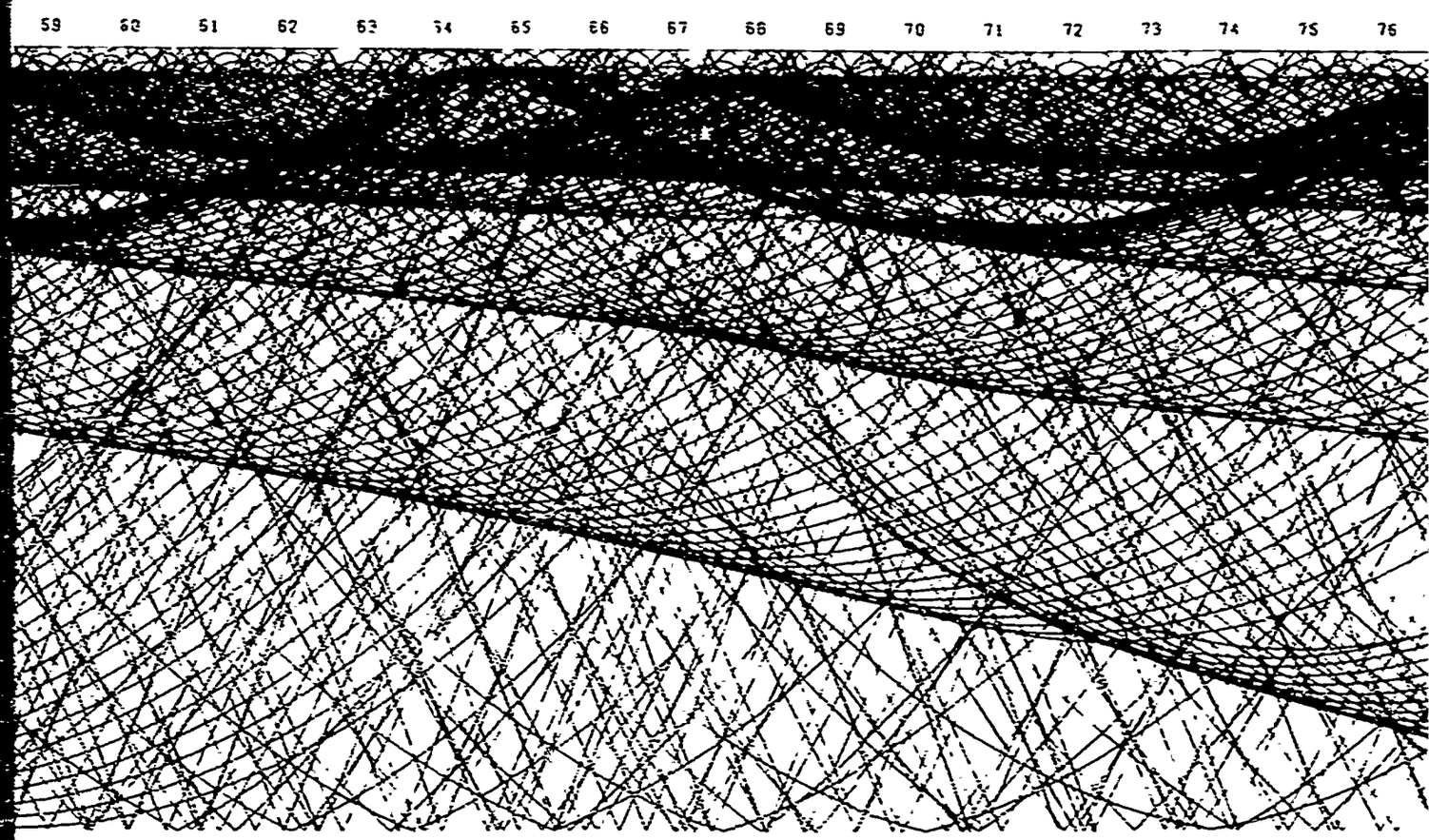
59 60 61 62 63 64 65 66 67 68 69 70 71 72 73 74 75 76

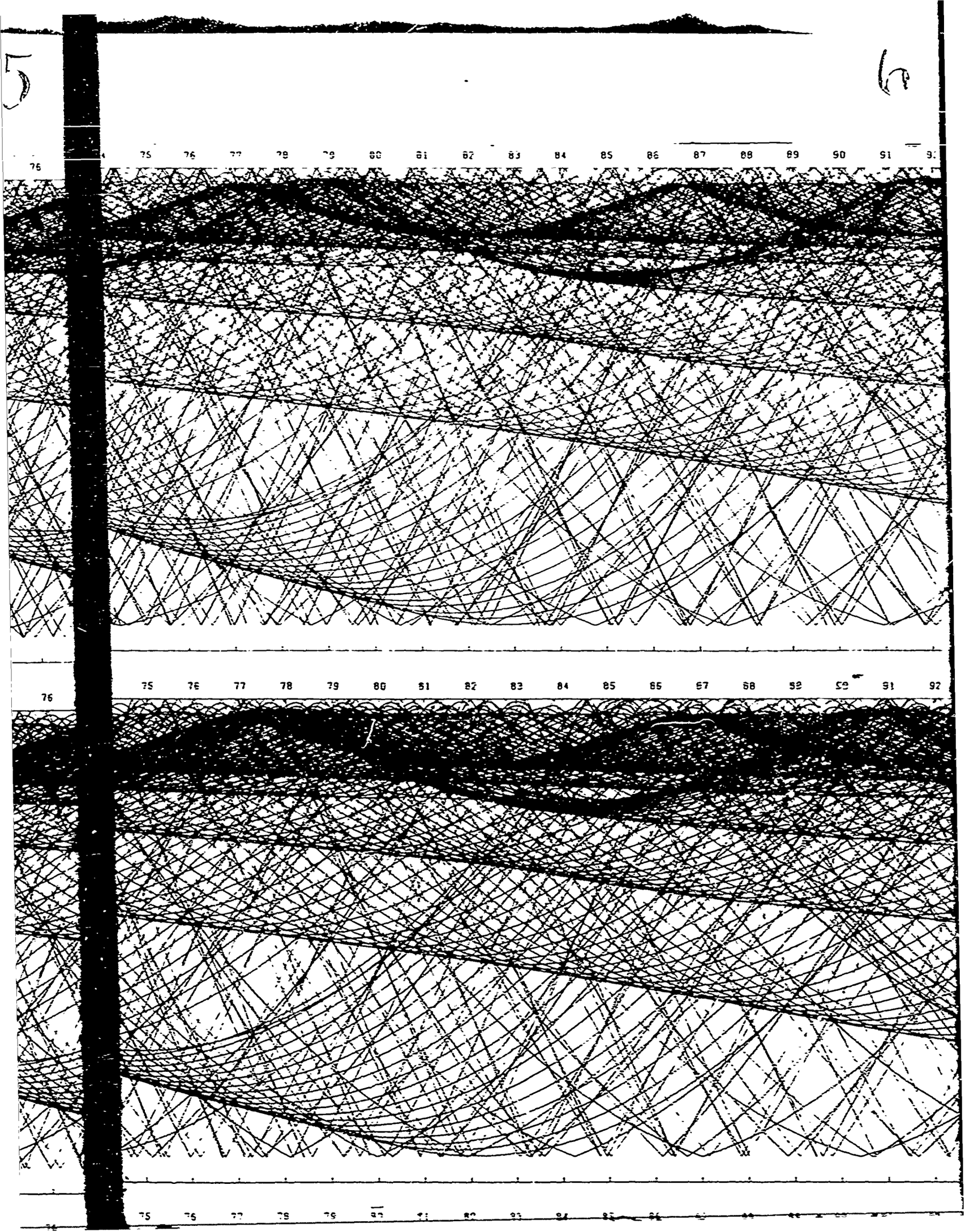
75 76 77 78 79 80 81 82 83 84 85 86 87 88 89 90 91
76
75 76 77 78 79 80 81 82 83 84 85 86 87 88 89 90 91 92
76
75 76 77 78 79

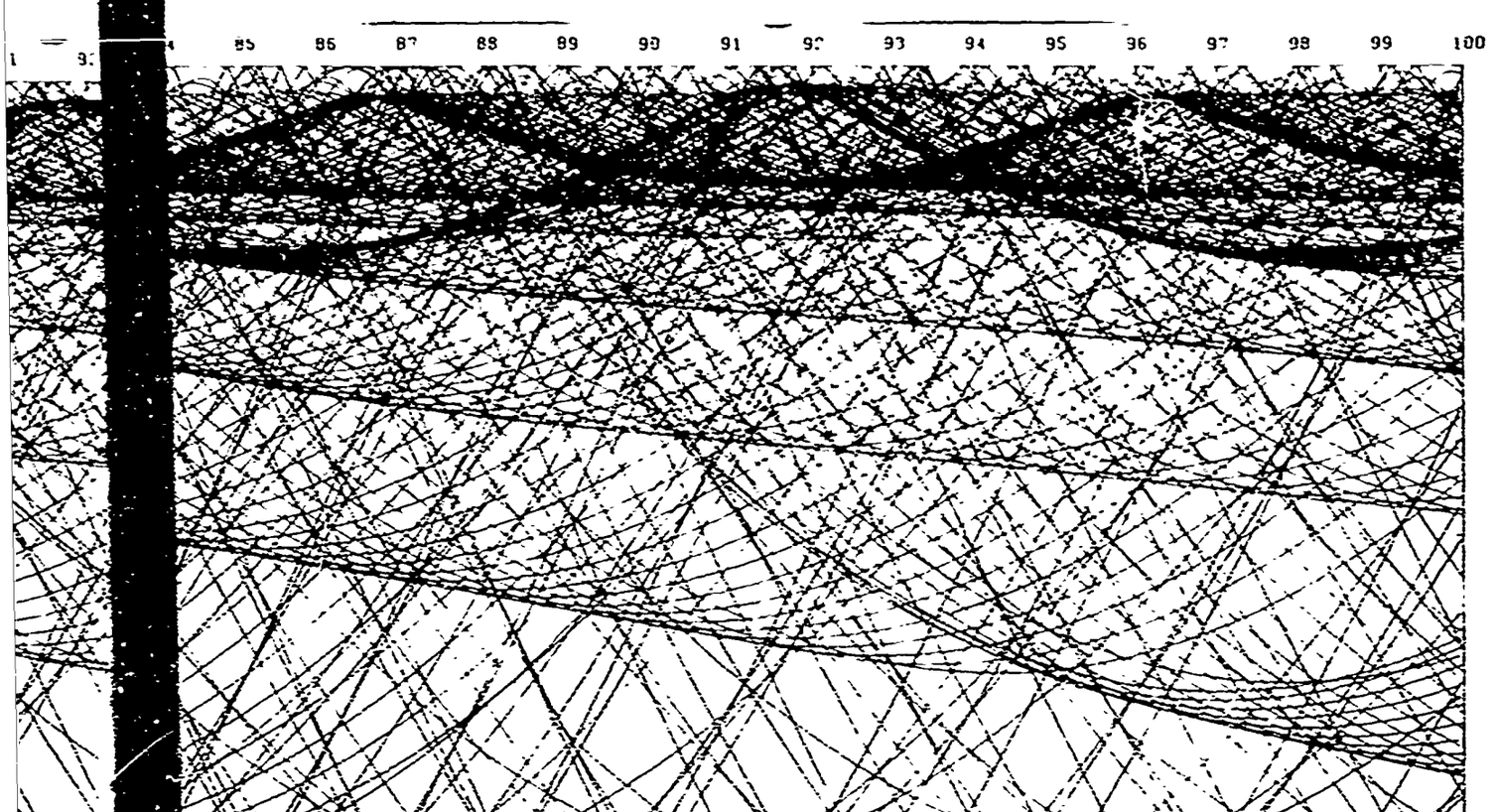
85 86 87 88 89 90 91 92 93 94 95 96 97 98 99 100

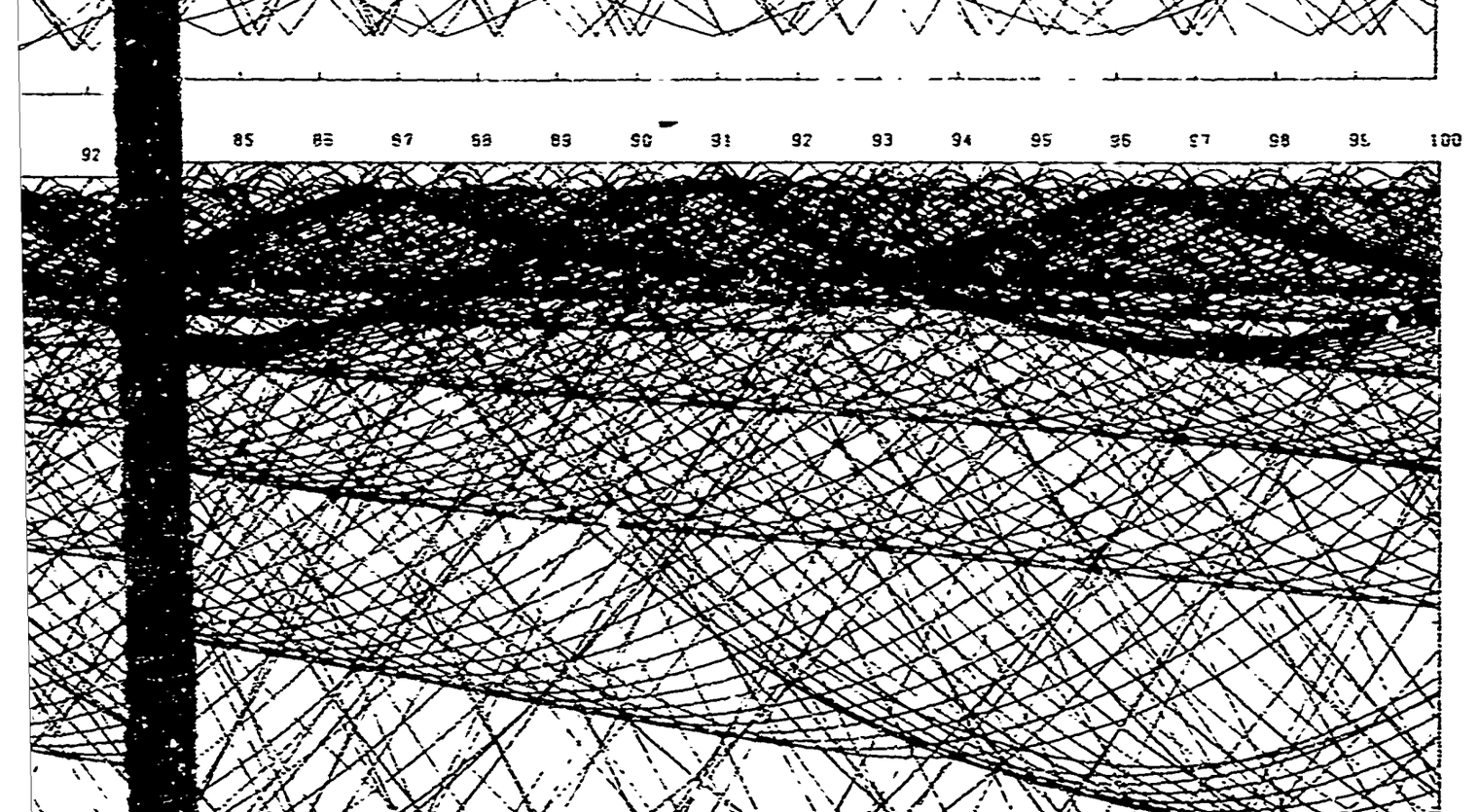
85 86 87 88 89 90 91 92 93 94 95 96 97 98 99 100

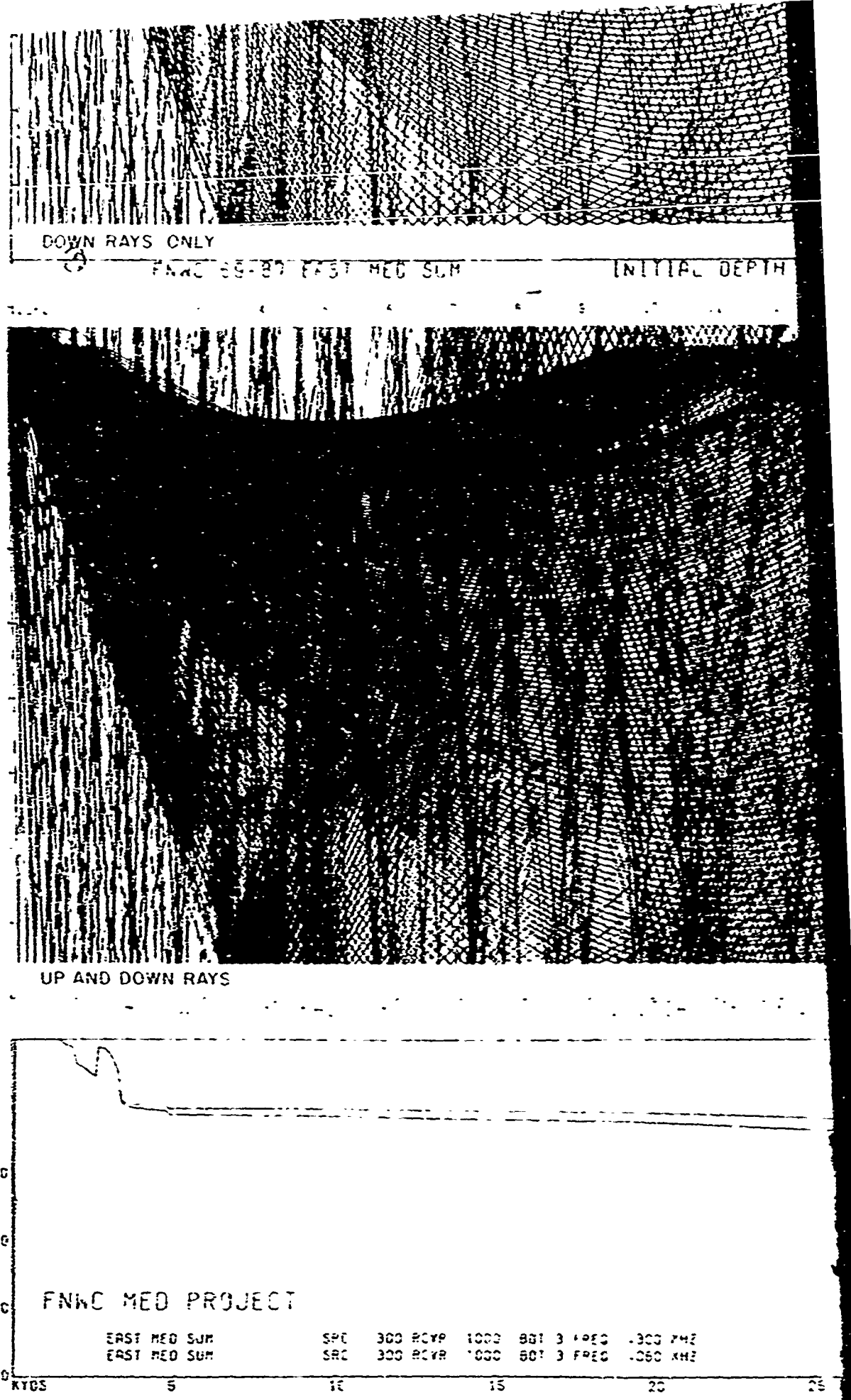
DOWN RAYS ONLY
INITIAL DEPTH
UP AND DOWN RAYS
DB LOSS
60
80
100
120
140
160
KYDS
5
10
15
20
25
FNWC MED PROJECT
EAST MED SUM SPC 300 RCVR 1000 BOT 3 FREQ .300 KHZ
EAST MED SUM SRC 300 RCVR 1000 BOT 3 FREQ .060 KHZ

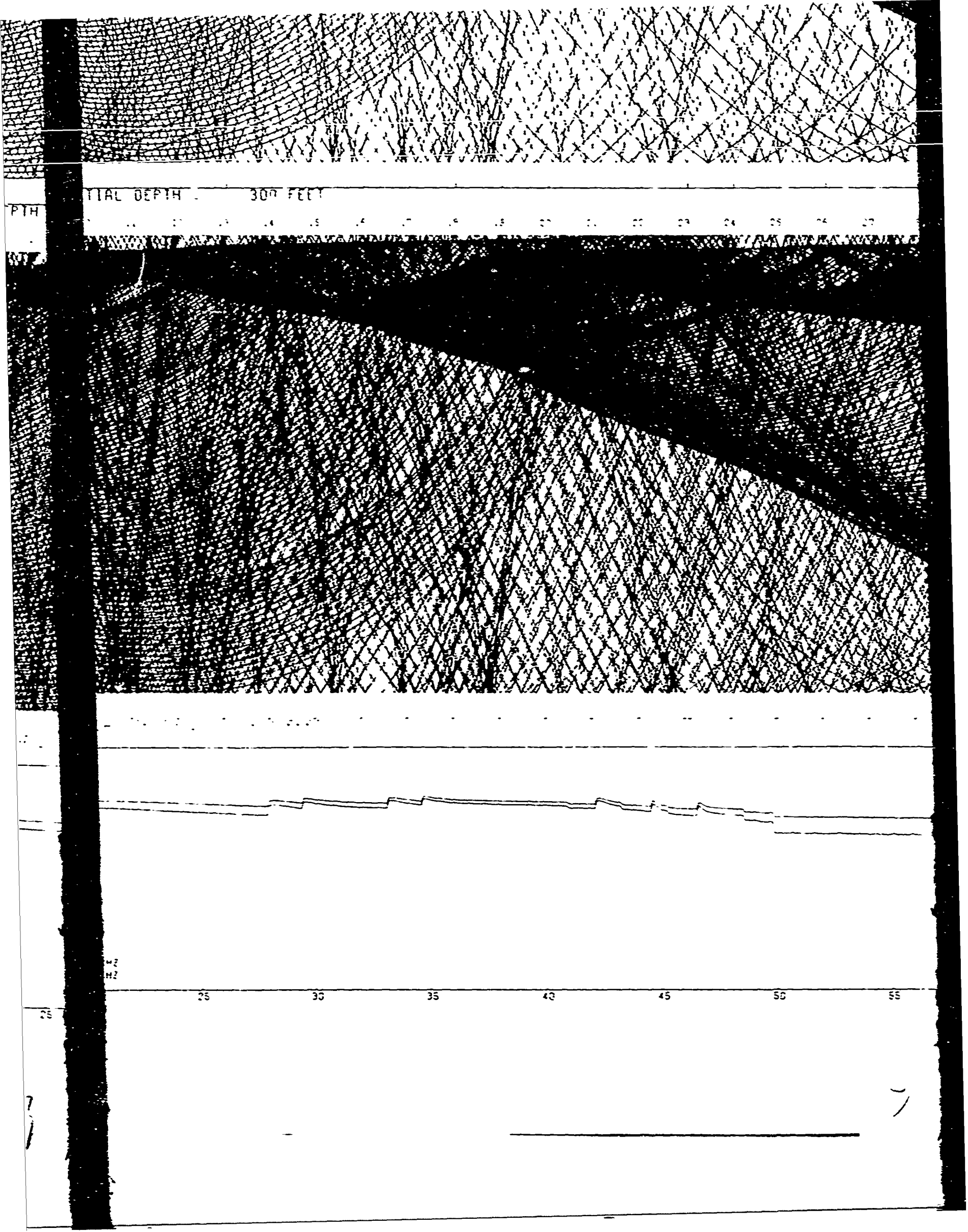
TIAL DEPTH - 30 FEET
PTH
25
30
35
40
45
50
55

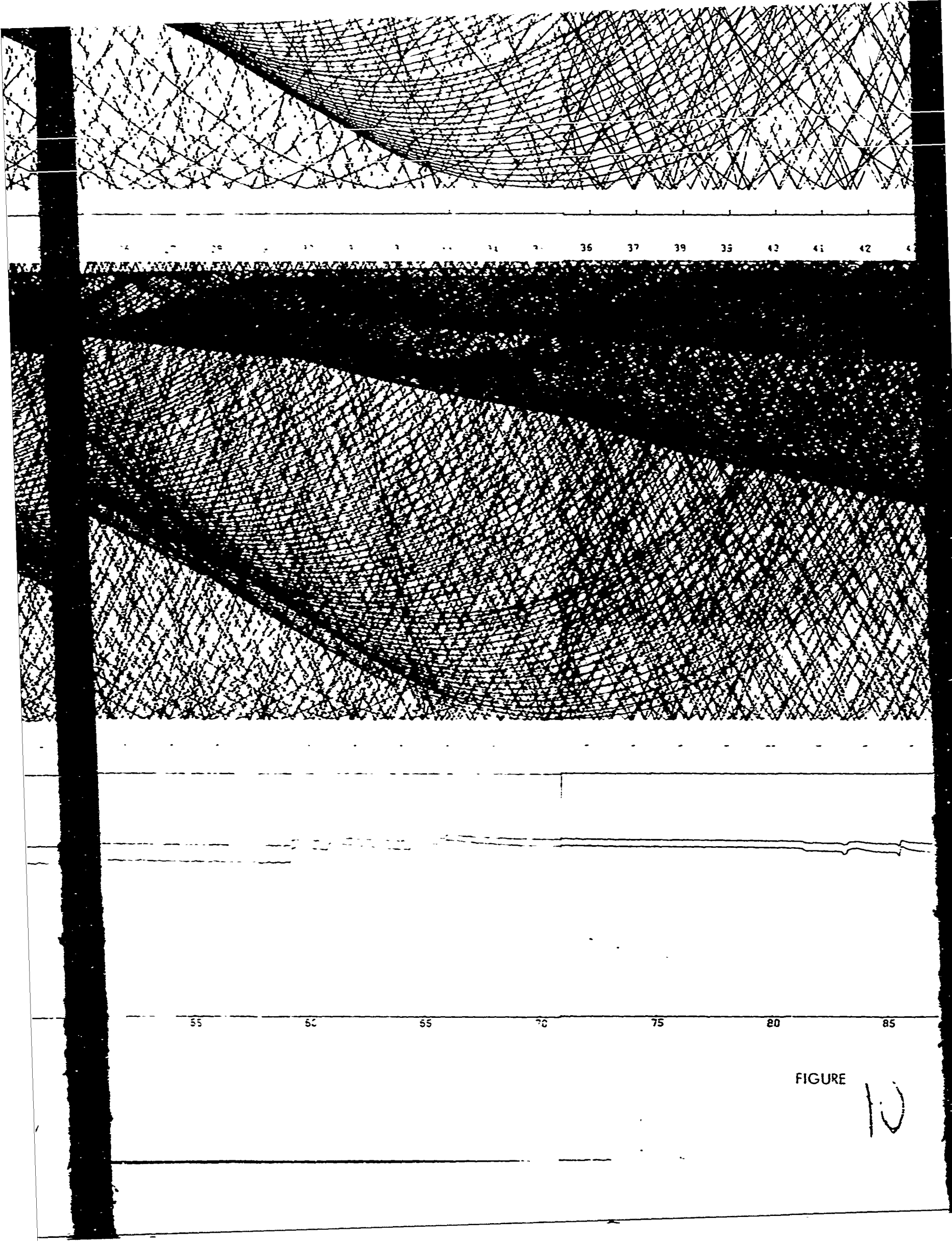

FIGURE 12

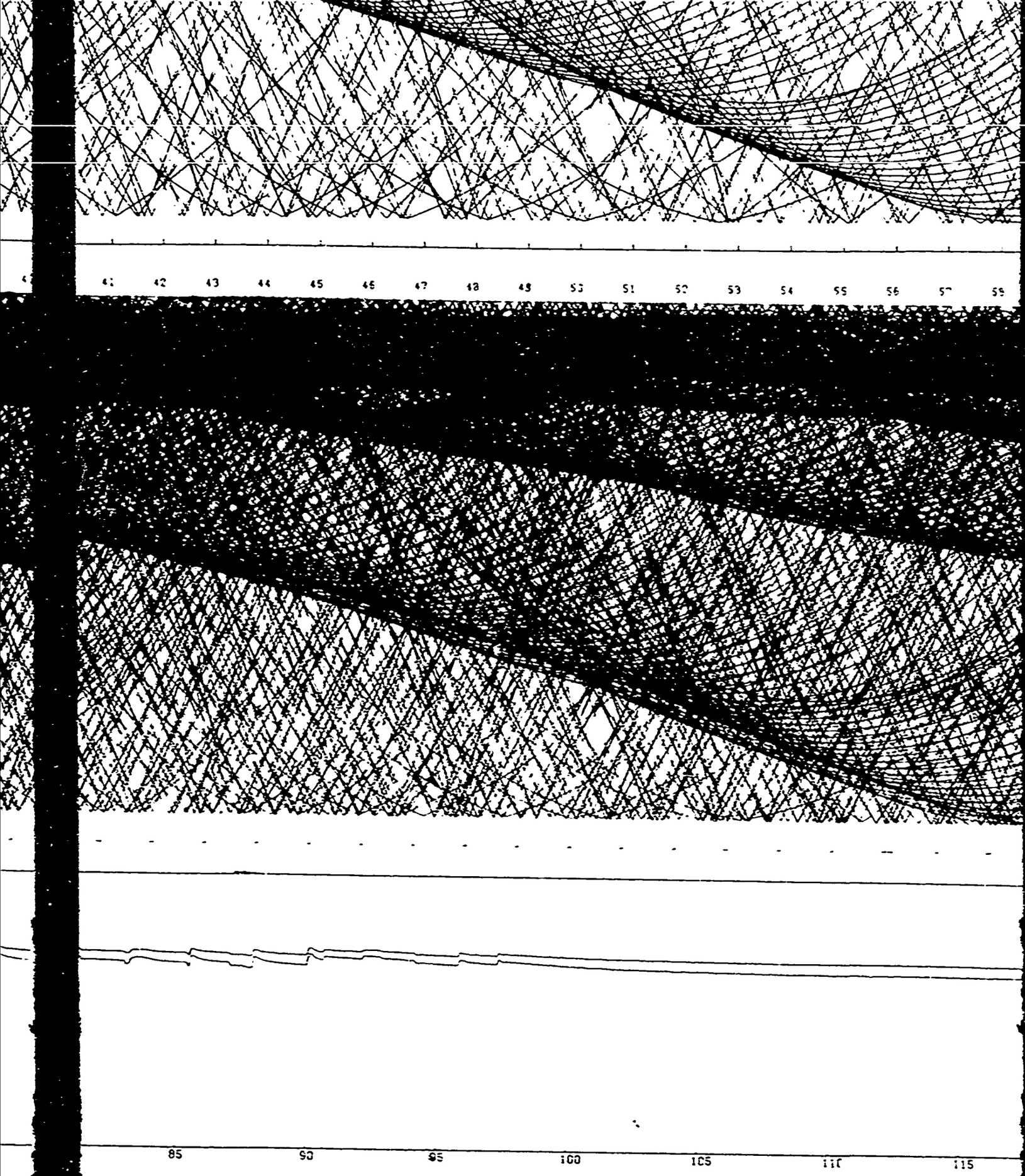

FIGURE 75. RAY PATHS AND TRANSMISSION LOSS -- EASTERN MEDITERRANEAN SUMMER

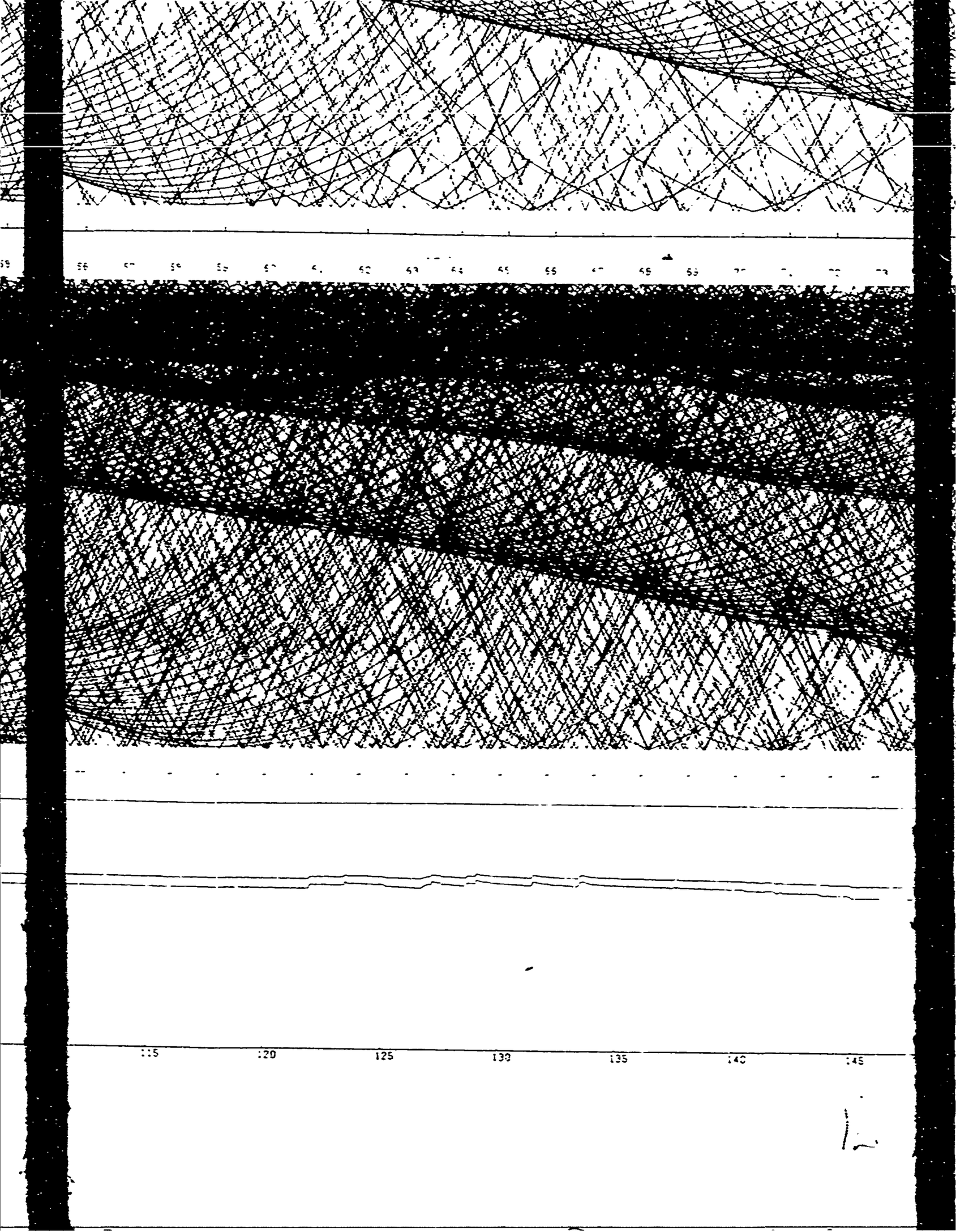

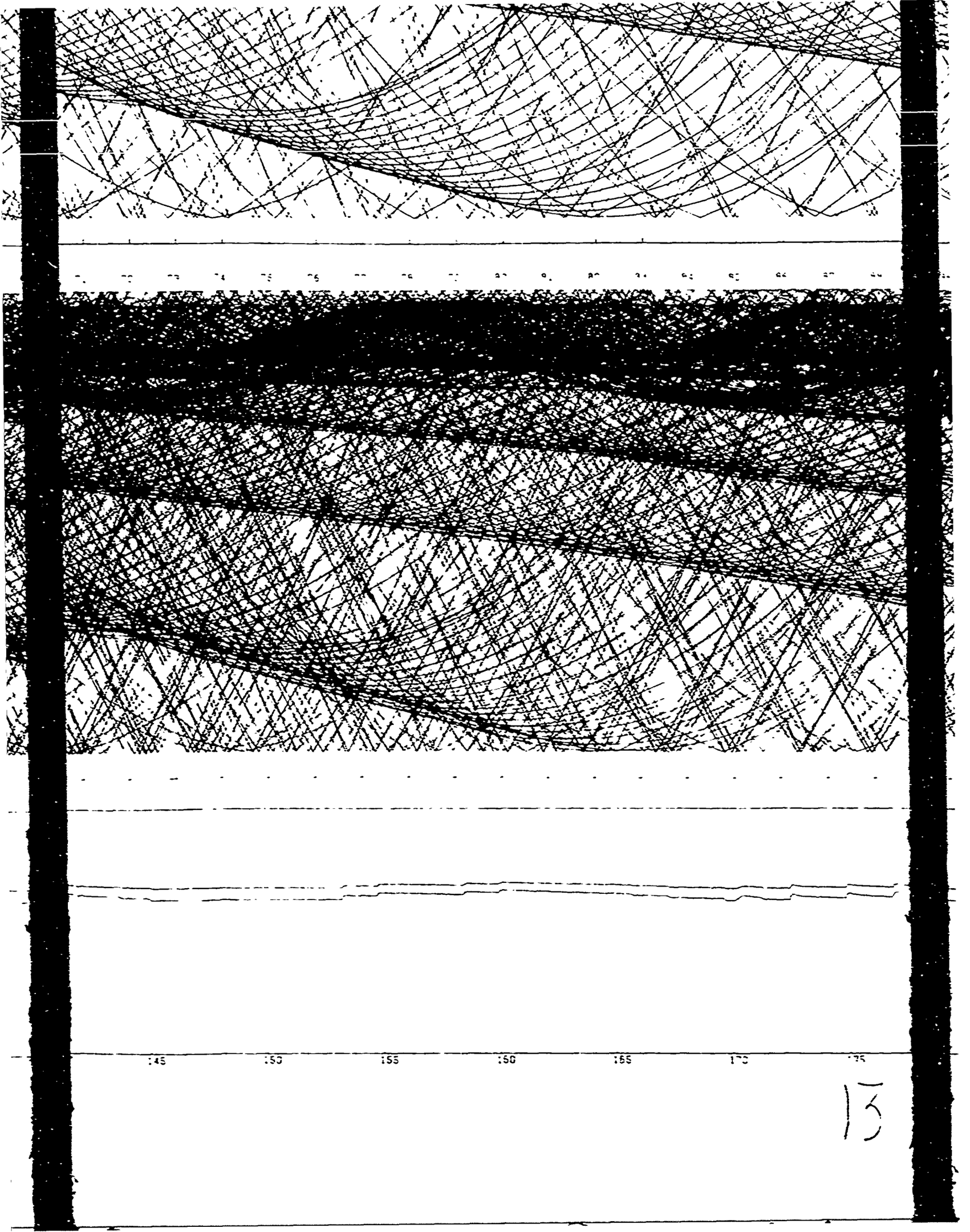

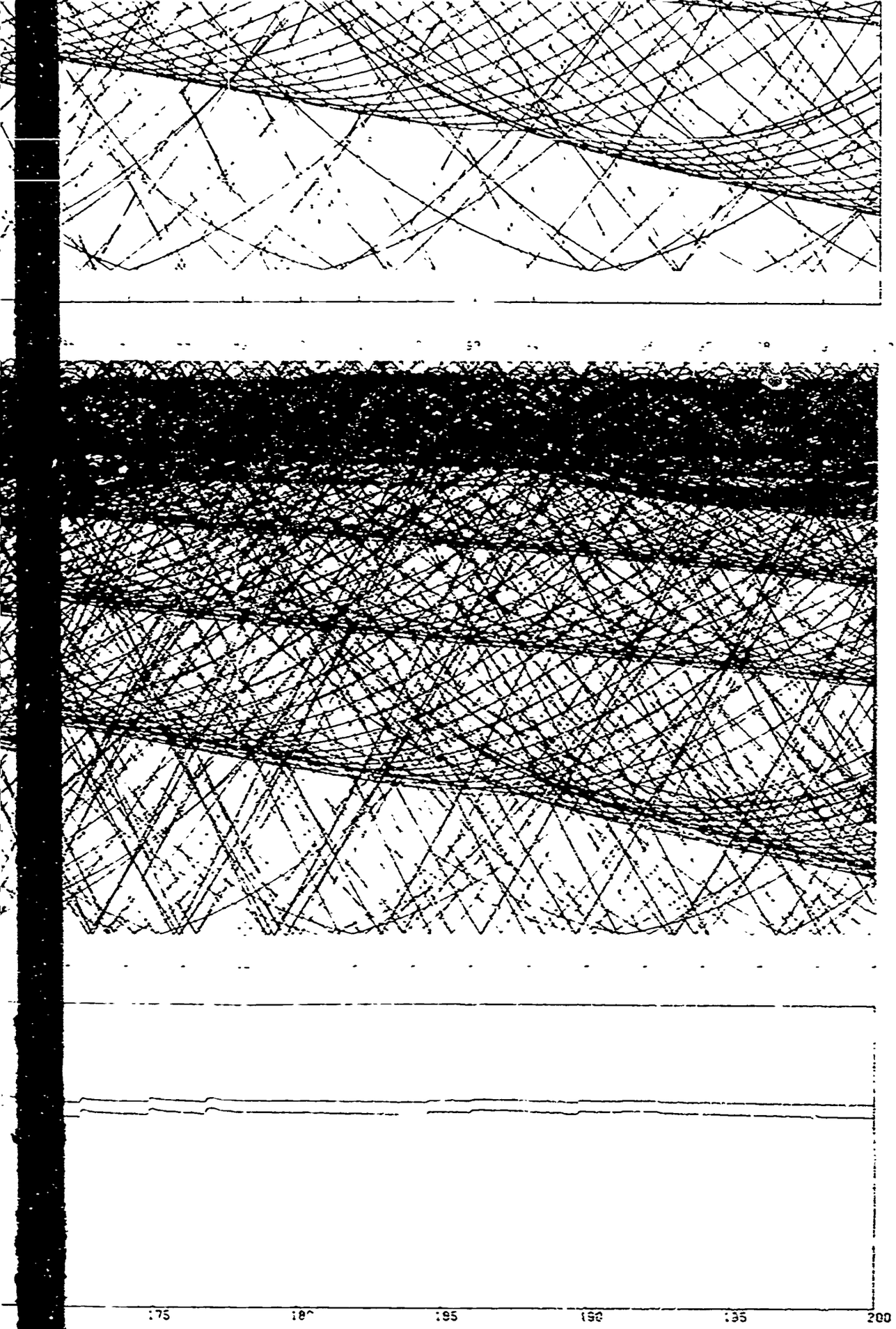
175
180
185
190
195
200

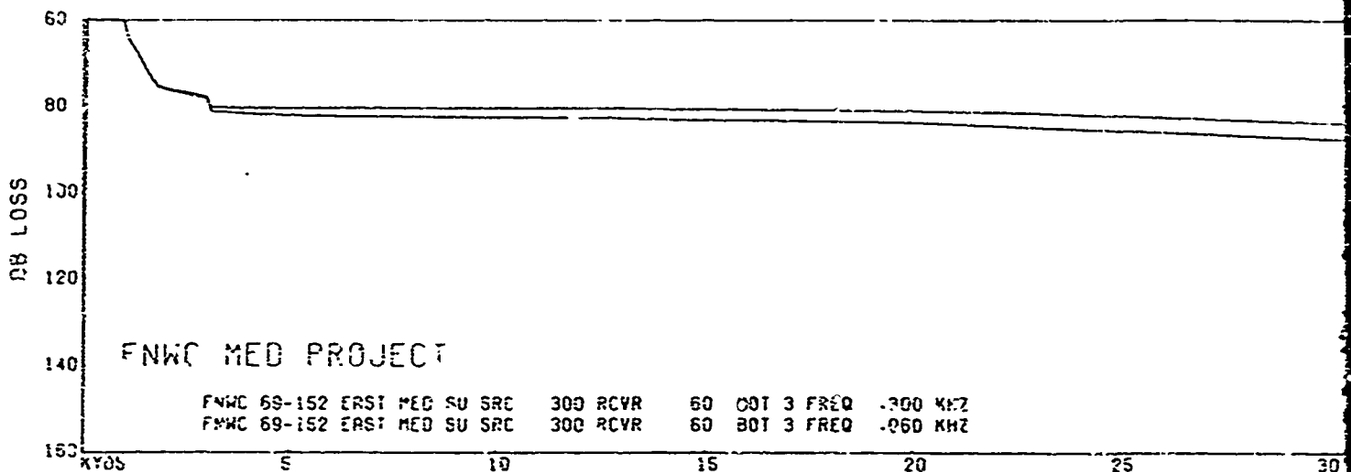
DB LOSS
60
80
100
120
140
160
KYDS
5
10
15
20
25
30
FNWC MED PROJECT
FNWC 69-152 EAST MED SU SRC 300 RCVR 60 BOT 3 FREQ .300 KHZ
FNWC 69-152 EAST MED SU SRC 300 RCVR 60 BOT 3 FREQ .060 KHZ

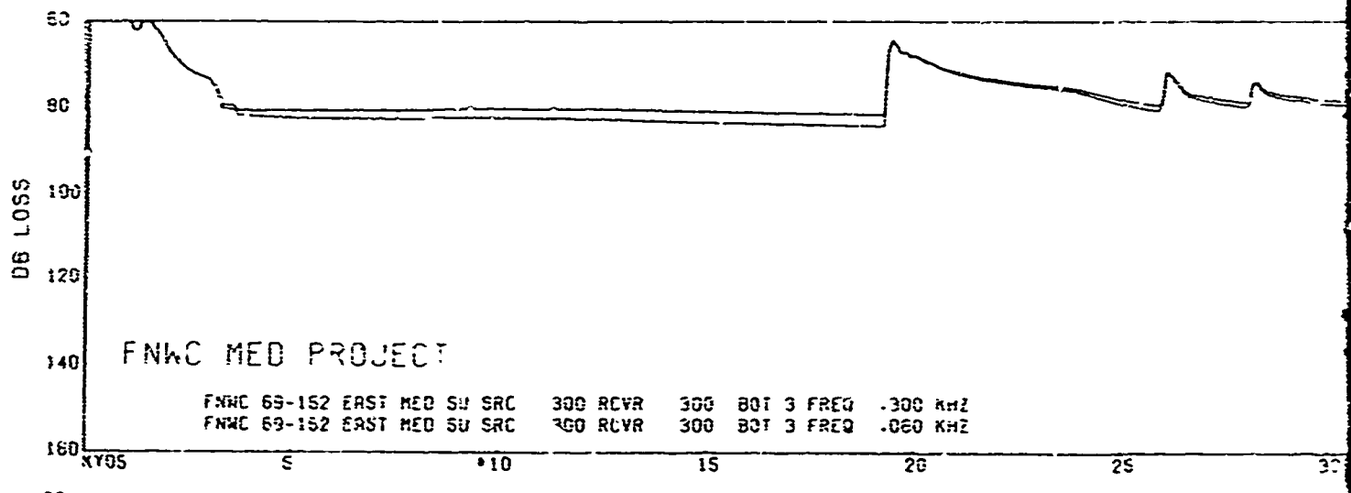
DB LOSS
60
80
100
120
140
160
KYDS
5
10
15
20
25
30
FNWC MED PROJECT
FNWC 69-152 EAST MED SU SRC 300 RCVR 300 BOT 3 FREQ .300 KHZ
FNWC 69-152 EAST MED SU SRC 300 RCVR 300 BOT 3 FREQ .060 KHZ

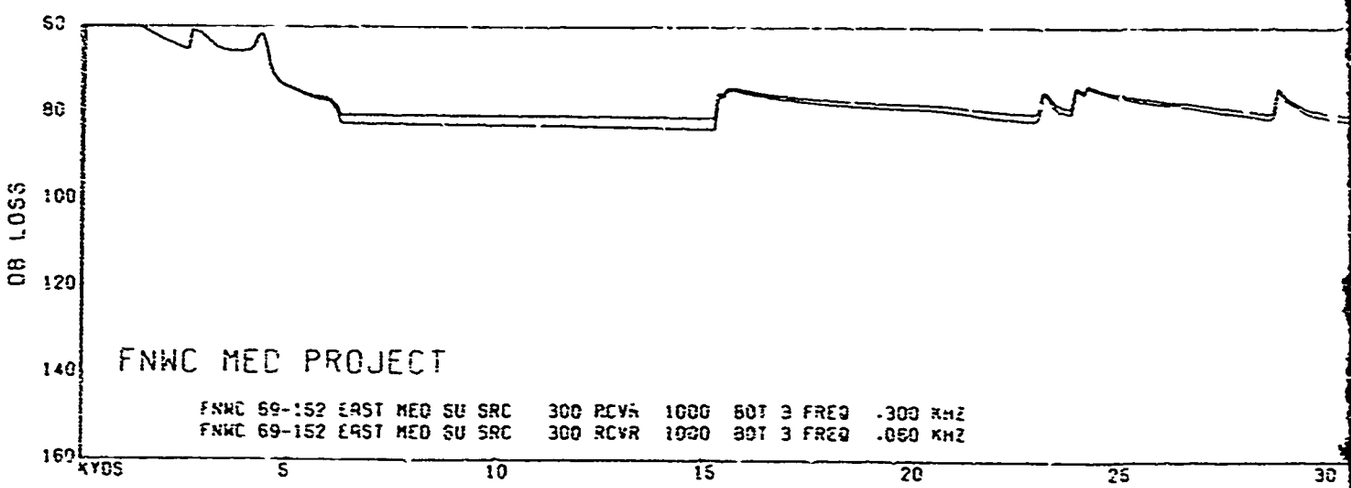
DB LOSS
60
80
100
120
140
160
KYDS
5
10
15
20
25
30
FNWC MED PROJECT
FNWC 69-152 EAST MED SU SRC 300 RCVR 1000 BOT 3 FREQ .300 KHZ
FNWC 69-152 EAST MED SU SRC 300 RCVR 1000 BOT 3 FREQ .060 KHZ

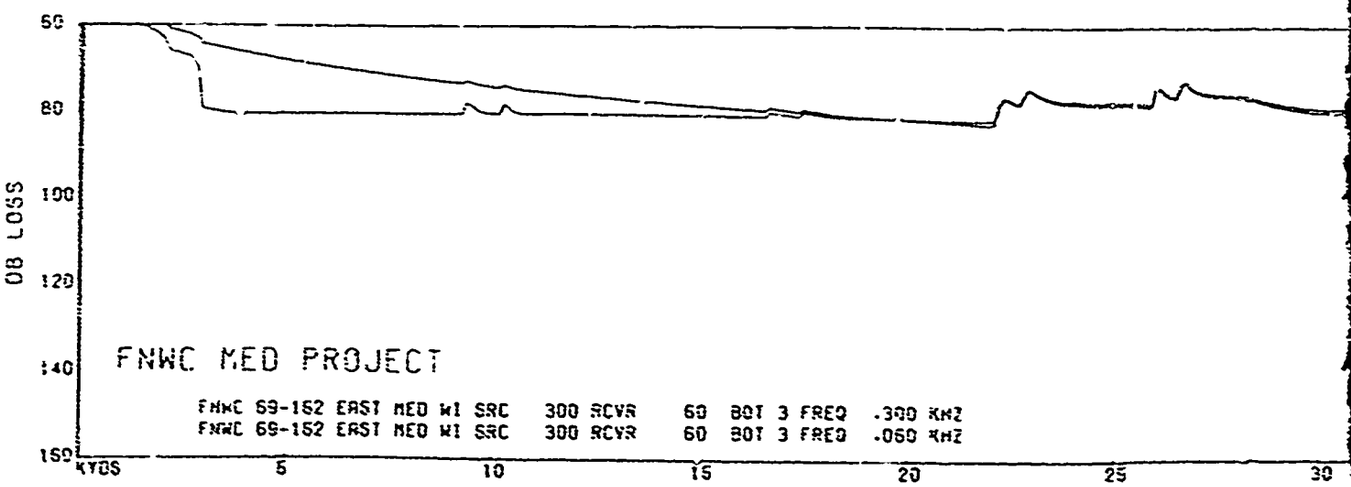
DB LOSS
60
80
100
120
140
160
KYDS
5
10
15
20
25
30
FNWC MED PROJECT
FNWC 69-152 EAST MED WI SRC 300 RCVR 60 BOT 3 FREQ .300 KHZ
FNWC 69-152 EAST MED WI SRC 300 RCVR 60 BOT 3 FREQ .060 KHZ

2

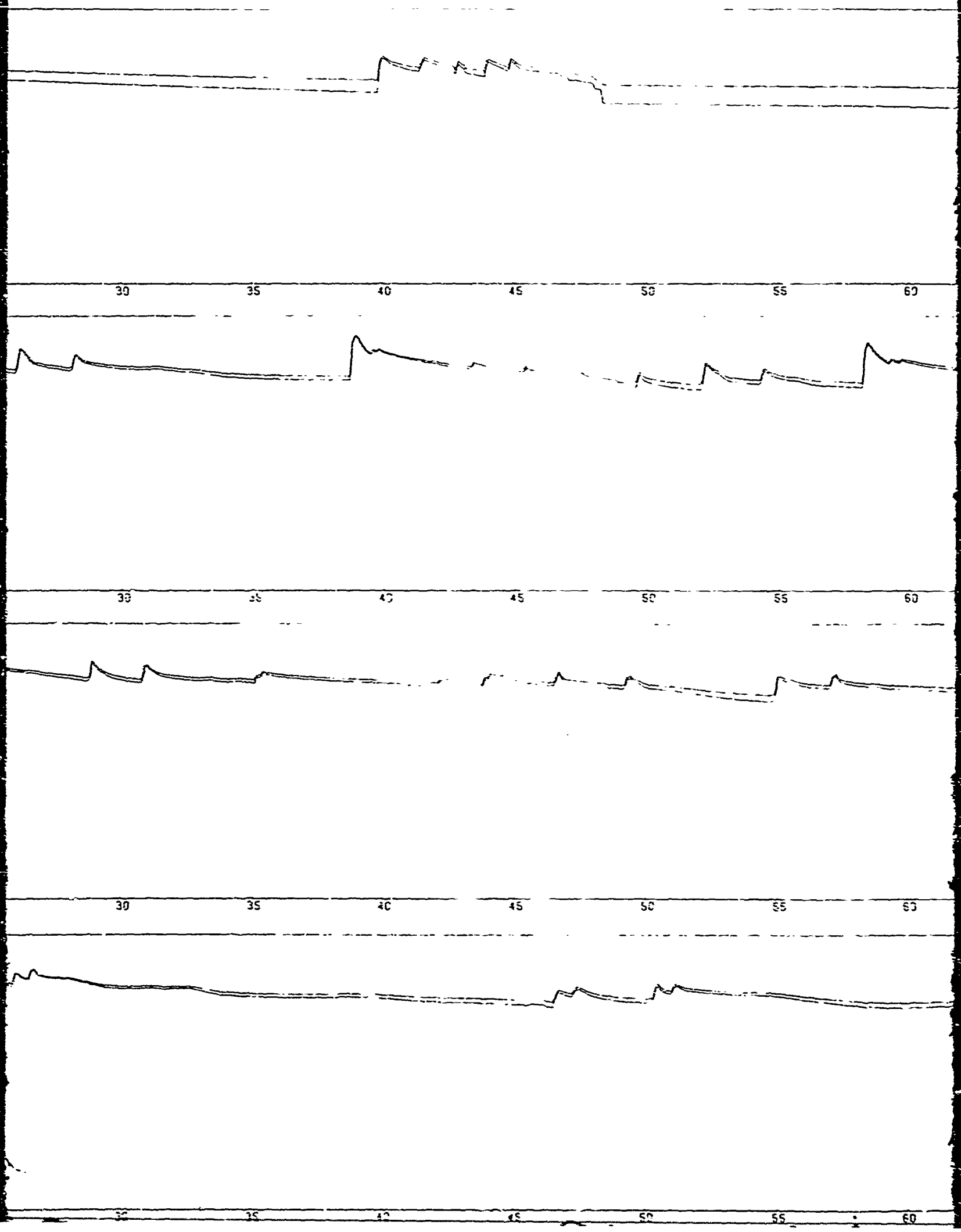

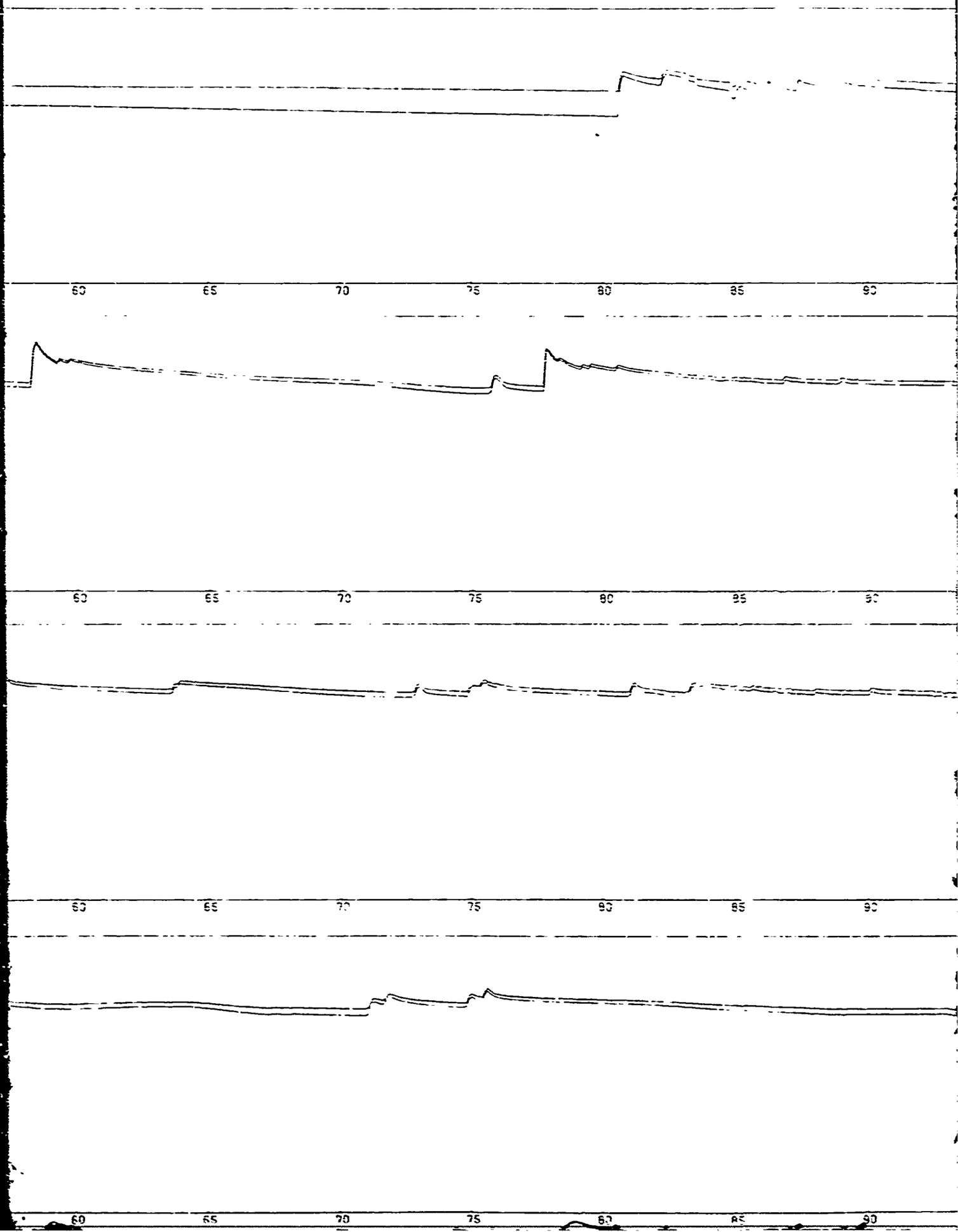
60
65
70
75
80
85
90
60
65
70
75
80
85
90
60
65
70
75
80
85
90
60
65
70
75
80
85
90

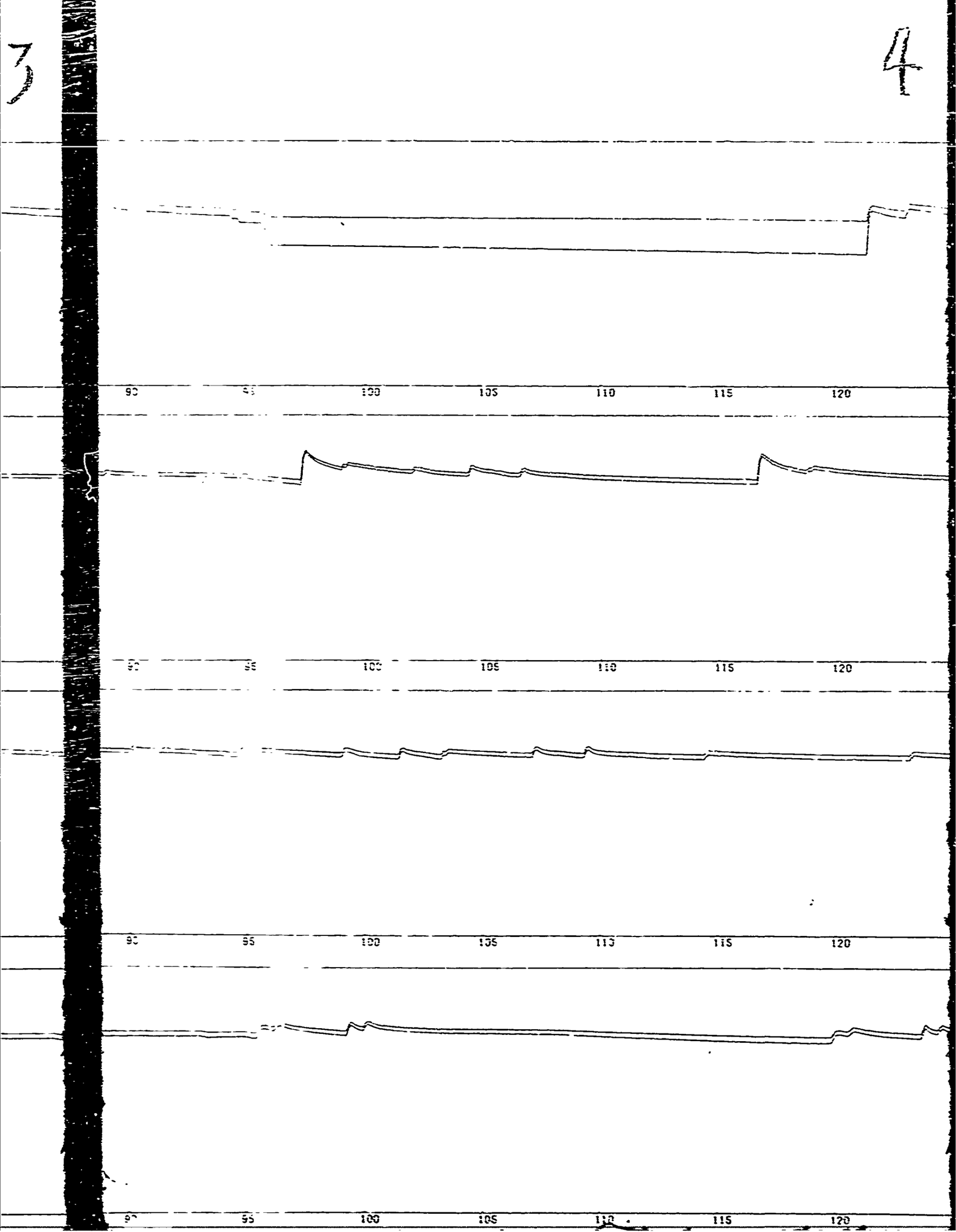
90
95
100
105
110
115
120
90
95
100
105
110
115
120
90
95
100
105
110
115
120
90
95
100
105
110
115
120

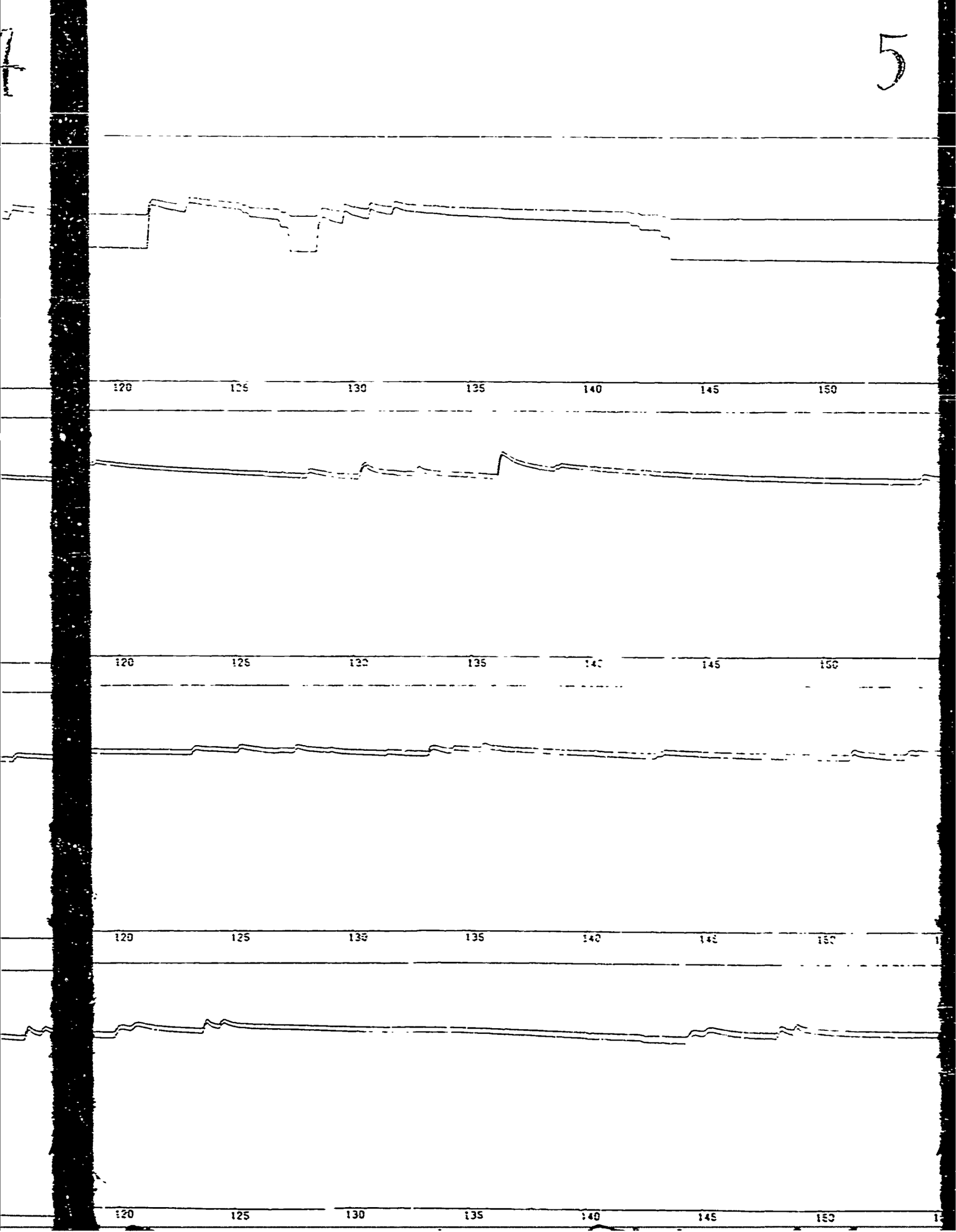
120
125
130
135
140
145
150
120
125
130
135
140
145
150
120
125
130
135
140
145
150
120
125
130
135
140
145
150

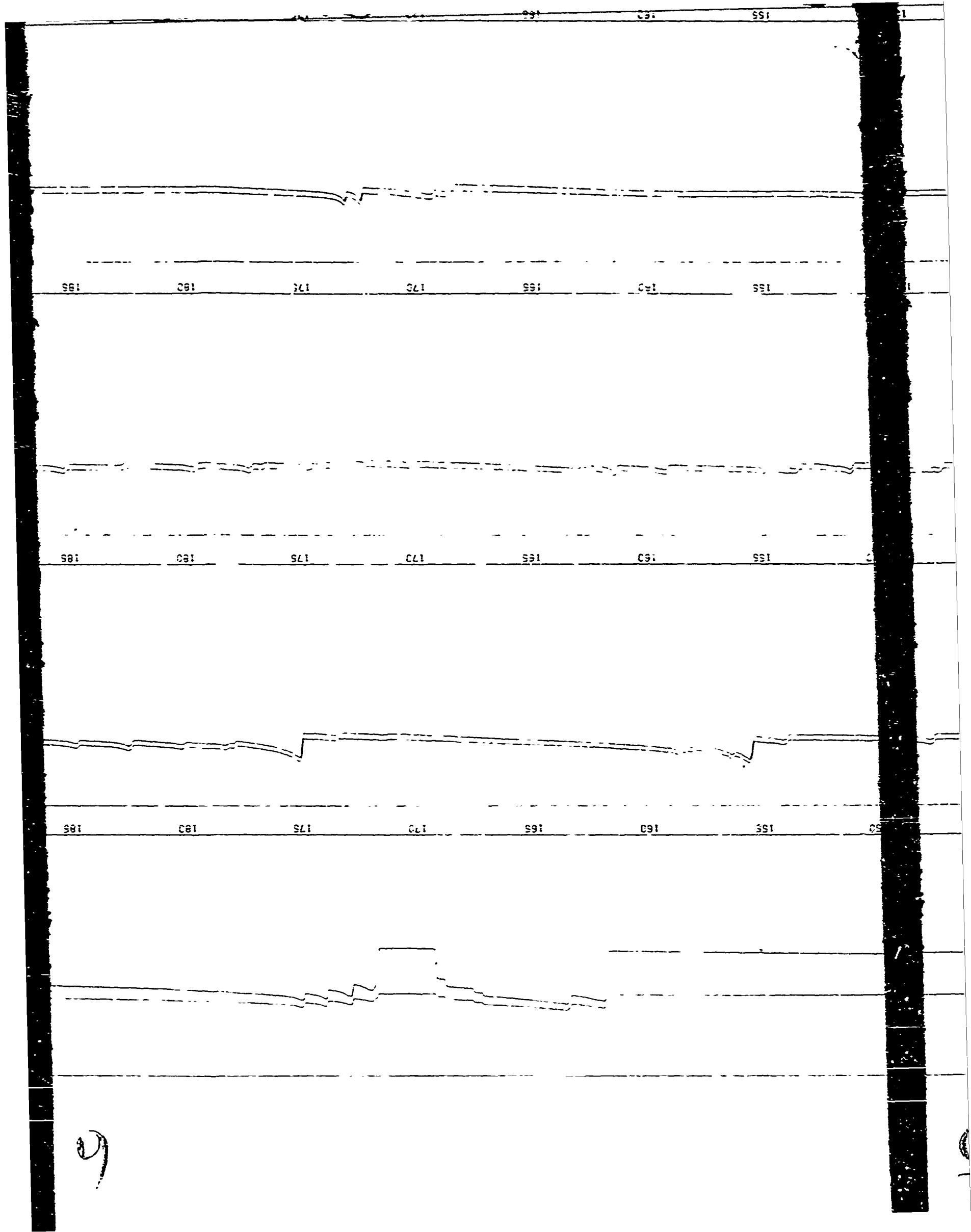
185
180
175
170
165
160
155
185
180
175
170
165
160
155
185
180
175
170
165
160
155

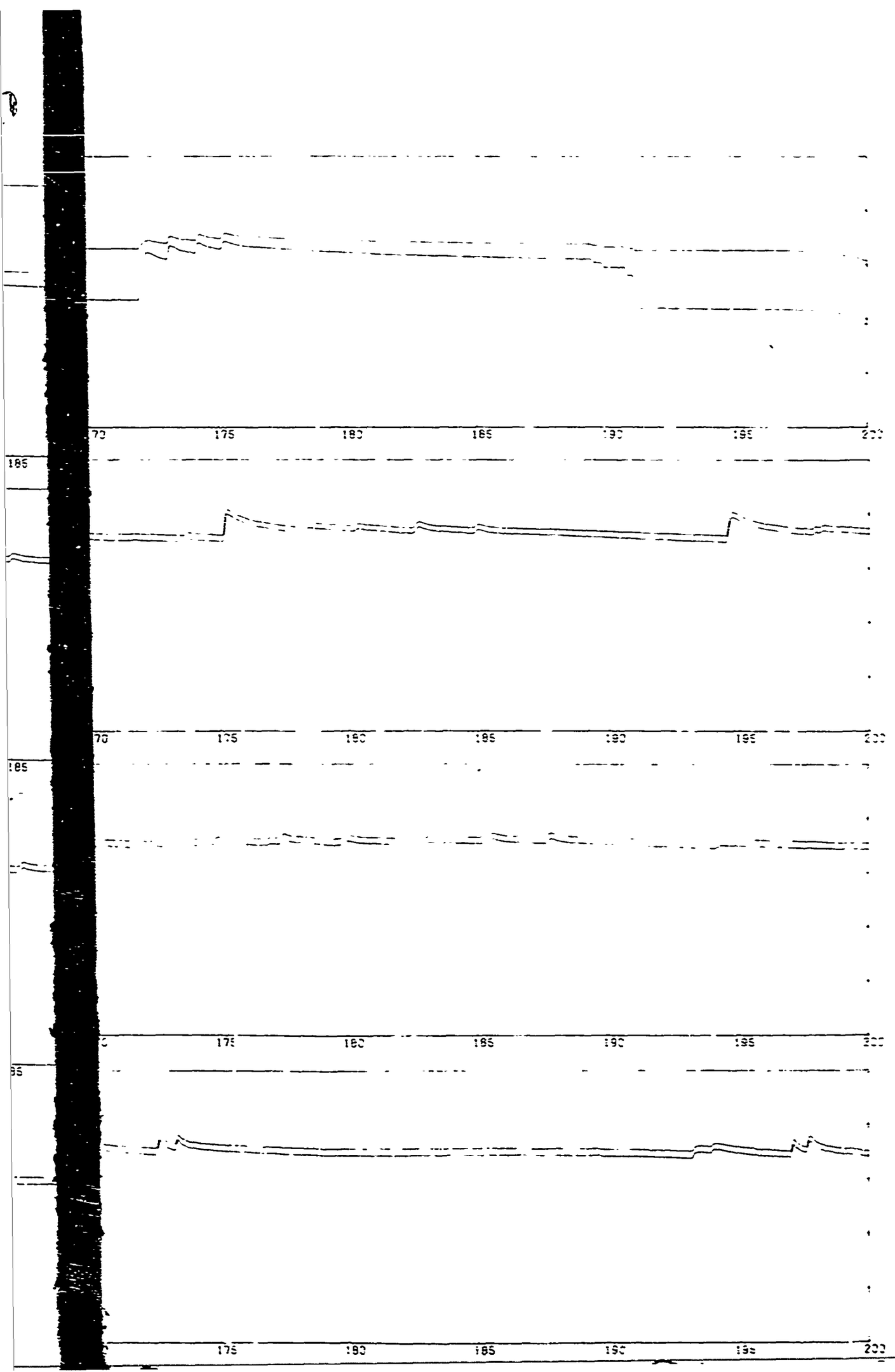
175
180
185
190
195
200

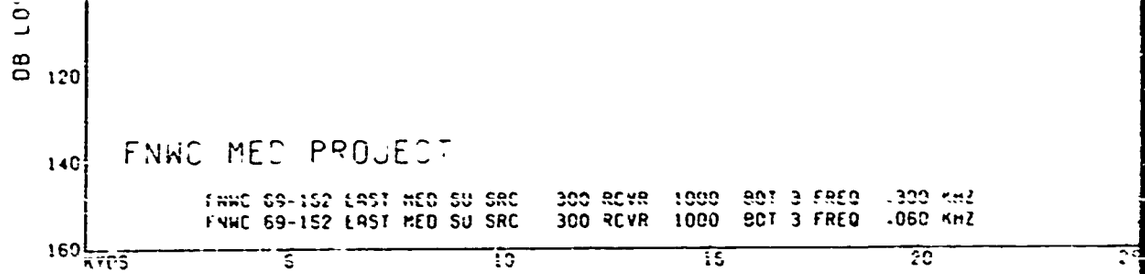
DB LOSS
120
140
160
FNWC MED PROJECT
FNWC 69-152 EAST MED SU SRC 300 RCVR 1000 BOT 3 FREQ .300 KHZ
FNWC 69-152 EAST MED SU SRC 300 RCVR 1000 BOT 3 FREQ .060 KHZ
KYDS
5
10
15
20

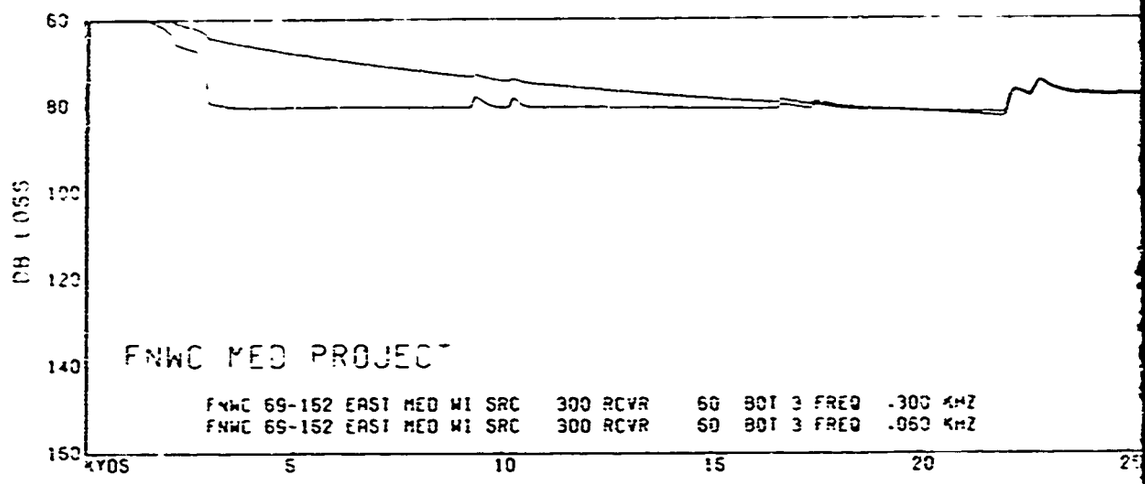
DB LOSS
60
80
100
120
140
160
FNWC MED PROJECT
FNWC 69-152 EAST MED WI SRC 300 RCVR 60 BOT 3 FREQ .300 KHZ
FNWC 69-152 EAST MED WI SRC 300 RCVR 60 BOT 3 FREQ .060 KHZ
KYDS
5
10
15
20

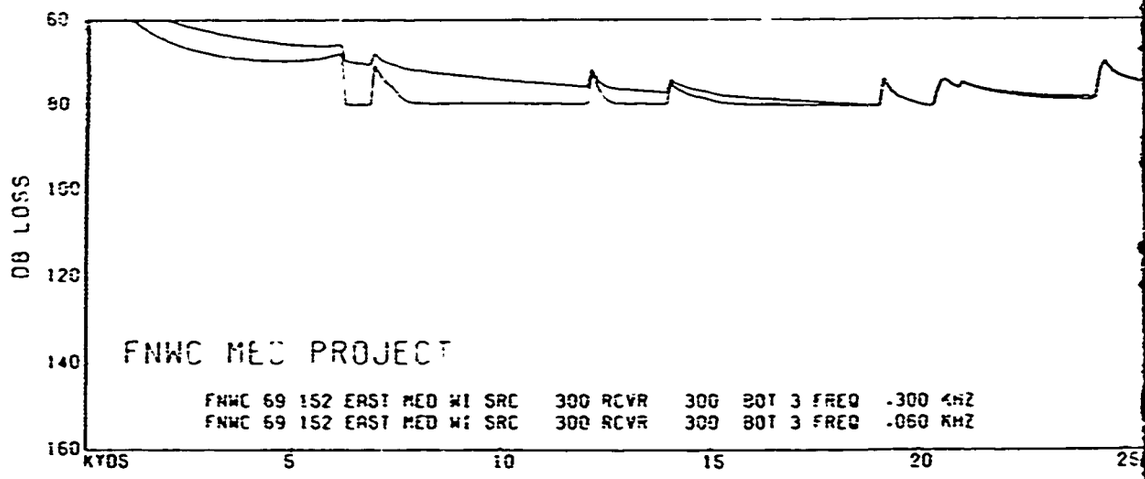
DB LOSS
60
80
100
120
140
160
FNWC MED PROJECT
FNWC 69 152 EAST MED WI SRC 300 RCVR 300 BOT 3 FREQ .300 KHZ
FNWC 69 152 EAST MED WI SRC 300 RCVR 300 BOT 3 FREQ .060 KHZ
KYDS
5
10
15
20

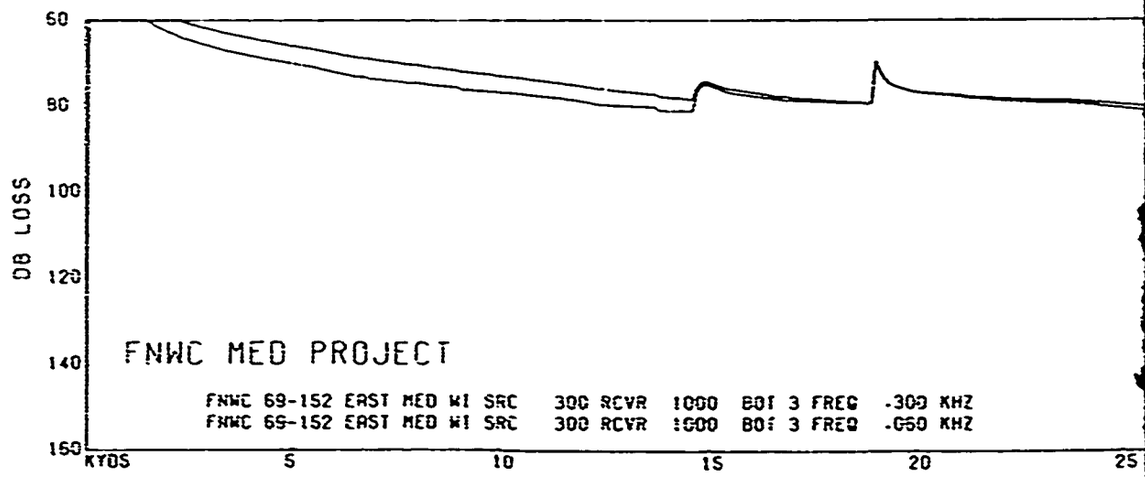
DB LOSS
60
80
100
120
140
160
FNWC MED PROJECT
FNWC 69-152 EAST MED WI SRC 300 RCVR 1000 BOT 3 FREQ .300 KHZ
FNWC 69-152 EAST MED WI SRC 300 RCVR 1000 BOT 3 FREQ .060 KHZ
KYDS
5
10
15
20
25

8

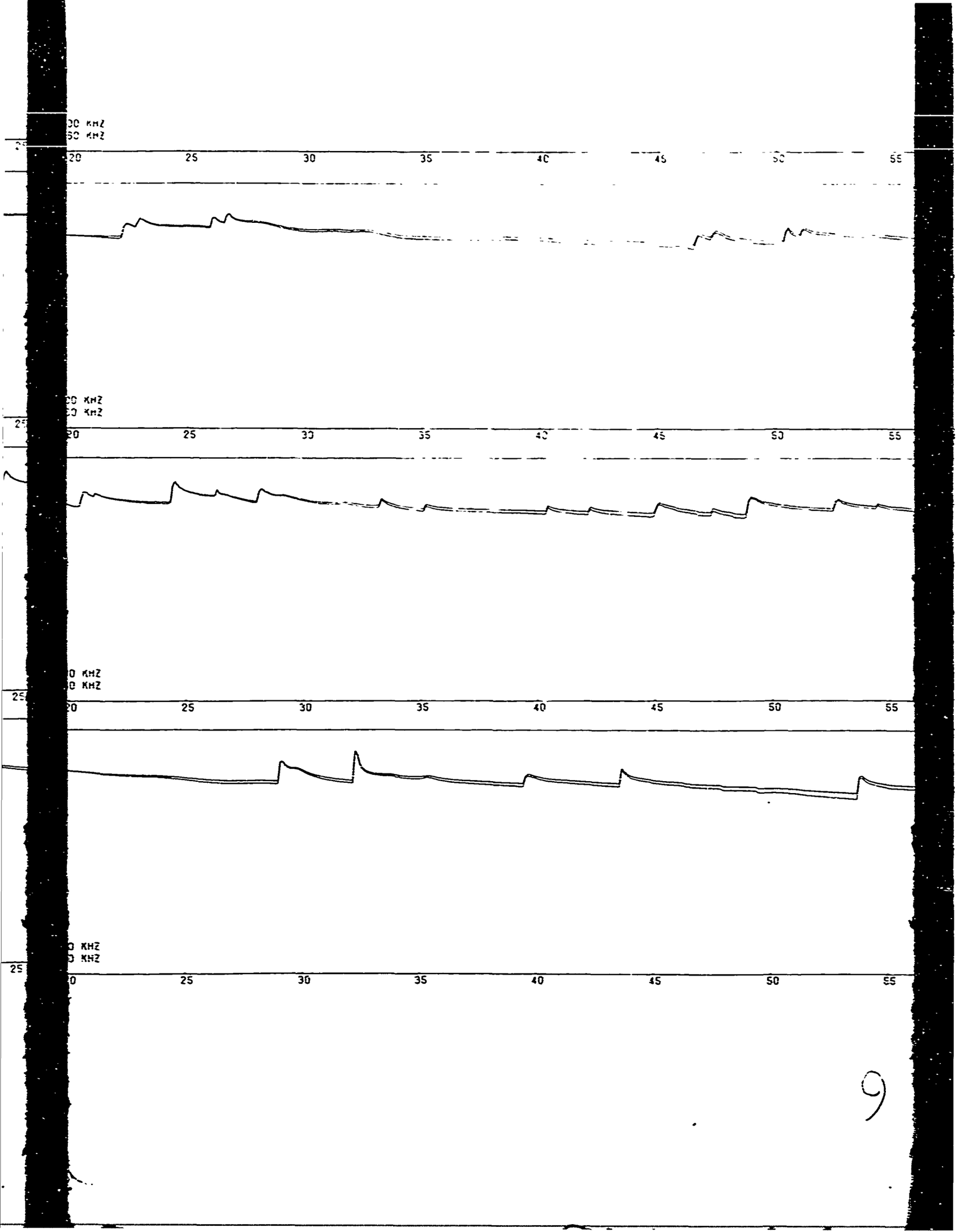
20
25
30
35
40
45
50
55

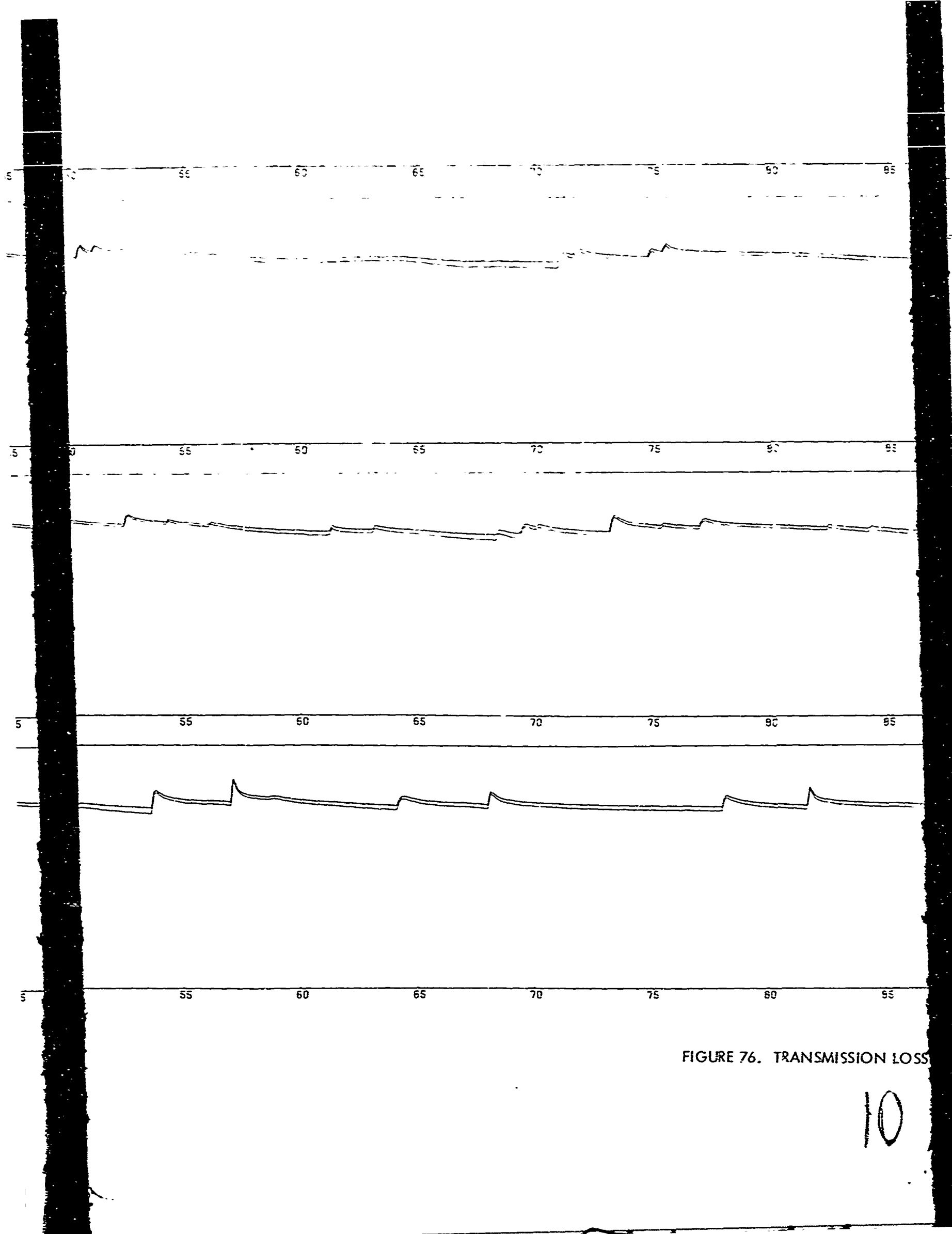

FIGURE 76. TRANSMISSION LOSS

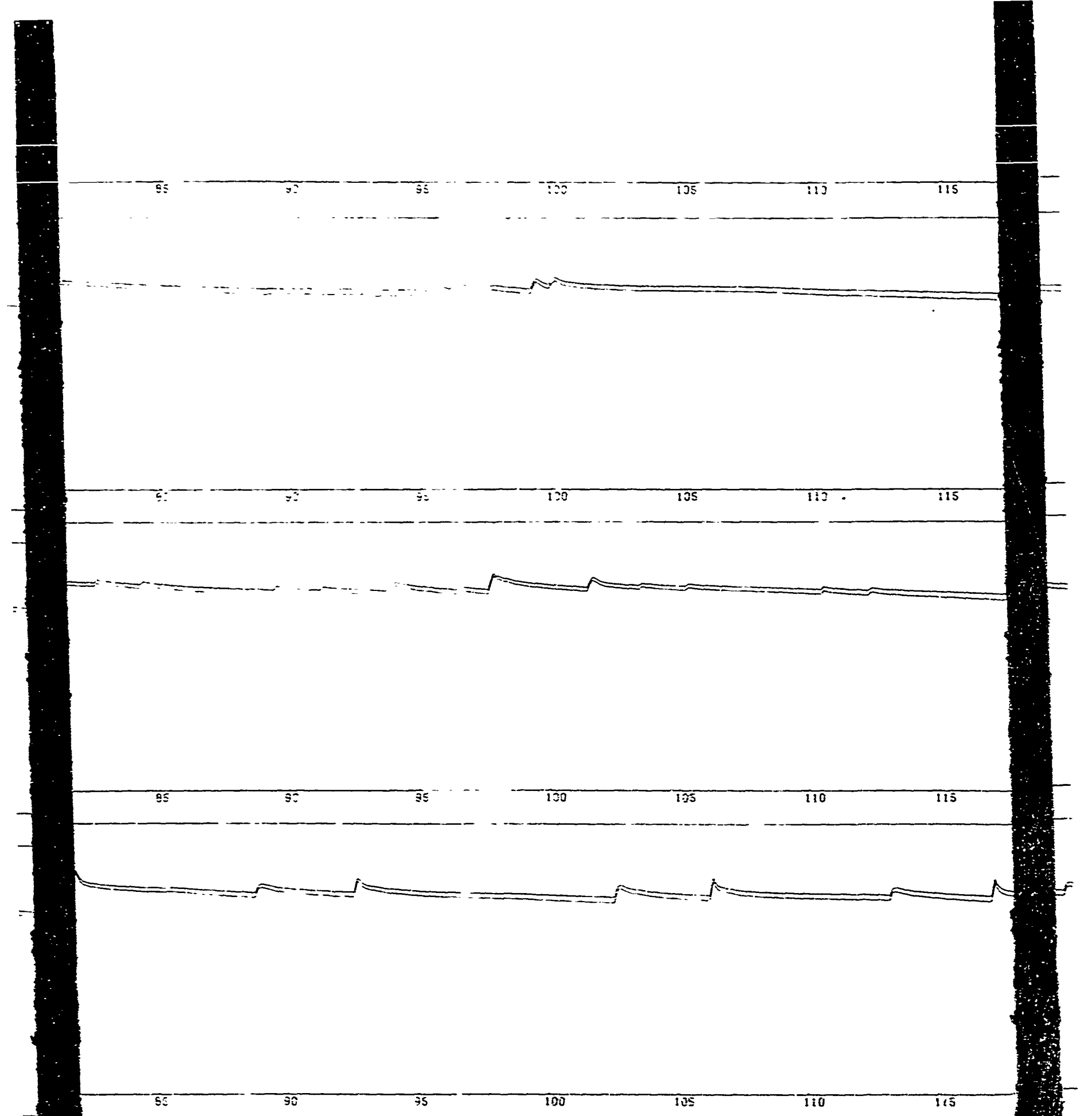

SMISSION LOSS -- EASTERN MEDITERRANEAN SUMMER AND WINTER

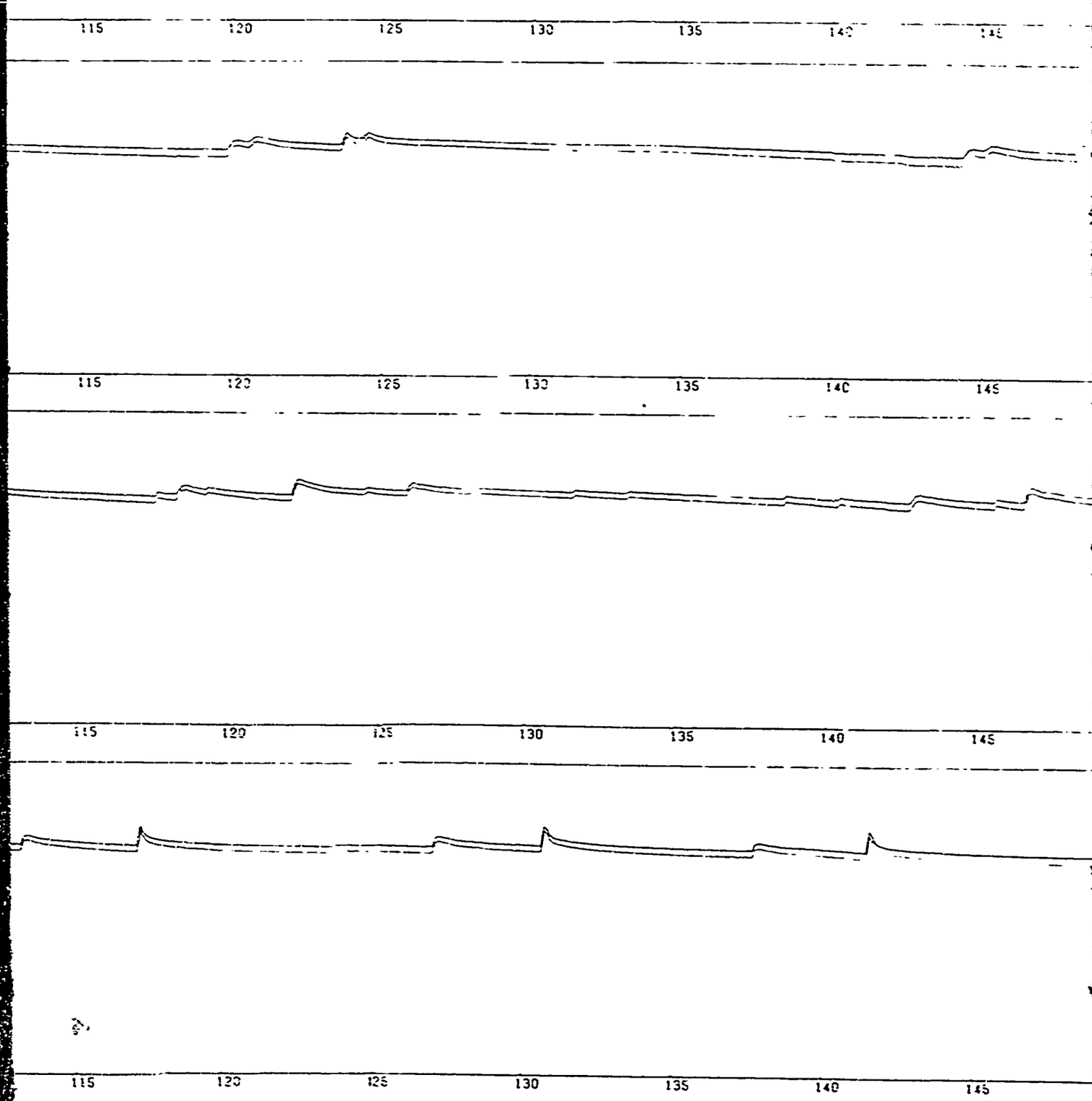
115
120
125
130
135
140
145
115
120
125
130
135
140
145
115
120
125
130
135
140
145
115
120
125
130
135
140
145

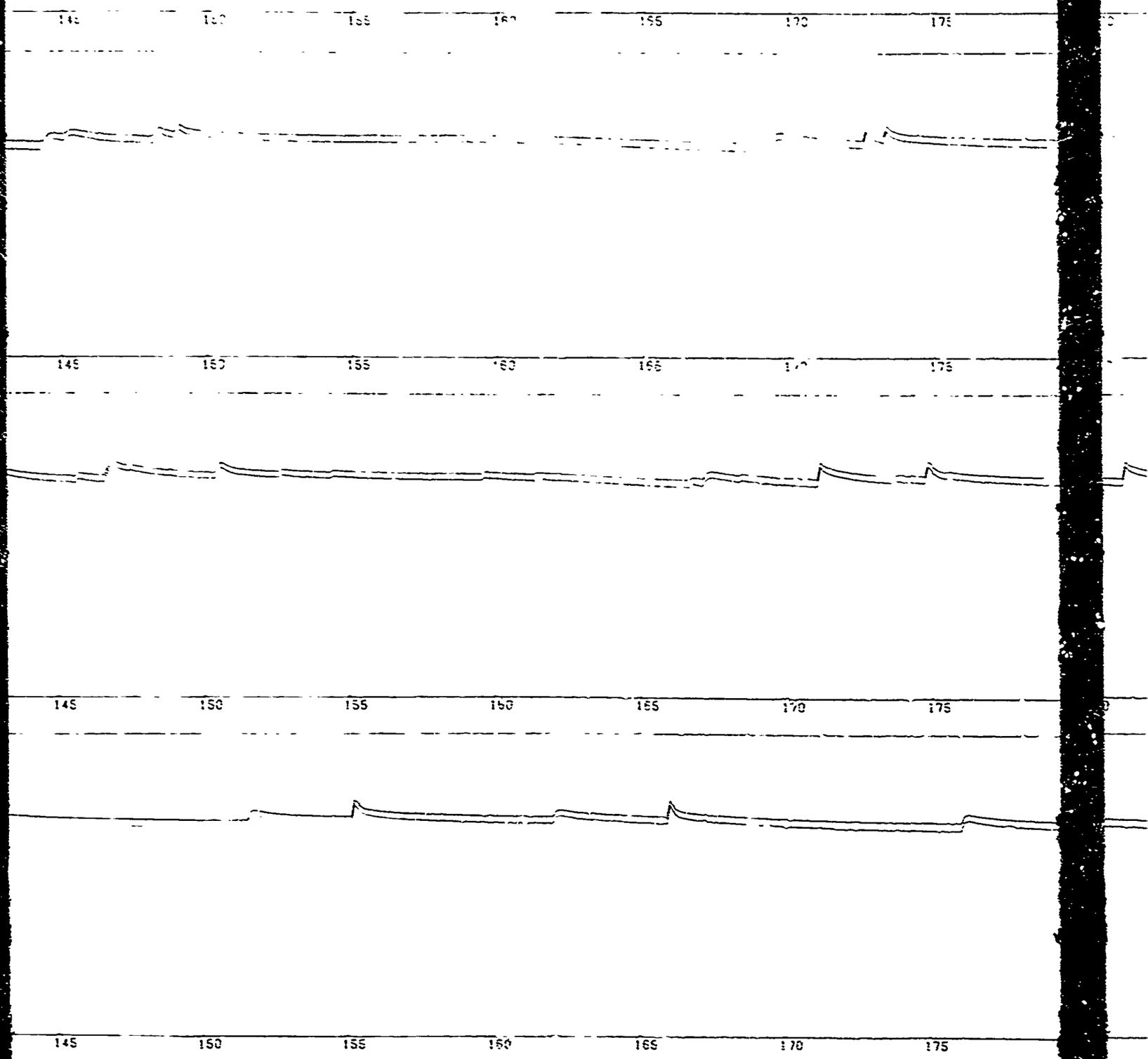
145
150
155
160
165
170
175

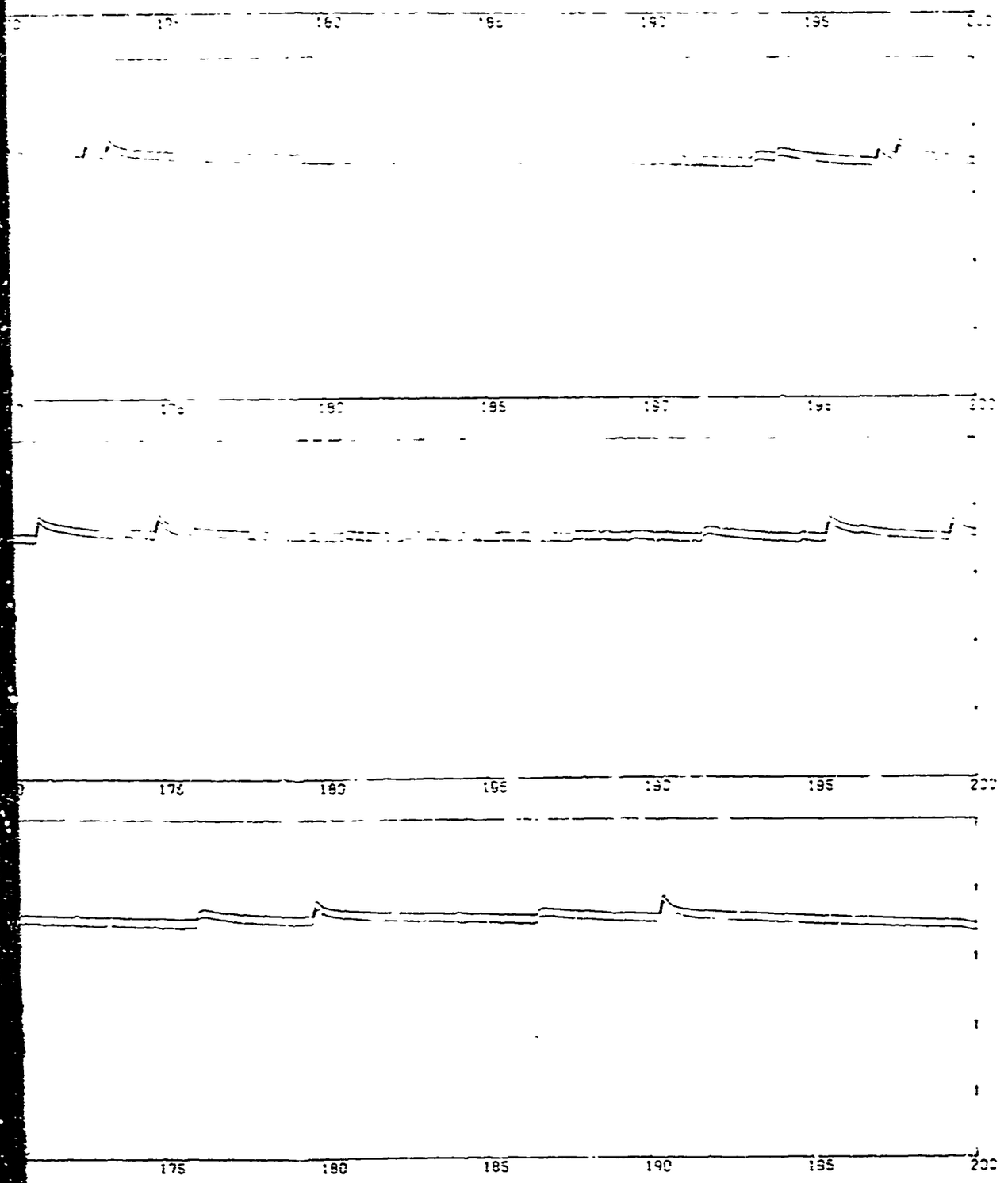

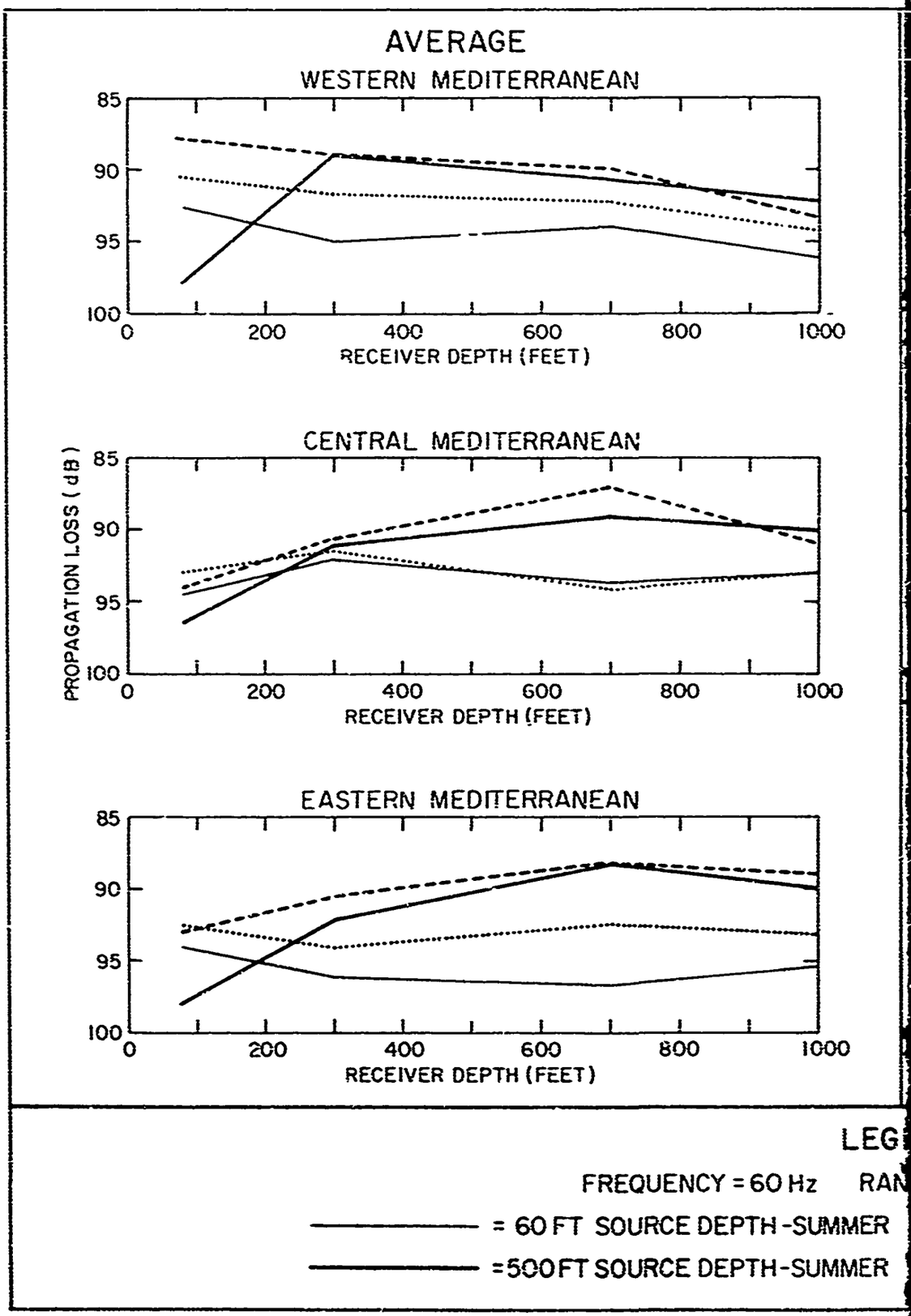

FIGURE 77. CALCULATED AVERAGE AND MINIMUM PROPAGATION LOSS — WE

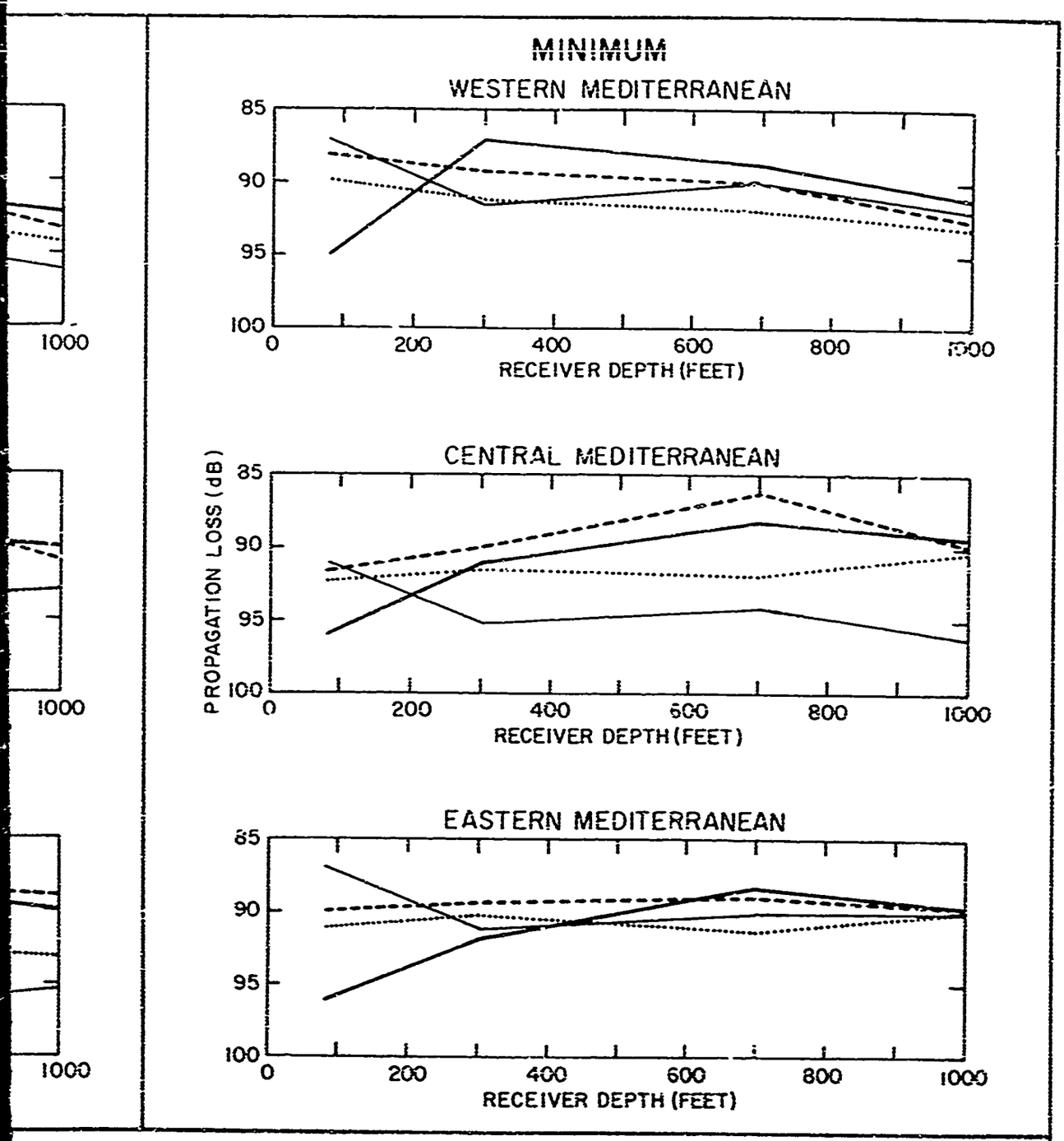

ON LOSS — WEST, CENTRAL AND EASTERN MEDITERRANEAN SEA

FIGURE 77. AVERAGE AND MINIMUM PROPAGATION LOSS

CONFIDENTIAL

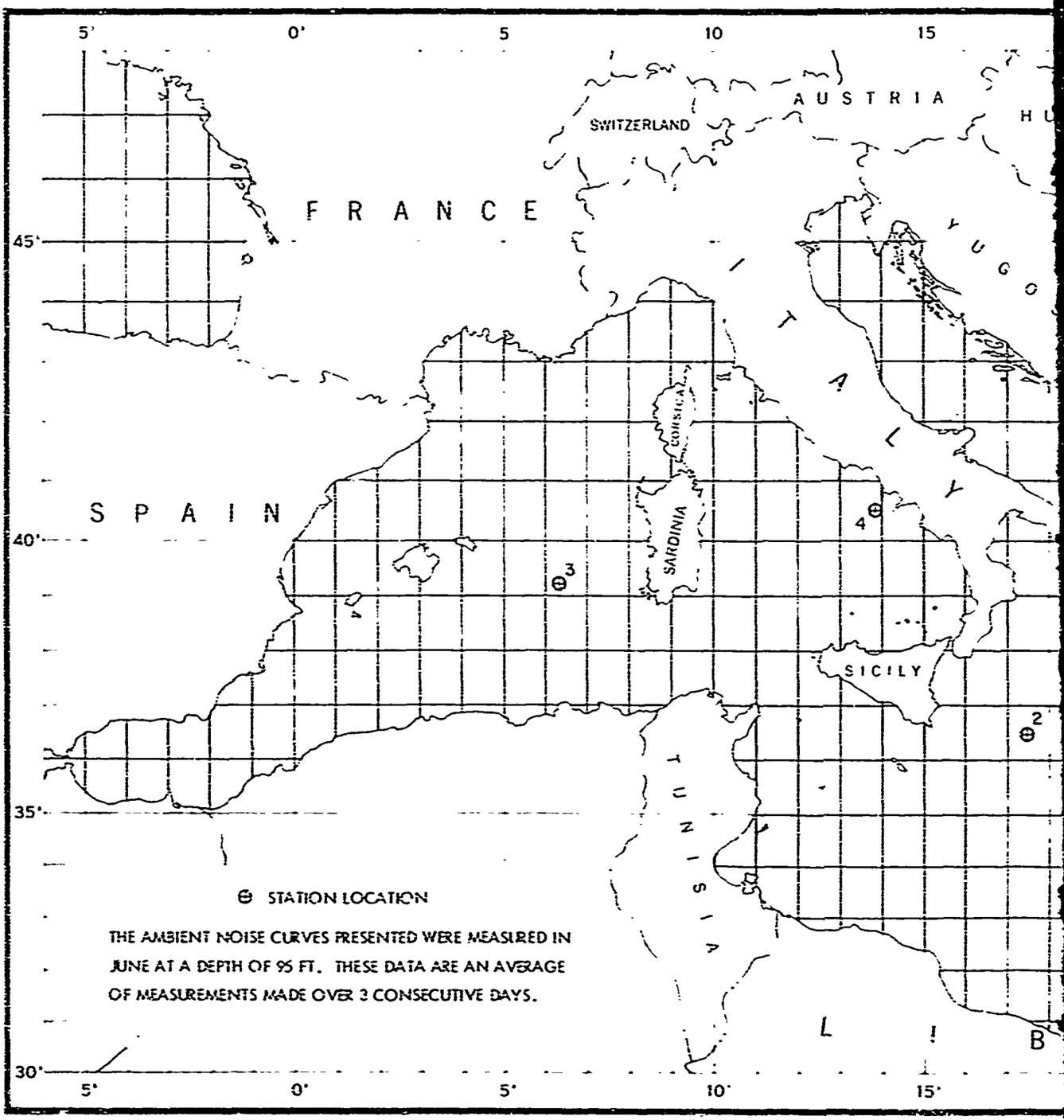

FIGURE 78. AMBIENT NOISE I

LOSS
TIAL

2

1

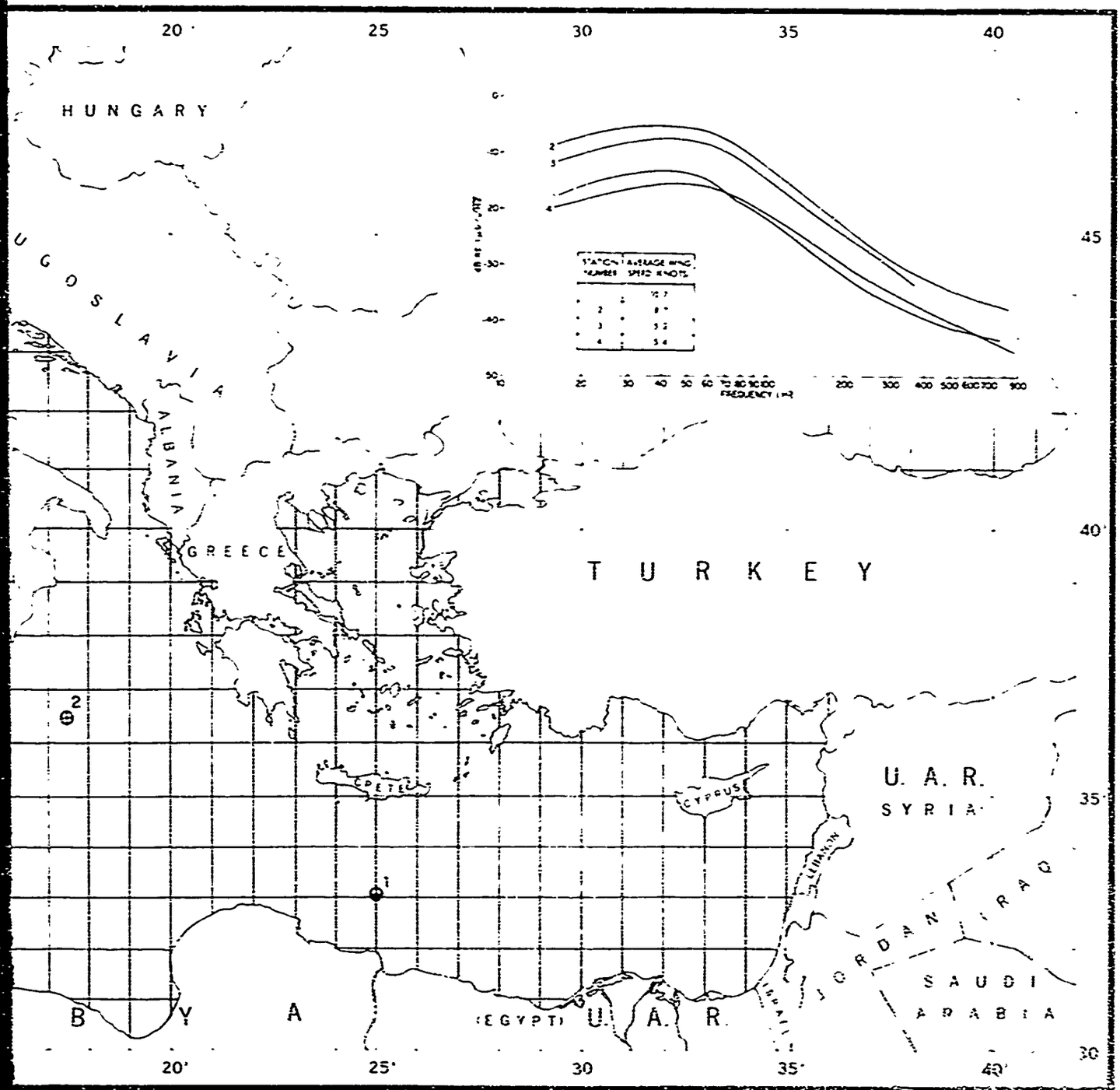

NT NOISE IN THE MEDITERRANEAN SEA

FIGURE 78. AMBIENT NOISE

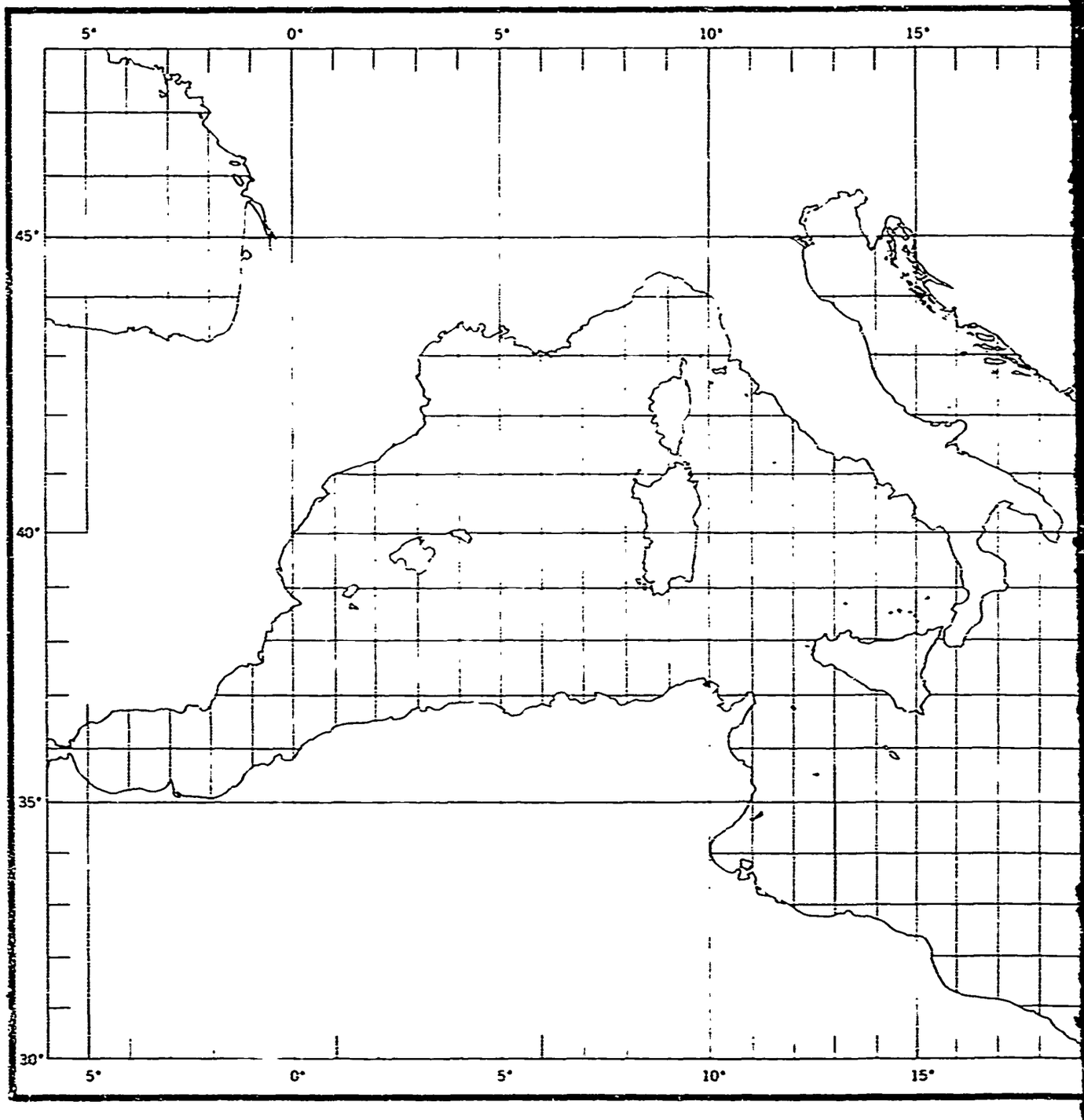
5°
0°
5°
10°
15°
45°
40°
35°
30°

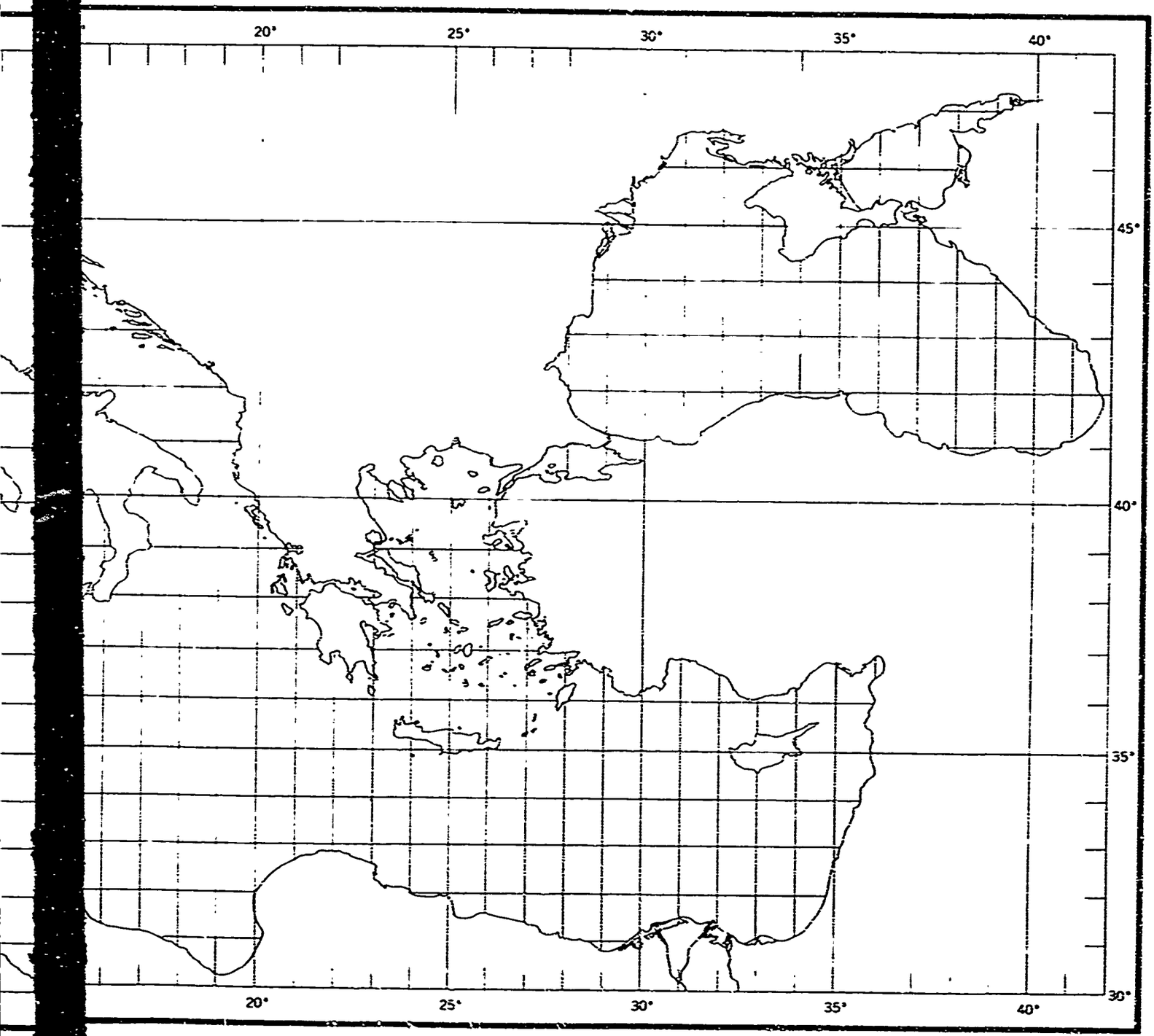

BLANK BASE CHARTS

DEPARTMENT OF THE NAVY
OFFICE OF NAVAL RESEARCH
875 NORTH RANDOLPH STREET
SUITE 1425
ARLINGTON VA 22203-1995

IN REPLY REFER TO:

5510/1
Ser 321OA/011/06
31 Jan 06

MEMORANDUM FOR DISTRIBUTION LIST

Subj: DECLASSIFICATION OF LONG RANGE ACOUSTIC PROPAGATION PROJECT (LRAPP) DOCUMENTS

Ref: (a) SECNAVINST 5510.36

Encl: (1) List of DECLASSIFIED LRAPP Documents

1. In accordance with reference (a), a declassification review has been conducted on a number of classified LRAPP documents.

2. The LRAPP documents listed in enclosure (1) have been downgraded to UNCLASSIFIED and have been approved for public release. These documents should be remarked as follows:

   Classification changed to UNCLASSIFIED by authority of the Chief of Naval Operations (N772) letter N772A/6U875630, 20 January 2006.

   DISTRIBUTION STATEMENT A: Approved for Public Release; Distribution is unlimited.

3. Questions may be directed to the undersigned on (703) 696-4619, DSN 426-4619.

BRIAN LINK
By direction

Subj: DECLASSIFICATION OF LONG RANGE ACOUSTIC PROPAGATION PROJECT (LRAPP) DOCUMENTS

DISTRIBUTION LIST:

NAVOCEANO (Code N121LC – Jaime Ratliff)
NRL Washington (Code 5596.3 – Mary Templeman)
PEO LMW Det San Diego (PMS 181)
DTIC-OCQ (Larry Downing)
ARL, U of Texas
Blue Sea Corporation (Dr.Roy Gaul)
ONR 32B (CAPT Paul Stewart)
ONR 321OA (Dr. Ellen Livingston)
APL, U of Washington
APL, Johns Hopkins University
ARL, Penn State University
MPL of Scripps Institution of Oceanography
WHOI
NAVSEA
NAVAIR
NUWC
SAIC

Declassified LRAPP Documents

Current availability key: NS - NRL Stennis; ND - NRL D.C.; AU - ARL:UT; ADXXXXXXX-DTIC

Report Number	Personal Author	Title	Publication Source (Originator)	Pub. Date	Current Availability	Class.
HLR167; CU-195-69-ONR-266-PHYS	Hardy, W. A.	PROJECT APTERYX: FINAL REPORT (U) (HUDSON LABORATORIES OPERATION 245)	Columbia Univ./ Hudson Labs	690301	NS; ND	C
MCR002	Unavailable	MEDITERRANEAN SEA ENVIRONMENTAL ATLAS FOR ITASS (U)	Maury Center for Ocean Science	691001	NS; ND AD516976	C
NUSCNL3018	Unavailable	TECHNICAL PLAN FOR IMPLANTMENT OF THE TEST BED ARRAY FOR THE LONG RANGE ACOUSTIC PROPAGATION PROGRAM (LRAPP) (U)	Naval Underwater Systems Center	700810	NS; ND	C
Project469 149429855R700	Balaban, M. M.	LRAPP TEST BED ARRAY CABLE FAILURE ANALYSIS (U)	TRW Systems Group	710730	AD0516710; NS; ND	C
BKDCN667	Bernard, P. G., et al.	TECHNICAL DIAGNOSTIC ANALYSIS OF LRAPP TEST BED PROGRAM FAILURE (U)	B-K Dynamics, Inc.	710802	AD0516656; NS; ND	C
NUSCPUB6002	Unavailable	IOMED EXPERIMENT. PRELIMINARY DATA REPORT (U)	Naval Underwater Systems Center	711206	NS; ND	C
ADL ED 15316; ADL-116-672	Unavailable	SQUARE DEAL EXERCISE PLAN (U)	Arthur D. Little, Inc.	720301	ND	C
ADLR4560372	Sullivan, D. L., et al.	PRELIMINARY ANALYSIS OF ACODAC MEASUREMENTS NEAR MADEIRA ON 13-16 OCTOBER 1971 (U)	Arthur D. Little, Inc.	720331	AD0595812; NS; ND	C
MCR07	Gaul, R. D., et al.	IOMEDEX SYNOPSIS ON ENVIRONMENTAL ACOUSTIC EXERCISE IN THE IONIAN BASIN OF THE MEDITERRANEAN SEA NOVEMBER 1971.	Maury Center for Ocean Science	720401	NS; ND	C
P1243	Unavailable	FINAL REPORT ACOUSTIC TEST ARRAY (U)	Raytheon Co.	720831	AD0522104; NS; ND	C
Unavailable	Unavailable	CHART-BATHYMETRIC-SQUARE DEAL EXERCISE (U)	Naval Oceanographic Office	730601	AU	C
TM SA23-C275-73	Wilcox, J. D.	A DESCRIPTION OF THE LRAPP ATLANTIC TEST BED ARRAY FOR MOTION PREDICTION STUDIES (U)	Naval Underwater Systems Center	731212	ND	C
Unavailable	Unavailable	CHURCH ANCHOR AMBIENT NOISE REPORT (U)	Texas Instruments, Inc.	740501	AU	C
Unavailable	Hoffman, J., et al.	CHURCH ANCHOR CW PROPAGATION LOSS AND SIGNAL EXCESS REPORT(U)	Texas Instruments, Inc.	740701	AU; ND	C
MCR104	Unavailable	MEDITERRANEAN ENVIRONMENTAL ACOUSTIC SUMMARY (U)	Maury Center for Ocean Science	740701	NS; ND	C
OSTP-39	Romain, N. E.	OSTP-39 NER: ANALYSIS OF DATA FROM A FIELD TRIAL OF THE LAMBDA ARRAY (U)	Westinghouse Electric Corp. and Bell Laboratories	740930	ND	C
MC-103	Unavailable	MEDITERRANEAN ENVIRONMENTAL ACOUSTIC DATA CATALOG (U)	Office of Naval Research	750501	ND	C
Unavailable	Unavailable	SQUARE DEAL SUS TRANSMISSION LOSS (U)	Arthur D. Little, Inc.	750725	AU	C

ENCL (1)